Dark Cosmology Centre

Star Formation at High Redshifts and the Importance of Dust Obscuration

Michał Jerzy Michałowski

Supervisor: Jens Hjorth

Co-supervisor: Darach Watson

Thesis submitted for the degree of

Philosophiæ Doctor

Dark Cosmology Centre
Niels Bohr Institut
Det Naturvidenskabelige Fakultet
Københavns Universitet

Submitted *October 15th, 2009*
Defended *December 4th, 2009*

CONTENTS

LIST OF FIGURES

LIST OF TABLES

ACKNOWLEDGMENTS

I dedicate this PhD thesis to my wonderful wife Joanna Baradziej. I would like to thank her for her love, support and understanding during these three years.

I would like to express my deep gratitude to my supervisors Jens Hjorth and Darach Watson for so much help, for guiding me through scientific world, for inspiration, and for invaluable discussions and comments (also Darach's comments on Jens' desk). Without you this thesis would not have been possible.

I am grateful to José María Castro Cerón for numerous inspiring discussions; to Thomas Greve for help and comments on submillimeter galaxies and CSO data; to Daniele Malesani for extensive help with acquisition and interpretation of optical data; to Atish Kamble for taking care of GMRT observations; to Robert Reinfrank for operational introduction to ATCA, help with ATCA data reduction and willingness to spend significant time on observing for me; to Alexander van der Horst for help with WSRT data reduction; and to Jorge Iglesias-Páramo and Laura Silva for providing their SED models.

I would like to thank all people at Dark Cosmology Centre for creating so inspiring and lively environment. Special thanks to Andrew Zirm, Justyn Maund and Robert Reinfrank for proofreading my thesis.

Finally, thanks to my friends and my family, parents, parents-in-law, Anita, Jurek, Paweł and Gosia for their support.

I would like to acknowledge the financial support from the Faculty of Science, University of Copenhagen and Dark Cosmology Centre.

ABSTRACT

One of the aspects of the understanding of the Universe evolution is its star formation history. In order to gain a complete picture of the Universe evolution it is important to know when the stars we see today were formed. One of the method to study this problem is to use far-infrared and radio emission of galaxies. In this way it is possible to investigate the sites of star formation that are totally obscured by dust and therefore invisible at the optical wavelengths. It is because the energy absorbed by dust in the optical is re-emitted in the infrared, whereas radio emission is unaffected by dust obscuration.

My analysis is based on two samples of galaxies, which have been confirmed to be associated with recent star formation, namely gamma-ray burst (GRB) host galaxies and submillimeter-selected galaxies (SMGs). For GRB hosts the long-wavelength data are scarce, so I have started a large observing program targeting these galaxies at the radio wavelengths. The obtained data are analysed simultaneously together with the literature data by means of spectral energy distribution (SED) modelling. I use the radiative transfer code called GRASIL, which calculates the entire UV-to-radio SED of a galaxy taking into account the evolution of stars as well as dust reprocessing in both molecular clouds and diffuse interstellar medium.

Using SED modelling I explain the seeming discrepancy between long- and short-wavelength properties of the only four GRB hosts that were detected in the submillimeter and/or radio, namely their enhanced submillimeter / radio emission combined with optical faintness and blue colors. I find that these four galaxies are young, highly star-forming, low-mass and dusty. Their high dust temperatures hint at a possibility that GRB hosts are hotter counterparts of SMGs. Such hot galaxies are missed in submillimeter surveys because their dust peaks are shifted towards shorter wavelengths.

In order to gain insight into local environments of GRBs I analyse the SED of the host of the closest known GRB 980425, associated with supernova 1998bw and of the Wolf-Rayet region ~ 800 pc from the supernova site. I find that the mass of the host of GRB 980425 is dominated by an older stellar population in contrast to the majority of GRB hosts. The Wolf-Rayet region experienced a starburst episode during which the majority of its stellar population was built up. Unlike that of the entire galaxy, its SED is similar to those of cosmological submillimeter/radio-bright GRB hosts with hot dust content. These findings add to the picture that in general, the environments of GRBs on 1–3 kpc scales are associated with high specific star formation rate and hot dust.

I present extensive study of 76 SMGs with spectroscopic redshifts in a range 0.080–3.623. I find that they are highly star-forming, moderately dust-obscured, hosting significant stellar populations of which only a minor part has been formed in the ongoing starburst episode. This implies that in the past, SMGs experienced either another starburst episode or merger with several galaxies. The properties of SMGs suggest that they are progenitors of present-day elliptical galaxies. I find that these bright SMGs contribute significantly to the cosmic star

formation rate density and stellar mass density at redshifts 2–4. I find evidence that the linear infrared-radio correlation holds for SMGs in an unchanged form up to redshift of 3.6, though its normalization is offset from the local relation by a factor of ~ 2.3 towards higher radio luminosities.

Finally, in order to extend this study to even higher redshifts I analyse the SEDs of the only six SMGs, that are spectroscopically confirmed to be at $z > 4$. I find that their star formation rates, stellar and dust masses, extinction and gas-to-dust ratios are within the ranges for $1.7 < z < 3.6$ SMGs. The analysis suggests that infrared-to-radio luminosity ratios of SMGs do not change up to redshift ~ 5 and are lower by a factor of ~ 2.1 than the value corresponding to the local IR-radio correlation. However, I also find dissimilarities between $z > 4$ and lower-redshift SMGs. Those at $z > 4$ tend to be among the most star-forming, least massive and hottest SMGs and exhibit the highest fraction of stellar mass formed in the ongoing starburst. This indicates that at $z > 4$ we see earlier stages of evolution of submillimeter-bright galaxies. Using the derived properties for $z > 4$ SMGs I investigate the origin of dust at epochs less than 1.5 Gyr after the Big Bang. This is significant to our understanding of the evolution of the early Universe. For three $z > 4$ SMGs asymptotic giant branch stars could be the dominant dust producers. However, for other three only supernovae are efficient and fast enough to be responsible for dust production, though requiring a very high dust yield per supernova (0.15–0.65 $M_{\odot}$, such as that claimed in the Cassiopeia A and Kepler supernova remnants). The required dust yields are lower if a top-heavy initial mass function or significant dust growth in the interstellar medium are assumed.

1

INTRODUCTION

One of the issues in the understanding of the evolution of the Universe is its star formation history. It is quantitatively described by the so-called Madau diagram (Madau et al., 1996, 1998; Lilly et al., 1995), giving the total star formation rate (SFR) density in the Universe per unit volume as a function of redshift (Figure 1.1). There are many possible ways to estimate SFRs (see caption of Figure 1.1 and Kennicutt, 1998, for a review). Depending on the method used to select galaxies and to estimate their SFRs, different modes of star formation activity are probed. Ultraviolet (UV)/optical-selected galaxies trace processes unobscured by dust or only little obscured, whereas galaxies selected at the infrared (IR) wavelengths exhibit the dust-reprocessed emission of young stars.

Long-wavelength emission provides therefore crucial information about the star formation history of the Universe. The total energy outputs of the obscured and unobscured modes of star formation are approximately equal, because similar luminosities of extragalactic background light at the UV/optical and IR wavelengths were reported (e.g. Hauser & Dwek, 2001). Hence, approximately half of the cosmic star formation is obscured by dust.

In order to study this obscured star formation I investigated two samples of galaxies. The first is composed of galaxies selected by the presence of a long gamma-ray burst (GRB) associated with the explosions of massive stars. GRBs are believed, therefore, to trace star-forming environments. The second sample includes galaxies selected by their strong submillimeter emission. They were also confirmed to be dominated by a recent burst of star formation, known as a "starburst". Both samples are described below.

1.1 GAMMA-RAY BURST HOST GALAXIES

1.1.1 FIRST OBSERVATIONS

Gamma-ray bursts are intense transient events of γ-ray emission. γ-ray photons have energies of $E > 10^5$ eV corresponding to wavelengths of $\lambda < 0.01$ nm. A burst can last from a few milliseconds to several minutes. It overshines all other γ-ray sources and then fades away. It is followed by decaying emission in other wavelengths (X-ray to radio) known as an afterglow. The observed rate of GRBs is approximately one per day.

Since the Earth's atmosphere absorbs γ-ray photons, GRBs can only be observed from space with satellites. They were first detected in 1967 by the U.S. Air Force military satellite *Vela*, while looking for γ-ray emission which could indicate nuclear tests performed by the Soviet Union. The first detections were reported a few years later by Klebesadel et al. (1973).

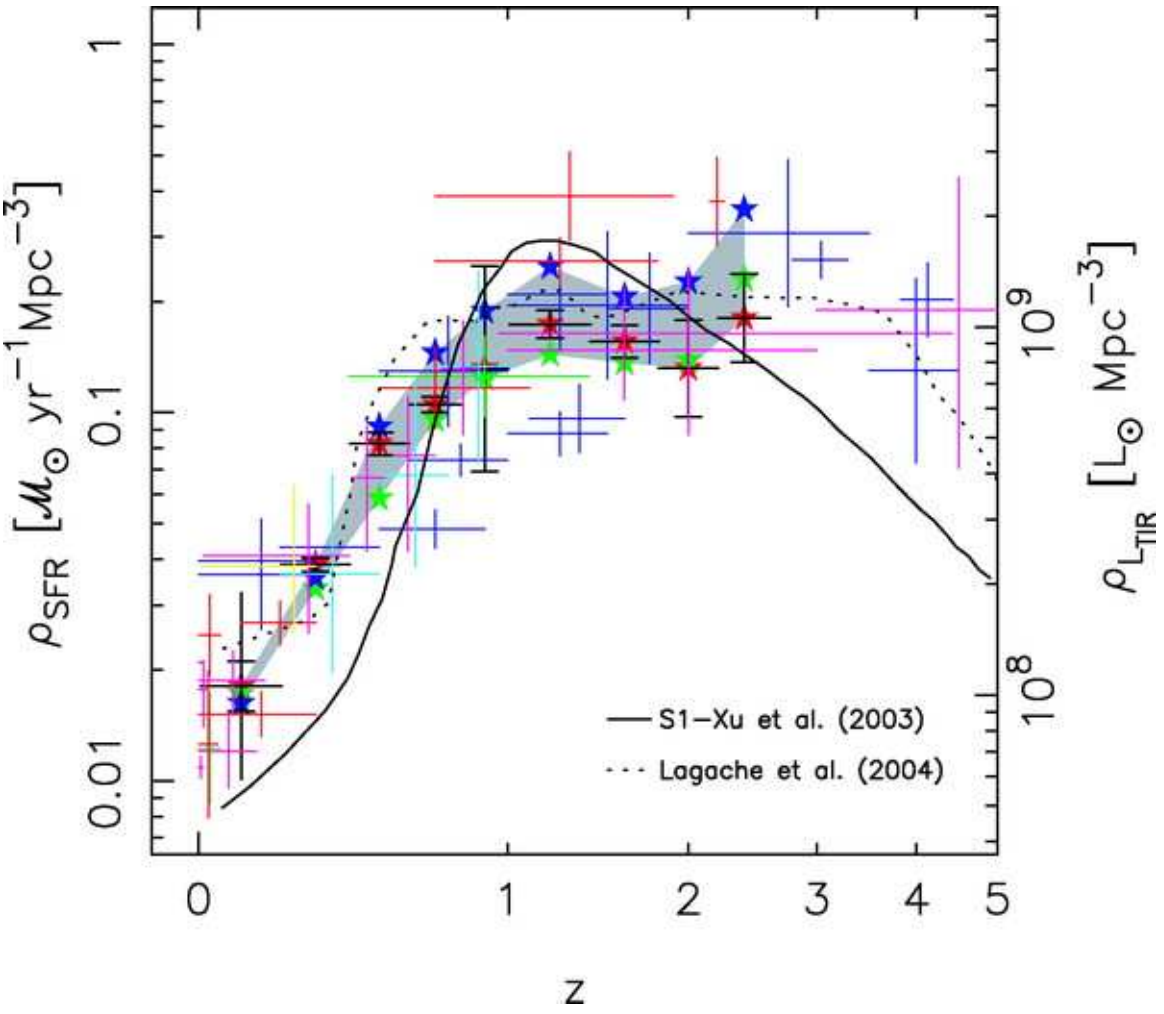

Figure 1.1: *The Madau diagram — the SFR density as a function of redshift. Different SFR indicators are shown with different colors: $H\alpha$ and $H\beta$ (red), [O II] (green), UV continuum (blue), MIR emission (cyan), submillimeter and radio emission (red), X-ray emission (yellow). Two theoretical models are given for comparison (Pérez-González et al., 2005).*

In the early 1990s there was a debate whether GRBs had Galactic or extra-Galactic origin. Finally, as reported by Paczyński (1991), the Burst and Transient Source Experiment (BATSE) on board of the Compton Gamma-Ray Observatory (CGRO) revealed the uniform distribution of GRBs on the sky as shown in Figure 1.2 (Greiner, 1999). Meegan et al. (1992) and Briggs (1995) reported only 0.9σ and 0.3σ deviation from complete isotropy in terms of dipole and quadrupole distributions, respectively. This supported the hypothesis of cosmological distances to GRBs. If GRBs were located in the Milky Way they would be preferentially distributed on the Galactic plane or concentrated towards the Galaxy center similar to halo objects (Paczyński, 1995).

An extragalactic origin of GRBs was confirmed when the first spectrum of the afterglow of GRB 970508 was taken and a redshift of $z = 0.835$ was measured (Metzger et al., 1997). The most distant GRB observed to date is GRB 090423 at the redshift of $z = 8.26$ (Tanvir et al., 2009;

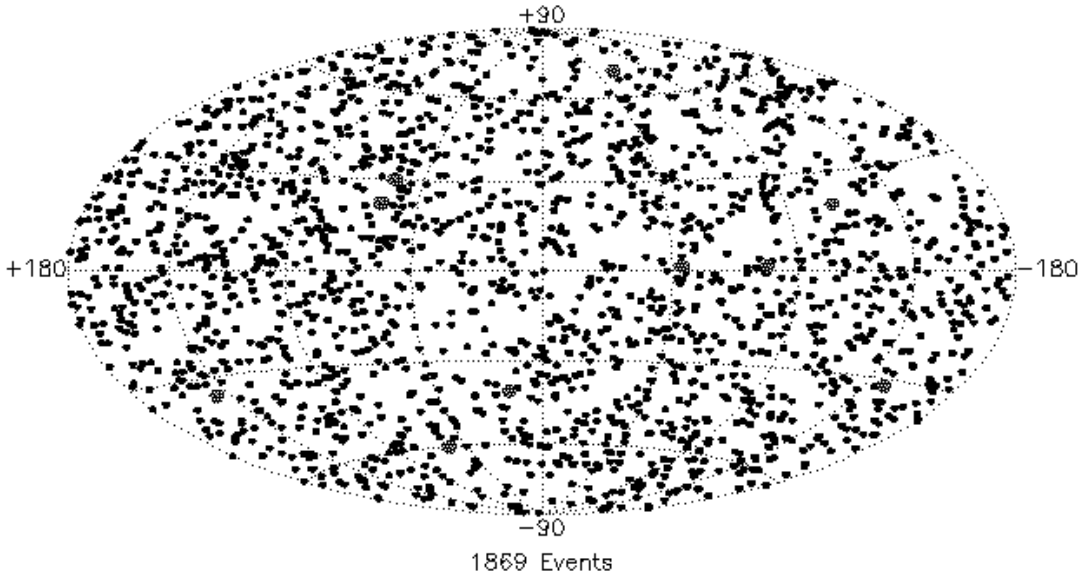

Figure 1.2: *Distribution of GRBs on the sky (Greiner, 1999). Uniformity is the argument in favour of their extra-galactic origin.*

Salvaterra et al., 2009). It exploded when the Universe was only 625 million years old (i.e. 5% of the present age).

1.1.2 PROGENITORS

GRBs are usually divided into two classes depending on their duration. Kouveliotou et al. (1993) noticed a bimodal distribution of the burst duration: long GRBs with $T > 2$ s and short GRBs with $T < 2$ s (Figure 1.3). Unless explicitly noted, a "GRB" refers to a long GRB in this thesis.

There are many proposed mechanisms for the engine of a GRB (Nemiroff, 1994; Cheng & Lu, 2001). However, there are two progenitor models that are favoured: 1) a collapse of a massive star either being a failed supernova or a hypernova (Woosley, 1993; Paczyński, 1998), and 2) the merger of two compact objects such as neutron stars or black holes (Paczyński, 1986). In the former case gravitational energy is released after the core collapse of the star and subsequently its outer parts are ejected with ultra-relativistic velocities. In the latter scenario the merger provides the burst energy. It is believed that the collapsar model may explain properties of long bursts whereas the merger model corresponds to short bursts (Narayan et al., 2001).

Discoveries of GRBs associated with supernovae (SNe) were important evidence in favour of the collapsar model. SN 1998bw was observed in an error box of the closest known GRB which occurred on 25 April 1998 (Galama et al., 1998). However, both GRB 980425 and SN 1998bw had a very peculiar nature, namely the isotropic energy released by the GRB was only $\sim 8 \times 10^{47}$ erg, four orders of magnitude less than a typical value and no "classical" afterglow was de-

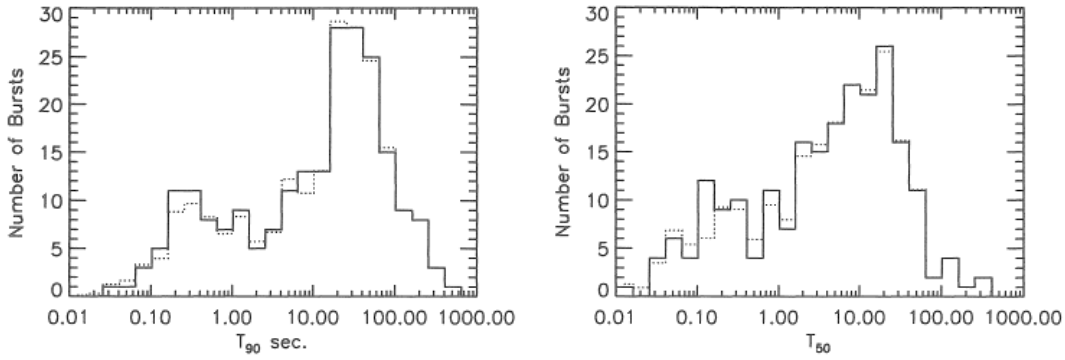

Figure 1.3: *Distribution of durations of GRBs: Left (Right) — time during which counts increases from 5% to 90% (50%) above the background (Kouveliotou et al., 1993). A clear bimodality of duration is especially visible in the case of* T_{90}.

tected (Hjorth et al., 2004). SN 1998bw had unusually high kinetic energy and radio emission. Moreover, according to the model of redshift and luminosity distributions of GRB hosts developed by Hogg & Fruchter (1999) it was highly unlikely to find such a close GRB. Hence, it was questionable if it provided any evidence that other, more "standard" GRBs can also be claimed to be associated with supernova explosions.

More evidence for GRB–SN association was presented by Hjorth et al. (2003b) and Stanek et al. (2003) for GRB 030329 and SN 2003dh. During the early epoch of the afterglow evolution the spectrum was a power-law, typical for this event. A few weeks later when the afterglow component had faded, observations revealed a supernova-like bump in the optical lightcurves as well as Fe-group lines and other spectral signatures similar to type Ic SNe[1]. A type Ic SN is believed to be the collapse of a very massive Wolf-Rayet star ($M > 20M_{\odot}$) after phase of extensive mass loss. It could also be a star in a binary system that loses its hydrogen envelope through Roche lobe overflow onto its companion (Nomoto et al., 1994).

The fact that a sample of GRBs associated with SNe consists only of a few events (e.g. Hjorth et al., 2003b; Matheson et al., 2003; Stanek et al., 2003; Cobb et al., 2004; Gal-Yam et al., 2004; Malesani et al., 2004; Thomsen et al., 2004; Ferrero et al., 2006; Mirabal et al., 2006; Modjaz et al., 2006; Pian et al., 2006; Soderberg et al., 2006; Sollerman et al., 2006) can be explained by a high mean redshift of GRBs, equal to ~ 1 in the pre-*Swift* era and ~ 2.8 for the *Swift* sample (Jakobsson et al., 2006c). It implies that any SN peak would be fainter than $R > 23$ mag, which is below the detectability threshold of most ground-based telescopes (Stanek et al., 2003).

1.1.3 HOST GALAXIES

The fact that GRBs signal the deaths of very massive and very short-lived stars hints at the possibility to use them to study star formation in the Universe. It is because if a galaxy hosts a GRB, then it must also have undergone a recent period of star formation. Therefore by examining the host galaxies of GRBs, we are taking a census of the sites of massive star formation directly, rather than via the proxy of the total galaxy light. This means that the luminosity function of GRB hosts should be directly related to instantaneous massive SFR in all types of galaxies (e.g.

[1]Type Ic SNe are defined as ones with no hydrogen, helium and silicon absorption lines (Wheeler & Harkness, 1990; Filippenko, 1997), see Figure 1.4

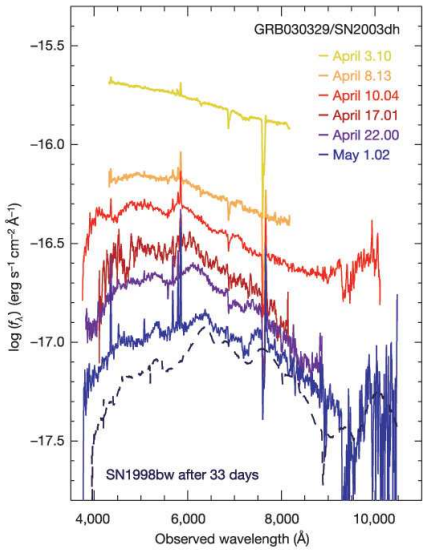

Figure 1.4: *Spectrum of GRB 030329 (solid lines) and SN 1998bw (dashed line) for comparison. The early-time afterglow spectrum was a typical power-law but later a supernova-like spectral features dominated (Hjorth et al., 2003b).*

Trentham et al., 2002). Ultimately the goal is to study cosmic star formation history using the GRB rate as a function of redshifts. Before this is possible the properties of GRB hosts must be investigated in detail to test whether indeed the GRB rate is proportional to cosmic SFR.

Le Floc'h et al. (2003) reported that GRB host galaxies were very blue ($R - K \lesssim 3$), even more so than nearby irregular galaxies. Moreover, they were sub-luminous ($K > 20$, $M_K \sim -22.25 = 0.08 M_\star$) implying low stellar masses. This could indicate that they were young galaxies undergoing the first episode of star formation. Similar results were reported by Castro Cerón et al. (2006, 2009) and Savaglio et al. (2009) finding that most of GRB hosts have stellar masses $< 10^{11} M_\odot$, ages of a few 100 Myr and high specific SFR.

As expected, GRBs were found to occur in star-forming regions. For example, Holland & Hjorth (1999) investigated the Hubble Space Telescope (HST) image of the surroundings of GRB 990123 and found that it occurred in an irregular galaxy, consisting of three knots with sizes comparable to star-forming and HII regions in the local Universe, as well as having luminosities and flat spectra consistent with ongoing star formation. Similarly, Bloom et al. (1998a, 1999); Galama et al. (1998); Kulkarni et al. (1998); Paczyński (1998); Castro-Tirado & Gorosabel (1999); Fruchter et al. (1999a,b); Hjorth et al. (1999, 2000, 2002); Fynbo et al. (2000); Holland (2001); Prochaska et al. (2004) claimed that GRBs resided in star-forming regions. In the case of GRB 980425 the region within 100 pc from the GRB contained three stars with blue colors consistent with being massive main-sequence stars (Holland, 2001). Moreover, Fruchter et al. (2006) found that GRBs traces the UV-bright (i.e. star-forming) parts of their host.

Thus, GRB hosts seem to be similar to the population of faint blue star-forming galaxies at high redshift. Most of them were not detected at the radio and submillimeter wavelengths (Berger et al., 2001b, 2003a; Frail et al., 2002; Tanvir et al., 2004). This implies that in the GRB host population there are only few highly star-forming galaxies in the class of (Ultra)Luminous Infrared Galaxies ([U]LIRGs).

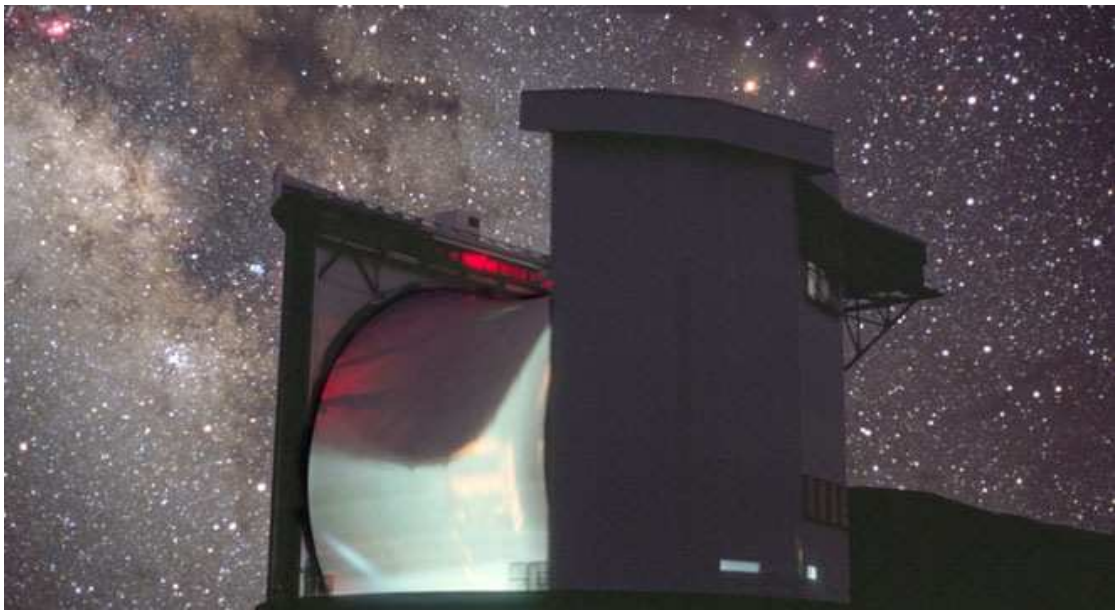

Figure 1.5: *Night view of James Clerk Maxwell Telescope. From:* `http://www.jach.hawaii.edu/JCMT/`

These findings can be explained by theoretical models. MacFadyen & Woosley (1999) predicted that the formation of massive rotating helium stars — progenitors of GRBs — was favored in low metallicity regions. This is because, in the case of high metallicity, strong stellar winds induce strong mass and angular momentum losses, which hamper the formation of GRBs. Hence, dwarf and subluminous galaxies would be preferred as hosts, since they usually have a lower metal content. Metal-poor environments of GRB hosts are also implied from their enhanced Lyα emission (Fynbo et al., 2003; Jakobsson et al., 2005), low oxygen abundances (Stanek et al., 2006), characteristics of emission lines (Vreeswijk et al., 2001b; Bloom et al., 2003; Gorosabel et al., 2005), SMC[2]-type of extinction (Kann et al., 2006), values of dust-to-gas ratios similar to, or even lower than, that of the SMC (Hjorth et al., 2003a; Stratta et al., 2004; Kann et al., 2006) and somewhat small sizes and irregular morphologies (Fruchter et al., 2006). Savaglio et al. (2003, 2006, 2009) found that the metallicity of GRB hosts is usually less than $0.6Z_{\odot}$, which is typical for starburst galaxies.

The utility of GRBs as star formation traces was studied by Hogg & Fruchter (1999) based on luminosity distributions of GRB hosts. They investigated three models in which a GRB rate was proportional to the SFR (consistent with the collapsar model), to the total integrated stellar density (consistent with the merger model) or was constant at any redshift. They found that the first model was slightly favored, whereas the second was most strongly disfavored by the data (with the likelihoods' ratio of $1.00 : 0.12 : 0.57$). Proportionality between the GRB rate and SFR was also claimed by Totani (1997); Mao & Mo (1998); Wijers et al. (1998); Kommers et al. (2000)

However, recent studies suggested that GRBs trace cosmic star formation history, but in a biased way towards low-metallicity environments (Li, 2008; Lapi et al., 2008; Kocevski et al., 2009). This means that at low redshift, when the average metallicity is high, GRBs do not trace the total star formation activity in the Universe.

[2]Small Magellanic Cloud

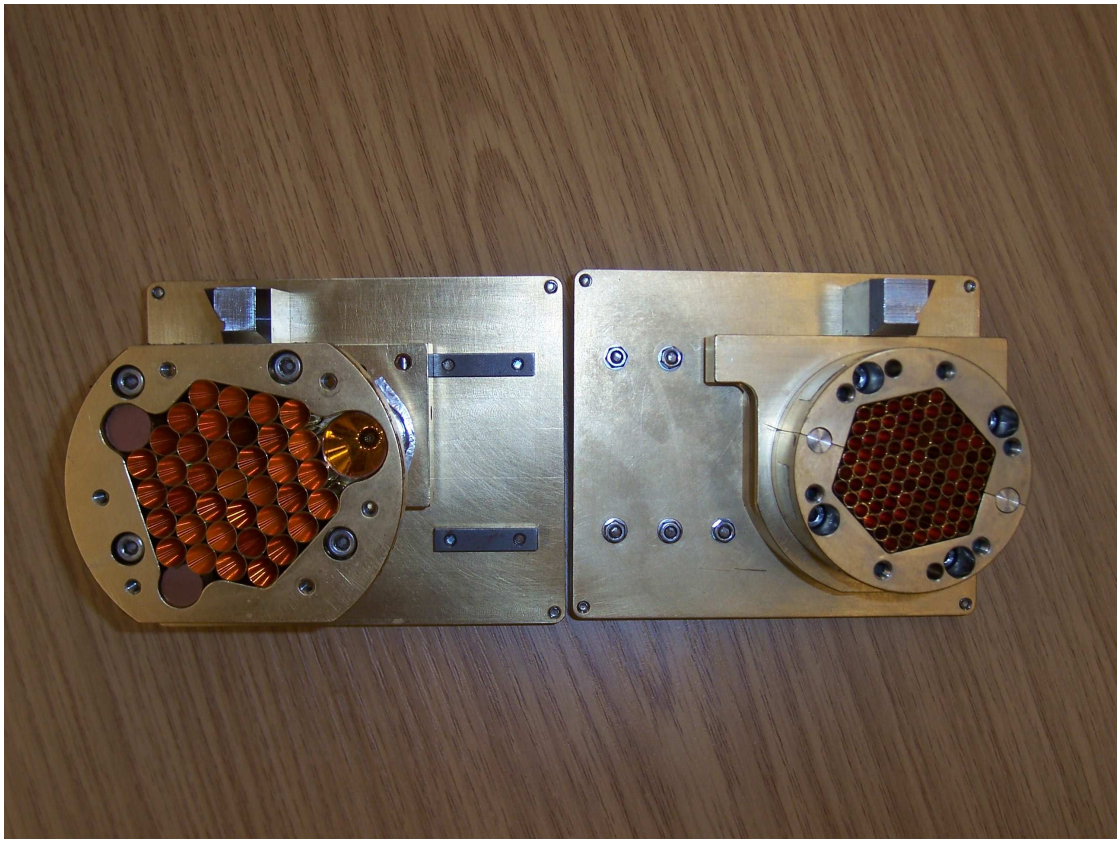

Figure 1.6: *The pixel layout of the SCUBA long-wavelength (850 μm) and short-wavelength (450 μm) arrays. This picture has been taken during my visit in the Royal Observatory in Edinburgh.*

1.2 SUBMILLIMETER GALAXIES

1.2.1 FIRST DISCOVERY

Study of high-redshift galaxies selected at submillimeter wavelengths (submillimeter galaxies, SMGs) was first possible when Submillimeter Common-User Bolometer Array (SCUBA; Holland et al., 1999) was mounted on James Clerk Maxwell Submillimeter Telescope (JCMT, Figure 1.5). This is because SCUBA was the first submillimeter instrument capable of reasonable fast mapping of given sky area making it possible to undertake submillimeter surveys. High mapping speed was not easy to achieve before, because detectors were usually single-pixel receivers (e.g. UKT14; Duncan et al., 1990). SCUBA consisted of two arrays working at $850\,\mu$m (37 pixels, see Figure 1.6) and $450\,\mu$m (91 pixels) taking advantage of minima in atmospheric opacity (see Figure 1.7). The arrays had a significant field of view of 2.3 arcmin, which also helped mapping large areas. The primary beam size (the diffraction limit of the resolution) was 14 and 7.5 arcsec for $850\,\mu$m and $450\,\mu$m, respectively. Both arrays could be used simultaneously by means of a dichroic beamsplitter.

Before the first SCUBA observations were performed, it had already been anticipated that a new population of distant dusty galaxies could be revealed, at redshifts as high as $z \sim 10$ (Blain & Longair, 1996; Blain, 1997). This is because of so-called negative K-correction. Namely

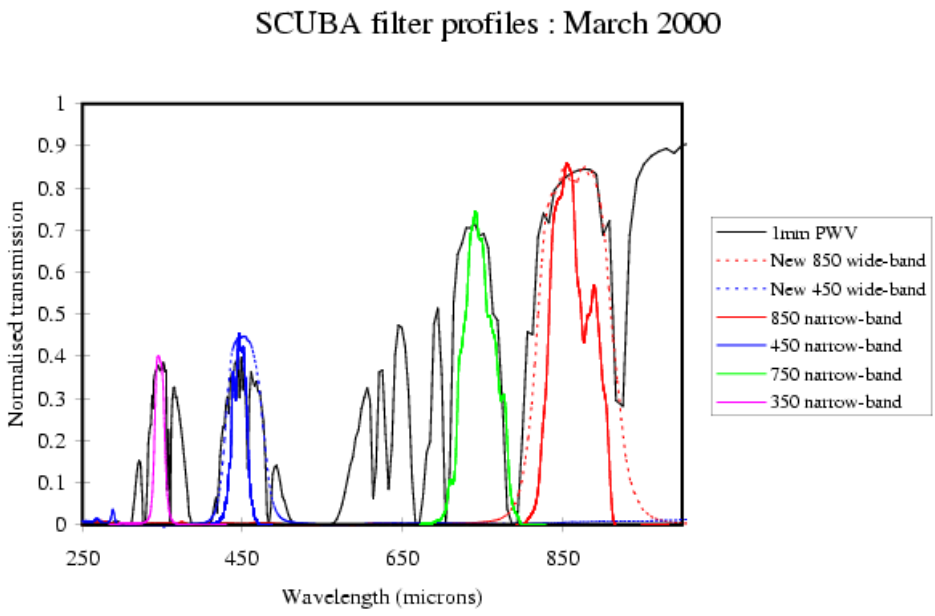

Figure 1.7: *Atmospheric transmission (black) and profiles of SCUBA filters (Holland et al., 1999).*

if a galaxy observed at the submillimeter wavelengths is shifted to higher redshifts, the observations probe closer to the dust peak where a galaxy is brighter. This effect compensate the $1/\text{distance}^2$ dimming and results in an almost invariant submillimeter flux of a galaxy through a wide range of redshifts (see red lines in Figure 1.8).

First SMGs were detected more than 10 years ago (e.g. Smail et al., 1997; Barger et al., 1998; Hughes et al., 1998; Ivison et al., 1998). Based on these pioneering data the number density of SMGs was measured and it turned out that they were much more numerous than expected under the assumption of nonevolving local luminosity function (Smail et al., 1997). This implies that there was a dramatic change between number of highly star-forming galaxies in the local and high-redshift Universe. The crude estimates of SFR were of the order of several $100\ M_{\odot}\ \text{yr}^{-1}$ implying that SMGs are significant contributors to star formation history at high redshifts. The detected sources already accounted for $\sim$ 20–50% of the extragalactic background at submillimeter wavelengths (Hughes et al., 1998; Barger et al., 1999) . This also hints at the importance of SMGs, because, as mentioned earlier, studies of extragalactic background light revealed that in the Universe there is approximately equal amount of energy emitted in the UV/optical and IR domains (e.g. Hauser & Dwek, 2001).

1.2.2 Leap forward: precise localisations

In these early times it was virtually impossible to study the nature of SMGs in details. In fact, even redshifts of this sources were unknown. This was because the coarse SCUBA beamsize of 14 arcsec prevented identifications of optical counterparts of SMGs, on which slits of optical spectrographs could be placed (bandwidths of (sub)millimeter spectrographs were too narrow, but now it is getting possible to measure redshifts of SMGs independently of optical emission; e.g. Daddi et al., 2009b,a; Weiß et al., 2009).

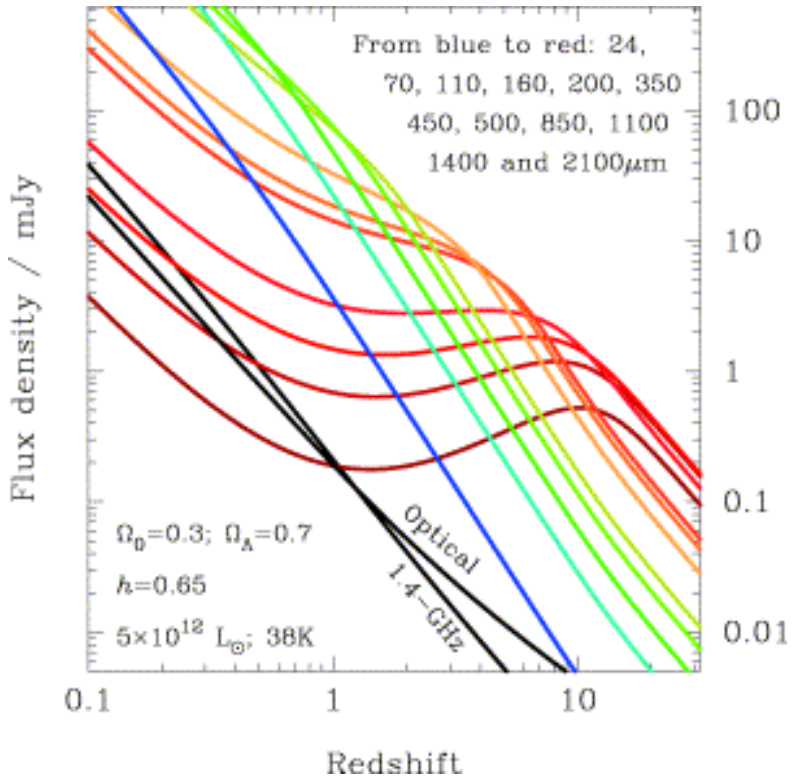

Figure 1.8: *K-correction at the submillimeter wavelengths makes it possible to detect SMGs as distant as at $z \sim 10$ (Blain et al., 2002). Lines shows fluxes of a galaxy at variety of wavelengths as a function of redshift.*

This was solved by high-resolution interferometric observations at the radio wavelengths (the principles are described in Chapter 2). It is known that a galaxy bright at the IR wavelengths is also bright in the radio. This FIR-radio correlation was found locally to be very tight and holds over several orders of magnitude in luminosity (Helou et al., 1985; Condon, 1992). Therefore galaxies detected at the submillimeter wavelengths should also be bright at the radio wavelengths. Moreover, the surface density of radio sources is much lower than that of optical sources, so a radio source coincident with a submillimeter peak is unlikely to be a chance superposition (Blain et al., 2002).

Therefore radio observations with sub-arsec resolution was used to pinpoint the locations of SMGs (e.g. Ivison et al., 2002). This enabled identifications of their optical counterparts and subsequently, measurement of their redshift. The big redshift survey of 76 SMGs was undertaken and the majority of them were found to be distant galaxies at $z \sim 1.7$–2.8 (Chapman et al., 2003b, 2005).

A multi-wavelength approach was applied in the largest submillimeter survey to date containing 120 SMGs, SCUBA Half-Degree Extragalactic Survey (SHADES; Mortier et al., 2005; Coppin et al., 2006). Counterparts of SMGs were identified at the radio and mid-IR wavelengths (Ivison et al., 2007). The photometric redshifts were measured using all the available data (Aretxaga et al., 2007; Dye et al., 2008).

1.2.3 THE NATURE OF SUBMILLIMETER GALAXIES

Having the precise localisations and redshifts, the nature of SMGs was studied in detail using both Chapman et al. (2005) and SHADES samples.

SMGs were confirmed to be among the bolometrically most luminous galaxies. Their infrared luminosities of $L_{\rm IR} \sim 10^{12-13}\,L_{\odot}$ (Chapman et al., 2005; Kovács et al., 2006; Coppin et al., 2008) imply huge SFRs of several hundred solar masses per year (using e.g. Kennicutt, 1998). These luminosities hint also at significant amount of cold dust ($M_d \sim 10^{8-9}\,M_{\odot}$; Kovács et al., 2006; Coppin et al., 2008) radiating at a temperature $T_d \sim 30$-45 K (Chapman et al., 2005; Kovács et al., 2006; Coppin et al., 2008)

SMGs were found to host significant stellar population too ($M_* \sim 10^{11-12}\,M_{\odot}$ Borys et al., 2005; Dye et al., 2008). The question is when these stars formed — either during the ongoing starburst if it is powerful and long enough, or in the past. Dye et al. (2008) found that approximately half of the stellar masses in SMGs have been formed over a long ($\sim$ 1–2 Gyr) period of approximately constant star formation activity.

It is generally found that a significant fraction of SMGs host AGNs, but their bolometric luminosities are dominated by star formation. This was inferred from X-ray properties (Alexander et al., 2005), mid-IR colors (Hainline et al., 2009), mid-IR spectroscopy (Valiante et al., 2007; Pope et al., 2008; Menéndez-Delmestre et al., 2007, 2009; Watabe et al., 2009) and near-IR spectroscopy (Swinbank et al., 2004) of SMGs.

1.3 THIS THESIS

In this thesis I present the study of obscured star formation in the Universe using the samples of GRB hosts and SMGs. I characterize their nature and investigate what we can learn from them about the formation of stars throughout the evolution of the Universe. In Chapter 2 I describe the principles of observations at the radio wavelengths and the data reduction. Moreover, I show preliminary results of the ongoing radio GRB host program. My main methodology tool, spectral energy distribution (SED) modeling, is described in Chapter 3. The main results of my thesis are discussed in the following four chapters. The sample of submillimeter/radio bright GRB hosts is investigated in Chapter 4. In Chapter 5 I analyse in detail the host galaxy and the immediate environment of the closest known GRB, namely GRB 980425, associated with SN 1998bw. In Chapter 6 I investigate the sample of 76 SMGs with spectroscopic redshifts, whereas in Chapter 7 I extend this work by analysing the recently found SMGs at redshifts $z > 4$. Finally, I present the conclusion and future prospects in Chapter 8.

2

OBSERVATIONS AT RADIO WAVELENGTHS

2.1 RADIO EMISSION

Radio observations provide a source of information complementary to that from other wavelengths. This is because radio emission traces different objects than, for example, the optical. This is illustrated in Figure 2.1, where the sky emission at radio wavelengths is shown. Most of the objects seen on the radio map are high-redshift galaxies and quasars, unlike in the optical, at which stars dominate the sky appearance.

Indeed, individual stars are very weak radio emitters, i.e. their contribution to the integrated radio emission of a galaxy is negligible. In order to emit at radio wavelengths, an object has to produce electrons, which are in turn responsible for radio emission. Two major mechanisms of continuum radio emission of galaxies are discussed below.

2.1.1 FREE-FREE EMISSION

Free-free emission (or thermal bremsstrahlung) originates when electrons scatter off ions The electron is not bound to the ion either before or after the interaction (hence the name of the mechanism). The energy lost by the electron is radiated at radio wavelengths.

This mechanism takes place in ionized H II regions surrounding hot young stars. Their strong UV radiation ionizes the medium, which is dense enough to ensure that free electrons have significant probability to interact with ions.

As given by Yun & Carilli (2002) the strength of the free-free emission depends on a thermal distribution of the electrons (with temperature T_e) and a free-free optical depth $\tau_{\rm ff}$ in the following way:

$$S_{\rm ff}(\nu) \propto B(\nu, T_e)(1 - e^{-\tau_{\rm ff}}), \tag{2.1}$$

where ν is the frequency, $B(\nu, T)$ is a black-body Planck curve

$$B(\nu, T) = \frac{2h}{c^2} \frac{\nu^3}{\exp(h\nu/kT) - 1}. \tag{2.2}$$

h, c and k are the Planck constant, the speed of light and the Boltzmann constant, respectively.

A normalization factor for an entire galaxy can be derived from its star formation rate (SFR) because it governs the production rate of the Lyman continuum photons (only young hot stars can ionize the medium around them). The results can be written as

$$S_{\rm ff}(\nu_{\rm obs}) = 0.71 \nu_{\rm em}^{-0.1} \frac{\rm SFR(1+z)}{D_L^2} \quad \text{[Jy]}, \tag{2.3}$$

Figure 2.1: *Appearance of the sky seen at radio wavelengths. Point-like objects are distant galaxies and quasars; ring-like objects are remnants of supernovae explosions in our Galaxy; whereas extended structures are star-forming clouds also in our Galaxy. From:* `web.njit.edu/~gary/728/RadioNightSky_med.jpg`*. Copyright: National Radio Astronomy Observatory / Associated Universities, Inc. / National Science Foundation.*

where z is redshift of a galaxy, $\nu_{\mathrm{em}} = (1+z)\nu_{\mathrm{obs}}$ is a galaxy rest frame frequency in GHz, and D_L is a luminosity distance in Mpc. The flux is measured in units called janskys defined as $1\,\mathrm{Jy} = 10^{26}$ watt per square meter per hertz.

2.1.2 Synchrotron Emission

Synchrotron emission is generated by ultra-relativistic electrons moving through a magnetic field. The magnetic field applies a force to the electrons causing them to radiate and follow curved paths.

Galactic synchrotron emission comes from relativistic electrons emitted by supernova remnants and spiralling in their magnetic fields. A supernova rate and in turn a supernova remnant

Figure 2.2: *Australia Telescope Compact Array. One of the antennas guarded by a kangaroo. This picture was taken during my visit at ATCA to observe the host of GRB 980425 (Chapter 5).*

rate are closely related to the SFR so the flux density of synchrotron emission is given by

$$S_{\rm nth}(\nu_{\rm obs}) = 25 f_{\rm nth} \nu_{\rm em}^{-\alpha} \frac{\rm SFR(1+z)}{D_L^2} \quad [\rm Jy]. \tag{2.4}$$

$f_{\rm nth}$ is a factor of the order of unity and accounts for possible changes in proportionality between SN rate and SFR. $\alpha = 0.7 - 0.8$ is a synchrotron spectral index.

2.1.3 WHY RADIO?

As indicated above, radio wavelength observations are an important source of information about astronomical objects, in particular galaxies. From equations (2.3) and (2.4) one can see

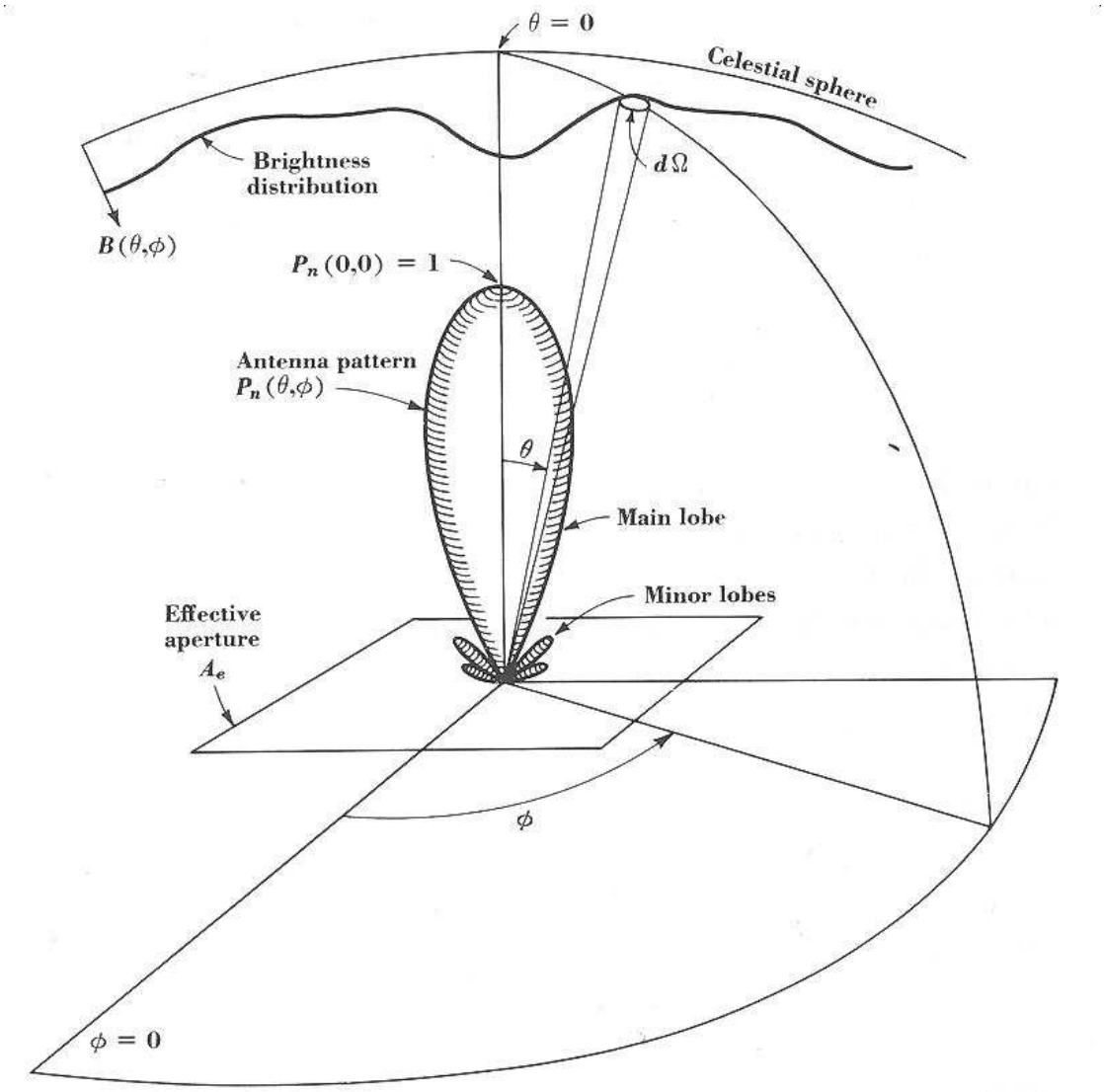

Figure 2.3: *Power pattern of a beam of a radio array giving the response as a function of angle from the main axis (Kraus, 1966). The received signal is a convolution of sky brightness distribution and the beam pattern.*

that the SFR of a galaxy can be estimated once their radio flux is measured (see also Bell, 2003, for a discussion about radio luminosity–SFR relation). A radio-determined SFR has the advantage that is unaffected by dust extinction which can be a large and uncertain factor for optical data (factor > 10 for star-forming galaxies, Bell et al., 2005). The assumption of the SED shape at radio wavelengths (spectral slope) is also not as crucial as in the submillimeter at which the 20% change of the assumed dust temperature leads to 85% change in SFR (Chapman et al., 2005). On the other hand, mid-infrared emission is strongly influenced by polycyclic aromatic hydrocarbon features.

Moreover, current (and future) radio interferometers (Section 2.2) can reach angular resolution of sub-arcsec, typical for optical observations. Therefore the morphology and kinematics of a galaxy can be studied in great details using radio wavelengths.

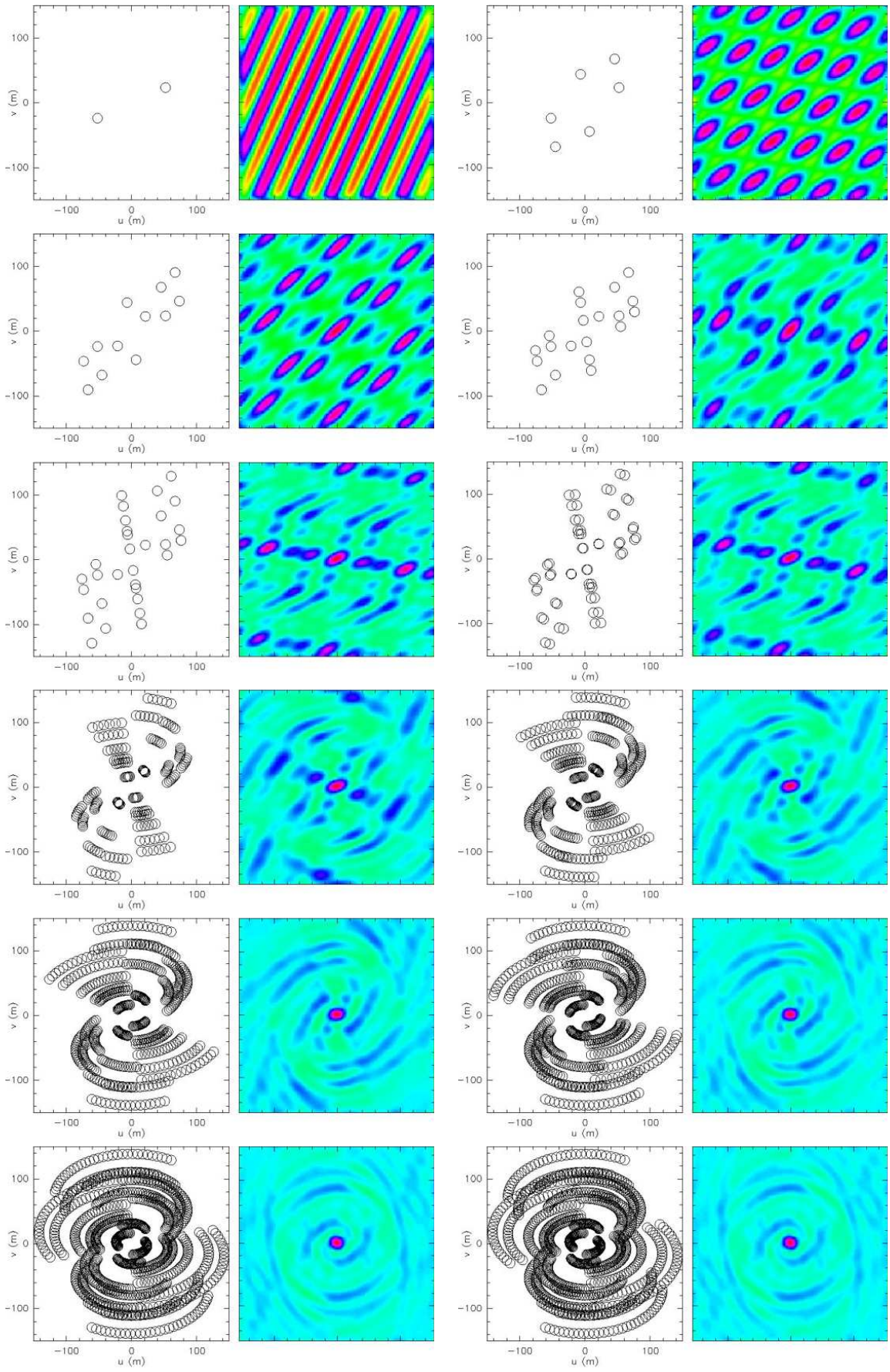

Figure 2.4: *Radio aperture synthesis. Left images: uv-plane. Right images: reconstructed map for a point source. See text for discussion. From:* `iram.fr/IRAMFR/IS/IS2004/presentations/pety-24nov04.pdf`.

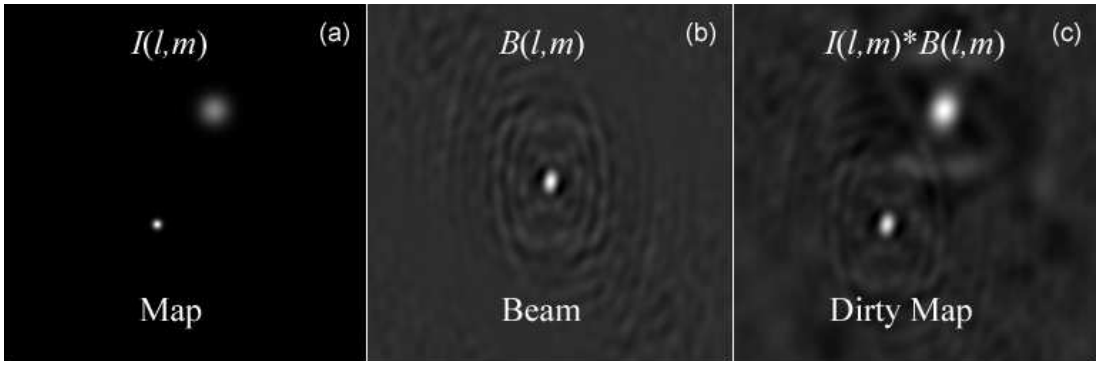

Figure 2.5: *Clean image, beam and dirty image. Dirty map is a convolution of the clean map and the beam. From:* `http://web.njit.edu/~gary/728/image_ft_relation.gif`.

Finally, spectral index (slope of the radio SED) provides valuable information on starburst ages and masses, gas densities and strength of activity (Bressan et al., 2002; Hirashita & Hunt, 2006).

2.2 RADIO INTERFEROMETRY

As mentioned above, radio observations can reach very fine angular resolution, but this requires a specific technical setup. The resolution of a telescope (θ, minimal angular distance at which two sources can be separated) is inversely proportional to its diameter D and proportional to the wavelength λ:

$$\theta('') = \frac{2.5 \times 10^5 \lambda}{D}. \tag{2.5}$$

Therefore for radio wavelengths a diameter of a telescope would need to be enormous in order to keep the same resolution as in optical wavelengths. For example to reach $1''$ resolution at 21 cm the diameter has to be ~ 50 km, exceeding capabilities of the current technology by at least two orders of magnitude.

This problem has been solved by applying interferometry. Instead of building huge antennas, it is much cheaper to combine signal received by several smaller antennas into an array. The resulting resolution is similar to that obtained by a single dish with diameter equal to the maximum distance between antennas (so-called maximum baseline). An example of a radio interferometer Australia Telescope Compact Array (ATCA) is shown in Figure 2.2. Its maximum baseline of 6 km gives resolution of $\sim 8''$ at 21 cm.

The response of an array on a point-like source is called a beam of an array and is shown in Figure 2.3. The majority of the signal of such source would be spread in the main lobe, but some part is distributed in side lobes. The angular distance between points at which the response has a value equal to a half of that at the maximum (half-power beamwidth, HPBW) is an estimate of the resolution of an array.

Each antenna pair measures signal in a form of so-called visibilities (fourier components of the signal), which are electric signals with amplitude A and phase ϕ[1]:

$$V = A \exp(i\phi) \tag{2.6}$$

[1] `iram.fr/IRAMFR/IS/IS2004/presentations/downes-22nov04.ppt`

Visibilities are fourier transform of original signal convolved with a beam plus noise[2]:

$$V = \mathrm{FT}(\mathrm{Beam} \star \mathrm{Source}) + \mathrm{Noise} \tag{2.7}$$

Each antenna pair provides therefore one datapoint on the fourier plane (so-called uv-plane). This is illustrated in Figure 2.4. In each panel the left image corresponds to the distribution of visibilities on the uv-plane, whereas the right image is the intensity map of a point source resulting from the inverse fourier transform of the visibilities. On the left images each circle corresponds to one antenna pair (one baseline). The first 5 panels (from top-left towards bottom-right) corresponds to snapshot observations using 2, 3, 4, 5, 6 antennas. There are $N(N-1)$ baselines for N antennas. When number of antennas increases there is an improvement in coverage of the uv-plane and reconstruction of the intensity map. However, considerably more antennas would be necessary to fill the uv-plane and obtain an acceptable image.

This is solved by applying the aperture supersynthesis method (Ryle & Vonberg, 1946). The idea is to use the Earth rotation to fill the uv-plane. This is illustrated on panels 6–12 of Figure 2.4. Once the Earth rotates, a given antenna pair tracks a source at different orientation and therefore provides additional point on the uv-plane. The full ~ 12 hr synthesis (last panel) provides a well-sampled uv-plane with a reasonable reconstruction of the intensity map.

The intensity map is reconstructed by the inverse fourier transform. During this process a beam of an array (response on a point source) is also calculated. The intensity map shown in the bottom-right corner of Figure 2.4 is called a dirty map because it contains the artifacts (e.g. side lobes) resulting from finite sampling of the uv-plane (corresponding beam is called dirty beam). In order to correct for that the CLEAN algorithm (Högbom, 1974; Schwarz, 1978) is applied[3]:

1. Find the strength and location of the brightest point in the image.
2. Subtract from the dirty image at this location the dirty beam multiplied by peak strength (Record the position and the subtracted flux).
3. Go to (1) unless any remaining peak is below some user-specified level. What is left are the residuals.
4. Convolve the accumulated point source model with an idealized clean beam (i.e. add back components) usually an elliptical gaussian of the same size and shape as the inner part of the dirty beam.
5. Add the residuals from step (3) to the clean image.

If the cleaning works reasonably for all the sources then the output clean map contains sources smeared by a gaussian corresponding to the resolution of an array plus the noise. This is shown in Figure 2.5. Right panel shows a dirty map - signal (two sources) convolved with a dirty beam, which is represented on the middle panel. After cleaning the original intensity map is reconstructed (left panel).

The last issue, which has to be taken into account during interferometric observations is correction for changes of amplitudes and phases due to instrumental effects. This process is called calibration (see Section 2.3.3). This is done by observing bright point sources — calibrators. A primary calibrator is used to set the absolute flux scale and determine the gain of the antennas (their amplitude response). It is observed once during an observing run, typically at the beginning or the end. To monitor the phase changes another calibrator is observed every 30–45

[2] iram.fr/IRAMFR/IS/IS2004/presentations/pety-24nov04.pdf
[3] http://web.njit.edu/~gary/728/Lecture7.html

minutes. It has to be bright, but also close to a target source in order to minimize slewing time. The idea of the calibration is that it is known how an array should respond on a point source, so comparing the obtained and expected signals one can derive appropriate corrections.

2.3 DATA REDUCTION

The reduction of radio data, i.e. the process from the raw data to the intensity map ready to be analysed, will be shown using an example of ATCA observations. I use the software package called MIRIAD (Sault et al., 1995; Sault & Killeen, 2004).

In order to speed-up typing the commands I usually define the following variables containing the names of the file with raw data, target source, primary and secondary calibrators as well as frequencies used, for example:

```
uvfilename=2008-01-27_0550.C1741
target=grb050915a
primary=1934-638
secondary=0451-282
freq1=1344
freq2=1432
```

The following description of the reduction steps is mostly based on the Miriad User's Guide (Sault & Killeen, 2004) unless stated otherwise. The entire reduction script is listed in Appendix B.

2.3.1 DATA PREPARATION

The raw ATCA data are written in the RPFITS format[4] and need to be converted into the MIRIAD file format by the task `atlot`:

```
task atlod
in=$uvfilename
out=$uvfilename.uv
options=birdie,xycorr,noauto
go
```

The `birdie` option ensures that the ATCA channels affected by self-interference at frequencies, which are a multiple of 128 MHz are flagged out. In order to correct for the phase difference between the polarization X and Y channels the option `xycorr` is set. The option `noauto` cause that autocorrelation data are discarded.

The output MIRIAD file (`$uvfilename.uv`) contains all the data for a particular run. In order to handle them it is necessary to split the data corresponding to individual objects (target source, primary and secondary calibrators). Moreover, if observations were performed at two different frequencies, they need to be treated separately, so the corresponding data should also be split according to frequency into two separate files. All these is done by the task `uvsplit`:

```
task uvsplit
vis= $uvfilename.uv
unset options
go
```

[4] `www.atnf.csiro.au/computing/software/rpfits.html`

The command `unset options` clears the entry for `options`, which is remembered from the last task.

The last step of the data preparation is to check how much time was spent on a target source using the task `uvindex`:

```
task uvindex
vis = $target.$freq1
unset interval
unset log
unset options
```

As an output a summary of the observations is given, e.g. number of antennas and spectral channels. Additionally the following line is given: `Total observing time is 8.64 hours`. This number does not include the time spent on calibrators or slewing.

2.3.2 Flagging bad data

Radio observations are often affected by interferences, namely strong transient signals not originating in astronomical sources. In most cases they are human-made signals from e.g. satellites, broadcast stations, mobile phones, or even microwave ovens. These must be removed before analysing the data. This step is the most time-consuming, because all interferences have to be identified and removed by hand (at least in the current implementation of MIRIAD). Moreover all datasets, i.e. for a target source, primary and secondary calibrators as well as for each frequency band have to be flagged separately.

I applied the following modes of flagging:

Flagging data in the whole periods was applied when an interference was clearly visible over extended period (i.e. amplitude rises to an extremely high level). First, task `uvplt` was used to plot the amplitudes as a function of time to localize interferences:

```
task uvplt
vis = $target.$freq1
unset line
unset select
stokes = i
axis = time,amp
options = 2pass,nofqav
device = /xs
nxy = 1
go
```

The parameter `axis` is set so that amplitude of the signal is shown as a function of time. I chose to show only `stokes` I parameters for better visibility of the data. The `options` are set, so that MIRIAD makes two passes through the data (`2pass`), first to estimate how big buffer is needed and the second to plot the data. The `nofqav` disables frequency-averaging of the data. Only one plot per page is required (`nxy=1`) and the output device is a terminal window (`/xs`).

Then I zoomed in to better localize an interference:

```
select=time(10:15:00,10:45:00)
go
```

Finally I flagged the chosen period:

```
task uvflag
vis= $target.$freq1
flagval=flag
options=brief
select=time(6:00:00,7:45:00),ant(1)(2)
go
```

In this example only the data corresponding to the baseline 1–2 are removed, because other baselines are unaffected.

Flagging data at individual channels was used in order to check whether the interference occurs at very narrow frequency range i.e. only at a few channels. Hence all the channels were examined individually:

```
task blflag
vis=$target.$freq1
unset options
axis =time,amp
stokes=ii
unset select
line=channel,1,1,1,1
go
line=channel,1,2,1,1
go
...
line=channel,1,13,1,1
go
```

The task `blflag` allows interactive removal of outlying datapoints.

Flagging averaged data was used mainly for a primary calibrator, which is usually very bright, so the data is of high quality and inspection of channel-averaged data is sufficient:

```
task blflag
vis=$primary.$freq1
unset options
axis =time,amp
unset line
go
vis=$primary.$freq2
go
```

In such setup if a datapoint is marked, then the corresponding data in all channels are flagged. The data at both frequency bands are flagged separately.

2.3.3 CALIBRATION

The first step of the calibration is to correct the data for the fact that each antenna reacts slightly differently on the incoming radiation. Namely, antenna gains (amplitude response), delay terms

(phase response) and passband shapes (frequency response) are calculated based on the data obtained for calibrators. As mentioned in Section 2.2, a calibrator is a bright point-source of known flux. Therefore it is possible to estimate how a radio array should respond when pointed at this object. The difference between the expected and observed signals allows to work out the calibration corrections. This is done by the task `mfcal`:

```
task mfcal
vis=$primary.$freq1
refant=4
unset stokes
interval =0.1
unset options
go
vis=$primary.$freq2
go
vis=$secondary.$freq1
go
vis=$secondary.$freq2
go
```

As a reference antenna (`refant`) one should use the one, which is close to the middle of an array and did not cause any obvious problem during the run. The keyword `interval` sets the maximum time interval between the calibration solutions.

The next step is to determine a polarization leakage, i.e. artificial impurities causing instrumental polarization. This means that an unpolarized source would appear slightly polarized if the polarization leakage is not removed[5] . This is done by the task `gpcal`:

```
task gpcal
vis=$primary.$freq1
options=xyvary
go
vis=$primary.$freq2
go
options=xyvary,qusolve
vis=$secondary.$freq1
go
vis=$secondary.$freq2
go
```

The option `xyvary` means that the polarization leakage is allowed to vary with time, which gives more accurate correction. A secondary calibrator is usually observed much more frequently than the primary, so it is also possible to compute corrections in the Q and U polarisation. Hence for the secondary `options=xyvary,qusolve` is used.

The absolute value of the flux (e.g. in Jy) of a primary calibrator is known with a high accuracy. This information is used to set the absolute scales for a secondary calibrator and a target source (similar concept as standard stars in optical observations). Namely, it is assumed that the gains (the ratio between correct and measured fluxes) should be the same for primary and

[5] `www.aoc.nrao.edu/~gtaylor/calman/polcal.html`

secondary calibrators. Hence if the gains determined by the task `mfcal` for primary and secondary calibrators differ, then the gain of a primary calibrator is assumed to be correct, and the gain of a secondary calibrator is scaled to match that of a primary, setting the absolute flux scale. This is done by the task `gpboot`:

```
task gpboot
vis=$secondary.$freq1
cal=$primary.$freq1
go
vis=$secondary.$freq2
cal=$primary.$freq2
go
```

Finally, all the calibration information obtained above should be copied to a target source:

```
task gpcopy
vis=$secondary.$freq1
out=$target.$freq1
unset options
go
vis=$secondary.$freq2
out=$target.$freq2
go
```

2.3.4 IMAGING

I performed imaging using the script `robust-weighting_imaging.pl` written by Robert Reinfrank (version November 2006) listed in Appendix B. In the following I explain how it works.

As mentioned in Section 2.2 interferometric data are recorded in forms of visibilities, i.e. amplitude vs. phase for each baseline on the so-called uv-plane. In order to obtain an image corresponding to the brightness distribution on the sky, the inverse fourier transform have to be performed by the task `invert`:

```
task invert
vis= grb050915a.1344,grb050915a.1432,
     ../a/grb050915a.1344,../a/grb050915a.1432
map=tmp_Imaging.imap,tmp_Imaging.qmap,tmp_Imaging.umap,tmp_Imaging.vmap
beam=tmp_Imaging.beam
imsize=1000,1000
cell=2.0
unset sup
unset robust
unset select
stokes=i,q,u,v
options=mfs,double
```

All the data from different runs as well as different frequency bands (if they are supposed to be averaged) should be inverted simultaneously, as given in the `vis` keyword. The file names of

the maps at all polarisations and the beam are given by the `map` and `beam` keywords, respectively. The size of the map (in pixels) is given by `imsize` and size of one pixel (in arcsec) by `cell`. Empty entry for the keyword `sup` restores the default of sidelobe suppression area equal to the whole image. Empty `robust` keyword gives uniform weighting as opposed to natural weighting giving higher sidelobes (but may result in smaller noise). The keyword `select` is also empty to use all the available data, but it is possible to restrict the fourier transform to some part of the data, e.g. `select = -ant(6)` removes the longest baselines (connected with antenna no. 6). All `stokes` parameters are usually used. Since the observations are in the continuum mode, all the frequency channels should be used in forming a single map, so multi-frequency synthesis (`mfs`) is used. In order to increase the accuracy of subsequent cleaning (see below), the beam pattern is set to be twice as large as the original image (`double`).

The image created in this step is usually referred to as a dirty image (and corresponding beam — dirty beam), because its quality is hampered by the finite sampling on the uv-plane (finite number of antennas). In order to reconstruct the real brightness distribution, the signal is assumed to be a superposition of point-like sources, which are iteratively removed from the map using the shape of the dirty beam (see Section 2.2). In this way it is possible to restore the positions and amplitudes of all the point sources, that are above the noise in the dirty map. This is done by the task `clean`:

```
task clean
map=tmp_Imaging.imap
beam=tmp_Imaging.beam
out=tmp_Imaging.iclean
niters=50000
region=abspix,box(1,1,1000,1000)
```

Number of iteration (`niters`) should be large enough so that all sources are properly cleaned. In order to clean the entire image the `region` have to contain the coordinates of the bottom-left (`1,1`) and top-right (`1000,1000`) pixels.

Finally a clean image can be produced using information about the point sources from the previous step and the dirty beam . Namely, signal from each source is convolved with the dirty beam, subtracted from the dirty map (it leaves map with noise structure only) then convolved with a gaussian (clean beam) and added to the map. This is done by the task `restor`:

```
task restor
model=tmp_Imaging.iclean
beam=tmp_Imaging.beam
map=tmp_Imaging.imap
out=image.irestor
```

The resulting clean map `image.irestor` is ready to be analysed.

2.3.5 Data analysis

To view the image one can use the task `cgdisp`:

```
task cgdisp
in = image.irestor
type = contour
region = arcsec,box(-400,-400,400,400)
```

```
slev = p,1
levs1 = -5,1,2,3,4,5,6,7,8,9,10,20,30,40,50,60,70,80
device = /xs
nxy = 1
labtyp = hms,dms
beamtyp = b,l
olay = $target.olay
```

In this example the central 400×400 arcsec (`region`) are shown as contours (`type`) with percentage levels (as oppose to absolute levels for which `slev=a` should be set) given in `levs1` keyword. One panel per plot (`nxy=1`) is shown in a terminal window (as oppose to a postscript file for which `device=file.ps/ps` should be set) with axes labelled with right ascension and declination (`labtyp=hms,dms`). The beam is shown in the bottom-left corner of the plot (`beamtyp=b,l`) and the symbol to overplot (e.g. a circle at the expected coordinates of the source) is read from a file (`olay`).

In order to perform the photometry one have to determine the position(s) and amplitude(s) of the peak(s) close to the expected target position as well as the pixel coordinates of the box in which fitting is going to be performed. This is done by the `cgcurs` task, which allows to click on the desired position to get coordinates of the pixel and its intensity:

```
task cgcurs
in = image.irestor
type = contour
region = arcsec,box(-100,-150,150,40)
slev = p,1
levs = -5,1,2,3,4,5,6,7,8,9,10,20,30,40,50,60,70,80
device = /xs
nxy = 1
labtyp = hms,dms
options = cursor
```

Both steps above can also be done in the `kvis` tool within KARMA package[6] (Gooch, 1996). This is a window-based tool allowing to view and analyse an image much easier and faster than in MIRIAD.

Once the position(s) of the peak(s) corresponding to a target are determined it is possible to measure its flux by fitting a 2-dimensional gaussian function. This is done by the task `imfit`:

```
task: imfit
in = image.irestor
region = arcsec,box(-100,-150,150,40)
object = gaussian,gaussian
spar = 3.5657E-04,3.11009778E+01,-1.66885578E+01,10,5,80,
       4.2465E-04,1.94225856E+01,-6.46589538E+01,10,5,80
out = model.im
go
```

In this example two gaussian functions (`object`) are fitted to a section of the image (`region`). Initial parameters for the fit are given in the keyword `spar` (amplitude, x and y position of

[6] `wwwatnf.atnf.csiro.au/computing/software/karma/`

the peak, major and minor axes FWHM and position angle for both gaussians). The image containing the resulting model is stored in the file determined by the `out` keyword.

As an output `imfit` gives `Total integrated flux`, which is a reasonable estimate of the flux of a target.

In order to check the accuracy of the fitting above it is advisable to *i*) overplot the model map on top of the original map to check wether the model represents reasonable the original map; and *ii*) overplot the residuals on top of the original map to check wether all the emission of a target was accurately subtracted. Both steps can be easily done in `kvis`, which allows loading several images and displaying one of them as contours on top of the other. Residual image is created also in `imfit` by changing the following keywords:

```
out = residual.im
options = residual
go
```

The final step of the data analysis is error estimation. This is done by measuring the RMS in the region close to a target, which does not contain other sources. The pixel coordinates of such region can be found either by the `cgcurs` task or in `kvis` (see above). Then the calculation is done by the task `imstat`:

```
task imstat
in = image.irestor
region = box(452.43,473.83,480.52,522.53)
plot = rms
axes = RA,DEC
device = /xs
```

As the output the rms is given.

As an additional check of the error value, the rms can also be calculated from the residual image on the position of the subtracted source:

```
task imstat
in = residual.im
region = box(494,532,506,547)
plot = rms
axes = RA,DEC
device = /xs
go
```

2.4 RADIO SURVEY OF GRB HOSTS

In the following I describe the ongoing observational program concentrated on GRB hosts and show the preliminary results. We have obtained radio data for 22 GRB hosts with the aim to constrain their SFR.

2.4.1 SAMPLE

Our target sample is composed of two subsets. The first includes GRBs that were spectroscopically or photometrically confirmed to be associated with SNe, namely the sample of Ferrero et al. (2006) plus GRB 980425 / SN 1998bw (Galama et al., 1998). We targeted GRB-SN hosts

because their progenitors are securely established to be connected with recent star formation. Since the detection of a SN component in a fading GRB afterglow is difficult at high redshift, this selection imposes a practical limit of $z \lesssim 1$. In total 15 hosts were selected of which 8 were observed and for the remaining 7 the deep upper limits from the literature were used.

The second subset is drawn from the 'unbiased' GRB sample based on the *Swift* satellite and the Very Large Telescope (VLT) Large Program (Jakobsson et al., 2006b, 2009; Fynbo et al., 2009) with a restriction of $z < 1$ to obtain meaningful radio constraints on SFRs (GRB 060814 at $z = 1.338$ is also in our target sample, because initially redshift of 0.84 was reported by Thöne et al., 2007b). The *Swift*/VLT sample is constructed in a way that it is not biased against dusty systems and the selection does not depend on the host luminosity. Redshift was measured for $\sim 60\%$ of *Swift*/VLT GRBs and the completeness is even higher at $z < 1$, because many GRBs without redshifts are confirmed to be at $z > 1$ and therefore would not enter our target sample even if the redshift was known. The 'unbiased' subset consists of 16 hosts (with an overlap of 2 hosts with the 'GRB-SN' subset) of which all were observed.

2.4.2 Data Reduction and Analysis

The radio data were collected using Australian Telescope Compact Array (ATCA) in 6A configuration (H168 for GRB 980425), Giant Metrewave Radio Telescope (GMRT), Very Large Array (VLA) in A configuration and Westerbork Synthesis Radio Telescope (WSRT) in maxi-short configuration. The log of observations is presented in Table 2.1.

Data reduction and analysis was done using the MIRIAD package (Sault & Killeen, 2004) as described in Section 2.3. Calibrated visibilities were Fourier transformed using 'robust' or 'uniform' weighting depending on which gives a better result for a particular field. The resulting rms noise, beam sizes and calibrators for targets, for which the data has been already analysed, are shown in Table 2.1.

Fluxes were measured by fitting 2-D Gaussian functions to the region around the host and the error was determined from the rms on the images. The hosts of GRBs 980425 and 031203 slightly overlap with radio objects $\sim 70''$ south (see Michałowski et al., 2009a) and $\sim 6''$ northwest, respectively, so their flux densities were estimated by simultaneous fitting of two Gaussian functions with their centroids, sizes and orientations as free parameters. The lack of residuals left after the subtraction of these two Gaussians rules out a significant contamination of the nearby objects to the measured flux of the hosts.

2.4.3 Results

The results of our photometry for analysed targets with addition of the results found in the literature are presented in Table 2.2. The SFRs were calculated from the empirical formula of Bell (2003) (see Section 4.2 of Michałowski et al., 2009a, for discussion of its applicability to GRB hosts).

Already with the presented sample it is evident that the highly star-forming galaxies (SFR $> 100\,M_\odot$) are very rare among the GRB hosts at $z < 1$. The larger sample will enable detailed study.

In order to test whether radio emission is a reliable tracer of SFR we compare SFRs of SMGs based on radio and IR emission (derived in Chapter 6). As shown in Figure 2.6, SFRs derived from these two indicators agree reasonably well, except of a few outliers, likely dominated by AGNs. As given in Chapter 6, median value of $\mathrm{SFR_{radio}}$ is $\sim 30\%$ higher than $\mathrm{SFR_{IR}}$, so this number should be regarded as systematic uncertainty of SFR based on radio emission.

Table 2.1: *Observation log*

GRB	Array	Obs. Dates	t^{a} (h)	Rms (μJy beam^{-1})	Beam size ($''$)	Calibrators[b] (PKS B)
980425 [c,d]	ATCA	18 Aug 2007	9.00	46, 27	76×38, 37×21	1934-638
991208	WSRT	2-3 Aug 2007	12			
020903	GMRT	18-19 Jan 2008	12			
021211	VLA	14 Jul 2007	6			
031203 [d]	ATCA	26 Jan 2008	6.97	46, 37	8.5×3.4, 6.3×2.3	1934-638, 0826-373
041006	GMRT	7-8 Aug 2007	12			
050416A	WSRT	27-28 Apr 2008	12			
050525A	WSRT	13-14 Aug 2007	12			
050824	WSRT	26-27 Dec 2007	12			
050915A	ATCA	25,27 Jan 2008	15.62	29	18.3×5.5	1934-638, 0451-282
051016B	WSRT	28-29 Dec 2007	12			
051117B	ATCA	12 August 2009	12			
060218	WSRT	16-17 Aug 2007	11.57			3c48
060505	GMRT	20-21 Jan 2008	12			
	ATCA	10-11 August 2009	12			
060614	ATCA	9-10 August 2009	13			
060729	ATCA	26,28 Jan 2008	11.36	35	7.4×6.4	1934-638, 0515-674
060814	WSRT	30 Dec 2007	12			
060912A	GMRT	1-2 June 2009	10			
061021	ATCA	18 Apr 2008	7.90	36	20.0×4.8	1934-638, 0919-260
061110A	WSRT	29 Dec 2007	12			
070318	ATCA	19 Apr 2008	9.74	47	7.2×4.2	1934-638, 0405-385
070808	GMRT	2-3 June 2009	10			

[a] Total integration time on-source.

[b] The first object was used as a primary and second as a secondary calibrator.

[c] The data published in Michałowski et al. (2009a).

[d] This object was observed simultaneously at two frequencies, see Table 2.2

Note. — The horizontal line divides the 'GRB-SN' and 'unbiased' subsets (see Section 2.4.1). GRBs 050525A and 060218 belong to both subsets.

Acknowledgements

M. J. M. would like to acknowledge support from The Faculty of Science, University of Copenhagen. The Dark Cosmology Centre is funded by the Danish National Research Foundation. The Australia Telescope Compact Array is part of the Australia Telescope which is funded by the Commonwealth of Australia for operation as a National Facility managed by CSIRO. We thank the staff of the GMRT who have made these observations possible. GMRT is run by the National Centre for Radio Astrophysics of the Tata Institute of Fundamental Research. The National Radio Astronomy Observatory is a facility of the National Science Foundation operated under cooperative agreement by Associated Universities, Inc. The Westerbork Synthesis Radio Telescope is operated by the ASTRON (Netherlands Foundation for Research in Astronomy) with support from the Netherlands Foundation for Scientific Research NWO.

Facilities: ATCA, GMRT, VLA and WSRT.

Table 2.2: *Radio fluxes and star formation rates*

GRB	z	Ref	Flux (μJy)	Frequency (GHz)	Ref	SFR [a] ($M_\odot$ yr^{-1})
970228	0.6950	1	< 69	1.43	15	<72.35
980425	0.0085	2	420 ± 50	4.80	16	0.23 ± 0.02
980425	0.0085	2	< 180	8.64	16	<0.17
990712	0.4337	3; 4	< 105	1.39	17	< 36.02
000911	1.0580	5	< 57	8.46	18	<608.06
010921	0.4510	6	< 83	1.43	15	<31.83
011121	0.3600	7	< 120	4.80	15	<68.11
020405	0.6910	8	< 42	8.46	19	<164.82
030329	0.1680	9	< 420	1.40	20	<17.41
031203	0.1050	10	254 ± 46	1.39	‡	3.83 ± 0.69
031203	0.1050	10	191 ± 37	2.37	‡	4.29 ± 0.83
050915A	0.4440		333 ± 29	1.39	‡	120.58 ± 10.50
060729	0.5400	12	< 105	1.39	‡	<59.80
061021	0.3463	13	< 108	1.39	‡	<22.15
070318	0.8360	14	< 141	1.39	‡	<223.27

[a] Assuming radio spectral index $\alpha = -0.75$ and applying the calibration of Bell (2003).

Note. — References: ‡: This work, 1: Bloom et al. (2001), 2: Tinney et al. (1998), 3: Galama et al. (1999), 4: Hjorth et al. (2000), 5: Price et al. (2002a), 6: Price et al. (2002b), 7: Infante et al. (2001), 8: Price et al. (2003), 9: Hjorth et al. (2003b), 10: Prochaska et al. (2004), 12: Thöne et al. (2006), 13: Fynbo et al. (2009), 14: Jaunsen et al. (2007), 15: Frail et al. (2003), 16: Michałowski et al. (2009a), 17: Vreeswijk et al. (2001a), 18: Berger et al. (2003a), 19: Berger et al. (2003b), 20: van der Horst et al. (2005),

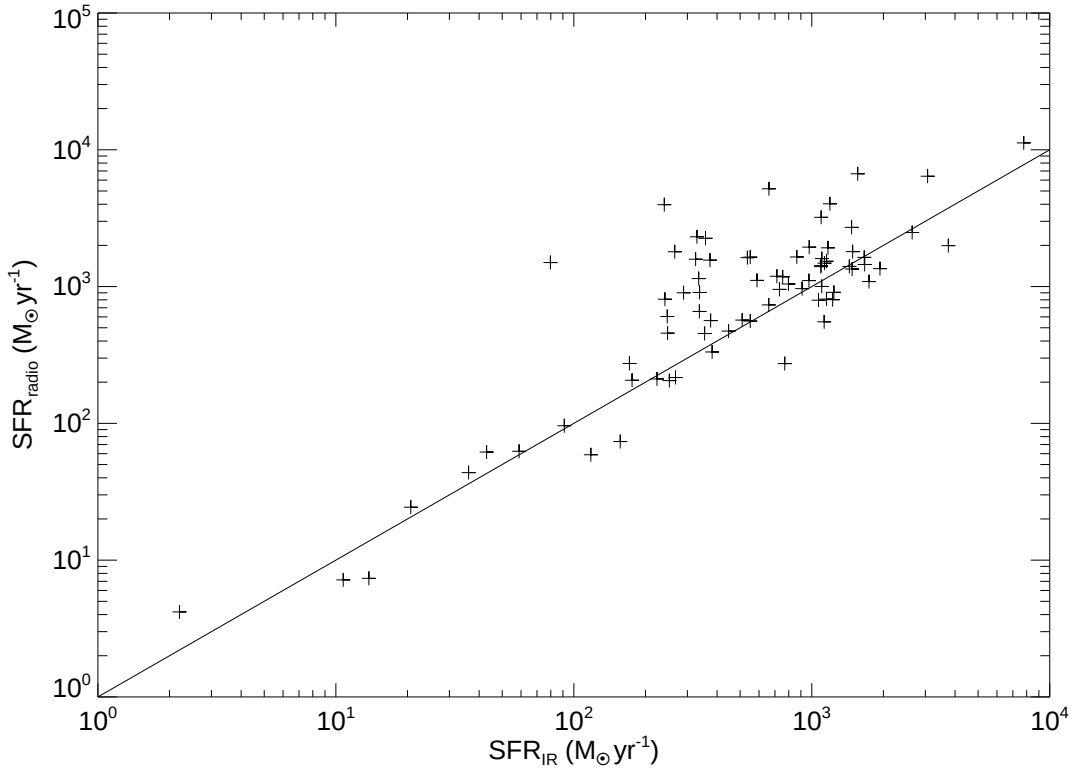

Figure 2.6: *Comparison of SFRs derived from radio and IR emission based on SMG data (Chapter 6). Solid lines indicates where* $SFR_{\rm radio} = SFR_{\rm IR}$.

3

SPECTRAL ENERGY DISTRIBUTION MODELING

A significant fraction of the results presented in this thesis (Chapters 4–7) is based on spectral energy distribution (SED) modeling using all available photometric data simultaneously for a given galaxy. This has the advantage that all the galaxy properties are derived consistently regardless of the wavelength regime in which those properties shape the SEDs (for example, recent star formation governs the UV and far-IR parts of a spectrum of a galaxy, whereas accumulated stellar mass is responsible for near-IR emission). Moreover, in the full SED modeling no single datapoint will drive the fit.

3.1 GRASIL PRINCIPLES

I used the GRASIL[1] software developed by Silva et al. (1998). It is a numerical code that calculates the spectrum of a galaxy by means of a radiative transfer method, applied to photons produced by a stellar population, and reprocessed by dust. The advantage of this code is that it produces self-consistent results. It obeys the principle of energy conservation between the energy absorbed by dust in the UV/optical wavelengths and the energy re-emitted in the infrared. Photons are influenced by dust, mostly for $\lambda \lesssim 1\,\mu$m (Silva et al., 1998) and the absorption is, on average, stronger for shorter wavelengths (e.g. Cardelli et al., 1989). However the density in molecular clouds (MCs) is so high that even IR photons are absorbed. Approximately 30% of the starlight is reprocessed by dust. This effect is especially important in galaxies with high star formation because of their high dust content.

3.2 STELLAR POPULATION

The first step implemented by Silva et al. (1998) involves calculation of the chemical evolution of a galaxy following the work of Tantalo et al. (1996). A galaxy is assumed to be an open system with gas infall and galactic winds taken into account. The star formation history is user-defined. Usually a smooth, Schmidt-type, law is adopted, where SFR is non-linearly proportional to the gas mass. In addition, a starburst episode can be included with a user-defined duration and strength (Figure 3.1). The program calculates the number and spectral types of stars at any given time of the galaxy's evolution.

The UV/optical/near-IR emission of stars present in a galaxy is summed up from the grid

[1] http://adlibitum.oat.ts.astro.it/silva/default.html

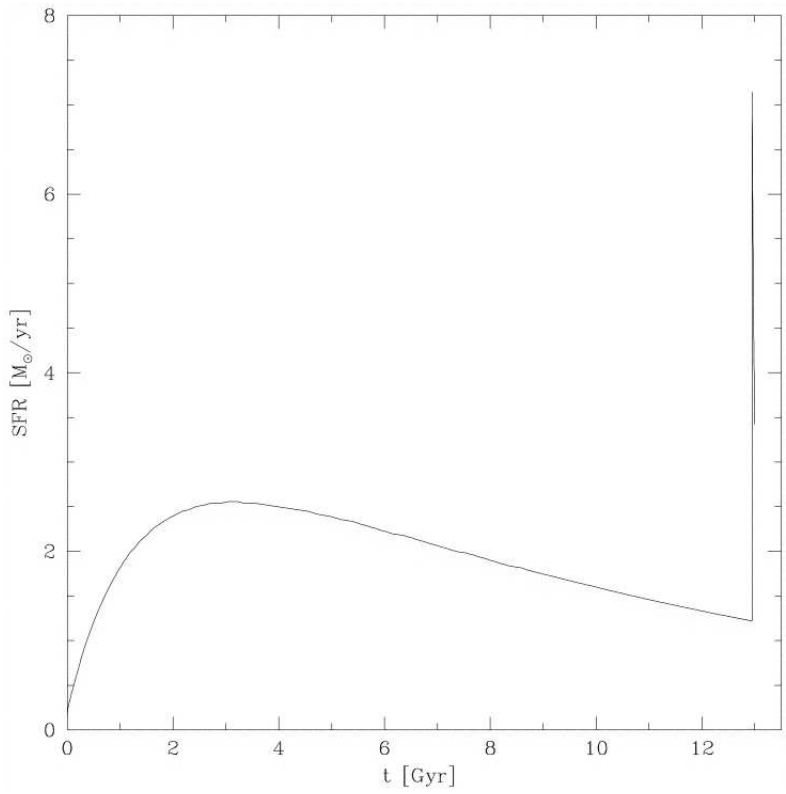

Figure 3.1: *Example of star formation history of a galaxy in GRASIL (Silva et al., 1998). Smooth evolution of SFR is followed by a starburst episode.*

of simple stellar populations (SSPs). An SSP is a group of stars born at the same time and place, sharing the same age and metallicity, and with a particular type of initial mass function (IMF). The Salpeter (1955) IMF is assumed with $M_{\rm min} = 0.15 M_\odot$ and $M_{\rm max} = 120 M_\odot$. The evolution of each star depends on its mass and metallicity and is tracked by evolutionary models. SSPs are taken from stellar spectral libraries developed by Bertelli et al. (1994). They include stars with ages from 1 Myr to 20 Gyrs and metallicities $Z = 0.004$, 0.008, $0.02 (= Z_\odot)$, 0.05, 0.1. In the calculation of stellar SEDs the effects of dusty envelopes around AGB stars are taken into account.

3.3 GEOMETRY

A galaxy is assumed to be an axially symmetric system. Free gas not incorporated into stars and dust are distributed throughout a galaxy in two forms: as a diffuse medium and inside star-forming MCs, as shown in Figure 3.2. New stars are born in MCs and then gradually escape their parent cloud. Hence the fraction f of SSP energy produced inside MCs at time t is:

$$f = \begin{cases} 1 & \text{if } t \leq t_0 \\ 2 - t/t_0 & \text{if } t_0 < t \leq 2t_0 \\ 0 & \text{if } t > 2t_0, \end{cases} \tag{3.1}$$

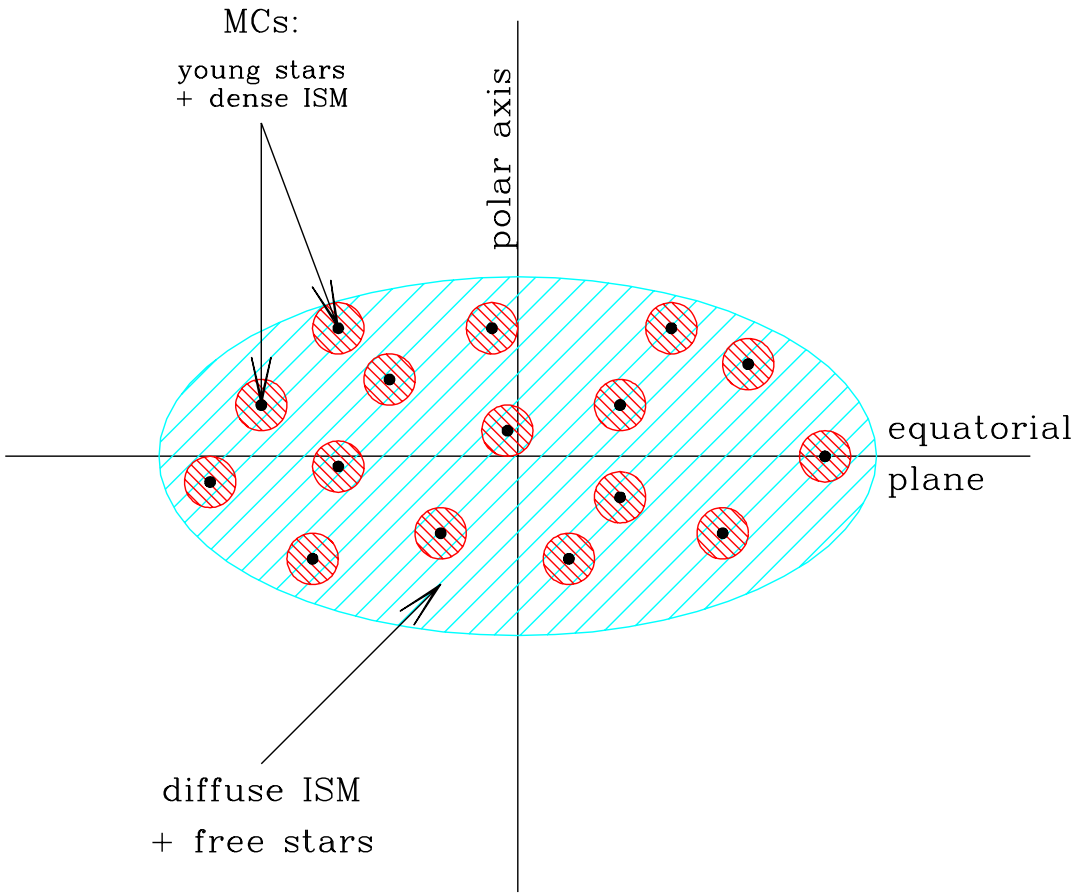

Figure 3.2: *The distribution of stars and gas in the model of Silva et al. (1998).*

where t_0 is the model parameter indicating the time, after the onset of star formation, when the first stars escape from MCs. The first epoch of star-forming activity is almost totally obscured in optical wavelengths because stars are formed in dense MCs.

3.4 Dust and radiative transfer

The starlight computed as above is attenuated by dust by means of radiative transfer. First, the fraction of light given by equation (3.1) is extinguished by dust in MCs. Then all the remaining emission plus the emission from free stars is extinguished by the diffuse medium. During this process, the IR emission is calculated so that its energy is equal to the absorbed energy.

The model includes the following dust grains: big grains, small grains, and polycyclic aromatic hydrocarbon (PAH) molecules. Dust grains vary in size between 8 Å and $2\,500$ Å following a broken power-law distribution with an index of -3.5 for sizes above 50 Å and -4.0 for smaller grains. Grains bigger than 100 Å are assumed to be in thermal equilibrium with the radiating field, emitting a gray body spectrum, whereas smaller grains fluctuate in temperature. The photon absorption cross-section of PAHs depends on the wavelength. PAHs are responsible for emission/absorption features at 3.3, 6.2, 7.7, 8.6 and 11.3 μm.

3.5 DERIVATION OF GALAXY PROPERTIES

In Chapters 5–7 (but not in Chapter 4) I utilized the set of 35 000 GRASIL models from Iglesias-Páramo et al. (2007). They cover a broad range of galaxy properties from quiescent to starburst. In this way instead of fitting for the best parameters directly in GRASIL I fitted all the templates to the data and choose the one with the best χ^2.

Once the SED is chosen I extract the SFR, stellar and starburst masses as a function of time from the GRASIL output. Extinction in the MCs is given by the radiative transfer routine. Infrared luminosity is obtained by integrating the SED over the range of $8 - 1000\,\mu$m and rest-frame K-band luminosity is interpolated from the model. Dust temperature is estimated by fitting a grey-body curve to the part of the SED near the dust peak ($\sim 100\,\mu$m, e.g. Yun & Carilli, 2002). Finally, the average extinction outside MCs can be calculated as: $A_V = 2.5\log(V\text{-band starlight extinguished by MCs only} \;/\; V\text{-band starlight observed})$; see Silva et al. (1998).

Published as: Michałowski, M. J., Hjorth, J., Castro Cerón, J. M., & Watson, D. – *The nature of GRB-selected submillimeter galaxies: hot and young* Astrophysical Journal, vol. 672, pp. 817–824, Januar 2008.

4

THE NATURE OF GRB-SELECTED SUBMILLIMETER GALAXIES: HOT AND YOUNG

ABSTRACT –

We present detailed fits of the spectral energy distributions (SEDs) of four submillimeter (submm) galaxies selected by the presence of a gamma-ray burst (GRB) event (GRBs 980703, 000210, 000418 and 010222). These faint ~ 3 mJy submm emitters at redshift ~ 1 are characterized by an unusual combination of long- and short-wavelength properties, namely enhanced submm and/or radio emission combined with optical faintness and blue colors. We exclude an active galactic nucleus as the source of long-wavelength emission. From the SED fits we conclude that the four galaxies are young (ages < 2 Gyr), highly starforming (star formation rates $\sim 150\,\mathrm{M}_\odot\ yr^{-1}$), low-mass (stellar masses $\sim 10^{10}\,\mathrm{M}_\odot$) and dusty (dust masses $\sim 3 \times 10^8\,\mathrm{M}_\odot$). Their high dust temperatures ($T_d \gtrsim 45$ K) indicate that GRB host galaxies are hotter, younger, and less massive counterparts to submm-selected galaxies detected so far. Future facilities like Herschel, JCMT/SCUBA-2 and ALMA will test this hypothesis enabling measurement of dust temperatures of fainter GRB-selected galaxies.

4.1 INTRODUCTION

It has been claimed that submillimeter (submm) galaxies (SMGs, see Blain et al., 2002, for a review) are significant contributors to the star formation history of the Universe at redshifts $z \sim 2{-}3$ (Chapman et al., 2005) and have built up a substantial fraction of the present-day stellar population (Lilly et al., 1999). SMGs are luminous (with infrared luminosities $L_{\rm IR} \sim 10^{12-14}\,L_\odot$) and cold (with mean dust temperature $T_d = 36 \pm 7$ K, Chapman et al., 2005). Galaxies with similar luminosities but with higher dust temperatures ($T_d > 45$ K) are difficult to detect in the submm with current technology due to the fact that the peak of the infrared dust emission is shifted out of the sensitive $850\,\mu$m band towards shorter wavelengths (Blain et al., 2004; Chapman et al., 2004a, 2005) in such galaxies.

At the other end of the galaxy luminosity function, the host galaxies of long-duration gamma-ray bursts (GRBs, originating in the collapses of very massive stars at the end of their evolution, e.g. Stanek et al., 2003; Hjorth et al., 2003b) do not have much in common with SMGs except for the fact that this type of galaxies is also thought to contribute significantly to, or at least trace, the global star formation (e.g. Jakobsson et al., 2005, 2006c). In contrast to SMGs, GRB hosts are found to be blue, subluminous in the optical (Le Floc'h et al., 2003; Fruchter et al., 2006) and metal-poor (Fynbo et al., 2003). The majority of them have not been detected at mid-infrared

(MIR), submm or radio wavelengths (Hanlon et al., 2000; Le Floc'h et al., 2006; Tanvir et al., 2004; Berger et al., 2003a; Priddey et al., 2006) indicating that, as a class, they are not heavily obscured or violently star forming galaxies. A low internal dust content is consistent with low extinction found in the analysis of optical afterglows (Stratta et al., 2004; Chen et al., 2006; Kann et al., 2006) and optical spectral energy distributions (SEDs) of the host galaxies (Christensen et al., 2004).

However, four GRB hosts (980703, 000210, 000418 and 010222) have been firmly detected in submm and/or radio (Tanvir et al., 2004; Berger et al., 2001b, 2003a) providing a somewhat complex picture: assuming that this emission is powered by starbursts, the derived star formation rates (SFRs) are of the order of a few hundred solar masses per year and the amount of dust in these galaxies is significant. On the other hand, they exhibit blue colors, low extinction and low extinction-corrected optical/UV SFRs (Djorgovski et al., 1998; Holland et al., 2001; Sokolov et al., 2001; Chary et al., 2002; Gorosabel et al., 2003a,b; Galama et al., 2003; Berger et al., 2003a; Savaglio et al., 2003; Christensen et al., 2004; Chen et al., 2006; Kann et al., 2006), like the majority of known GRB hosts. This puzzling situation was highlighted by Berger et al. (2003a, their Figure 3) — these GRB hosts are much fainter in the optical than the prototypical Ultra Luminous Infrared Galaxy (ULIRG) Arp 220 and have much bluer spectra, but are more luminous in submm and radio. In fact, no template SED model (e.g. Silva et al., 1998; Dale et al., 2001; Dale & Helou, 2002) could give consistency with the data (see also Michałowski & Hjorth, 2007; Michałowski, 2006). Moreover, none of these hosts have been detected at $24\ \mu$m (Le Floc'h et al., 2006; Castro Cerón et al., 2006, Le Floc'h, private communication).

The location of the GRB events within their hosts adds further complexity to this picture. As found by Fruchter et al. (2006), GRBs trace the location of the brightest rest-UV parts of their hosts (see also Bloom et al., 2002). If the majority of the star formation in the hosts of GRBs 980703, 000210, 000418 and 010222 was hidden by dust, then they should preferentially be found in obscured (UV-dim) parts of their hosts (as long as GRBs trace star formation), contrary to observations.

In this chapter we investigate this seeming discrepancy between short- and long-wavelength data through stellar population model SED fitting. In particular we discuss the possibility that these submm-bright GRB hosts may represent the long-sought hotter (and less luminous) counterparts of SMGs. In Section 4.2 we describe the model and the fitting procedure, in Section 4.3 we show the results, discuss their implication in Section 4.4, and finally in Section 4.5 conclude this work. We use a cosmological model with $H_0 = 70$ km s^{-1} Mpc^{-1}, $\Omega_\Lambda = 0.7$ and $\Omega_M = 0.3$.

4.2 GRASIL SED Modeling

In order to model the SEDs of GRB hosts we used the GRASIL[1] software developed by Silva et al. (1998). It is a numerical code that calculates the spectrum of a galaxy by means of a two-dimensional radiative transfer method, applied to photons produced by a stellar population, and reprocessed by dust. This model is self-consistent in that it fulfills the principle of energy conservation between the energy absorbed by dust in the UV/optical wavelengths and the energy re-emitted in the infrared. Two extinction media are implemented, dense star forming molecular clouds (MCs, applied only to the youngest stellar population) and diffuse cirrus. The dust is composed of small grains (not in thermal equilibrium with radiation and hence fluctuating in temperature), big grains (silicates and graphites) and polycyclic aromatic hydrocarbon (PAH) molecules. The emission of grains with given size is assumed to be a grey-body, so the

[1] http://web.pd.astro.it/granato/grasil/grasil.html

composite spectrum is a sum of all grey-bodies with different temperatures. A galaxy is assumed to be an axially symmetric system. Different geometries of the stellar and diffuse dust distributions are allowed but were not used here. The SFR is assumed to be proportional to the available gas content following the Schmidt-law. On top of this smooth SFR history a violent starburst epoch is added. Star formation is unevenly distributed throughout the galaxy in MCs. The SFR given as a GRASIL output is the sum of the SFRs of each MC.

We gathered photometric data from the literature at optical (Sokolov et al., 2001; Vreeswijk et al., 1999; Gorosabel et al., 2003a,b; Galama et al., 2003), infrared (Castro Cerón et al., 2006; Le Floc'h et al., 2006), submm (Tanvir et al., 2004; Berger et al., 2003a) and radio (Berger et al., 2001b, 2003a; Frail et al., 2002; Sagar et al., 2001) wavelengths. For the host of GRB 000210 we performed the photometry on the archival *Spitzer* images (see Castro Cerón et al., 2006, 2009, for a decription of the procedure) and obtained the following fluxes: at $4.5\,\mu$m: $3.3 \pm 2.1\,\mu$Jy; at $8.0\,\mu$m: $15.0 \pm 5.1\,\mu$Jy and at $24\,\mu$m: $< 31.5\,\mu$Jy (3σ).

We performed SED modeling investigating a wide range of the following GRASIL parameters: age of the galaxy (defined as the time since the beginning of its evolution when the stellar population started to build up), dust-to-gas ratio, and mass of gas converted into stars during the current starburst episode (lasting 50 Myr). We used a clearing time for MCs, $t_{\rm esc} = 50$ Myr (see Panuzzo et al., 2007, for discussion of this parameter).

4.3 RESULTS

The best fits[2] are shown in Figure 4.1 and the results for each parameter listed in Table 4.1 together with several properties of the galaxies derived from the SEDs. SFRs, stellar masses, dust masses and extinction in the MCs are given as output from GRASIL. Infrared luminosities were obtained by integrating the SEDs over the range of $8 - 1000\,\mu$m. Dust temperatures were estimated by fitting a grey-body curve to the part of the SEDs near the dust peak ($\sim 100\,\mu$m, e.g. Yun & Carilli, 2002). Finally, the average extinction outside MCs was calculated as: $A_V = 2.5\log(V\text{-band starlight extinguished by MCs only} \,/\, V\text{-band starlight observed})$; see Silva et al. (1998). This parameter describes the extinction averaged throughout the galaxy as opposed to the line-of-sight extinction derived from optical GRB afterglows.

We checked the consistency of our results with those reported in the literature (Berger et al., 2001a, 2003a; Björnsson et al., 2002; Castro Cerón et al., 2006, 2009; Chen et al., 2006; Christensen et al., 2004; Galama et al., 2003; Gorosabel et al., 2003a,b; Le Floc'h et al., 2006; Michałowski, 2006; Michałowski & Hjorth, 2007; Sokolov et al., 2001; Stratta et al., 2004; Takagi et al., 2004, see Section 4.6). We generally found good agreement except for the following points. Our estimate of the age for GRB 980703 (which has the most significant old stellar component) is considerably larger than that derived by Christensen et al. (2004). The discrepancy arises because we calculated the time from the beginning of the galaxy evolution, not the beginning of the starburst. Our SFRs for GRB 980703 and 010222 are inconsistent with the reported upper limits of Le Floc'h et al. (2006). However our analysis, based on the full SED rather than only $24\,\mu$m datapoints, seems to be more reliable as admitted by Le Floc'h et al. (2006) who assigned a factor of $\gtrsim 5$ error to their estimates (see also the results of Castro Cerón et al., 2006, based on the same data). Berger et al. (2003a) obtained systematically higher SFRs by a factor of 2–5 based on submm alone. This may be the effect of uncertainty of the dust properties (we could reproduce the results of Berger et al. (2003a) using Yun & Carilli (2002), but when we used a

[2]The SED fits can be downloaded from
`http://archive.dark-cosmology.dk`

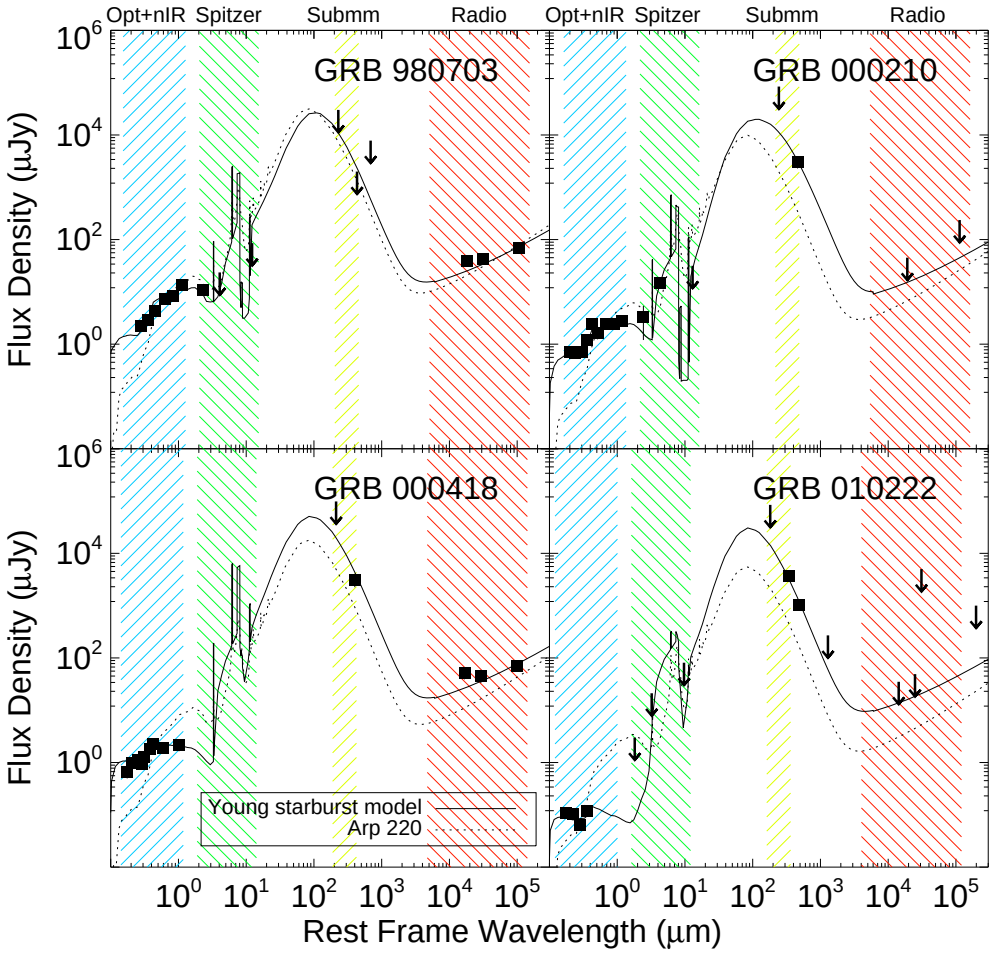

Figure 4.1: *SEDs of GRB hosts. Solid lines: the young starburst galaxy models calculated using GRASIL and consistent with the data. Dotted lines: Arp 220 model (from Silva et al., 1998). Squares: detections with errors, in most cases, smaller than the size of the symbols. Arrows: 3σ upper limits (values marked at the base). Hashed columns mark the wavelengths corresponding to optical/near-infrared filters, MIR Spitzer filters, SCUBA submm bands and the radio domain. It is apparent that the ULIRG Arp 220 model underpredicts the radio and submm fluxes of GRB hosts while fitted to the optical data. The optical color of this model is also too red compared to GRB hosts. In contrast, the emission of young starbursts is blue in optical and strong in submm/radio at the same time. In the case where we lack Spitzer data the MIR part of the SED is unconstrained due to the possible absorption or emission of PAH and silicate features.*

temperature 10 K higher and an emissivity index 0.35 lower than Berger et al. (2003a) did, we obtained values consistent with our results reported here) as well as of the contribution of older stellar populations to the submm fluxes (see for example the discussion in Vlahakis et al., 2007), that leads to an overestimation of SFRs using only submm data. For the hosts of GRB 000210, 000418 and 010222, Takagi et al. (2004) predicted much higher SFRs, of the order of a few thousand $\mathrm{M}_\odot$ yr^{-1} and stellar masses of $\sim 10^{11}\,\mathrm{M}_\odot$. Such a high SFR is unlikely to be necessary to

explain the submm emission of GRB hosts and hence the accumulated stellar masses seem to be too high as well. We derived much higher extinction for the host of GRB 000210 than Christensen et al. (2004), but our model predicts that the majority of the extinction in the V-band has a grey nature, which would be undetectable in any reddening measurements (we found $E(B-V) = 0.07$, which is consistent with their results if one assumes the Galactic extinction curve slope $R_V = 3.1$). Moreover, it is possible that a GRB event destroys the dust along the line of sight, so study of an afterglow results in low dust content.

The determination of the infrared luminosity suffers from systematic uncertainties depending on the choice of the SED template. Our approach of using all the optical, submm and radio data to constrain the shape of the SED results in a moderate systematic error in luminosity. Using the templates of Dale et al. (2001) and Dale & Helou (2002) fitted to long-wavelength data we obtained values only 30% lower. Similar analysis on a bigger sample of galaxies led Bell et al. (2007) to the conclusion that the systematic uncertainty of infrared luminosity is usually less than a factor of ~ 2. The arbitrary choice of the Salpeter (1955) IMF with the cutoffs of 0.15 and $120\,\mathrm{M}_\odot$ introduces a systematic error of a factor of ~ 2 in the determination of the stellar masses and SFRs (Erb et al., 2006). Bell et al. (2007) have also found that random errors in stellar mass are less than a factor of ~ 2. Dust mass estimates are uncertain up to a factor of a few (Silva et al., 1998). Estimates of dust temperatures based on submm and radio alone have uncertainties of ~ 10 K (Chapman et al., 2003b).

4.4 Discussion

4.4.1 Solving the puzzle

The key property of GRB hosts that explains their blue colors and enhanced submm/radio emission is their young ages (Table 4.1). On one hand the majority of the stars still reside in dense MCs, so a significant part of the energy is absorbed and re-emitted. This increases the dust emission. On the other hand there are lots of young, hot, blue stars in such a galaxy, because they have not finished their lives yet. Hence the total optical spectrum of the galaxy is blue. GRBs may indeed reside in or close to MCs (possibly causing hydrogen ionization and dust sublimation along the line of sight, Watson et al., 2007) and it was found that gas column densities derived from *X*-ray afterglows in a sample of 8 GRBs (including GRB 980703, discussed here) were in the range corresponding to the column densities of giant MCs in the Milky Way (Galama & Wijers, 2001). A similar conclusion for high-redshift GRBs was recently drawn by Jakobsson et al. (2006a) by means of modeling Lyα absorption features (see also Castro-Tirado et al., 1999; Hjorth et al., 2003a; Savaglio et al., 2003; Stratta et al., 2004; Vreeswijk et al., 2004; Chen et al., 2005, 2006; Watson et al., 2006; Campana et al., 2007; Prochaska et al., 2007a,b; Ruiz-Velasco et al., 2007, for a discussion of similar results).

Table 4.1: *GRASIL parameters yielding SEDs consistent with the data and characteristics of the galaxies derived from the SED modeling.*

GRB host	z	Age (Gyr)	dust/gas (10^{-2})	$M_{\rm burst}$ ($10^9\,{\rm M}_\odot$)	$L_{\rm IR}$ ($10^{12}L_\odot$)	SFR (${\rm M}_\odot\ {\rm yr}^{-1}$)	M_* ($10^9\,{\rm M}_\odot$)	M_d ($10^9\,{\rm M}_\odot$)	T_d (K)	$A_{1\mu{\rm m}}^{\rm MC}$	$A_V^{\rm av}$
(1)	(2)	(3)	(4)	(5)	(6)	(7)	(8)	(9)	(10)	(11)	(12)
980703	0.97	2	0.3	2.3	1.9	212	21.0	0.15	44	54	0.42
000210	0.85	0.19	2.4	1.2	0.9	179	10.1	0.33	45	27	1.01
000418	1.12	0.14	1	5.0	4.6	288	18.7	0.82	50	31	0.70
010222	1.48	0.09	0.7	5.9	4.3	278	13.5	0.32	51	25	0.58
Arp 220	0.018	13	1	25	1.16	580	153.2	0.30	55	63	0.59
NGC 6946	0.00016	13	1	-	0.05	6	104.1	0.10	29	36	0.06

Note. — (1) GRB name, (2) redshifts from Djorgovski et al. (1998), Piro et al. (2002), Bloom et al. (2003), Jha et al. (2001), Soifer et al. (1984) and Huchra et al. (1999), (3) age of the galaxy defined as the time since the beginning of its evolution, (4) dust-to-gas ratio, (5) mass of gas converted into stars during starburst, (6) total $8-1000\,\mu$m infrared luminosity (7) total star formation rate for $0.15-120\,{\rm M}_\odot$ stars averaged over the last 50 Myr, (8) stellar mass, (9) dust mass, (10) dust temperature, (11) extinction in molecular cloud (MC) at 1 μm measured from its center, (12) average extinction of stars outside MCs at 0.55 μm. Values corresponding to Arp 220 (ULIRG) and NGC 6946 (spiral) are given for comparison.

Since the stars formed during the starburst do not dominate the stellar mass of the GRB hosts discussed here (only from 10 to 40% of these masses have been formed during the ongoing starburst epoch — compare columns 5 and 8 of Table 4.1) and are still embedded in MCs providing strong extinction (so-called age-dependent extinction, see Panuzzo et al., 2007), it is apparent that the optical/UV light is dominated by somewhat older stars, which are already outside MCs and suffer only moderate extinction (column 12 in Table 4.1, see Plante & Sauvage, 2002, for an example of a totally obscured, metal-poor star-forming region). This is why optical measurements of extinction resulted in low values suggesting low dust content whereas enhanced submm emission is consistent with being emitted by dusty galaxies. In light of this, we provide support for the hypothesis of Gorosabel et al. (2003a) claiming that the optical and submm emission of the GRB 000210 host are dominated by different populations of stars (the same explanation was proposed by Goldader et al., 2002, for a sample of dusty ULIRGs with UV colors bluer than expected for starburst galaxies).

The location of GRBs in the brightest UV parts of the galaxy (Fruchter et al., 2006) is also consistent with our model. Although the GRBs discussed here trace regions of obscured rather than non-obscured star formation (because the majority of star formation is obscured and under the assumption that GRBs trace star formation), these regions are not spatially distinct in the galaxy. Regions of obscured star formation evolve into non-obscured regions by destroying the MCs without changing their location. Unless individual MCs can be resolved, obscured star formation within them and less-obscured star formation on their outskirts cannot be spatially separated.

Our results are based on the assumption that the detected submm/radio sources are indeed related to GRB hosts. It is however possible that the emission comes from unrelated sources falling into the coarse beam of SCUBA ($15''$) as noted by Smith et al. (2001, 2005), Gorosabel et al. (2003a) and Le Floc'h et al. (2006). The most suspicious case is the GRB 010222 host which is undetected at $24\,\mu$m, but accompanied by several spatially close MIR-bright galaxies that could dominate the submm emission (Le Floc'h et al., 2006). On the other hand, the nondetections of GRB hosts in the MIR are easily explained by silicate absorption features and the steep infrared spectrum of the galaxies (see Figure 4.1). The situation is less severe for GRB 980703 and GRB 000418, both detected by VLA in the radio, for which accurate astrometry decreases the chance of confusion.

4.4.2 The nature of the GRB hosts

From the results presented in Table 4.1 a common characteristic of submm GRB hosts emerges (although our sample is too small to draw a very robust conclusion). For all four galaxies we obtained young ages ($\lesssim 2$ Gyr) and relatively low stellar masses ($\lesssim 2 \times 10^{10}\,\mathrm{M}_{\odot}$). These are usual properties among GRB hosts (Christensen et al., 2004; Sollerman et al., 2005; Castro Cerón et al., 2006; Savaglio et al., 2006). Galaxies with such stellar mass are believed to dominate the star formation of the Universe at redshifts $z \lesssim 1$ (Zheng et al., 2007; Bell et al., 2007).

What is special about the four galaxies discussed here is that they are highly star forming (as opposed to the other known GRB hosts, see Berger et al., 2003a; Le Floc'h et al., 2006; Tanvir et al., 2004) and have high dust content. Hence they can be representative only of the bright end of the infrared luminosity function of GRB hosts. More sensitive observations in submm (by JCMT/SCUBA-2 and ALMA) and far-infrared (FIR, by *Herschel*) are therefore necessary to detect fainter hosts and test this hypothesis.

The optical afterglow of GRB 000418 was exceptionally red (Klose et al., 2000) while no opti-

cal afterglow was detected for GRB 000210 in spite of deep searches (Piro et al., 2002) (its *X*-ray luminosity was high enough to place it at the borderline of the category of dark GRBs, Jakobsson et al., 2004; Rol et al., 2005), both hinting at significant obscuration in the hosts. However the "darkness" of GRBs cannot easily be linked with obscuration in the hosts, because the remaining three members of our submm/radio sample were associated with bright optical afterglows (Berger et al., 2001a; Bloom et al., 1998b; Björnsson et al., 2002; Castro-Tirado et al., 1999; Galama et al., 2003; Holland et al., 2001; Klose et al., 2000; Vreeswijk et al., 1999). Moreover, Barnard et al. (2003) did not detect submm emission from the hosts of three GRBs classified as dark. This issue should be addressed by targeting a more significant sample of dark GRBs in the submm and radio.

4.4.3 Rejection of an AGN contribution

In general, GRB hosts are typically starburst galaxies and this selection makes the presence of an AGN component quite unlikely. Here we present additional indications that the long-wavelength emission from GRB hosts discussed here is not dominated by AGNs.

In order to assess the probability that there is an AGN component in our sample of GRB hosts we compared their FIR and radio luminosities using the q coefficient of Helou et al. (1985): $q = \log(\mathrm{FIR}/3.75 \cdot 10^{12}/S_{1.4})$. The FIR luminosity was integrated in the range 42.5–$122.5\,\mu$m. The rest 1.4 GHz luminosity ($S_{1.4}$) was calculated from the observed 1.4 GHz (or 4.86 GHz for GRB 010222) flux assuming a steep radio slope $\alpha = -0.75$ to obtain a robust lower limit on q. (Assuming a shallower slope, the expected rest 1.4 GHz radio luminosity would be even lower). The resulting q values are 2.28, > 1.93, 2.41 and > 2.06 for GRBs 980703, 000210, 000418 and 010222, respectively. It is known that starburst galaxies follow the so-called FIR–radio correlation with a mean $q = 2.21 \pm 0.14$ (Helou et al., 1985) or 2.3 ± 0.2 (Condon, 1992). Hence the GRB hosts are consistent with being starburst-dominated galaxies. Emission dominated by radio-loud AGN would show $q < 2$ (Yun et al., 2001; Chanial et al., 2007; Yang et al., 2007) which would only be the case for GRB 000210 if the actual radio flux is just below the 3σ upper limit. We therefore conclude that the FIR-radio correlation shows that the emission from GRB hosts is probably not dominated by radio-loud AGNs. Even if a non-dominating AGN is present its contribution to the radio and submm emission is insignificant since the hosts fulfill the FIR-radio correlation. It would be rather unlikely that AGN-domianted emission is coincidentally consistent with tight FIR–radio correlation.

This is supported by several other diagnostics. Berger et al. (2001b) detected no variability in the radio flux of GRB 980703 host over 650 days contrary to what would be expected if an AGN dominates its radio emission. Moreover, GRB hosts have optical spectra typical for starbursts, not AGNs (i.e. no high-ionization AGN lines have been found, Djorgovski et al., 1998; Berger et al., 2001b; Bloom et al., 2003; Prochaska et al., 2004). This excludes non-obscured AGNs in our sample. Moreover, GRB hosts are dwarf galaxies and the fraction of AGNs (without optical high ionization lines) in a galaxy sample with stellar mass of $M_* \sim 10^{10}\,\mathrm{M}_\odot$ is negligible ($< 0.01\%$ from Figure 2 of Best et al. 2005; see also Woo et al. 2005). AGNs are also more luminous than GRB hosts as is shown in Figure 4.2. In summary, AGNs cannot dominate the emission of the GRB hosts discussed here unless they are atypically small, obscured and radio-quiet. Since submm- and radio-faint hosts are even less probably connected with AGN activity (because it would require even smaller AGNs) we conclude that GRB hosts in general are unlikely powered by AGNs.

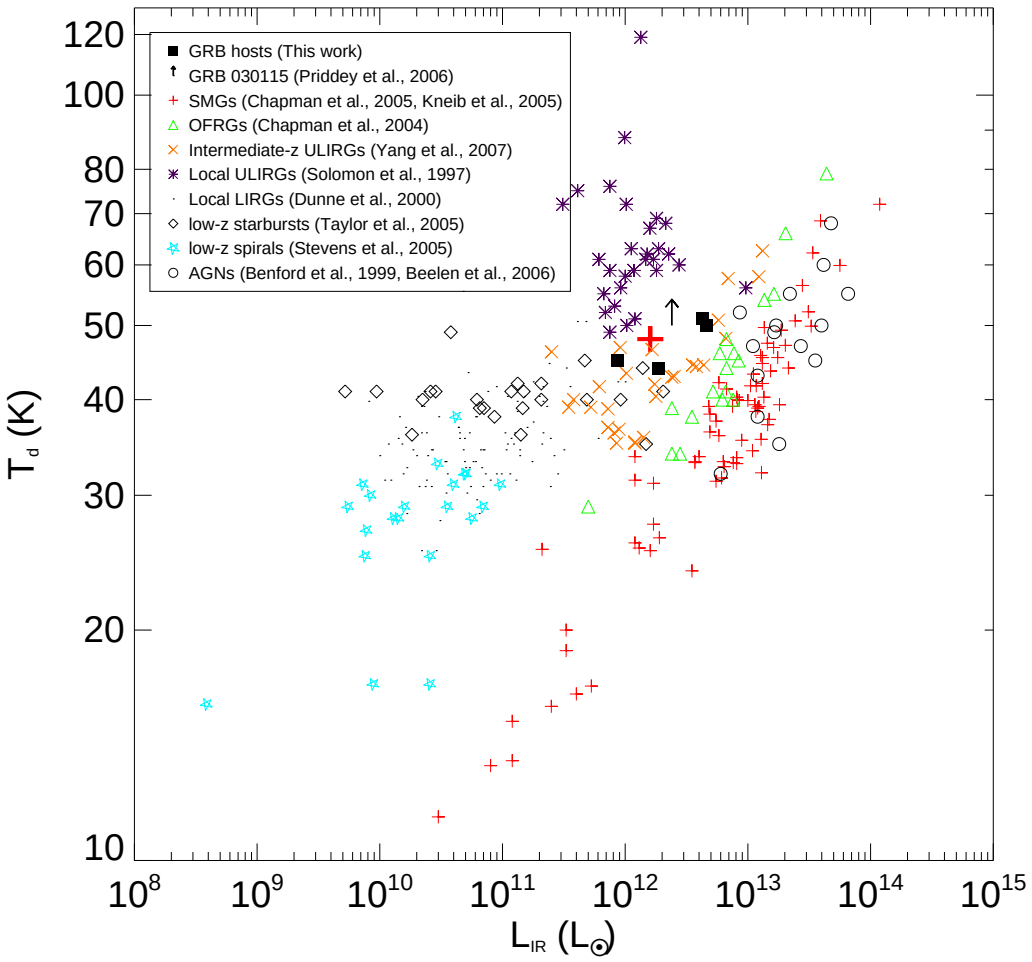

Figure 4.2: *Dust temperature as a function of infrared* ($8 - 1000\ \mu m$) *luminosity. GRB hosts discussed here (filled squares) and GRB 030115 (arrow indicating lower limit on temperature, Priddey et al., 2006) are compared with submm galaxies (pluses, Chapman et al., 2005; Kneib et al., 2005, large symbol denotes a hot lensed galaxy found behind a cluster), optically faint radio galaxies (triangles, note that symbols indicate lower limits on temperature, Chapman et al., 2004a), intermediate-z ULIRGs (crosses, Yang et al., 2007), local ULIRGs (asterisks, Solomon et al., 1997), local LIRGs (dots, Dunne et al., 2000), low-z starburst galaxies (diamonds, Taylor et al., 2005), low-z spirals and cirrus galaxies (stars, Stevens et al., 2005; Taylor et al., 2005) and millimeter-selected radio-quite AGNs (circles, Benford et al., 1999; Beelen et al., 2006). GRB hosts seem to reflect the properties of intermediate-z ULIRGs, the bright end of starburst galaxies and optically faint radio galaxies — the candidates for hotter counterparts of SMGs. Moreover, the hot, faint SMG found behind the cluster (large plus) falls in the same region as GRB hosts.*

4.4.4 The general picture of dust properties

In Figure 4.2 we compare the total infrared luminosities and dust temperatures of GRB hosts with well-studied galaxies both local and at high-z. We included the four hosts studied here as well as the host of GRB 030115 which has an upper limit to the temperature of 50 K. This limit was derived by Priddey et al. (2006) using SED modeling of optical and near-infrared data,

which led to the estimation of the infrared luminosity via the UV-slope method. This, in turn, allowed them to exclude a low dust temperature, because cold dust would be inconsistent with the non-detection in the submm.

GRB hosts seem to overlap with intermediate-z ULIRGs from Yang et al. (2007). This is not very surprising since both galaxy classes have ULIRG characteristics. GRB hosts are however much more distant. As opposed to a mean redshift of 0.37 for intermediate-z ULIRGs, our sample has a mean redshift of 1.1 compared to 2.8 for GRBs in general (Jakobsson et al., 2006c), 2.2 for SMGs (Chapman et al., 2005) and 2.1 for optically faint radio galaxies (OFRGs, Chapman et al., 2004a).

The GRB hosts discussed here occupy the same region of Figure 4.2 as the brightest starbursts from Taylor et al. (2005). Moreover, dust masses of GRB hosts (Table 4.1) are close to the upper boundary for starburst galaxies derived by these authors.

As noted above, the GRB hosts discussed here must form the bright end of the infrared luminosity function of GRB hosts. The remaining members of the sample are still undetected at long wavelengths making it impossible to measure luminosities and dust temperatures. One can speculate from Figure 4.2 that they may follow the "starburst" sequence having similar temperatures ($T \sim 40 - 50$ K) and infrared luminosities in the range $10^9 - 10^{12}\,L_\odot$. *Herschel* should be able to detect these sources in the FIR. There is also the possibility that we can detect even brighter (but rare) GRB hosts — the counterparts of the brightest ULIRGs of Yang et al. (2007) with luminosities $\sim 10^{13}\,L_\odot$ and temperatures ~ 60 K. These should be bright enough to be searched for by sensitive submm instruments (JCMT/SCUBA-2, ALMA).

It is known that GRB hosts are much bluer than massive, star forming SMGs (compare Christensen et al., 2004; Le Floc'h et al., 2003; Berger et al., 2003a; Smail et al., 2004). From Figure 4.2 it seems that they are also hotter than SMGs with the same luminosity (or dimmer than SMGs with the same temperature). This gives a hint that GRB events may pinpoint a population of ULIRGs at high redshifts with dust hotter than in typical SMGs. The search for such galaxies is important because they likely contribute to the star formation history at the same level as SMGs. High dust temperatures of GRB hosts were hypothesized by Barnard et al. (2003) and Tanvir et al. (2004) as a possible way to explain their faintness in submm. Here we provide evidence that this is the case. Moreover, Trentham et al. (2002) suggested that GRB hosts may be low-luminosity SMGs. Indeed, very faint sub-mJy SMGs magnified by clusters of galaxies are found to be hotter than those found in blind surveys (limited by confusion to ~ 2 mJy): the $z \sim 2.5$ SMG behind the cluster A 2218 found by Kneib et al. (2005) has very similar dust properties to the GRB hosts discussed here ($T_d \sim 50$, $L_{\rm IR} \sim 10^{12}\,L_\odot$).

Hotter dust temperatures indicate that the star formation sites in GRB hosts are more compact than those in SMGs (Chanial et al., 2007; Yang et al., 2007). It is consistent with the fact that GRB hosts have higher specific SFRs (per unit mass) than SMGs (Castro Cerón et al., 2006). The blue optical colors of GRB hosts compared to SMGs can also be explained by the compactness of the former galaxies. If they are compact then the stellar population suffers strong extinction. This would lead to redder colors, but it is likely (see Section 4.4.1) that this extinction is so strong that very young stars are totally obscured, so optical light is dominated by relatively less obscured stars outside star forming regions leading to blue colors.

We note that the majority of the galaxies shown in Figure 4.2 also have higher dust temperatures compared to SMGs. However, all of them are local galaxies, so cannot be considered as counterparts of high-redshift SMGs and their submm emission has been detected only because of their proximity.

GRB hosts may be consistent with a population of OFRGs having similar infrared luminosi-

ties and (likely) temperatures. Although the majority of OFRGs lie at $z \sim 2$ (Chapman et al., 2004a), some of them are within the redshift range of the GRB hosts discussed here. OFRGs have been suggested to be hotter counterparts of SMGs (Chapman et al., 2004a), so the same may be true for GRB hosts.

Indeed SMG samples are clearly biased against the high-T_d–low-L galaxies (upper-left part of Figure 4.2, see Chapman et al., 2005). The lack of SMGs in low-T_d–high-L (lower-right corner) is probably real, because such sources would be detected if present (see Figure 2 of Blain et al., 2004, for a discussion of selection effects). Similarly, the lack of very luminous sources with $L > 10^{14}\,L_{\odot}$ is probably real. If such powerful sources exist, they are very rare and do not contribute to the presented sample. Taking into account all the galaxies shown in Figure 4.2, the lack of high-T_d–low-L galaxies is probably not a selection effect (at low redshift) because the hotter counterparts of $10^{10}\,L_{\odot}$ galaxies should be easily detected in MIR and FIR.

Therefore the apparent trend (also seen in our GRB host sample) that more luminous galaxies have higher dust temperatures is a real effect called the luminosity-temperature relation (Soifer et al., 1987; Chanial et al., 2007; Yang et al., 2007). The spread has been interpreted as variation in the size of a star forming region (Chanial et al., 2007) or in the dust emissivity index and amount of dust in each galaxy (Yang et al., 2007). Galaxies with large dust content tend to occupy the lower-right corner of Figure 4.2 whereas those with low dust content occupy the upper-left corner. The GRB hosts discussed here with $M_d \sim 10^8\,\mathrm{M}_{\odot}$ are placed near the average of all the galaxies shown in Figure 4.2. The rest of the population is probably aligned along the diagonal of Figure 4.2 fulfilling the luminosity–temperature relation. It is expected that some of the IR-faint GRB hosts have much lower dust content so are possibly located in the lower-L—higher-T_d regime.

4.5 Conclusions

The short- and long-wavelength properties of the host galaxies of GRBs 980703, 000210, 000418 and 010222 can be linked assuming that they are very young and powerful starbursts. We conclude that they are galaxies with the highest star formation rates among known GRB hosts, but their optical properties, starburst nature, stellar masses and ages are not distinctive. We also found that AGNs are probably not responsible for boosting their long-wavelength emission.

We have shown that GRB host galaxies at cosmological redshifts may constitute a population of hot submillimeter galaxies. This hypothesis makes GRB hosts of special interest, placing them in the same category as optically faint radio galaxies, and should be confirmed by future sensitive long-wavelength observations. Future instruments (*Herschel*, JCMT/SCUBA-2 and ALMA) will be able to build up a statistically significant sample of GRB hosts with accurately measured infrared luminosities and temperatures.

4.6 Comparison of our results with the literature

In the following section we compare our results with those found by other authors applying different methods, to show that our modeling in most cases gives consistent values, but also provides additional galaxy properties that cannot be inferred from previous approaches. We stress that some inconsistency with methods based on optical/UV is expected because optical/UV light traces only a minor (i.e. unobscured) portion of the bolometric luminosity of the galaxies. Some authors used different IMFs, but the necessary correction to total SFRs and stellar masses is not larger than 15%, and does not affect the conclusions of the comparison.

4.6.1 AGES

Based on galaxy SEDs fitted to the optical data only, Gorosabel et al. (2003a,b) and Christensen et al. (2004) derived the ages of the starbursts in the hosts of GRBs 980703, 000210 and 000418. Our estimates are considerably larger only for GRB 980703. The discrepancy is because we calculated the time from the beginning of the galaxy evolution, not the beginning of the starburst. Sokolov et al. (2001) derived ages of both old stellar populations and starbursts. Our estimation for GRB 980703 agrees with the age of the old component, which is conceptually closer to our definition of the galaxy age. Ages derived by Takagi et al. (2004) for GRB 000210, 000418 and 010222 agree with our results within a factor of a few.

4.6.2 STAR FORMATION RATES

See Michałowski & Hjorth (2007) for details of the comparison between SFR estimates. Since the starburst is still hidden in MCs and its optical light is extinguished, SFRs derived from optical indicators (Christensen et al., 2004; Gorosabel et al., 2003a,b; Berger et al., 2003a) are two orders of magnitude lower than our estimates. Our results are consistent with radio-derived SFRs (Berger et al., 2003a). This is because the calibration of SFR to radio flux requires the prior assumption of only two parameters (a normalization factor and a spectral index, see Yun & Carilli, 2002), which are relatively well constrained. Our values also agree with the upper limits derived by Castro Cerón et al. (2006) using the template of Arp 220. Finally, Berger et al. (2003a) obtained systematically higher SFRs by a factor of $2-5$ based on submm alone. We have checked that the SFRs derived from our SED models using the total infrared emission (Kennicutt, 1998) are consistent with our values derived here (see Michałowski & Hjorth, 2007).

4.6.3 STELLAR MASSES

Our results for the GRB 980703 host agree with the stellar mass derived by Castro Cerón et al. (2006) and with both stellar and burst masses derived by Sokolov et al. (2001). The stellar mass derived by Castro Cerón et al. (2009) for GRB 000210 is also in agreement with our value.

4.6.4 DUST PROPERTIES

Our value of the dust mass for GRB 980703 host agrees within a factor of 1.5 with the one derived by Castro Cerón et al. (2006). Dust masses derived by Takagi et al. (2004) for GRB 000210, 000418 and 010222 agree with our results within a factor of a few. We have checked that for these three hosts, values of dust masses computed directly from submm fluxes (using Hildebrand, 1983; Taylor et al., 2005) agree with those reported here (see Michałowski, 2006).

The near-infrared extinction derived for MCs (column 11 in Table 4.1) is within the typical values found in observations of compact star forming regions (e.g. Scoville et al., 1998; Plante & Sauvage, 2002; Hunt et al., 2005) and numerical simulations (e.g. Indebetouw et al., 2006; Goicoechea & Le Bourlot, 2007; Panuzzo et al., 2007). Our values of average extinction outside MCs, A_V (column 12 in Table 4.1), are consistent with those derived from optical host SED modeling by Sokolov et al. (2001, for 980703) and Christensen et al. (2004, for 980703, 000210, 000418) and from optical afterglow modeling by Berger et al. (2001a, for 000418), Björnsson et al. (2002, for 010222), Stratta et al. (2004, for 980703, 010222) and Chen et al. (2006, for 980703), except for the host of GRB 000210 for which we predict higher extinction, but with grey nature undetectable in any reddening measurements To the best of our knowledge we present the first A_V determination from the host galaxy SED fitting for GRB 010222.

Acknowledgements
We wish to thank J. Baradziej, D. Alexander, B. Cavanagh, F. Economou, J. Fynbo, T. Greve, T. Jenness, E. Le Floc'h, A. Levan, P. Natarajan, C. Skovmand for help, discussion and comments and L. Silva for making the GRASIL code available. The Dark Cosmology Centre is funded by the Danish National Research Foundation. MJM would like to acknowledge support from The Faculty of Science, University of Copenhagen. JMCC gratefully acknowledges support from the Instrumentcenter for Dansk Astrofysik and the Niels Bohr Institutet's International PhD School of Excellence.

Published as: Michałowski, M. J., Hjorth, J., Malesani, D., Michałowski, T., Castro Cerón, J. M., Reinfrank, R. F., Garrett, M. A., Fynbo, J. P. U., Watson, D. & Jørgensen, U. G. – *The properties of the host galaxy and the immediate environment of GRB 980425 / SN 1998bw from the multi-wavelength spectral energy distribution* Astrophysical Journal, vol. 693, pp. 347–354, March 2009.

5

PROPERTIES OF THE HOST GALAXY AND THE IMMEDIATE ENVIRONMENT OF GRB 980425

ABSTRACT – *We present an analysis of the spectral energy distribution (SED) of the galaxy ESO 184-G82, the host of the closest known long gamma-ray burst (GRB) 980425 and its associated supernova (SN) 1998bw. We use our observations obtained at the Australia Telescope Compact Array (the third $> 3\sigma$ radio detection of a GRB host) as well as archival infrared and ultraviolet (UV) observations to estimate its star formation state. We find that ESO 184-G82 has a UV star formation rate (SFR) and stellar mass consistent with the population of cosmological GRB hosts and of local dwarf galaxies. However, it has a higher specific SFR (per unit stellar mass) than luminous spiral galaxies. The mass of ESO 184-G82 is dominated by an older stellar population in contrast to the majority of GRB hosts. The Wolf-Rayet region ~ 800 pc from the SN site experienced a starburst episode during which the majority of its stellar population was built up. Unlike that of the entire galaxy, its SED is similar to those of cosmological submillimeter/radio-bright GRB hosts with hot dust content. These findings add to the picture that in general, the environments of GRBs on 1–3 kpc scales are associated with high specific SFR and hot dust.*

5.1 INTRODUCTION

Long gamma-ray bursts (GRBs) are associated with the death of massive stars (e.g. Galama et al., 1998; Hjorth et al., 2003b; Stanek et al., 2003). This makes them of special interest in cosmology because they possibly trace the evolution of the rate of star formation in the Universe (e.g. Lamb & Reichart, 2000; Jakobsson et al., 2005, 2006c). Indirect evidence of the nature of GRBs was found by studying their host galaxies (e.g. Bloom et al., 1998a; Christensen et al., 2004; Sollerman et al., 2005; Castro Cerón et al., 2009; Savaglio et al., 2009).

Moreover, several studies on the immediate environments of GRBs suggest a close connection of long GRBs with regions of star formation, and therefore that their progenitors are likely massive stars. Fruchter et al. (2006) found that GRBs trace the ultraviolet (UV) brightest parts of their host (see also Bloom et al., 2002). Thöne et al. (2008) studied in detail the environment (in 3 kpc bins) of GRB 060505, concluding that it originated in the youngest, most metal-poor and most intense star-forming region in the host galaxy. Similarly, Östlin et al. (2008) found that the 0.3 kpc environment of GRB 030329 is much younger than the entire galaxy and its estimated age suggests a conservative lower limit on the mass of the GRB progenitor equal to $12\,M_{\odot}$. Finally, a significant number of other GRBs were reported to reside in dense star-forming re-

gions (Castro-Tirado et al., 1999; Holland & Hjorth, 1999; Hjorth et al., 2003a; Savaglio et al., 2003; Vreeswijk et al., 2004; Chen et al., 2005, 2006; Fynbo et al., 2006a; Watson et al., 2006, 2007; Prochaska et al., 2007a,b; Ruiz-Velasco et al., 2007) and molecular clouds (Galama & Wijers, 2001; Stratta et al., 2004; Jakobsson et al., 2006a; Campana et al., 2007; Prochaska et al., 2008).

GRB 980425 is the closest known GRB ($z = 0.0085$; Tinney et al., 1998), therefore it is an excellent laboratory for local GRB studies. Galama et al. (1998) reported the Type Ic supernova (SN) 1998bw exploding inside the error box of GRB 980425. Its lightcurve was well modeled by an explosion of a Wolf-Rayet (WR) star (Iwamoto et al., 1998), which is a highly evolved and massive star that has lost its outer hydrogen layers. Up to now, three other GRBs have also been spectroscopically confirmed to be associated with SNe: GRB 030329 (Hjorth et al., 2003b; Matheson et al., 2003; Stanek et al., 2003), 031203 (Cobb et al., 2004; Gal-Yam et al., 2004; Malesani et al., 2004; Thomsen et al., 2004) and 060218 (Ferrero et al., 2006; Mirabal et al., 2006; Modjaz et al., 2006; Pian et al., 2006; Soderberg et al., 2006; Sollerman et al., 2006), while two GRBs were confirmed to be SN-less: GRB 060505 and 060614 (Fynbo et al., 2006b; Della Valle et al., 2006; Gal-Yam et al., 2006).

The host galaxy of GRB 980425 / SN 1998bw (ESO 184-G82; Holmberg et al., 1977) is a dwarf (0.02 of the characteristic blue luminosity, L_B^*; Fynbo et al., 2000) barred spiral (SBc; Fynbo et al., 2000) with axis diameters of 12 and 10 kpc (down to $B = 26.5$ mag arcsec^{-2}; Sollerman et al., 2005), dominated by a large number of star-forming regions (Fynbo et al., 2000; Sollerman et al., 2005). SN 1998bw occurred inside one of these, ~ 800 pc southeast of a region displaying a Wolf-Rayet type signature spectrum (hereafter: WR region; Hammer et al., 2006). The WR region dominates the galaxy's emission at $24\,\mu$m (Le Floc'h et al., 2006) and is the youngest region within the host exhibiting very low metallicity (Christensen et al., 2008).

In this chapter we present fits to the spectral energy distribution (SED) of ESO 184-G82 and the WR region and compare their properties to other galaxies. Section 5.2 lists the data sources (including the third radio detection of a GRB host after those reported by Berger et al., 2001b, 2003a) used for the SED modeling of Section 5.3. We derive properties of the host galaxy and WR region in Section 5.4, discussing their implications in Section 5.5. Section 5.6 closes with our conclusions. We use a cosmological model with $H_0 = 70$ km s^{-1} Mpc^{-1}, $\Omega_\Lambda = 0.7$ and $\Omega_m = 0.3$, so ESO 184-G82 is at a luminosity distance of 36.5 Mpc and $1''$ corresponds to 175 pc at its redshift.

5.2 DATA

We undertook deep radio observations of the host galaxy of GRB 980425 on 2007 August 18 using the Australia Telescope Compact Array (proposal no. C1651, PI: Michałowski) using the hybrid H168 configuration, with antennas positioned on both east-west and north-south tracks, and baselines of 60–4500 m. Simultaneous observations were made at 6 cm (4.8 GHz) and 3 cm (8.64 GHz), with a bandwidth of 128 MHz at each frequency. A total of 10.5 hr of data were obtained. Calibrator source PKS B1934-638 was utilized to set the absolute flux calibration of the array as well as to calibrate phases and gains. Data reduction and analysis was done using the MIRIAD package (Sault & Killeen, 2004). Antenna #1 was excluded from the analysis due to phase instabilities, thus reducing the number of possible baselines from 15 to 10. Calibrated visibilities were Fourier transformed using "robust weighting", which combines high signal-to-noise ratio with enhanced sidelobe suppression. The final synthesized beam sizes for 6 and 3 cm images were $76'' \times 38''$ and $37'' \times 21''$, respectively, with root-mean-square (rms) values of 46 and $27\,\mu$Jy beam^{-1}. The host galaxy, ESO 184-G82, was only detected at 6 cm. This is only

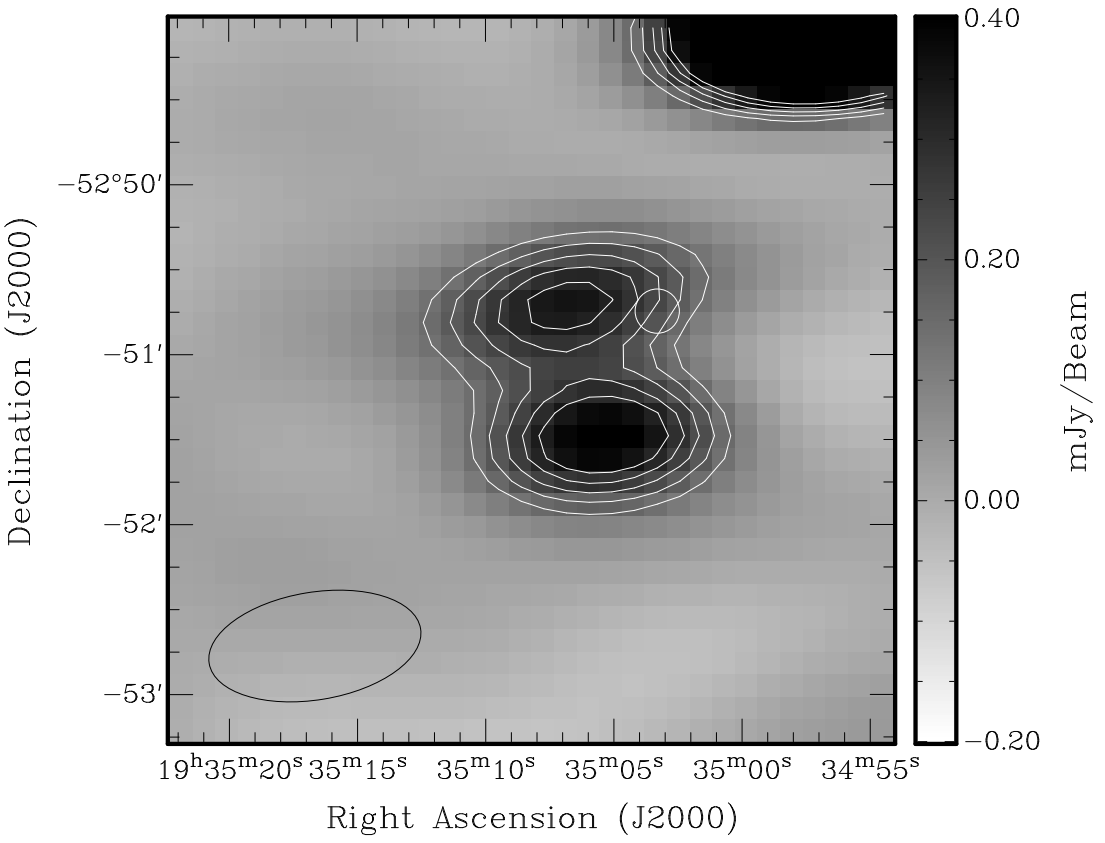

Figure 5.1: *6 cm ATCA image with size of* $5.7'$ *or* 60 *kpc at the redshift of* 0.0085*. The circle marks the position of SN 1998bw. The two overlapping objects in the middle are the ESO 184-G82 (north) and galaxy A of Foley et al. (2006) (south). The contours are* 3*,* 4*,* 5*,* 6*, and* 7σ*, where* $\sigma = 46$ *μJy beam*$^{-1}$*. The beam is shown in the bottom left corner.*

the third $> 3\sigma$ radio detection of a GRB host, after those of GRB 980703 and GRB 000418 (Berger et al., 2001b, 2003a). Note that the radio observations of GRB 000301C and GRB 000911 were also reported to be $> 3\sigma$ detection, but after removal of the afterglow signal, the significance of the host detections drops below 3σ. As ESO 184-G82 slightly overlaps Galaxy A, reported by Foley et al. (2006), $\sim 70''$ south (see Figure 5.1), its flux density was estimated by simultaneous fitting of two two-dimensional Gaussian functions to the data with their centroids, sizes, and orientations as free parameters. The lack of residuals left after the subtraction of these two Gaussians rules out a significant contamination of the Galaxy A to the measured flux of the host. ESO 184-G82 was not detected at 3 cm down to a 3σ limiting flux of 0.18 mJy.

We obtained U-band photometry on the Danish 1.5m Telescope on La Silla during the period 2007 May-June. In total 3.75 hr were spent on the target. The data were reduced in a standard manner using IRAF (Tody, 1986, 1993).

We performed photometry on archival JHK images from NTT/SofI (Patat et al., 2001), VLT/ISAAC (Sollerman et al., 2002) and Two Micron All Sky Survey (2MASS Jarrett et al., 2000)[1], as well as $BVRI$ images from VLT/FORS1 (Sollerman et al., 2005) and UV images from

[1]2MASS XSC Final Release (Two Micron All Sky Survey Extended Source Catalog) released on 2003 March 25; `http:`

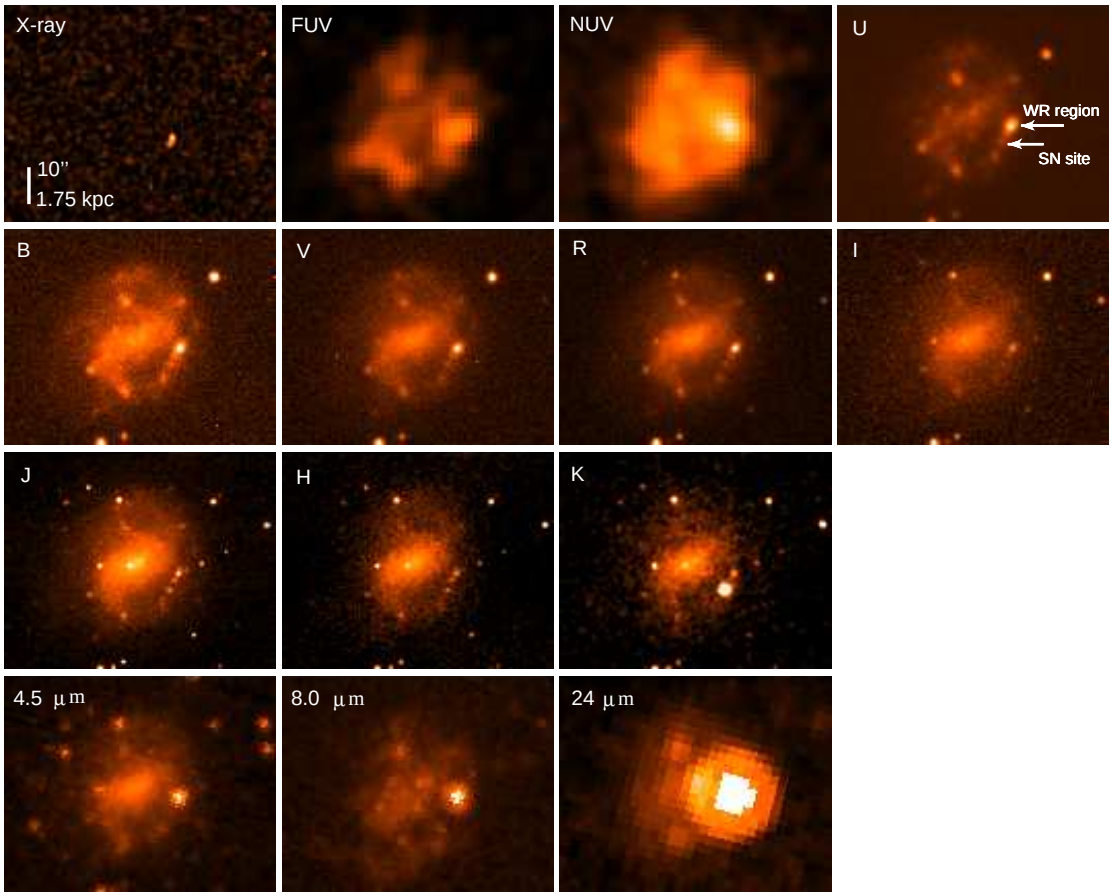

Figure 5.2: *Mosaic of images of ESO 184-G82, the host galaxy of GRB 980425 / SN 1998bw. North is up and east is to the left. Images are* $70'' \times 60''$ *(*12×10 *kpc at the redshift of* 0.0085*). The scale is also shown on the first panel. From top left to bottom right: X-ray, far-UV, near-UV,* U, B, V, R, I, J, H, K, 4.5 μm, 8.0 μm *and* 24 μm*. The arrows on the U-band image mark the SN site and the WR region. The WR region is bright in the UV and mid-IR and faint in the near-IR (see Figure 5.3) hinting at a very young stellar population with overall small mass (compare with Table 5.2). Note that the* K*-band image was obtained when the SN was still bright. The X-ray image reveals two compact sources* $1.5''$ *apart (overlapping at the image shown): the SN and an ultra-luminous X-ray source (Kouveliotou et al., 2004).*

GALEX (Martin et al., 2003, 2005)[2]. The flux was measured in an aperture of $50''$ diameter for the whole galaxy and 2.4–3.6″ (depending on the seeing of the particular image) for the WR region. The results of our photometry and the fluxes obtained from the literature are presented in Table 5.1 and a mosaic of images is shown in Figure 5.2.

Finally we analyzed the X-ray (2–10 keV) image from Kouveliotou et al. (2004). It was, however, not used in the modeling since our SED templates do not cover this wavelength regime.

//www.ipac.caltech.edu/2mass/

[2]*Galaxy Evolution Explorer*; http://galex.stsci.edu/

Table 5.1: *Results of the photometry of the GRB 980425 host and the WR region.*

Filter	X-ray	FUV	NUV	U	B	V	R	I	J	H	K	*Spitzer*			ATCA	
λ (μm)	6 keV	0.1516	0.2267	0.36	0.428	0.553	0.656	0.767	1.25	1.64	2.17	4.5	8.0	24	3 cm	6 cm
Host	3.6×10^{-7}	1.26	1.54	2.44	4.5	5.56	6.80	8.21	9.8	8.8	6.5	2.95	11.9	27.3	< 0.18	0.42
Error	1.6×10^{-7}	0.13	0.16	0.26	...	...	...	...	0.4	0.5	0.4	0.10	0.3	0.2	...	0.05
WR	...	0.095	0.120	0.170	0.116	0.162	0.135	0.0690	0.078	0.071	0.044	0.22	1.815	21	...	...
Error	...	0.023	0.017	0.016	0.006	0.008	0.006	0.0034	0.013	0.012	0.009	...	...	...	...	...
(%)	...	7.5	7.8	7.0	2.6	2.9	2.0	0.8	0.8	0.8	0.7	7.5	15.3	76.9	...	...
Ref.	1	2	2,3	2	2,4	2,4	2,4	2,4	2	2	2,3	5	5	5	2	2

Note. — Flux densities are given in mJy and are corrected for Galactic extinction assuming $E(V-B) = 0.059$ (Schlegel et al., 1998) and the extinction curve of Cardelli et al. (1989). The row marked by % shows the percentage contribution of the WR region to the total galaxy emission. The upper limit is 3σ and errors are 1σ. References: 1: Watson et al. (2004), 2: This work, 3: Castro Cerón et al. (2009), 4: Sollerman et al. (2005), 5: Le Floc'h et al. (2006).

Table 5.2: *Properties of the host galaxy ESO 184-G82 and its WR region derived from the SED modeling.*

Region (1)	Age (Gyr) (2)	$L_{\rm IR}$ ($10^9 L_\odot$) (3)	$\rm SFR_{SED}$ ($M_\odot$ yr^{-1}) (4)	$\rm SFR_{UV}$ ($M_\odot$ yr^{-1}) (5)	$\rm SFR_{IR}$ ($M_\odot$ yr^{-1}) (6)	$\rm SFR_{radio}$ ($M_\odot$ yr^{-1}) (7)	M_* ($10^9 M_\odot$) (8)	$M_{\rm burst}$ ($10^6 M_\odot$) (9)	$M_{\rm dust}$ ($10^5 M_\odot$) (10)	T_d (K) (11)	$A^{\rm MC}_{1\mu\rm m}$ (mag) (12)	$A^{\rm av}_V$ (mag) (13)
Host	$12.00^{+0.00}_{-4.00}$	$2.64^{+0.13}_{-0.31}$	$0.38^{+0.05}_{-0.05}$	$0.25^{+0.04}_{-0.06}$	$0.45^{+0.02}_{-0.05}$	0.23 ± 0.04	$1.6^{+0.25}_{-0.10}$	...	28^{+72}_{-14}	38	0.34	0.07
WR	$3.56^{+8.44}_{-1.98}$	$0.36^{+0.28}_{-0.26}$	$0.10^{+0.05}_{-0.05}$	$0.03^{+0.01}_{-0.02}$	$0.06^{+0.05}_{-0.04}$	...	$0.0057^{+0.0063}_{-0.0025}$	$4.5^{+2.4}_{-2.4}$	$0.05^{+0.14}_{-0.03}$	92	0.78	0.04
(%)	...	14	26	12	13	...	0.4	...	0.2	...	...	...

Note. — Column (1): the entire host galaxy / only WR region / percentage contribution of the WR region to the cumulative properties of the galaxy. Column (2): age, defined as the time since the beginning of its evolution. Column (3): total $8 - 1000$ μm infrared luminosity. Column (4): total star formation rate (SFR) for $0.15 - 120\,M_\odot$ stars averaged over the last 50 Myr derived from the SED model. Column (5): SFR from UV emission (Table 5.1, using Kennicutt, 1998). Column (6): SFR from IR emission (Column 3, using Kennicutt, 1998). Column (7): SFR from radio emission (Table 5.1, using Bell, 2003). Column (8): stellar mass. Column (9): mass of gas converted into stars during starburst. Column (10): dust mass. Column (11): dust temperature. Column (12): extinction in molecular cloud (MC) at 1 μm measured from its center. Column (13): average extinction of stars outside MCs at 0.55 μm.

5.3 SED Modeling

In order to model the SEDs of ESO 184-G82 and of the WR region we utilized the set of 35 000 SED models from Iglesias-Páramo et al. (2007) developed in GRASIL (Silva et al., 1998)[3] based on numerical calculations of the radiative transfer within a galaxy. They cover a broad range of galaxy properties from quiescent to starburst. We scaled all the SEDs to match the observational data and chose the one with the lowest χ^2 to derive the galaxy characteristics.

The radio parts of model SEDs were scaled down by an appropriate factor to account for the decreased efficiency of nonthermal radio emission of dwarf galaxies (see Equation (5.1) and discussion in Section 5.4.2 and in Bell, 2003). Namely a dwarf galaxy has a lower radio flux than it would result from scaling down the high-luminosity SED template and the GRASIL model does not take into account this effect. From the SFR–radio flux relation of Bell (2003, see equation (5.1) below) we inferred that the radio part of the SED template corresponding to ESO 184-G82 should be ≈ 3.5 times lower than in the original template. Anyway, even such corrected templates overpredict the value of radio data points so we excluded them from the fitting (see Section 5.5.2 for a discussion).

The best fits[4] are shown in Figure 5.3 and the resulting properties of the galaxy are listed in Table 5.2 (see Michałowski et al., 2008, and Sections 5.4.2 and 5.4.3 for details on how these were derived from the SEDs).

5.4 Results

5.4.1 Stellar Masses

The broadband SED of the host of GRB 980425 is consistent with that of a galaxy with an old stellar population (the time since the beginning of the galaxy evolution is equal to 12 Gyr, see Column 2 of Table 5.2) built up quiescently without any starburst episode (consistent with the conclusion of Sollerman et al., 2005) at a rate comparable to the present value. The age estimate is however uncertain due to degeneracy between age and dust extinction as well as metallicity, namely that if one increases the assumed metallicity or decreases the extinction then the resulting age will increase. The derived stellar mass agrees with previous estimates (Castro Cerón et al., 2009; Savaglio et al., 2009).

On the other hand, the comparison of Columns 8 and 9 of Table 5.2 reveals that the stellar mass of the WR region is dominated by a starburst episode, so that it has built up a negligible fraction of the stellar mass before the starburst. According to our SED model, this starburst is still ongoing and started 50 Myr ago. Interestingly this is the starburst age predicted for GRB hosts by Lapi et al. (2008) based on the argument that for older starbursts the metallicity becomes too high to produce a GRB.

5.4.2 Star Formation Rates

The SFR of the entire galaxy, as well as that of the WR region, was calculated from UV and infrared (IR) fluxes (Table 5.1) using the conversions of Kennicutt (1998). The radio SFR ($M_\odot$ yr^{-1}) was calculated from the radio luminosity $L_{1.4\,\mathrm{GHz}}$ (erg s^{-1} Hz^{-1}) using the method proposed

[3] `http://adlibitum.oat.ts.astro.it/silva/default.html`.
[4] The SED fits can be downloaded from `http://archive.dark-cosmology.dk`

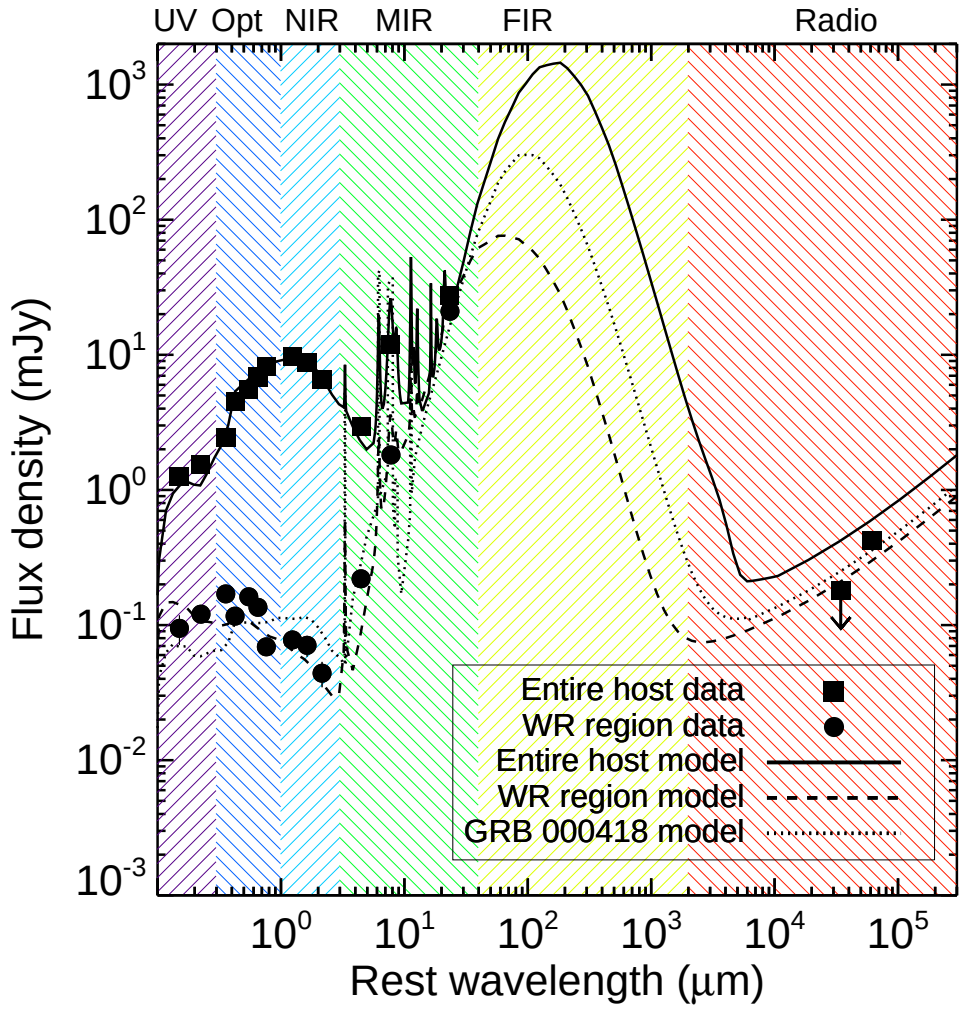

Figure 5.3: *Spectral energy distribution of ESO 184-G82, the host of GRB 980425 / SN 1998bw, compared to the model corresponding to the host of GRB 000418 (Michałowski et al., 2008). Solid line: spiral galaxy model (entire host). Dashed line: young starburst model (WR region). Both models have been calculated using GRASIL (Silva et al., 1998) by Iglesias-Páramo et al. (2007). Dotted line: model based on the host of GRB 000418 from Michałowski et al. (2008) (slightly modified; see Section 5.5.3). Squares and circles: detections of the host galaxy and the WR region, respectively, with errors, in most cases, smaller than the size of the symbols. Arrow: 3σ upper limit (values marked at the base). The hashed columns mark the wavelength ranges corresponding to the UV, optical, near-IR, mid-IR, far-IR, and radio domains. For a discussion of the discrepancy between the data and models at radio wavelengths see Section 5.5.2.*

by Bell (2003):

$$\mathrm{SFR} = \begin{cases} 5.52 \times 10^{-29} L_{1.4\,\mathrm{GHz}} & L_{1.4\,\mathrm{GHz}} > L_c \\ \dfrac{5.52 \times 10^{-29} L_{1.4\,\mathrm{GHz}}}{0.1 + 0.9 (L_{1.4\,\mathrm{GHz}}/L_c)^{0.3}} & L_{1.4\,\mathrm{GHz}} < L_c, \end{cases} \tag{5.1}$$

where $L_c = 6.4 \times 10^{28}$ erg s^{-1} Hz^{-1} is a critical luminosity (see below). This relation was derived based on a sample of 249 galaxies spanning a wide range in luminosities including normal and intensely star-forming galaxies, starbursts, ultraluminous IR galaxies and blue compact dwarfs. The luminosity at the rest frequency of 1.4 GHz, $L_{1.4\,\mathrm{GHz}}$ (erg s^{-1} Hz^{-1}), of a galaxy at redshift z and luminosity distance D_L (cm), can be calculated from the flux density F_ν (Jy) at the observed radio frequency ν_{obs} (GHz) assuming the radio spectral slope $\alpha = -0.75$ (Yun & Carilli, 2002):

$$L_{1.4\,\mathrm{GHz}} = \frac{4\pi \times 10^{-23} D_L^2 F_\nu}{1+z} \times \left[\frac{\nu_{\mathrm{obs}}(1+z)}{1.4}\right]^{-\alpha}. \tag{5.2}$$

This relation (Equation (5.1)) diverges significantly from the usual methods (Condon, 1992; Yun & Carilli, 2002) for low-luminosity galaxies, because the nonthermal radio emission is not effective in such galaxies and the relation between SFR and radio luminosity becomes nonlinear below L_c (SFR $\lesssim 3\,M_\odot$ yr^{-1}). This effect is likely caused either by the fact that cosmic-ray electrons responsible for the radio emission escape from galaxies of small sizes (Bell, 2003) or that the ordered magnetic field in dwarf galaxies is weaker and therefore magnetic field due to SNe (responsible for acceleration of electrons) is less efficient because it results from contraction and amplification of the global field.

The SFR derived from SED modeling (Column 4 of Table 5.2) agrees (within a factor of 2) with the estimates derived from UV, IR, and radio for the entire galaxy, suggesting little extinction (see also Section 5.4.3). All the estimates are also consistent with the X-ray SFR upper limit of $2.8\,M_\odot$ yr^{-1} derived by Watson et al. (2004).

As noted by Le Floc'h et al. (2006) the contribution of the WR region to the galaxy luminosity at 24 μm is $\sim 75\%$ (see Table 5.1 and Figure 5.3). However, according to our SED fit, it only emits 15% of the total IR luminosity (it would require high-resolution far-IR or submillimeter imaging to confirm this result). Under the assumption that the total IR luminosity is proportional to the SFR (Kennicutt, 1998), this is consistent within a factor of 2 with the finding of Sollerman et al. (2005) and Christensen et al. (2008) that the WR region harbors about one-third of the host star formation (as also suggested by the SFRs derived directly from SED fits, see Column 4 of Table 5.2).

5.4.3 Dust Properties

We derived the dust temperature by fitting a graybody curve to the model SED near the dust peak (as in Michałowski et al., 2008). The dust in the WR region is much hotter than the average over the entire galaxy (see Column 11 of Table 5.2 and note on Figure 5.3 that the SED of the WR region peaks at shorter wavelengths than that of the entire galaxy). This hints at a very intense starburst episode and a strong radiation field, consistent with the discussion in Section 5.4.1. High dust temperatures are not uncommon for GRB hosts. They were found for higher-redshift ($z = 0.9$–1.5) GRBs with similar conclusions about their origin (Michałowski et al., 2008). Moreover, Bloom et al. (2003) and Djorgovski et al. (2001) noted that high flux ratios between the [Ne 3] and [O 2] lines in GRB hosts suggest the presence of very hot H 2 regions.

The total dust mass, M_d, was estimated using the method of Taylor et al. (2005) based on the formalism developed by Hildebrand (1983):

$$M_d = \frac{F_\nu D_L^2}{(1+z)\kappa(\nu_r)B(\nu_r, T)}, \tag{5.3}$$

where F_ν is the flux density (either observed or interpolated from an SED model) at the rest frequency dominated by dust thermal emission ($200\,\mathrm{GHz} \lesssim \nu_r \lesssim 5000\,\mathrm{GHz}$), $B(\nu_r, T)$ is the

Planck function, T is dust temperature, κ is the mass absorption coefficient

$$\kappa(\nu_r) = 0.067 \left[\frac{\nu_r\,(\mathrm{GHz})}{250}\right]^{\beta} \quad \mathrm{m^2\,kg^{-1}} \tag{5.4}$$

and β is the emissivity index. Equations (5.3) and (5.4) can be combined into the following easy-to-use formula where the resulting dust mass M_d ($M_\odot$) is computed from the quantities in the following units: F_ν (Jy), D_L (cm), $\nu_{\rm obs}$ (GHz), and T (K):

$$M_d = 3.24 \times 10^{-44} \frac{F_\nu D_L^2 \left\{\exp\left[\frac{0.048\nu_{\rm obs}(1+z)}{T}\right] - 1\right\}}{(1+z)\left[\frac{\nu_{\rm obs}(1+z)}{250}\right]^{\beta+3}}. \tag{5.5}$$

We estimated the flux at $450\ \mu$m from the SED models. The results of dust masses are given in Column 10 of Table 5.2 assuming $\beta = 1.3$. There exists a degeneracy between the value of this parameter and resulting dust mass in a way that more dust is expected if lower β is assumed. The uncertainties quoted in Table 5.2 are large, because we allowed a broad range of β ($0 - 2$; Yun & Carilli, 2002).

Hatsukade et al. (2007) derived an upper limit on the molecular mass of the host of GRB 980425 $M_{\rm H_2} < 3 \times 10^8\,M_\odot$. Therefore from our dust mass estimate we derive a molecular gas-to-dust ratio $M_{\rm H_2}/M_d < 107$. This value is lower than the molecular gas-to-dust ratio for the Milky Way ($\sim 140-400$; Sodroski et al., 1997; Draine et al., 2007) and other spirals ($\sim 1000 \pm 500$; Devereux & Young, 1990; Stevens et al., 2005), but consistent with the values for high-redshift submillimeter galaxies (54^{+14}_{-11}; Kovács et al., 2006), and for the nuclear regions of local luminous IR galaxies (LIRGs), ultraluminous IR galaxies (ULIRGs) (120 ± 28; Wilson et al., 2008) and of local, far-IR-selected galaxies (~ 50; Seaquist et al., 2004). It indicates that the host of GRB 980425 harbors a relatively large amount of dust, or that its gas reservoir is significantly depleted. However this conclusion is based on an uncertain dust mass estimate, so should be checked with deep submillimeter observations.

Our SED fits are consistent with negligible extinction for both the entire galaxy and the WR region (Column 13 of Table 5.2). Very low reddening for the entire galaxy was also found by Patat et al. (2001) and Sollerman et al. (2005) from the width of the Na 1 D doublet and SED fitting, respectively. On the other hand, using the Balmer decrement, Savaglio et al. (2009) and Christensen et al. (2008) derived $A_{\rm V} = 1.73$ and 0.93, respectively, for the entire galaxy, whereas Hammer et al. (2006) and Christensen et al. (2008) obtained $A_{\rm V} = 1.51$ and 0.53, respectively, for the WR region. However, extinction derived from emission lines of the H 2 regions is usually higher than from the SED modeling (Savaglio et al., 2009).

5.5 Discussion

5.5.1 The Host Galaxy

From the SED modeling it is apparent that ESO 184-G82, the host galaxy of GRB 980425 / SN 1998bw, is a normal dwarf star-forming spiral. None of its properties (Table 5.2) are exceptionally high or low. In particular its mass, SFR, and size are broadly consistent with the range obtained for a sample of local dwarf galaxies (Fiigures 5 and 17 of Woo et al., 2008, in this respect ESO 184-G82 is very similar to the Large Magellanic Cloud) and for a sample of local blue compact galaxies (Figure 2 of Sollerman et al., 2005).

Its specific SFR ($\phi \equiv \mathrm{SFR}/M_* = 0.23\,\mathrm{Gyr^{-1}}$) is consistent with the range of ϕ found for other GRB hosts by Castro Cerón et al. (2009) based on UV (but lower than for a subsample detected

in mid-IR; Castro Cerón et al., 2006). However its ϕ is higher than for the majority of nearby spiral galaxies hosting SNe (see Figure 8 of Thöne et al., 2009). High ϕ for other GRB hosts were also reported by, e.g., Christensen et al. (2004) and predicted theoretically by Courty et al. (2004, 2007) and Lapi et al. (2008). This is in agreement with the finding of Iglesias-Páramo et al. (2006, 2007) and Zheng et al. (2007) that low-mass galaxies in general have high ϕ.

As stated in Section 5.4.1, the SED of ESO 184-G82 is consistent with being of a nonstarburst nature. This is also supported by its stellar building time ($T_{\rm SFR} \equiv \phi^{-1} = 4$ Gyr) being not much less than the Hubble time and low SFR per unit area equal to $0.004\,M_{\odot}$ yr^{-1} kpc^{-2} (see the relevant discussion in Heckman, 2005).

ESO 184-G82 is the only GRB host with a clear $\sim 1.6\,\mu$m bump in the SED (compare Figure 5.3 with Figure 4 of Savaglio et al., 2009). According to Sawicki (2002) this feature starts to be apparent for a galaxy older than 100 Myr (see his Figure 1). The preference of not having the bump for other GRB hosts likely indicates that on average they are very young galaxies, although we stress that in many cases the optical and near-IR data presented by Savaglio et al. (2009) do not cover the wavelengths into where the bump is redshifted.

5.5.2 Radio Detection

The SED model presented in Figure 5.3 (solid line) overpredicts the radio fluxes by a factor of 1.5 (> 2.3) in the 6 (3) cm band. We suggest that this may result from the following effect. Radio wavelengths probe current star formation activity ($\lesssim 10^8$ yr; Condon, 1992; Cannon & Skillman, 2004), unlike UV (Kennicutt, 1998; Christensen et al., 2004) and IR (Calzetti et al., 2007), at which even older galaxies can be luminous. Therefore it seems likely that only a limited part of the galaxy is younger than 10^8 yr, so the galaxy is fainter in radio than its UV and IR fluxes would imply. This is supported by Sollerman et al. (2005) who noticed that the colors of the GRB 980425 host are consistent with a constant SFR over 5–7 Gyr without any starburst episode. Therefore if we assume that the IR probes the total SFR, then the radio data point would be a factor of ~ 2 ($\approx {\rm SFR_{IR}/SFR_{radio}}$) higher if the radio were also sensitive to star formation older than 10^8 yr.

We calculated the radio spectral index α defined as $F_{\nu} \propto \nu^{\alpha}$, so $\alpha_{\nu_1}^{\nu_2} = \log[F_{\nu}(\nu_2)/F_{\nu}(\nu_1)]/\log(\nu_2/\nu_1)$. The radio SED of ESO 184-G82 (see Table 5.1) is very steep with $\alpha_{4.8}^{8.64} < -1.44$. This is consistent with the steepest slopes in the sample of ULIRGs discussed by Clemens et al. (2008) and interpreted as an indication of spectral aging of relativistic electrons (the lifetime of high-energy electrons emitting high-frequency radiation is shorter than for low-energy electrons). The same conclusion is drawn by Hirashita & Hunt (2006) who predicted a steepening of the radio slope ~ 10 Myr after a starburst when synchrotron radiation starts to dominate over free-free emission from H 2 regions (see also Bressan et al., 2002; Cannon & Skillman, 2004). In summary, such a steep radio slope indicates that the bulk of star formation activity in the host of GRB 980425 is not recent.

As mentioned in Section 5.4.2 the radio SFR for dwarf galaxies can underpredict the true value if derived using usual methods. Since GRB hosts are in general subluminous at all wavelengths (Hogg & Fruchter, 1999; Hanlon et al., 2000; Hjorth et al., 2000, 2002; Vreeswijk et al., 2001b; Fynbo et al., 2002, 2003, 2006b; Berger et al., 2003a; Le Floc'h et al., 2003, 2006; Christensen et al., 2004; Courty et al., 2004; Tanvir et al., 2004, 2008; Jakobsson et al., 2005; Sollerman et al., 2005, 2006; Fruchter et al., 2006; Priddey et al., 2006; Chary et al., 2007; Ovaldsen et al., 2007; Thöne et al., 2007a; Wiersema et al., 2007; Castro Cerón et al., 2009; Savaglio et al., 2009) we suggest that the Bell (2003) relation (Equation (5.1)) should be used to calculate their radio SFRs. Indeed, in the case of the host of GRB 980425, one would get a value of $0.068\,M_{\odot}$ yr^{-1} using the

method of Yun & Carilli (2002), a value much smaller than the UV SFR. The radio luminosity is supposed to trace both unobscured and obscured SFRs (because radio is not affected by dust), so such a low value is clearly an underestimation of the true SFR. The relation of Bell (2003) is however not necessary (but gives reasonable results) for the high-luminosity subsample of GRB hosts where usual methods result in radio SFRs consistent with other diagnostics (see Table 1 of Michałowski & Hjorth, 2007).

5.5.3 WR Region

The WR region emits 7% of the host's UV flux. Its contribution falls to below 1% in the near-IR and rises steeply to 75% in the mid-IR. As mentioned in Sections 5.4.1 and 5.4.3, an intense starburst episode together with low stellar mass provide a consistent explanation of the shape of the SED. Indeed our SED fit suggests that the WR region harbors as much as 12–26% of the total star formation activity, but its contribution to the galaxy stellar and dust masses is negligible (see Columns 8 and 10 of Table 5.2).

The ϕ of the WR region is 22 Gyr^{-1}. High ϕ in the immediate environment of GRBs was also found by Thöne et al. (2008, see their Figure 4; the spatial resolution was 3 kpc in this case) and is consistent with the findings of Fruchter et al. (2006). We stress that we do not claim here that GRB 980425 is physically connected with the WR region, just that it occurred in the most intense star-forming part of the galaxy (note in Figure 5.2 that the Southern spiral arm is the only part of the galaxy where X-ray point sources are found, indicative of intense star formation; Kouveliotou et al., 2004). Because of the proximity of the SN region to the WR region, it is very likely that their star formation was triggered by the same mechanism and therefore that the nature of their star formation is similar.

The starburst nature of the WR region is confirmed by its stellar building time ($T_{\rm SFR} = 57$ Myr) being much less than the Hubble time, and its very high SFR per unit area equal to $6\,M_{\odot}$ yr^{-1} kpc^{-2} (Heckman, 2005).

It is worth noting that the SED of the WR region is qualitatively similar to the SEDs presented by Michałowski et al. (2008) for submillimeter/radio-bright GRB hosts: blue in the optical, luminous in the mid-IR, and indicating hot dust content. The similarities are highlighted in Figure 5.3 where the WR region model (dashed line) and the model corresponding to GRB 000418 (dotted line) are compared. The agreement is striking, but note that in order to suppress the very high IR luminosity of the host of GRB 000418, we needed to modify the SED model presented by Michałowski et al. (2008) by changing the escape parameter from 50 to 10 Myr (the time after which stars begin to escape from molecular clouds; see Panuzzo et al., 2007, for a discussion of this parameter).

The WR region was also found to be similar to high-z GRB hosts with respect to emission line ratios (indicative of age and metallicity), unlike the entire host galaxy ESO 184-G82, which appears to be older than other GRB hosts (Christensen et al., 2008).

The picture that emerges from these findings is that the $\sim$1–3 kpc scale environment of a GRB represents the youngest and most intensely star-forming region of a host galaxy, harboring the hottest dust. If present at high redshifts such regions may dominate the emission (and therefore, derived properties) of distant GRB hosts.

5.6 CONCLUSIONS

In this chapter we have presented the UV-to-radio SED fitting of the host galaxy of GRB 980425 / SN 1998bw and of the WR region close to the SN position.

The host galaxy of GRB 980425 is a normal dwarf spiral galaxy with somewhat elevated star formation activity compared to other spirals (though it is not necessary to invoke any starburst episode to explain its SED). The steep radio slope and the presence of the $\sim 1.6\,\mu$m bump in the SED indicate the existence of an old stellar population. Its low radio luminosity can be explained by the suppression of synchrotron emission in dwarf galaxies and the fact that radio is only sensitive to recent star formation.

The emission of the WR region close to the GRB position is dominated by an ongoing starburst episode, during which almost all of its stars were formed. It contributes significantly to the star formation of the entire galaxy. In many aspects the WR region is similar to high-redshift GRB hosts: it is a blue, young region of intense star formation containing hot dust. The presence of the GRB close to this region indicates that GRBs appear to be associated with regions of high specific SFR and high dust temperatures.

Acknowledgements

We thank Joanna Baradziej, Eelco van Kampen, Robin Wark, Mark Wieringa for discussion and comments; our referee Sandra Savaglio for help in improving this paper; Jorge Iglesias-Páramo for kindly providing his SED templates; Naomi McClure-Griffiths for help with ATCA observations; Paul M. Vreeswijk, Jesper Sollerman, Ferdinando Patat, and Chris Lidman for providing the reduced optical and near-infrared images; Andreas O. Jaunsen for help on the data reduction; and Laura Silva for making the GRASIL code available.

The Dark Cosmology Centre is funded by the Danish National Research Foundation. M. J. M. would like to acknowledge support from The Faculty of Science, University of Copenhagen. J. M. C. C. gratefully acknowledges support from the Instrumentcenter for Dansk Astrofysik and the Niels Bohr Institutet's International PhD School of Excellence. The Australia Telescope Compact Array is part of the Australia Telescope which is funded by the Commonwealth of Australia for operation as a National Facility managed by CSIRO. The authors acknowledge the data analysis facilities provided by the Starlink Project which is run by CCLRC on behalf of PPARC. This research has made use of the NASA's Astrophysics Data System; the GHostS database (`http://www.grbhosts.org/`*), which is partly funded by Spitzer/NASA grant RSA Agreement No. 1287913; the Gamma-Ray Burst Afterglows site (*`http://www.mpe.mpg.de/~jcg/grb.html`*), which is maintained by Jochen Greiner; IRAF, distributed by the National Optical Astronomy Observatories, which are operated by the Association of Universities for Research in Astronomy, Inc., under cooperative agreement with the National Science Foundation; the NASA/IPAC Extragalactic Database (NED) which is operated by the Jet Propulsion Laboratory, California Institute of Technology, under contract with the National Aeronautics and Space Administration; and SAOImage DS9, developed by Smithsonian Astrophysical Observatory.* Galaxy Evolution Explorer *(*GALEX *) is a NASA Small Explorer, launched in 2003 April. We gratefully acknowledge NASA's support for construction, operation, and science analysis for the* GALEX *mission, developed in cooperation with the Centre National d'Etudes Spatiales of France and the Korean Ministry of Science and Technology.*

Published as: Michałowski, M. J., Hjorth, J., & Watson, D. – *Cosmic evolution of submillimeter galaxies and their contribution to stellar mass assembly* Monthly Notices of the Royal Astronomical Society, submitted, arXiv:0905.4499.

6

COSMIC EVOLUTION OF SUBMILLIMETER GALAXIES

ABSTRACT –

The nature of galaxies selected at submillimeter wavelengths (SMGs, $S_{850} \gtrsim 3$ mJy), some of the bolometrically most luminous objects at high redshifts, is still elusive. In particular their star formation histories and source of emission are not accurately constrained. In this chapter we introduce a new approach to analyse the SMG data. Namely, we present the first self-consistent UV-to-radio spectral energy distribution fits of 76 SMGs with spectroscopic redshifts using all photometric datapoints from ultraviolet to radio simultaneously. We find that they are highly star-forming (median star formation rate $659\,M_{\odot}\ yr^{-1}$), moderately dust-obscured (median $A_V \sim 2$ mag), hosting significant stellar populations (median stellar mass $3.5 \times 10^{11}\,M_{\odot}$) of which only a minor part (7%) has been formed in the ongoing starburst episode. This implies that in the past, SMGs experienced either another starburst episode or merger with several galaxies. The properties of SMGs suggest that they are progenitors of present-day elliptical galaxies. We find that these bright SMGs contribute significantly to the cosmic star formation rate density ($\sim 20\%$) and stellar mass density ($\sim$ 30–50%) at redshifts 2–4. Using number counts at low fluxes we find that as much as 80% of the cosmic star formation at these redshifts took place in SMGs brighter than 0.1 mJy. We find evidence that a linear infrared-radio correlation holds for SMGs in an unchanged form up to redshift of 3.6, though its normalization is offset from the local relation by a factor of ~ 2.3 towards higher radio luminosities. We present a compilation of photometry data of SMGs and determinations of cosmic SFR and stellar mass densities.

6.1 INTRODUCTION

Submillimeter galaxies (SMGs; see Blain et al., 2002) were discovered at $850\,\mu$m ($S_{850} \gtrsim 3$ mJy) by the Submillimetre Common-User Bolometer Array (SCUBA; Holland et al., 1999) mounted on the James Clerk Maxwell Telescope (JCMT). Due to the coarse resolution of SCUBA, localizations derived from high-resolution radio maps had to be used to measure their spectroscopic redshifts (Chapman et al., 2005). Lots of studies have addressed the issue of characterizing the nature of SMGs (Egami et al., 2004; Greve et al., 2004, 2005; Smail et al., 2004; Swinbank et al., 2004, 2006, 2008; Takagi et al., 2004; Alexander et al., 2005; Borys et al., 2005; Kovács et al., 2006; Laurent et al., 2006; Pope et al., 2006; Tacconi et al., 2006, 2008; Takata et al., 2006; Younger et al., 2007, 2008b, 2009a; Clements et al., 2008; Coppin et al., 2008; Dye et al., 2008, 2009; Hainline, 2008; Hainline et al., 2009; Perera et al., 2008; Scott et al., 2008; Austermann et al., 2009; Devlin et al., 2009; Eales et al., 2009; Murphy et al., 2009; Murphy, 2009; Tamura et al., 2009). However they were usually based on limited samples ($\lesssim$ 20 sources), limited wavelength coverage or

photometric redshifts. These limitations have made it difficult to solve several issues, including the characterization of the star formation histories of SMGs and their dominant source of emission.

An important open question concerns the contribution of SMGs to cosmic stellar mass assembly. This is important, because in order to understand galaxy evolution, the build-up of stellar mass must be mapped out to high redshifts. It is usually parametrized by the total star formation rate (SFR) density per unit comoving volume, ($\rho_{\rm SFR}$; see e.g. Hopkins, 2004; Hopkins & Beacom, 2006). At high redshifts it is difficult to disentangle the contribution to $\rho_{\rm SFR}$ from galaxy populations of different masses due to incompleteness at low luminosities.

Another approach to study stellar mass assembly is to consider directly the stellar mass density per unit comoving volume, ρ_*, which is equivalent to the integrated $\rho_{\rm SFR}$ over the age of the Universe. It is established that ρ_* grows with cosmic time (stellar mass is accumulating; Drory et al., 2005; Fontana et al., 2006; Elsner et al., 2008; Pérez-González et al., 2008; Marchesini et al., 2009), but the contribution from different galaxy populations is not well-determined. *Spitzer* observations of SMGs (Egami et al., 2004; Frayer et al., 2004; Ivison et al., 2004; Borys et al., 2005; Ashby et al., 2006; Laurent et al., 2006; Pope et al., 2006; Dye et al., 2008; Hainline, 2008; Hainline et al., 2009) have enabled studies of the rest-frame near-infrared (near-IR) part of the spectrum, where old stellar populations are dominant – an important step forward in getting full spectral energy distributions and accurate estimates of stellar masses of SMGs. The results indicate that SMGs are among the most massive galaxies in the Universe.

The dominant source of emission from SMGs is dust reprocessed emission either from young stars or active galactic nuclei (AGNs). One way to test it is to compare the infrared (IR) and radio luminosities of SMGs, because, at least locally, star-forming galaxies follow a remarkably tight correlation between IR and radio luminosities (Helou et al., 1985; Condon, 1992). The correlation is believed to result from the fact that both IR and radio emissions are related to short-lived massive stars: the former originates from dust heated by ultraviolet (UV) light from blue, massive stars and the latter from synchrotron emission of electrons produced in supernova remnants. Therefore, a relation consistent with the local one is an indication of star formation dominating both the IR and radio emissions. There is growing evidence that the correlation holds at redshifts $z \lesssim 1$ (Garrett, 2002; Gruppioni et al., 2003; Appleton et al., 2004; Boyle et al., 2007; Marleau et al., 2007; Vlahakis et al., 2007; Yang et al., 2007). At higher redshifts sample sizes are small making it difficult to draw robust conclusions (Appleton et al., 2004; Kovács et al., 2006; Beswick et al., 2008; Ibar et al., 2008; Sajina et al., 2008; Garn et al., 2009; Murphy et al., 2009; Murphy, 2009; Rieke et al., 2009; Seymour et al., 2009; Younger et al., 2009b). The only sign of evolution was reported by Ivison et al. (2009) based on stacking analysis of the $24\,\mu$m-selected galaxies, though possibly interpreted as a selection effect.

The objectives of this chapter is to model for the first time the entire UV-to-radio spectral energy distributions of a statistically significant sample of SMGs in a self-consistent way. Using these models we *i*) consistently derive the properties of a statistically significant sample of SMGs using all available data to characterize their nature and determine the dominant emission mechanism; *ii*) estimate the contribution of SMGs to the cosmic SFR and stellar mass densities; *iii*) investigate whether the local IR-radio correlation holds at high redshifts in an unchanged form. In Section 6.2 our SMG sample is presented. Our methodology is outlined in Section 6.3. We derive the properties of SMGs in Section 6.4 and discuss the implications in Section 6.5. Section 6.6 closes with our conclusions. We use a cosmological model with $H_0 = 70$ km s^{-1} Mpc^{-1}, $\Omega_\Lambda = 0.7$ and $\Omega_m = 0.3$.

6.2 SAMPLE

We base our analysis on 76 SMGs ($S_{850} \gtrsim 3$ mJy) from the sample of Chapman et al. (2005), all with spectroscopically measured redshifts spanning a range of 0.080–3.623.

The way the sample is selected involves complex biases, which are difficult to fully quantify and account for. The parent sample of Chapman et al. (2005) consists of 150 SMGs out of which 104 have radio identifications. The sample discussed here (76 galaxies) consists of the SMGs for which redshifts have been measured (spectroscopic completeness $\sim 75\%$). All this implies that the sample is biased against: *i*) faint submillimeter emitters (low dust content and/or hot dust, influence mostly the low-z portion of the sample); *ii*) faint radio emitters (high-z and cold dust, see Figure 3 of Chapman et al., 2005); *iii*) faint optical emitters (difficult to obtain spectra); *iv*) $z \sim 1.2$–1.8 ("redshift desert" where no emission lines enter the observable wavelengths). At low redshifts ($z < 1$) the sample may also be incomplete due to a limited sky area (and therefore – volume) coverage making it difficult to detect rare strong submillimeter emitters (for details on the SMG selection effects see also Figure 2 of Blain et al. (2004) and discussion in Section 4.4 of Michałowski et al. (2008)).

It is important to estimate what the influence of these selection effects on our results is. In total we analyse $\sim 50\%$ (76/150) of the parent sample. Additionally, 25 radio-detected SMGs without spectroscopic redshifts have similar long-wavelength properties compared to the redshift sample (see Figure 1 of Chapman et al., 2005), so their absence from the sample probably does not significantly bias our results. The same is true for the SMGs in the "redshift desert", since they are missed not due to their inherent properties. The remaining 46 radio-nondetected SMGs ($\sim 30\%$) could in principle have very different properties than our sample resulting in a potential limitation in our analysis.

Even if most of the SMGs without spectroscopic redshifts are similar to those in our sample, the incompleteness at $z < 1.8$ implies that the estimates of SMG densities (Sections 6.5.3 and 6.5.2) in the two low-redshift bins (see Section 6.3.2) are strict lower limits.

The photometric datapoints (see Tables 2 and 3 in Michałowski et al., 2009b) were collected from the literature: Ivison et al. (2002, IK, radio), Ivison et al. (2005, R, 1.2 mm), Chapman et al. (2003c, VI), Chapman et al. (2005, BR, $850\,\mu$m, radio), Capak et al. (2004, $UBVRIzHK$), Clements et al. (2004, $UBVIK$), Egami et al. (2004, $24\,\mu$m), Greve et al. (2004, 1.2 mm), Smail et al. (2004, IJK), Fomalont et al. (2006, Rz), Kovács et al. (2006, $350\,\mu$m, 1.2 mm), Laurent et al. (2006, $350\,\mu$m, 1.1 mm), Tacconi et al. (2006, 1.3 mm), Pope et al. (2006, R, $24\,\mu$m), Huynh et al. (2007, $160\,\mu$m), Hainline (2008, $3.6, 4.8, 5.6, 8.0, 24, 70\,\mu$m).

6.3 METHODOLOGY

6.3.1 SED MODELING

In order to model the spectral energy distributions (SEDs) of SMGs, we use all the photometric datapoints simultaneously. This has the advantage that all the galaxy properties are derived consistently regardless of the wavelength regime in which those properties shape the SEDs (for example, recent star formation governs the UV and far-IR parts of a spectrum of a galaxy, whereas accumulated stellar mass is responsible for near-IR emission). Moreover in the full SED modeling no single datapoint drives the fit alone.

We utilized the set of 35 000 models from Iglesias-Páramo et al. (2007) developed in GRASIL (Silva et al., 1998)[1] based on numerical calculations of radiative transfer within a galaxy. They

[1] http://adlibitum.oat.ts.astro.it/silva/default.html

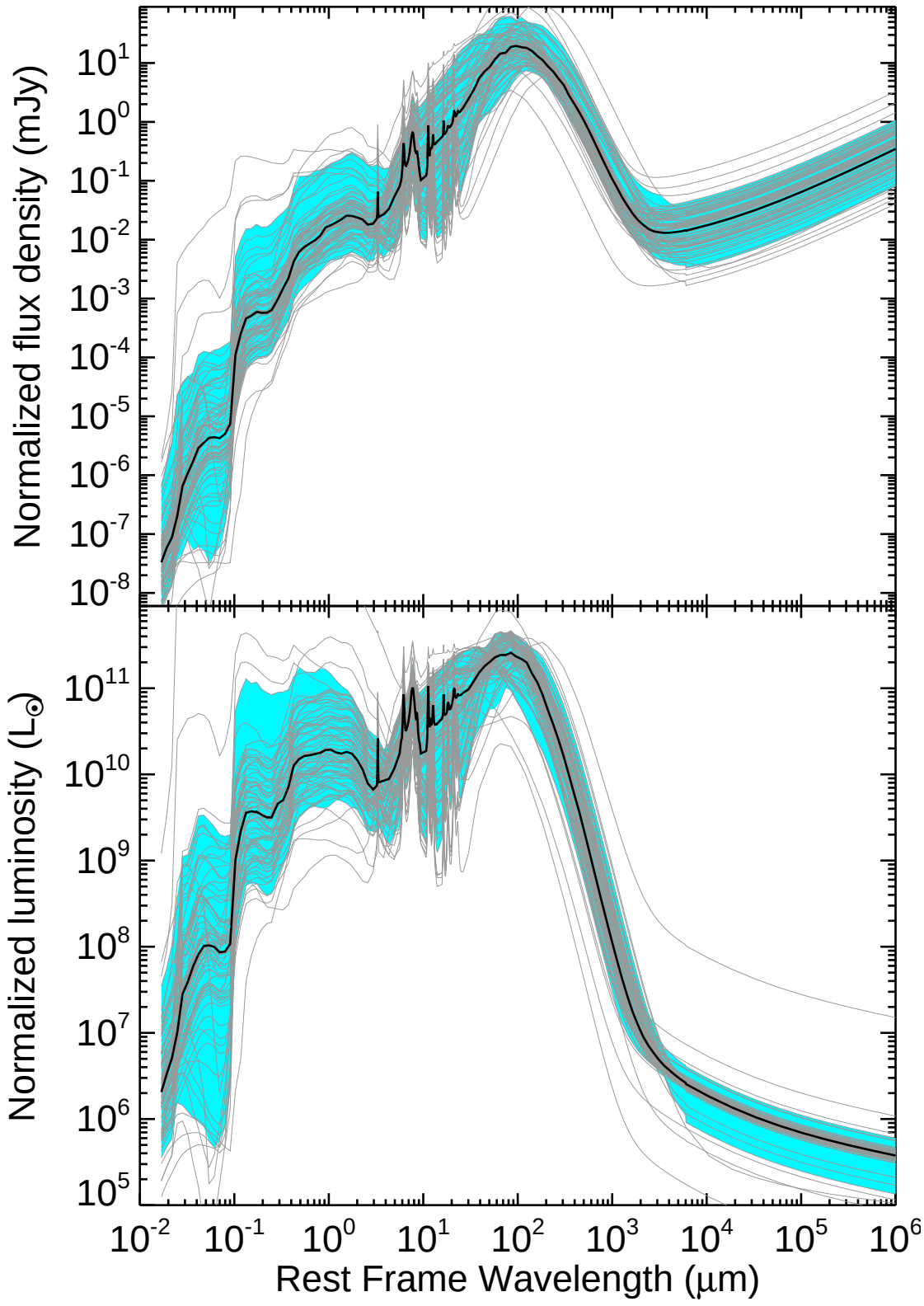

Figure 6.1: *Median spectral energy distribution (SED) of SMGs (thick lines) and SEDs of individual SMGs (thin lines). Shaded areas enclose* 90% *of the SEDs. Top: all SEDs were divided by the corresponding* 850 μm *datapoint and scaled, so that the median SED has a flux of* 5 *mJy at the rest-frame* 283 μm *(observed* 850 μm *at* $z = 2$*). Bottom: SEDs were normalized to an infrared star formation rate of* 100 $M_\odot\ yr^{-1}$.

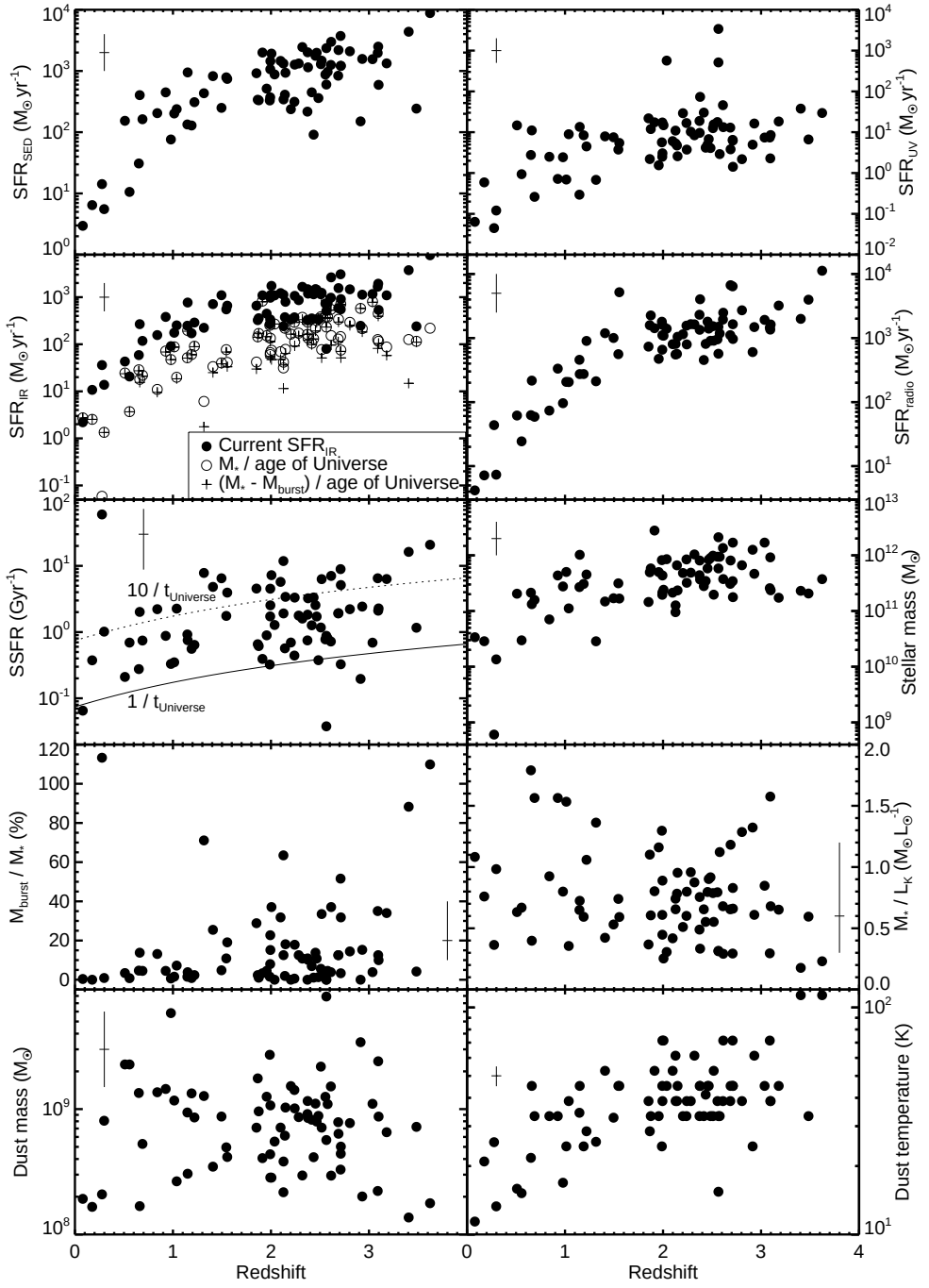

Figure 6.2: *Redshift evolution of the properties (full circles, see Table 6.2) of the sample of 76 SMGs with spectroscopic redshifts (Chapman et al., 2005). Typical errors (Section 6.4) are shown as crosses. From top-left to bottom-right: star formation rate (SFR) derived from spectral energy distribution modeling, ultraviolet, infrared and radio emission, SFR per unit stellar mass ($\equiv SFR_{\rm IR}/M_*$), stellar mass, fraction of stellar population formed during the ongoing starburst, stellar mass-to-light ratio, dust mass and temperature. In the $SFR_{\rm IR}$ panel, we also show the minimum average SFRs (see Section 6.5.2) required to build up the total stellar mass within the age of the Universe at a given redshift (empty circles) and to build up the fraction of stellar population that was not formed during the ongoing starburst (plus signs). The location of plus signs indicates that SMGs must have been highly star-forming even before the onset of the ongoing starburst. When empty circles and plus signs overlap, the contribution of the ongoing starburst to the total stellar mass of a galaxy is negligible (i.e. $M_{\rm burst}/M_* \sim 0$).*

cover a broad range of galaxy properties from quiescent to starburst. Their star formation histories are assumed to be a smooth Schmidt-type law (SFR proportional to the gas mass to some power, see Silva et al., 1998, for details) with a starburst (if any) on top of that starting 50 Myr ago. Additionally we fitted templates based on nearby galaxies (Silva et al., 1998) and gamma-ray burst host galaxies (Michałowski et al., 2008). We simultaneously used all the photometric datapoints from UV to radio. In cases where the data given by different authors were contradictory, we disregarded the obvious outliers. We scaled the SEDs to match the data and chose the one with the lowest χ^2.

Based on the best fits we derived the properties of the galaxies as explained in Michałowski et al. (2008, 2009a). In particular, SFRs, stellar (M_*) and starburst ($M_{\rm burst}$) masses were given as output from GRASIL, infrared (IR) and rest-frame K luminosities ($L_{\rm IR}$ and L_K), UV and IR SFRs ($\rm SFR_{IR}$ was adopted for all subsequent calculations, because $\rm SFR_{UV}$ is on average two orders of magnitude lower) were estimated from the SEDs (using Kennicutt, 1998), dust masses (M_d) were calculated from the 850 μm detections using equation (5) of Michałowski et al. (2009a) and radio SFRs were calculated from the 20 cm detections using the empirical formula of Bell (2003) (see Section 4.2 of Michałowski et al., 2009a). Dust temperatures (T_d) were estimated by identifying the peak of the dust emission and assuming an emissivity index $\beta = 1.3$. The average extinction in the rest-frame V-band was calculated from the unextinguished starlight given in GRASIL: $A_V = 2.5 \log$(unextinguished V-band starlight / observed V-band starlight). IR-radio correlation parameters were calculated according to the formula $q = \log(L_{\rm IR}/3.75 \times 10^{12}/I_{1.4})$, where $I_{1.4}$ is a rest-frame 1.4 GHz luminosity density computed from the observed 1.4 GHz flux assuming a spectral slope of -0.75.

6.3.2 VOLUME DENSITIES

In order to calculate the SFR density, the stellar density and the dust mass densities per unit comoving volume, $\rho_{\rm SFR}$, ρ_* and $\rho_{\rm dust}$, we used the following angular areas for the submillimeter surveys (Table 1 of Chapman et al., 2005): CFRS-03: 60 arcmin^2 and CFRS-14: 48 arcmin^2 (Webb et al., 2003b), Lockman Hole: 122 arcmin^2 and ELAIS-N2: 102 arcmin^2 (Scott et al., 2002), HDF-N: 100 arcmin^2 (Chapman et al., 2001), SSA-13 and SSA-22: 100 arcmin^2 each (Chapman et al., 2003a), totaling 632 arcmin^2.

We divided our sample into four redshift bins (Table 6.1) containing the same number of SMGs (19). The densities in each bin were calculated as a sum of $\rm SFR_{IR}$ (or M_*, or M_d) of all SMGs in this bin divided by its comoving volume (a similar approach to calculate the SFR and number volume densities of SMGs was taken by Coppin et al., 2009; Daddi et al., 2009b; Younger et al., 2009a; Wang et al., 2009). The volume densities (Column 2) were found using the total area from the previous paragraph.

We removed the contribution of ten SMGs[2], which were observed by SCUBA in the photometry mode targeting optically-faint radio galaxies (Chapman et al., 2005). These objects fall outside the fields discussed here.

The method is therefore to analyse the fraction of the sky observed by SCUBA and estimate the number of SMGs and their volume densities. However, the true number of SMGs in our fields could be higher. On the other hand, regardless of the selection effects, the true number of SMGs in our fields cannot be lower than the number of SMGs in our sample. In turn, the true values of SFR and M_* densities cannot be lower than the values we derive. Therefore our

[2]SMMJ123553.26+621337.7, SMMJ123555.14+620901.7, SMMJ123600.10+620253.5, SMMJ123600.15+621047.2, SMMJ123606.85+621021.4, SMMJ123716.01+620323.3, SMMJ163706.51+405313.8, SMMJ221804.42+002154.4, SMMJ221806.77+001245.7

results on volume densities should be regarded as robust lower limits.

Having this in mind we note that the parent sample of Chapman et al. (2005) includes only 29% of all the SMGs detected in the used survey fields (compare with Scott et al., 2002; Webb et al., 2003b,a). Therefore the estimated densities are conservative lower limits. We attempt to correct for this incompleteness by assuming that the parent sample of Chapman et al. (2005) is a fair representation of the total population. In this case our numbers should be multiplied by 3.5.

We have not applied a volume density correction for the AGN contribution, because it is at most minor. Even though a fraction of SMGs host AGNs and a few individual SMGs have been shown to exhibit a significant AGN contribution to their emission, it is established that on average AGN activity is responsible for at most ~ 10–20% of the bolometric infrared emission of SMGs (Alexander et al., 2005, 2008; Menéndez-Delmestre et al., 2007, 2009; Valiante et al., 2007; Pope et al., 2008; Hainline et al., 2009; Murphy et al., 2009; Watabe et al., 2009). Therefore a potential error associated with the AGN contribution in our analysis of a statistically significant sample is smaller than the systematic uncertainty (e.g. 30% error of luminosity-SFR conversion; Kennicutt, 1998).

The percentage contribution of SMGs to the SFR and M_* densities (Columns 5 and 7 of Table 6.1) was calculated as $\rho_{\rm SMG}/(\rho_{\rm SMG}+\rho_{\rm other})$, where $\rho_{\rm SMG}$ is the density of SMGs at each redshift bin (Columns 4 and 6) and $\rho_{\rm other}$ is the density of other galaxies assumed to be an average of determinations (excluding lower limits) reported by other authors (see Tables 5 and 6 in Michałowski et al., 2009b), for which the redshift ranges overlap with our bins. This way of calculating the contribution is justified if SMGs do not enter the "other" samples of galaxies. This is usually the case because SMGs are faint in the optical. However, if this was not fulfilled, the real percentage contribution of SMGs would be even higher.

6.4 RESULTS

The best fits[3] are shown in Figure 6.7 and the median SEDs (in flux and luminosity domains) are shown in Figure 6.1.

The resulting properties of the galaxies are listed in Table 6.2 and shown in Figure 6.2 as a function of redshift. We notice similar trends to Hainline (2008) that low-z SMGs are less luminous and colder (see her Figures 4.7 and 4.9).

In two cases we obtained much better fits using the templates of Silva et al. (1998) instead of those of Iglesias-Páramo et al. (2007), namely, an HR 10 template for SMMJ105151.69+572636.0 and a spiral Sc template for SMMJ221733.12+001120.2. In 9 cases[4] where our fits strongly underpredict the $850\,\mu$m datapoint we adopted the $L_{\rm IR}$ and T_d estimates of Chapman et al. (2005).

The determination of the IR luminosity suffers from systematic uncertainties depending on the choice of the SED template. Our approach of using all the optical, submillimeter and radio data to constrain the shape of the SED results in a moderate systematic error in the IR luminosity (less than a factor of ~ 2; Bell et al., 2007). The choice of a Salpeter (1955) IMF with the cutoffs of 0.15 and $120\,{\rm M}_\odot$ introduces a maximum systematic error of a factor of ~ 2 in the determination of the stellar masses and SFRs (Erb et al., 2006). Bell et al. (2007) have also found that random errors in stellar mass are less than a factor of ~ 2. Estimates of dust temperatures

[3]The SED fits can be downloaded from `http://archive.dark-cosmology.dk`

[4]SMMJ030226.17+000624.5, SMMJ030231.81+001031.3, SMMJ030236.15+000817.1, SMMJ030238.62+001106.3, SMMJ123636.75+621156.1, SMMJ123651.76+621221.3, SMMJ123721.87+621035.3, SMMJ163639.01+405635.9, SMMJ221724.69+001242.1

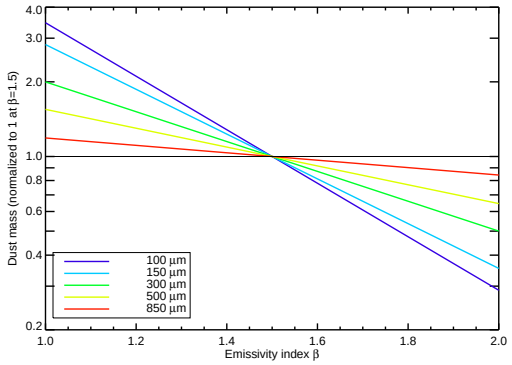

Figure 6.3: *Dust mass (normalized to 1 at $\beta = 1.5$) of a mock galaxy with $T_d = 40$ K derived from several infrared rest-wavelengths as a function of the assumed emissivity index β. The uncertainty of the dust mass resulting from unknown β is a factor of a few.*

have uncertainties of $\sim$ 5–10 K dominated by the unknown value of the emissivity index, β. The SFR determination based on radio observations is accurate up to 30% since it agrees with the detailed spectrophotometric SED fitting (Michałowski & Hjorth, 2007). The uncertainties in q (defined in Section 6.3.1) are ~ 0.3 (see also Kovács et al., 2006), dominated by the error in $L_{\rm IR}$.

In order to assess the influence of the choice of emissivity index $\beta = 1.3$ on the dust mass estimates, we recalculated the dust temperatures and masses in a range of β of 1–2. The resulting error was less than a factor of 3.5.

This is illustrated on Figure 6.3 where we present a more systematic analysis of this problem. We calculated the dust mass of a mock galaxy with $T_d = 40$ K (this choice does not influence the results) using β in a range of 1–2 assuming a flux density of 5 mJy at a variety of infrared rest-wavelengths. Then we normalized dust masses to 1 at $\beta = 1.5$. We conclude that as long as the observations probe wavelengths longer than $\sim 150\,\mu$m ($z \lesssim 4.7$ for observed wavelength of $850\,\mu$m), then the error on the dust mass resulting from unknown β is less than a factor of ~ 5.

None of these errors significantly affect our conclusions, because the inferred nature of SMGs would not be different even in the worst case scenario when all systematic errors work in one direction (increasing or decreasing the obtained values). Moreover, we analyse a statistically significant sample of 76 galaxies, so random errors of a factor of 2 are reduced to $< 20\%$ when an error of a mean is considered.

Table 6.1 contains the volume densities and mean IR-radio correlation parameter divided into four redshift bins (see Section 6.3.2). The uncertainties quoted on $\rho_{\rm SFR}$ and ρ_* include the systematic 30% uncertainty of the $L_{\rm IR}$ to SFR conversion (Kennicutt, 1998) and a factor of ~ 2 systematic uncertainty in the stellar mass (Michałowski et al., 2008). The systematic error resulting from our incompleteness correction (Section 6.3.2) is likely a factor of a few.

6.5 Discussion

6.5.1 Spectral energy distributions of SMGs

We have presented the first successful attempt to fit the entire UV-to-radio SEDs of SMGs in a self-consistent way taking into account all the available data simultaneously. Our study provides evidence that GRASIL models can reproduce the SMG data. Namely, we found good

Table 6.1: *Mean values for SMGs in redshift bins*

z	Volume	$\log \rho_{\rm IR}$	$\rho_{\rm SFR}$	%	$\log \rho_*$	%	q	$\log \rho_{\rm dust}$
	(10^6 Mpc^3)	($L_\odot$ Mpc^{-3})	($M_\odot$ yr^{-1} Mpc^{-3})		($M_\odot$ Mpc^{-3})			($M_\odot$ Mpc^{-3})
(1)	(2)	(3)	(4)	(5)	(6)	(7)	(8)	(9)
$0.080 - 1.316$	1.15	$7.77^{+0.06}_{-0.07}$	0.0102 ± 0.0014	11^{+3}_{-2}	$7.12^{+0.13}_{-0.08}$	4^{+2}_{-1}	2.52 ± 0.05	$5.42^{+0.11}_{-0.14}$
$1.408 - 2.142$	1.63	$8.12^{+0.05}_{-0.05}$	0.0228 ± 0.0027	11^{+3}_{-3}	$7.18^{+0.16}_{-0.11}$	11^{+6}_{-3}	2.29 ± 0.08	$4.32^{+0.03}_{-0.04}$
$2.148 - 2.565$	0.89	$8.45^{+0.05}_{-0.05}$	0.0486 ± 0.0054	18^{+7}_{-5}	$7.61^{+0.12}_{-0.08}$	51^{+20}_{-11}	2.27 ± 0.09	$4.90^{+0.05}_{-0.05}$
$2.578 - 3.623$	2.17	$8.30^{+0.05}_{-0.05}$	0.0341 ± 0.0040	20^{+5}_{-4}	$7.28^{+0.12}_{-0.07}$	31^{+14}_{-7}	2.25 ± 0.08	$4.43^{+0.03}_{-0.03}$

Note. — Column (1): redshift range of the bins containing equal number of SMGs. Column (2): comoving volume of these bins (calculated in Section 6.3.2). Column (3): IR luminosty density of SMGs. Column (4): Resulting IR SFR density of SMGs (Section 6.5.3). Column (5): contribution of SMGs to the cosmic SFR density (calculated in Section 6.3.2). Column (6): stellar mass density of SMGs (Section 6.5.3). Column (7): contribution of SMGs to the cosmic M_* density (calculated in Section 6.3.2). Column (8): mean (and error of the mean) FIR-radio correlation parameter for SMGs (Section 6.5.4). Column (9): dust mass density of SMGs (Section 6.5.2). Columns 3-7 and 9 have been corrected for incompleteness by a factor of 3.5 (Section 6.3.2).

fits for all SMGs in our sample with the best IR/submillimeter wavelength coverage[5] except of SMMJ105238.30+572435.8.

As is evident from Figure 6.1, regardless of whether SEDs were normalized to the same observed $850\,\mu$m datapoint or $\mathrm{SFR_{IR}}$, the scatter at optical and near-IR wavelengths is significant, showing that SMGs exhibit a wide range of stellar population properties (as also noted by Ivison et al., 2002). This implies the need for an SED template library in SMG studies, as opposed to single-template fitting.

Having constrained the SEDs of SMGs we now turn to a discussion of what we can learn about these galaxies using the best-fitting models.

6.5.2 Properties of SMGs

Star formation rates

The very high (current) SFRs of SMGs (median $659\,M_\odot$ yr^{-1}, Column 5 of Table 6.2 and Figure 6.2) place them among the most powerful starburst galaxies in the Universe. Such extreme SFRs likely result from major mergers (e.g. Chapman et al., 2004b; Swinbank et al., 2004; Greve et al., 2005; Tacconi et al., 2006, 2008; Younger et al., 2007, 2008b; Berciano Alba et al., 2009; Narayanan et al., 2009b,a) and cannot be sustained for a long period (after a few hundred Myr the gas reservoir would be depleted; see Greve et al., 2005; Hainline et al., 2006).

On the other hand, their extinction-uncorrected UV SFRs are two orders of magnitude lower (median $\sim 7\,M_\odot$ yr^{-1}, Column 4). This implies that the majority of star formation in SMGs is hidden by dust. Therefore, optical observations alone are not sufficient to investigate their nature and contribution to cosmic star formation.

Using stellar masses of SMGs we placed lower limits on the time-averaged SFRs required to build their stellar masses within the age of the Universe ($\equiv M_*$/age of the Universe at given redshift), shown as empty circles on Figure 6.2. Their median value of $\sim 130\,M_\odot$ yr^{-1} indicates that SMGs had to be relatively highly star-forming throughout the age of the Universe to build up their stellar populations at a constant rate.

[5]SMMJ105201.25+572445.7, SMMJ105230.73+572209.5, SMMJ163650.43+405734.5, SMMJ163658.19+410523.8, SMMJ163706.51+405313.8

Having constrained the mass of stars formed during the ongoing starburst episode, $M_{\rm burst}$, we can further constrain the minimum average SFR of SMGs *before* the onset of this starburst, $\equiv (M_* - M_{\rm burst})$/age of the Universe (plus signs on Figure 6.2). The median is still high, $\sim 100\,M_\odot$ yr^{-1}, so SMGs must have been highly star-forming in the past too. At redshifts 2–3 the age of the Universe is $\sim$ 3–2 Gyr and it is unlikely that a galaxy can sustain this high SFR over such a long period. *Therefore we conclude that either the stellar masses of SMGs have been formed in at least two strong* ($> 100\,M_\odot$ yr^{-1}) *starburst episodes or continuously over the period of* 2-3 *Gyr but in several smaller galaxies that eventually merged*. In order to build up the stellar mass of one SMG, five such galaxies would need to form stars continuously at a rate of $20\,M_\odot$ yr^{-1}, a value more likely to be sustainable over several Gyr. The latter scenario is consistent with the results of Dye et al. (2008) based on observed optical to mid-IR data of 51 SMGs with photometric redshifts. They found that approximately half the stellar mass in SMGs has been formed over a long ($\sim$ 1–2 Gyr) period of approximately constant star formation activity. The possibility that a significant part of stellar mass in SMGs was formed before the ongoing starburst has also been suggested by Hainline (2008), who compared the build-up timescale of stellar mass and the duration of the SMG phase.

The median value of the SFR per unit stellar mass (SSFR $\equiv$ SFR$_{\rm IR}/M_*$, Column 7 of Table 6.2) of $\sim 1.7\,$Gyr^{-1} is within the range for other high-z star-forming samples (compare with Figures 2 and 4 of Castro Cerón et al., 2006, 2009, respectively). This indicates that SMGs are forming stars intensely.

SSFRs are compared with (the inverse of) the age of the Universe in Figure 6.2. The SMGs close to the solid line could have formed their stellar populations at the present rate within the age of the Universe. However, the SMGs close to, or above the dashed line could have formed their stars at the present rate within less than 10% of the age of the Universe, i.e., within $\lesssim 300$ Myr at $z = 2$. These galaxies are experiencing a powerful starburst episode.

At the extreme there are three high-z SMGs[6] with very high SSFRs $> 10\,$Gyr^{-1} (Column 7 of Table 6.2). They are all hot ($T_d > 60$ K, Column 13) and formed the majority of their stellar populations during the ongoing starburst ($M_{\rm burst}/M_* > 60\%$, Column 9). Therefore they are likely the most powerful cases of SMGs formed in major mergers of galaxies with huge gas reservoirs that were subsequently converted into stars.

Our median SSFR at $z > 1.7$ ($1.83\,$Gyr^{-1}) is a factor of ~ 2 lower than that of Dunne et al. (2009a, 3–$4.5\,$Gyr^{-1}; see their Figure 12b) for $10^{11} < M_* < 10^{12}\,M_\odot$ galaxies at these redshifts. This difference can be explained if the radio luminosities (used by Dunne et al., 2009a, to estimate SFRs) are boosted by AGN activity more than the IR luminosities used here. Indeed, if we use SFR$_{\rm radio}$ instead of SFR$_{\rm IR}$ to calculate SSFRs the median for the SMGs at $z > 1.7$ increases to $3.20\,$Gyr^{-1} (see Section 6.5.4 for discussion of AGN contamination in our sample).

In order to assess the accuracy of SFR estimates based on radio emission (independent of SED modeling) we compared the ratio of SFR$_{\rm radio}$/SFR$_{\rm IR}$. Its median value is equal to ~ 1.3. Hence, assuming that IR emission is a good proxy for SFR, then radio estimates suffer from a $\sim 30\%$ systematic error. This is illustrated on Figure 6.5 where the dashed line denotes the relation between IR and radio luminosities required to make SFR$_{\rm IR}$ = SFR$_{\rm radio}$. Indeed the radio luminosity gives systematically higher SFRs for SMGs (most of the points are above the line). This can be caused by a significant AGN contamination boosting radio flux (see Section 6.5.4), or a strong bias favouring radio-bright galaxies, because those non-detected at radio do not enter our sample (Section 6.2). Alternatively, it could be that for luminous galaxies either the IR

[6]SMMJ131201.17+424208.1, SMMJ141802.87+523011.1, SMMJ221806.77+001245.7 plus a low-mass, low-z case, SMMJ030238.62+001106.3

conversion of Kennicutt (1998) should be scaled up by a factor of 1.3, or the radio conversion of Bell (2003) scaled down.

Stellar masses

SMGs having stellar masses of $\sim 10^{11}$–$10^{12}\,M_{\odot}$ (Column 8 of Table 6.2 and Figure 6.2) are among the most massive galaxies in the Universe, regardless of redshift (compare with Figures 2 and 4 of Castro Cerón et al., 2006, 2009, respectively). This property makes them natural candidates for the progenitors of the present-day ellipticals.

The relatively tight range of stellar masses is likely not a result of sensitivity limits at optical and near-IR. This is because *i*) galaxies with stellar mass as low as $\sim 10^{9}\,M_{\odot}$ would have been detected in deep *Spitzer* imaging at redshifts $z \sim 2$ (e.g. Reddy et al., 2006) *ii*) our sample accounts for 50% of the parent Chapman et al. (2005) sample (and only 30% of the parent sample may have different properties than our sample, see Section 6.2), so it is unlikely that we miss only the low-mass objects. Therefore, high M_{*} seems to be an intrinsic property of submillimeter-selected galaxies. Mergers of less massive galaxies could not result in a powerful starburst giving rise to detectable submillimeter emission (see also Davé et al., 2009).

Only a minor part (median ~ 7%, Column 9 of Table 6.2 and Figure 6.2) *of the stellar populations present in SMGs has been formed during the ongoing starburst episodes*. Hence, even though SMGs probably evolve into ellipticals, the majority of the stellar mass in such ellipticals had been created before the submillimeter-bright phase.

This could mean that the current SFRs and stellar masses of SMGs are only loosely connected and indeed this manifests itself in a very high spread (around two orders of magnitude) in SSFRs in our sample even though the stellar mass range is relatively tight: $\sim 10^{11}$–$10^{12}\,M_{\odot}$ (Figure 6.2). This behaviour is unusual compared to other galaxies (see Castro Cerón et al., 2006, 2009).

However we note that the low stellar masses created in the ongoing starburst may partially be an effect of the assumed starburst ages of 50 Myr. If a starburst duration of 100–200 Myr were adopted (Smail et al., 2004; Borys et al., 2005; Hainline, 2008; Tacconi et al., 2008) the resulting $M_{\rm burst}$ could be higher by a factor of ~ 2–4.

The mass-to-light ratios, M_{*}/L_{K}, of SMGs (Column 10 of Table 6.2 and Figure 6.2) are typical for massive galaxies. Specifically, the median ($0.68\,M_{\odot}\,L_{\odot}^{-1}$) is similar to the values for $M_{*} > 10^{11}\,M_{\odot}$ galaxies (Drory et al., 2004, their Table 1) and to simulated massive galaxies at $z \sim 1$ (Courty et al., 2007, their Figure 4).

Dust properties

Our fits suggest that SMGs are moderately dust-obscured with a median $A_{V} \sim 2$ mag (Column 14 of Table 6.2). Our estimates are consistent within 1–2σ with the mean/median values obtained by Smail et al. (2004, 1.70–2.44), Swinbank et al. (2004, 3.0 ± 1.0), Borys et al. (2005, 1.7 ± 0.2) and Hainline (2008, 1.7 ± 0.1) based on near-IR data. For individual SMGs we obtained systematically larger extinction (median difference of ~ 0.3 mag) than Hainline (2008). The difference may be accounted for if there is significant extinction even in *Spitzer* IRAC data.

The dust density of SMGs at low redshifts (Column 9 of Table 6.1) is similar to the local ($0.013 < z < 0.18$) value of $\log \rho_{\rm dust} = 5.57^{+0.12}_{-0.17}\,M_{\odot}\,{\rm Mpc}^{-3}$ given by Driver et al. (2007) based on an assumed dust-to-light ratio. Their and our samples are disjoint since only ~ 5% of SMGs are brighter than their flux limit $B < 20$ mag. Therefore SMGs contribute of order ~ 50% to the dust budget at low redshifts.

In our sample of SMGs $\rho_{\rm dust}$ does not change significantly from $z \sim 3.6$ to $z \sim 0$. We do not detect any evolution of dust mass in SMGs across the entire redshift range (Figure 6.2). A constant dust mass density across redshifts 0–3.5 was also found by Pascale et al. (2009) based on a stacking analysis at submillimeter wavelengths of galaxies selected at $24\,\mu$m.

The question is what happened to the dust produced in SMGs. If they evolve into dust-poor ellipticals, then the dust is not simply stored in their end-products (as is probably the case for stellar masses). It is therefore plausible that dust is either blown away (by stellar and/or AGN winds) or destroyed during subsequent evolution after the SMG event.

Comparison with GRB hosts

In Michałowski et al. (2008) we presented a hypothesis that gamma-ray burst (GRB) host galaxies may constitute a subsample of hotter/less luminous counterparts of SMGs. Indeed, the UV-to-IR SEDs of three $z \sim 2$–3 SMGs[7] are consistent with $z \sim 1$ submillimeter/radio bright GRB hosts (dashed lines on Figure 6.7 from Michałowski et al., 2008), but 1.2–3.9 times more luminous. These three SMGs are similar to GRB hosts with respect to their hot dust temperatures (~ 40–60 K), high SSFRs ($\gtrsim 2$ Gyr^{-1}, high fraction of stellar mass formed in the ongoing starburst ($> 10\%$) and blue optical colors.

If larger samples of GRB hosts shows a similar tendency that their brightest members overlap with the hotter subsample of SMGs, then GRB events will provide an effective way of selecting hot SMGs, otherwise difficult to localize.

6.5.3 Contribution to stellar mass assembly

Star formation rate volume density

SFR densities of SMGs were calculated as described in Section 6.3.2. In order to assess the accuracy of our simplified method of dividing the sum of the SFRs of the detected SMGs by the total survey volume, we compare our estimates with those resulting from detailed calculation of the volume contribution of individual SMGs done by Chapman et al. (2005, based on the same sample as we analyse) and Wall et al. (2008, based on 35 SMGs in GOODS-N field of which 17 have spectroscopic redshifts). The comparison is shown in Figure 6.4. Our results in two high-redshift bins ($z > 2$) corrected for incompleteness (Section 6.3.2) are consistent with that of Chapman et al. (2005) and Wall et al. (2008). At lower redshifts we find values similar to Chapman et al. (2005), but an order of magnitude lower than Wall et al. (2008). Therefore we conclude that *i*) our method to calculate volumes is accurate, since it gives consistent results with other estimates; and *ii*) our sample is incomplete in the two low-redshift bins as anticipated in Section 6.2.

From Figure 6.4 (and Columns 4 and 5 of Table 6.1) it is apparent that a $\rho_{\rm SFR}$ of SMGs starts to decline (with cosmic time) earlier (before $z \sim 2$) than that of other galaxies ($z \sim 1$). More quantitatively, SMGs harbour $\sim 20\%$ of the cosmic $\rho_{\rm SFR}$ at $z \sim 2$–3.6 (Column 5), but their contribution drops to $\sim 11\%$ at $z < 1.4$. It is likely that at lower redshifts, due to the decreased rate of mergers (e.g. Rawat et al., 2008; de Ravel et al., 2009), there are fewer galaxies left that can still sustain high SFRs to be detected at submillimeter wavelengths. However, part of the decrease of SMG $\rho_{\rm SFR}$ can be explained by the "redshift desert", which makes it difficult to detect $z \sim 1.2$–1.8 SMGs (see Section 6.2).

[7] SMMJ141750.50+523101.0, SMMJ141802.87+523011.1, SMMJ163627.94+405811.2

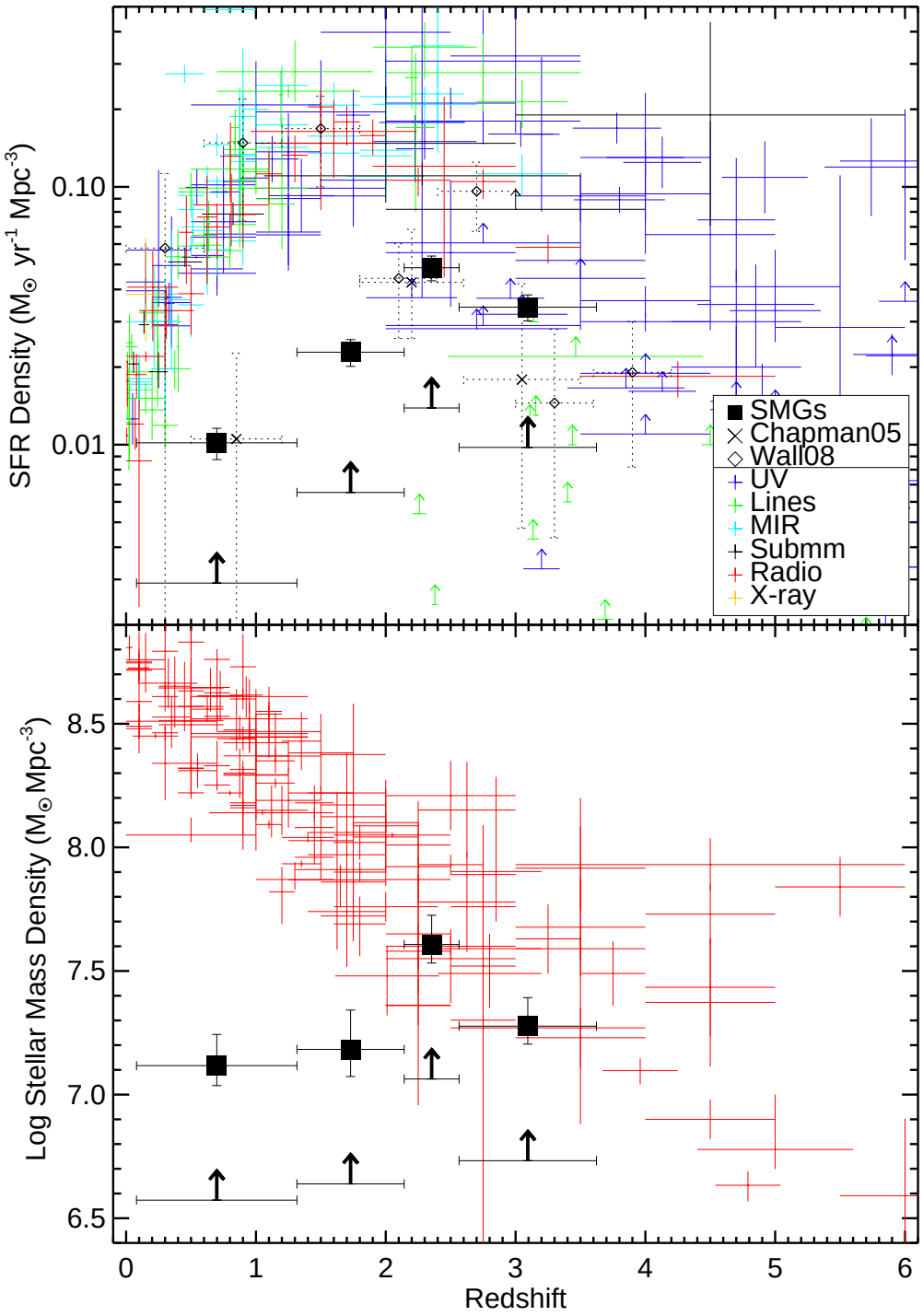

Figure 6.4: *Top: Cosmic star formation density. The SMGs' contribution rises with redshift from* $\sim$ 11% *to* $\sim$ 20% *(Section 6.5.3 and Table 6.1). Filled Squares: SMG data in four bins (Table 6.1 and Section 6.3.2). Thick black arrows: the SMG data without incompleteness correction (factor of* 3.5*, Section 6.3.2). Black crosses and diamonds: star formation density of SMGs determined by Chapman et al. (2005) and Wall et al. (2008), respectively. Colored points with error bars: determination of the cosmic value based on different estimates – ultraviolet (violet), emission lines: [O 2], [O 3], Hα, Hβ (green), mid-IR (light blue), submillimeter (black), radio (red), X-ray (yellow). Extinction correction and, in many cases, incompleteness correction have been applied by the authors. Arrows: lower limits. Bottom: Cosmic stellar mass density. The SMGs' contribution rises with redshift from* $\sim$ 4% *to* $\sim$ 50% *(Section 6.5.3 and Table 6.1). Filled Squares: SMG data in four bins (Table 6.1 and Section 6.3.2). Thick black arrows: the SMG data without incompleteness correction. Red points with error bars: determination of the cosmic value from literature.*

A high value of $\rho_{\rm SFR}$ of SMGs at $z \sim 2$–3 and the subsequent decline are consistent with the hypothesis that the SMG population is a manifestation of powerful starburst episodes evolving into the present-day ellipticals (as discussed in Section 6.5.2). In this scenario galaxies detected in the submillimeter at high-z do not enter the sample of SMGs at low-z because they have already evolved into passive galaxies. It has indeed been found that ellipticals contain old stars formed at $z \sim 1.5$–4 (Daddi et al., 2000; van Dokkum & Franx, 2001; van de Ven et al., 2003). The evolution of SMGs into ellipticals has also been claimed by several authors based on their luminosity function (Smail et al., 2004), huge luminosities (Eales et al., 1999) and gas reservoirs (Smail et al., 2002; Greve et al., 2005), strong clustering (Ivison et al., 2000; Almaini et al., 2003), space density and morphology (Barger et al., 1999; Lilly et al., 1999; Trentham et al., 1999; Swinbank et al., 2006) and evolutionary SED models (Takagi et al., 2004).

Knudsen et al. (2008b) analysed number counts of SMGs fainter than the SCUBA confusion limit, using those behind clusters of galaxies magnified by lensing. They concluded that the integrated light produced by the SMGs brighter than 0.1 mJy (i.e. LIRGs and ULIRGs with roughly $L_{\rm IR} > 8 \times 10^{10}\,L_\odot$ and SFR $> 15\,M_\odot$ yr^{-1}) is comparable to the extragalactic background light (EBL) at $850\,\mu$m (see also Blain et al., 1999; Cowie et al., 2002). This means that these galaxies host the majority of the cosmic *obscured* star formation. Knudsen et al. (2008b) also found that sources brighter than 2.5 mJy (roughly the limit of the survey considered here) contribute $\sim 25\%$ to the to EBL at $850\,\mu$m (see also Hughes et al., 1998; Barger et al., 1999; Wang et al., 2004; Coppin et al., 2006). Together with our results this implies that as much as $\sim 80\%$ ($4 \times 20\%$) of the cosmic star formation at $z \sim 2$–3.6 reside in SMGs brighter than 0.1 mJy. This is only true if the faint (< 2 mJy) SMGs have similar dust temperatures to the brighter ones. If they are colder (hotter) their submillimeter fluxes corresponds to lower (higher) SFRs (because it is calibrated to total IR emission) and therefore the total SMG population contribute less (more) than 80% to the cosmic $\rho_{\rm SFR}$. This picture is however complicated, because based on stacking analysis it has been claimed that the distribution of the faint SMGs peaks at lower redshifts ($z < 1.5$; Wang et al., 2006; Serjeant et al., 2008).

Our overall conclusion is that the SMG population plays a significant role at redshifts $z \sim 2$–4, namely sources brighter than ~ 3 (0.1) mJy at $850\,\mu$m host 20% (80%) of cosmic star formation. Their contribution can however be lower in reality if very small (but numerous) galaxies are missed in all high-z flux-limited galaxy surveys. In such a case the total SFR density (color points on Figure 6.4) would be underestimated. To solve this issue much deeper surveys at high-z are necessary, either blank-field or for well-selected dwarf galaxy samples (e.g., GRB hosts or Lyα emitters).

Zheng et al. (2007) estimated $\rho_{\rm SFR}$ at $z \sim 0.9$ for massive galaxies ($M_* > 10^{11}\,M_\odot$) down to $R < 24$ mag (only $\sim 40\%$ of SMGs satisfy the latter criterion) equal to $0.0052^{+0.0020}_{-0.0021}\,M_\odot$ yr^{-1} Mpc^{-3}. This value is only a factor of 2 lower than our estimate for the SMGs at $z < 1.4$ (Table 6.1). Therefore, although SMGs do not host a major fraction of the cosmic SFR at low redshifts, they contribute significantly ($0.0102/(0.0052 \times 0.6 + 0.0102) \sim 66\%$) to the SFR budget of massive galaxies.

Stellar mass volume density

Stellar mass densities of SMGs were calculated as described in Section 6.3.2. Figure 6.4 and Table 6.1 (Columns 6 and 7) show that *at $z \sim 2$–3.6 a significant part (~ 30–50%) of the cosmic stellar mass had been formed in the progenitors of SMGs*. At lower redshifts ρ_* of SMGs (and hence their contribution to the cosmic ρ_*) drops, likely because the majority of SMGs at higher redshifts

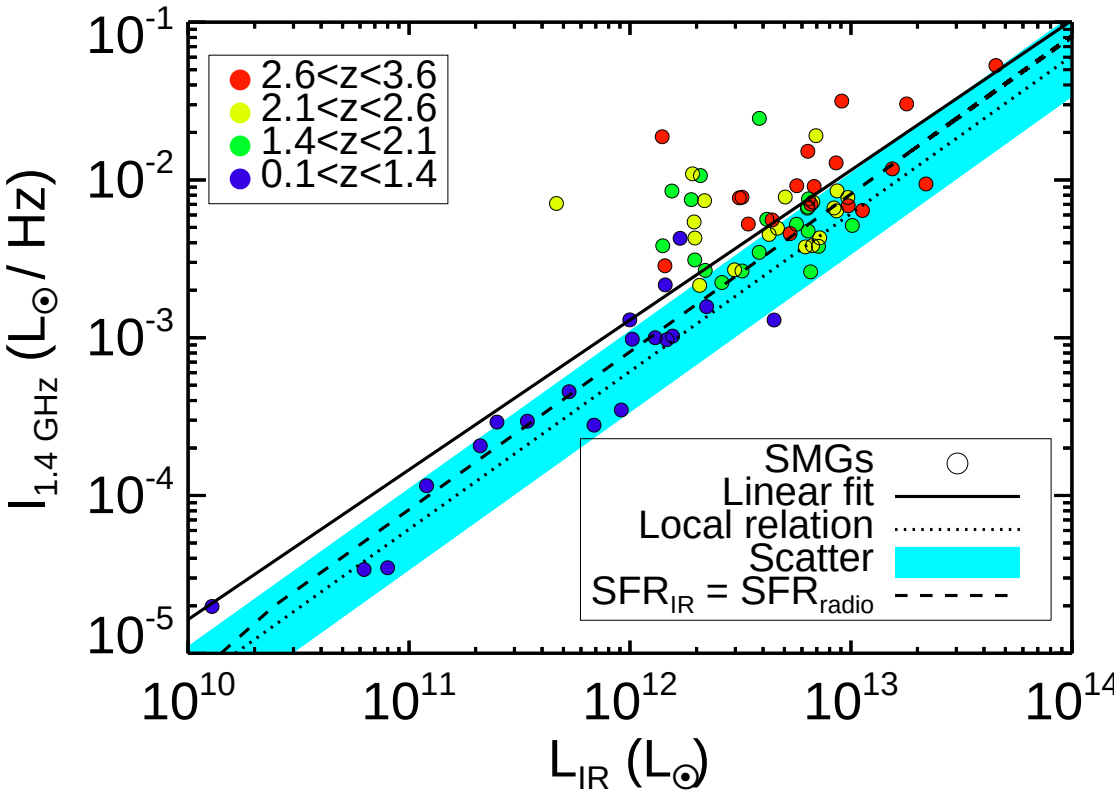

Figure 6.5: *Radio luminosity density as a function of infrared luminosity of SMGs showing a linear relation, though with a normalization offset from the local relation by a factor of* ~ 2.3 *towards higher radio luminosities (Section 6.5.4). Circles: values for individual SMGs color-coded by redshift. Solid line: linear fit to the data (eq. 6.1). Dotted line: the mean local relation (Bell, 2003). Shaded area: its scatter. Dashed line: the track where* $SFR_{\rm IR}$ *(Kennicutt, 1998) is equal to* $SFR_{\rm radio}$ *(Bell, 2003). The strong outliers (above the line) at high-luminosity end are probably caused by AGN activity increasing radio luminosities.*

had already evolved into passive galaxies at $z \sim 1.5$, and so dropped out of our submillimeter-selected sample. Moreover the sample is incomplete at $z \sim 1.2$–1.8 due to the "redshift desert" (see Section 6.2). This brings down the densities of SMGs in both low-z bins.

Since most of the stellar mass of SMGs has not been formed in the ongoing starburst (Section 6.5.2), their ρ_* reflects the integrated contribution of SMGs to the cosmic $\rho_{\rm SFR}$. Therefore the relatively high contribution of SMGs to the cosmic ρ_* in the last redshift bin ($\sim 31\%$, Column 7 of Table 6.1) means that SMGs play a non-negligible role in the cosmic stellar assembly even at $z > 3.6$. This can be checked by analysis of a sample of $z \gtrsim 4$ SMGs in a defined survey sky area, e.g. radio non-detected SMGs from the parent sample of Chapman et al. (2005). It has been confirmed that such distant SMGs exist (Capak et al., 2008; Knudsen et al., 2008a, 2009; Schinnerer et al., 2008; Coppin et al., 2009; Daddi et al., 2009b,a).

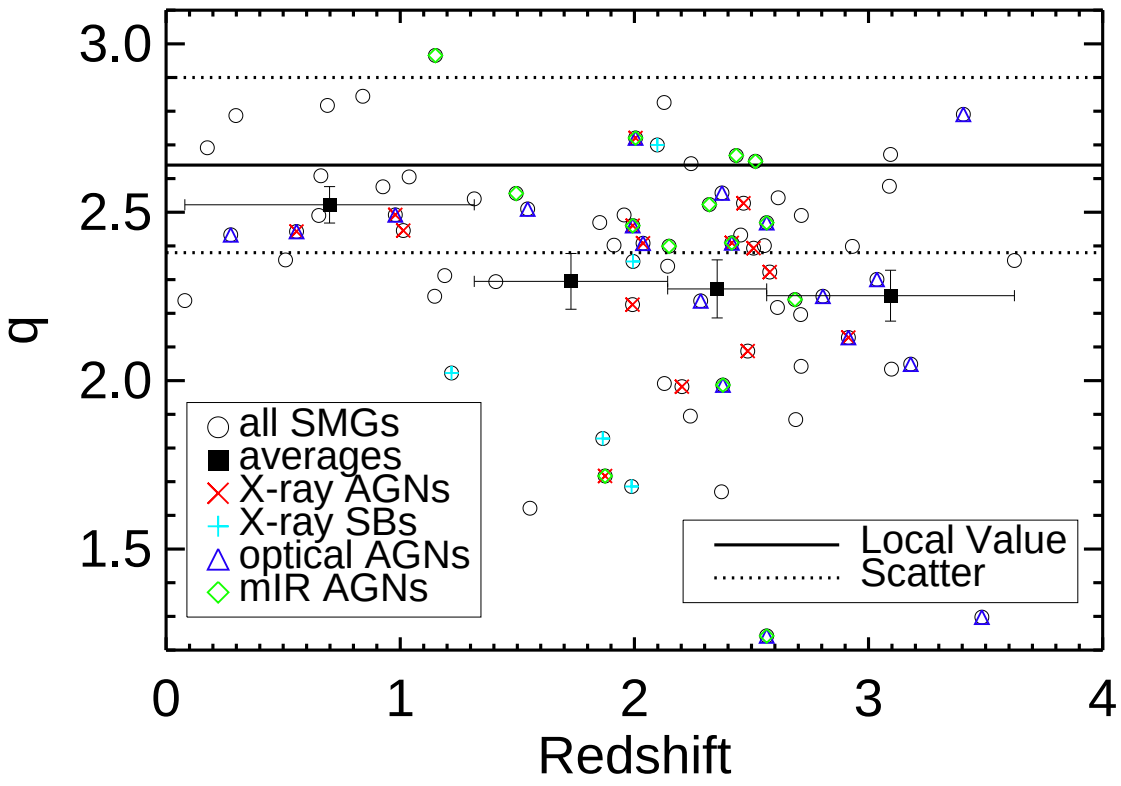

Figure 6.6: *The ratio of the infrared and radio luminosities q (defined in Section 6.3.1) as a function of redshift of SMGs. It provides evidence that a linear IR-radio correlation holds for SMGs up to $z \sim 3.6$, though with a normalization offset from the local relation by a factor of ~ 2.3 ($\Delta q \sim -0.36$) towards higher radio luminosities (Section 6.5.4). Circles: values for individual SMGs. Squares: the mean values (and errors on the mean) in four redshift bins containing equal number of galaxies (Table 6.1 and Section 6.3.2). Red crosses: SMGs classified as AGNs based on X-ray emission (Alexander et al., 2005). Light blue plus signs: SMGs classified as starbursts based on X-ray emission (Alexander et al., 2005). Violet triangles: SMGs classified as AGNs based on optical spectra (Chapman et al., 2005). Green diamonds: SMGs classified as AGNs based on a mid-IR power-law (Section 6.5.4). The mean local $q = 2.64$ (Bell, 2003) is shown as a solid line with 0.26 scatter (dotted lines). The q values for majority of AGN-classified SMGs do not differ from the rest of the SMG population (see Section 6.5.4).*

6.5.4 Source of emission

IR-radio correlation

With our full SED modelling of 76 SMGs we confirm the results of Hainline (2008) on the correlation between IR and radio luminosities. Figure 6.5 shows that SMGs follow a linear IR-radio correlation over almost four orders of magnitude in luminosity. The two outliers (with $q \sim 1.3$, see below) are probably caused by AGN activity contributing significantly to radio luminosities (see below). A linear fit gives:

$$\log(I_{1.4}/L_{\odot}\mathrm{Hz}^{-1}) \quad = \quad (0.95 \pm 0.07)\log(L_{\mathrm{IR}}/L_{\odot}) - (14.3 \pm 0.8). \tag{6.1}$$

The slope is consistent (within errors) with unity, suggestive of the linear relation between $I_{1.4}$ and L_{IR} at the high-end ($L_{\mathrm{IR}} \gtrsim 10^{11}\,L_{\odot}$) of the galaxy luminosity function (a similar value of

1.064 ± 0.025 was found by Hainline, 2008).

The IR-radio correlation is usually quantified by the ratio of IR and radio luminosities, q (see Section 6.3.1). The mean q for SMGs (2.34 ± 0.04, scatter: 0.34) is significantly lower than that of local star-forming galaxies (2.64 with a scatter of 0.26; Bell, 2003). Similar offsets were reported by Kovács et al. (2006), Murphy et al. (2009) and Murphy (2009) based on smaller samples of SMGs. *We conclude that at $z > 1.4$ SMGs have radio luminosities on average a factor of ~ 2.3 larger ($\Delta q \sim -0.36$) than what would result from the local relation.* The difference is significant at the level of 4–5σ and can be explained in three ways.

Radio-loud AGNs have on average low q values (see e.g. Miller & Owen, 2001; Yun et al., 2001; Yang et al., 2007). If $\gtrsim 50\%$ of the radio emission of SMGs is powered by AGNs, then the radio luminosities of SMGs higher by a factor of ~ 2.3 can be accounted for. However, there are indications that SMGs are starburst-dominated (see below), so we deem this explanation less likely.

Another explanation is that the radio excess is a result of the bias against radio-faint sources in our sample (see Section 6.2). This can be tested when a sample of SMGs with localizations (and hence redshifts) independent of radio detections is available (e.g. Daddi et al., 2009b,a; Knudsen et al., 2009; Weiß et al., 2009).

The third possibility is that some properties influencing the IR or radio emission are intrinsically different for SMGs and local galaxies. The sample of Bell (2003) includes local normal, star-forming spiral and irregular galaxies, blue compact dwarfs, starburst galaxies and ULIRGs. Therefore the difference in the properties between this sample and such extreme galaxies as SMGs is expected. Such explanation was offered by Lacki et al. (2009) and Lacki & Thompson (2009). Their numerical modelling showed that cosmic-ray electrons in "puffy starbursts" (vertically and radially extended galaxies with vertical scale heights ~ 1 kpc) experience weaker bremsstrahlung and ionization losses resulting in stronger radio emission. Indeed, there are indications that SMGs are extended on vertical scales of ~ 1 kpc (Lacki & Thompson, 2009; Tacconi et al., 2006, 2008; Genzel et al., 2008; Younger et al., 2008b; Law et al., 2009), so we find this explanation probable.

The q values for SMGs are shown in Figure 6.6 as a function of redshift. We do not detect any significant evolution across the redshift range 1.4–3.6. The only sign of evolution is that the mean q in the low-redshift bin ($z < 1.4$) is above the value found at higher redshifts (4.5σ). This can be explained either by the contribution of reprocessed emission from low-mass stars (cirrus emission, e.g. Yun et al., 2001, and references therein) to the IR, or by the fact that at low redshifts SMGs are more similar to other local galaxies and do not exhibit large vertical scale heights characteristic for "puffy starbursts" (see above).

It is important to note that the derived linear IR-radio correlation for SMGs is not a consequence of the use of the SED templates (which were tuned to fulfill this correlation locally), because the radio luminosities used here were derived based on the observational data only, independent of the SED modeling.

AGN activity

As discussed above, AGN activity could explain low q values of SMGs. This is at least true for the two SMGs with lowest q[8], spectroscopically classified as AGN (Chapman et al., 2005).

In the SEDs of SMGs there are clear signs that some of them host AGNs (though, not necessarily a bolometrically dominant ones). Radio datapoints are higher than model predictions by

[8]SMMJ131215.27+423900.9, SMMJ141813.54+522923.4

more than 3σ in 36% (27/76) of SMGs, whereas they are lower than models only for 8% (6/76). This may hint at an AGN contribution in these galaxies. However, 4 out of 5 X-ray identified starbursts (Column 16 of Table 6.2) also exhibit radio excess, so we find other explanations of radio excess presented above more reliable.

Another indication of an AGN contribution is that 18% (14/76) of SMGs show a mid-IR power-law AGN feature incompatible with our starburst models (see Figure 6.7 and Column 16 of Table 6.2). However, rest-frame 2–5 μm excess was also interpreted as a tracer of recent star formation (Mentuch et al., 2009).

Finally, three SMGs[9] have exceptionally high $\mathrm{SFR_{UV}}$ ($> 500\,M_\odot$ yr^{-1}, Column 4 of Table 6.2). Strikingly, all of them were fitted with non-starburst models ($M_{\mathrm{burst}} = 0$, Column 9), so modeling is consistent with these high SFRs being continuous (the same is true for three other non-starburst SMGs with high $\mathrm{SFR_{IR}}$). Such a scenario is unlikely, so this hints at an AGN contribution to the UV/IR emission.

However, the fact that we obtained reasonable SED fits for most of the SMGs using purely star-forming models (Figure 6.7) hints at the conclusion that AGN activity is not dominant in our sample.

We investigated the issue of AGN activity further by analysing the average q values of the following subsamples (see also Figure 6.6): X-ray identified (Alexander et al., 2005) AGNs: 2.32 ± 0.06 and starbursts: 2.12 ± 0.18; optically identified AGNs (Chapman et al., 2005): 2.27 ± 0.09; and mid-IR identified AGNs (see above): 2.36 ± 0.12. All subsamples are consistent with the value derived for the entire sample (2.34) Hence, we confirm the finding of Hainline (2008) that even the AGN-classified SMGs follow a linear IR-radio correlation. This means that even if an AGN is present it does not contribute to the emission of an SMG significantly (with the exception of the two $q \sim 1.3$ sources).

This is in line with *i*) the X-ray studies of SMGs indicating that the contribution of AGN activity to their IR emission is only $\sim 8\%$ on average (Alexander et al., 2005); *ii*) mid-IR colors of SMGs indicating that AGNs dominate the emission at these wavelengths only in 13–19% cases (Hainline et al., 2009); *iii*) mid-IR spectroscopy of SMGs revealing only weak AGN-like continua (Valiante et al., 2007; Pope et al., 2008; Menéndez-Delmestre et al., 2007, 2009; Murphy et al., 2009; Watabe et al., 2009); *iv*) near-IR spectroscopy revealing that starbursts dominate the emission of SMGs (Swinbank et al., 2004). Moreover, de Vries et al. (2007) found that star formation processes (if present) account for at least 75% of the radio luminosities of optically-selected AGNs.

Therefore we conclude that AGNs are present in a significant fraction of SMGs, but their contribution to the IR emission is at most minor.

6.5.5 Comparison of our results with the literature

For the sample of SMGs discussed in this chapter there are previous estimates of some of their properties. In this section we compare them with our results.

Chapman et al. (2005) derived L_{IR} and T_d based only on the $850\,\mu$m and 1.4 GHz data. There is no systematic difference between the determinations of T_d (our median of 38.7 K, theirs: 38.3 K). The mean difference between individual datapoints is 4 K ($\sim 10\%$). However, our values for L_{IR} are systematically lower than theirs (the median ratio of individual datapoints is 1.7). We find our values more reliable since they are based on data spanning a wider wavelength range. Overestimation of L_{IR} when using only $850\,\mu$m and 1.4 GHz was also noticed by Kovács et al.

[9] SMMJ123716.01+620323.3, SMMJ131215.27+423900.9, SMMJ131222.35+423814.1

(2006) and Pope et al. (2006).

Kovács et al. (2006) investigated a subsample observed at $350\,\mu$m. Their median dust mass ($9.04\,\log M_\odot$) and q value (2.20) are consistent with our estimates (9.01 and 2.35, respectively). The median difference between individual datapoints is $\sim 30\%$ for dust masses and $\sim 13\%$ for q. With our extended dataset we do not confirm the suggestion of Kovács et al. (2006) that q values of SMGs are lower than the local value.

The median stellar mass for a subsample of 13 SMGs investigated by Borys et al. (2005, $11.51\,\log M_\odot$) is close to our value (11.70). However, estimates of Hainline (2008, median $10.82\,\log M_\odot$) for 64 SMGs are a factor of ~ 5.6 smaller than our values (11.57). Hainline (2008) postulated that the discrepancy between her results and those of Borys et al. (2005) arose from a combination of systematic differences between the applied SED models and a higher AGN contribution in the K-band (used by Borys et al., 2005) with respect to the H-band. Our estimates are based on all the available photometric data, and so we find the former explanation more likely.

6.6 Conclusions

We have investigated the UV-to-radio SEDs of 76 SMGs ($S_{850} \gtrsim 3$ mJy) with spectroscopic redshifts (0.080–3.623). For the first time the properties of such a significant sample has been derived consistently using all available data. The resulting SFRs (median $659\,M_\odot$ yr^{-1}) and stellar masses ($11.54\,\log M_\odot$) are among the highest in the Universe.

Such high stellar masses, already present at redshifts $\sim$ 2–3, require that SMGs experienced either at least two starburst episodes, or a merger of several smaller galaxies. Our modeling suggests that only a minor fraction (7%) of their stellar populations was formed during the ongoing starburst episodes. This is supported by the fact that the SFRs and M_* of SMGs are basically disconnected, i.e. we observe two orders of magnitude spread in SSFRs whereas the range of M_* is relatively narrow: 10^{11}–$10^{12}\,M_\odot$. We concluded that dust is blown away or destroyed during the evolution of SMGs, since it is not stored in the likely end-products of SMGs, elliptical galaxies.

Indeed, the high stellar masses and the evolution of the SFR and stellar mass densities of SMGs are consistent with a scenario in which SMGs are progenitors of present-day ellipticals.

We found that SMGs contribute significantly to the cosmic SFR, $\rho_{\rm SFR}$ ($\sim 20\%$) and stellar mass, ρ_* (30–50%) densities at $z \sim$ 2–4. If we consider submillimeter sources down to 0.1 mJy the contribution to $\rho_{\rm SFR}$ rises to $\sim 80\%$.

Our analysis suggests that a linear IR-radio correlation holds for SMGs at least up to a redshift of 3.6, but they are ~ 2.3 times brighter at radio wavelengths than what would result from the local correlation.

Acknowledgements

We thank Joanna Baradziej, José María Castro Cerón, Thomas Greve, Brian Lacki, Kim Nilsson, Jesper Sommer-Larsen, Sune Toft, Bärbel Tress and Gunther Tress for discussion and comments; Scott Chapman for information on the survey areas; Jorge Iglesias-Páramo for kindly providing his SED templates; and Fabio Fontanot for kindly providing his model and data on star formation density. We acknowledge use of the extensive Spitzer database in the PhD thesis of Laura Hainline.

M. J. M. would like to acknowledge support from The Faculty of Science, University of Copenhagen. The Dark Cosmology Centre is funded by the Danish National Research Foundation. This research has made use of NASA's Astrophysics Data System Bibliographic Services.

6.7 LONG TABLES AND FIGURES

Table 6.2: *Properties of SMGs derived from the SED modeling*

		SFR ($M_\odot$ yr^{-1})				SSFR	$\log M_*$	$M_{\rm burst}/M_*$	M_*/L_K	$\log M_d$	$\log L_{\rm IR}$	T_d	A_V		
SMG	z	SED	UV	IR	radio	(Gyr^{-1})	($M_\odot$)	(%)	($M_\odot/L_\odot$)	($M_\odot$)	($L_\odot$)	(K)	(mag)	q	AGN?
(1)	(2)	(3)	(4)	(5)	(6)	(7)	(8)	(9)	(10)	(11)	(12)	(13)	(14)	(15)	(16)
SMMJ030226.17+000624.5	0.080	3	0.06	2	4	0.07	10.53	0.4	1.08	8.28	10.11	11.4	0.33	2.24	rad
SMMJ030227.73+000653.5	1.408	825	7.91	713	1190	4.81	11.17	25.5	0.42	8.54	12.62	52.6	1.81	2.29	rad
SMMJ030231.81+001031.3	1.316	433	0.68	224	211	7.81	10.46	71.1	1.36	9.10	12.11	25.6	4.38	2.54	…
SMMJ030236.15+000817.1	2.435	91	4.18	1152	810	3.33	11.54	1.1	0.55	8.62	12.83	41.3	0.27	2.67	mIR,rad
SMMJ030238.62+001106.3	0.276	14	0.04	36	44	59.74	8.78	113.3	0.36	8.32	11.32	25.5	4.22	2.43	spec,rad
SMMJ030244.82+000632.3	0.176	6	0.59	11	7	0.37	10.46	0.0	0.76	8.22	10.80	20.1	1.44	2.69	…
SMMJ105151.69+572636.0	1.147	134	0.30	248	457	0.92	11.43	1.5	0.65	8.97	12.16	34.4	4.00	2.25	rad
SMMJ105155.47+572312.7	2.686	837	12.95	589	1110	1.91	11.49	12.5	0.66	8.90	12.54	38.7	2.29	2.24	mIR
SMMJ105158.02+571800.2	2.239	314	16.77	373	1561	0.44	11.93	0.6	0.60	9.15	12.34	33.2	1.12	1.89	rad
SMMJ105200.22+572420.2	0.689	163	0.26	118	59	0.74	11.20	4.5	1.56	8.72	11.84	33.2	2.58	2.82	…
SMMJ105201.25+572445.7	2.148	935	2.58	798	1044	3.40	11.37	18.1	0.95	9.01	12.67	45.1	2.91	2.40	mIR
SMMJ105207.49+571904.0	2.689	2195	3.81	1559	6679	1.93	11.91	12.5	1.18	8.80	12.96	45.1	2.85	1.88	rad
SMMJ105225.79+571906.4	2.372	217	18.89	329	2310	0.75	11.64	0.0	0.49	8.96	12.28	33.2	1.16	1.67	rad
SMMJ105227.58+572512.4	2.142	410	4.73	376	564	0.57	11.82	1.9	0.78	8.79	12.34	38.7	1.71	2.34	…
SMMJ105227.77+572218.2	1.956	515	1.55	447	473	0.89	11.70	4.5	1.16	9.01	12.42	33.2	2.17	2.49	…
SMMJ105230.73+572209.5	2.611	1255	45.92	975	1942	0.72	12.13	3.8	0.68	9.18	12.75	38.7	1.51	2.22	…
SMMJ105238.19+571651.1	1.852	919	21.87	659	734	4.54	11.16	28.8	0.37	8.85	12.58	38.7	2.13	2.47	…
SMMJ105238.30+572435.8	3.036	1558	7.40	1169	1921	0.69	12.23	3.9	0.85	9.04	12.83	45.1	1.86	2.30	spec
SMMJ123549.44+621536.8	2.203	237	29.23	335	1144	0.70	11.68	0.0	0.51	9.18	12.29	33.2	1.11	1.98	X,rad
SMMJ123553.26+621337.7	2.098	1460	6.05	1223	802	5.73	11.33	31.8	0.42	8.85	12.85	52.6	2.99	2.70	SB
SMMJ123555.14+620901.7	1.875	332	11.94	358	2252	0.61	11.76	1.0	0.61	8.98	12.32	33.2	1.41	1.72	X,mIR,rad
SMMJ123600.10+620253.5	2.710	3733	6.49	3066	6407	8.92	11.54	51.6	0.29	8.52	13.25	71.5	3.64	2.20	rad
SMMJ123600.15+621047.2	1.994	1449	3.04	1102	1602	2.53	11.64	15.2	0.89	9.03	12.81	38.7	2.80	2.35	SB,rad
SMMJ123606.72+621550.7	2.416	448	30.23	354	454	1.27	11.45	6.9	0.65	8.92	12.32	33.2	1.15	2.41	X,spec,mIR
SMMJ123606.85+621021.4	2.509	1291	12.59	1153	1531	1.17	11.99	5.6	0.79	9.34	12.83	33.2	1.58	2.39	X,rad
SMMJ123616.15+621513.7	2.578	968	2.91	754	1179	0.80	11.97	4.5	1.12	9.04	12.64	33.2	2.17	2.32	X
SMMJ123618.33+621550.5	1.865	339	2.20	325	1585	0.66	11.70	2.4	1.10	9.25	12.28	28.5	2.33	1.83	SB,rad
SMMJ123621.27+621708.4	1.988	330	5.65	266	1797	0.32	11.91	1.5	1.30	9.43	12.19	24.4	1.92	1.69	SB,rad
SMMJ123622.65+621629.7	2.466	1981	6.78	1438	1403	1.72	11.92	10.8	0.90	8.90	12.92	45.1	2.40	2.53	X
SMMJ123629.13+621045.8	1.013	202	0.69	176	207	0.35	11.70	1.5	1.53	9.07	12.01	24.4	2.13	2.45	X
SMMJ123632.61+620800.1	1.993	1067	17.30	973	1107	4.52	11.33	22.7	0.45	8.45	12.75	71.5	1.70	2.46	X,spec,mIR,rad
SMMJ123634.51+621241.0	1.219	309	4.49	289	901	0.64	11.66	2.4	1.06	8.93	12.23	28.5	2.16	2.02	SB,rad
SMMJ123635.59+621424.1	2.005	1921	14.81	1740	1087	7.23	11.38	37.1	0.25	8.45	13.01	71.5	2.31	2.72	X,spec,mIR
SMMJ123636.75+621156.1	0.557	11	0.94	21	24	0.69	10.47	0.8	0.67	9.36	11.08	15.2	1.04	2.44	X,spec
SMMJ123651.76+621221.3	0.298	6	0.12	14	7	1.02	10.13	0.9	0.98	8.91	10.90	13.3	1.93	2.79	…
SMMJ123707.21+621408.1	2.484	361	4.01	338	905	0.38	11.95	1.3	0.92	8.95	12.29	33.2	1.65	2.09	X,rad
SMMJ123711.98+621325.7	1.992	371	2.50	337	658	1.72	11.29	8.0	0.61	8.64	12.29	45.1	2.30	2.23	X,rad
SMMJ123712.05+621212.3	2.914	150	4.96	247	604	0.20	12.10	0.0	1.32	9.53	12.16	24.4	1.91	2.13	X,spec,rad
SMMJ123716.01+620323.3	2.037	879	567.07	1091	1399	1.28	11.93	0.0	0.31	8.74	12.80	45.1	0.18	2.41	X,spec
SMMJ123721.87+621035.3	0.979	76	2.44	91	96	0.33	11.44	0.6	0.80	9.77	11.72	16.9	1.12	2.49	X,spec
SMMJ131201.17+424208.1	3.405	4375	37.82	3748	1992	16.26	11.36	88.3	0.18	8.14	13.34	113.3	3.08	2.79	spec
SMMJ131208.82+424129.1	1.544	787	3.75	551	560	1.75	11.50	10.9	0.74	8.70	12.51	45.1	1.99	2.51	spec
SMMJ131212.69+424422.5	2.805	2095	2.18	1470	2710	2.22	11.82	14.4	1.29	8.89	12.93	38.7	3.44	2.25	spec,rad
SMMJ131215.27+423900.9	2.565	2361	3387.93	80	1498	0.04	12.32	0.0	0.32	9.90	11.67	15.4	0.00	1.24	spec,mIR
SMMJ131222.35+423814.1	2.565	600	512.57	510	569	0.88	11.76	0.0	0.31	8.75	12.47	33.2	0.10	2.47	spec,mIR
SMMJ131225.20+424344.5	1.038	238	8.94	252	205	2.26	11.05	7.2	0.36	8.42	12.17	38.7	1.46	2.60	…
SMMJ131225.73+423941.4	1.554	742	5.47	661	5188	3.94	11.22	19.1	0.59	8.62	12.59	45.1	2.14	1.62	rad
SMMJ131228.30+424454.8	2.931	1572	16.32	1131	1482	2.43	11.67	15.3	0.61	8.30	12.82	61.3	1.75	2.40	…
SMMJ131231.07+424609.0	2.713	1212	1.42	910	966	5.13	11.25	31.8	0.66	8.70	12.72	45.1	3.95	2.49	…
SMMJ131232.31+423949.5	2.320	2457	8.41	1660	1635	1.60	12.02	10.8	0.87	8.47	12.99	61.3	2.40	2.52	mIR
SMMJ131239.14+424155.7	2.242	1271	3.75	1068	795	3.32	11.51	17.9	0.80	9.01	12.79	38.7	2.87	2.64	…

SMG	z	SFR ($M_\odot$ yr^{-1}) SED	UV	IR	radio	SSFR (Gyr^{-1})	$\log M_*$ ($M_\odot$)	$M_{\rm burst}/M_*$ (%)	M_*/L_K ($M_\odot/L_\odot$)	$\log M_d$ ($M_\odot$)	$\log L_{\rm IR}$ ($L_\odot$)	T_d (K)	A_V (mag)	q	AGN?
(1)	(2)	(3)	(4)	(5)	(6)	(7)	(8)	(9)	(10)	(11)	(12)	(13)	(14)	(15)	(16)
SMMJ141741.81+522823.0	1.150	948	13.50	770	274	0.75	12.01	3.8	0.72	8.48	12.65	45.1	1.28	2.97	mIR
SMMJ141742.04+523025.7	0.661	403	11.08	267	216	2.02	11.12	13.8	0.40	8.23	12.19	45.1	1.74	2.61	…
SMMJ141750.50+523101.0	2.128	343	5.31	241	808	1.91	11.10	12.5	0.66	8.58	12.15	38.7	2.29	1.99	…
SMMJ141800.40+512820.3	1.913	1999	17.45	1095	1424	0.39	12.44	3.3	0.80	8.61	12.80	52.6	0.89	2.40	…
SMMJ141802.87+523011.1	2.127	1325	10.95	1127	552	11.82	10.98	63.5	0.74	8.34	12.82	61.3	2.87	2.83	…
SMMJ141809.00+522803.8	2.712	1213	6.24	551	1641	0.33	12.23	3.3	0.83	8.64	12.51	45.1	1.09	2.04	…
SMMJ141813.54+522923.4	3.484	243	6.65	240	3967	1.16	11.31	4.2	0.60	8.86	12.15	33.2	1.35	1.30	spec,rad
SMMJ163627.94+405811.2	3.180	1332	18.32	1095	3210	6.32	11.24	34.0	0.65	8.82	12.80	45.1	2.41	2.05	spec
SMMJ163631.47+405546.9	2.283	1325	10.28	865	1646	1.77	11.69	12.5	0.96	8.94	12.70	38.7	2.62	2.24	spec
SMMJ163639.01+405635.9	1.495	250	7.51	1101	1002	6.49	11.23	4.8	0.53	8.94	12.81	32.7	1.46	2.56	mIR,rad
SMMJ163650.43+405734.5	2.378	1147	73.43	1191	4030	3.24	11.57	10.1	0.33	8.93	12.84	45.1	1.12	1.99	spec,mIR,rad
SMMJ163658.19+410523.8	2.454	1769	4.97	1485	1801	2.55	11.77	13.8	0.80	9.04	12.94	45.1	2.45	2.43	…
SMMJ163658.78+405728.1	1.190	129	8.41	171	274	0.56	11.49	0.9	0.59	9.13	11.10	24.4	1.14	2.31	…
SMMJ163704.34+410530.3	0.840	205	2.50	157	74	2.22	10.85	13.1	0.92	9.13	11.96	33.2	2.43	2.84	…
SMMJ163706.51+405313.8	2.374	2020	9.63	1478	1344	1.83	11.91	10.9	0.76	9.06	12.94	45.1	1.99	2.56	spec
SMMJ221724.69+001242.1	0.510	154	14.71	43	62	0.21	11.31	3.4	0.63	9.36	11.40	15.9	0.69	2.36	…
SMMJ221725.97+001238.9	3.094	2499	2.29	1935	1353	2.10	11.96	12.5	1.58	9.38	13.05	38.7	3.27	2.67	…
SMMJ221733.02+000906.0	0.926	447	0.72	381	333	0.88	11.64	4.5	1.56	9.16	12.35	33.2	2.58	2.58	…
SMMJ221733.12+001120.2	0.652	31	2.77	59	62	0.28	11.33	4.7	1.79	9.13	11.54	21.8	1.27	2.49	rad
SMMJ221733.91+001352.1	2.555	875	17.73	731	954	0.78	11.97	3.8	0.79	9.01	12.63	38.7	1.69	2.40	…
SMMJ221735.15+001537.2	3.098	594	8.51	536	1627	2.28	11.37	10.0	0.68	8.94	12.49	38.7	1.93	2.03	…
SMMJ221735.84+001558.9	3.089	1969	7.43	1668	1450	6.49	11.41	35.0	0.30	8.35	12.99	71.5	2.98	2.58	…
SMMJ221737.39+001025.1	2.614	2991	13.32	2641	2484	7.05	11.57	37.1	0.29	8.47	13.19	71.5	2.70	2.54	…
SMMJ221804.42+002154.4	2.517	1474	15.50	1239	908	6.30	11.29	33.5	0.55	8.85	12.86	52.6	2.11	2.65	mIR
SMMJ221806.77+001245.7	3.623	8825	29.59	7774	11225	20.81	11.57	109.9	0.23	8.25	13.66	113.3	3.76	2.36	rad
mean	2.002	1065	68.35	873	1429	3.51	11.71	15.6	0.75	9.02	12.71	40.1	2.03	2.34	…
median	2.148	825	6.78	659	1087	1.72	11.54	7.2	0.68	8.91	12.58	38.7	1.99	2.40	…
std dev	0.851	1271	395.38	1066	1731	7.44	0.55	23.2	0.36	0.36	0.60	18.3	0.95	0.34	…
min	0.080	3	0.04	2	4	0.04	8.78	0.0	0.18	8.14	10.11	11.4	0.00	1.24	…
max	3.623	8825	3387.93	7774	11225	59.74	12.44	113.3	1.79	9.90	13.66	113.3	4.38	2.97	…

Note. — Column (1): SMG name. Column (2): redshift (Chapman et al., 2005). Column (3): total star formation rate (SFR) for $0.15 - 120\,M_\odot$ stars averaged over the last 50 Myr derived from the SED model. Column (4): SFR from UV emission interpolated from the SED template (using Kennicutt, 1998). Column (5): SFR from IR emission (Column 12) used in all analysis throughout the paper (using Kennicutt, 1998). Column (6): SFR from radio emission derived directly from the radio data (using Bell, 2003). Column (7): specific SFR $\equiv$ SFR$_{\rm IR}/M_*$. Column (8): stellar mass. Column (9): Ratio of the mass of gas converted to star during the recent starburst episode to the total stellar mass. There are values greater than 100%, because the starburst episode is ongoing; 0% means that non-starburst template was adopted. Column (10): stellar mass to light ratio (luminosity at rest-frame K was intepolated using the best SED model). Column (11): dust mass. Column (12): total $8 - 1000$ μm infrared luminosity. Column (13): dust temperature. Column (14): Average extinction $A_V = 2.5\log(V$-band starlight unextinguished / V-band starlight observed). Column (15): FIR-radio correlation parameter (Section 6.5.4). Column (16): AGN flag — X: X-ray identified AGN; SB: X-ray identified starburst (Alexander et al., 2005); spec: spectroscopically identified AGN or QSO (Chapman et al., 2005); mIR: mid-IR identified AGN (Section 6.5.4); rad: radio datapoint is more than 3σ above the starburst model (Section 6.5.4). This table is available in a machine-readable form in the electronic edition of the Journal.

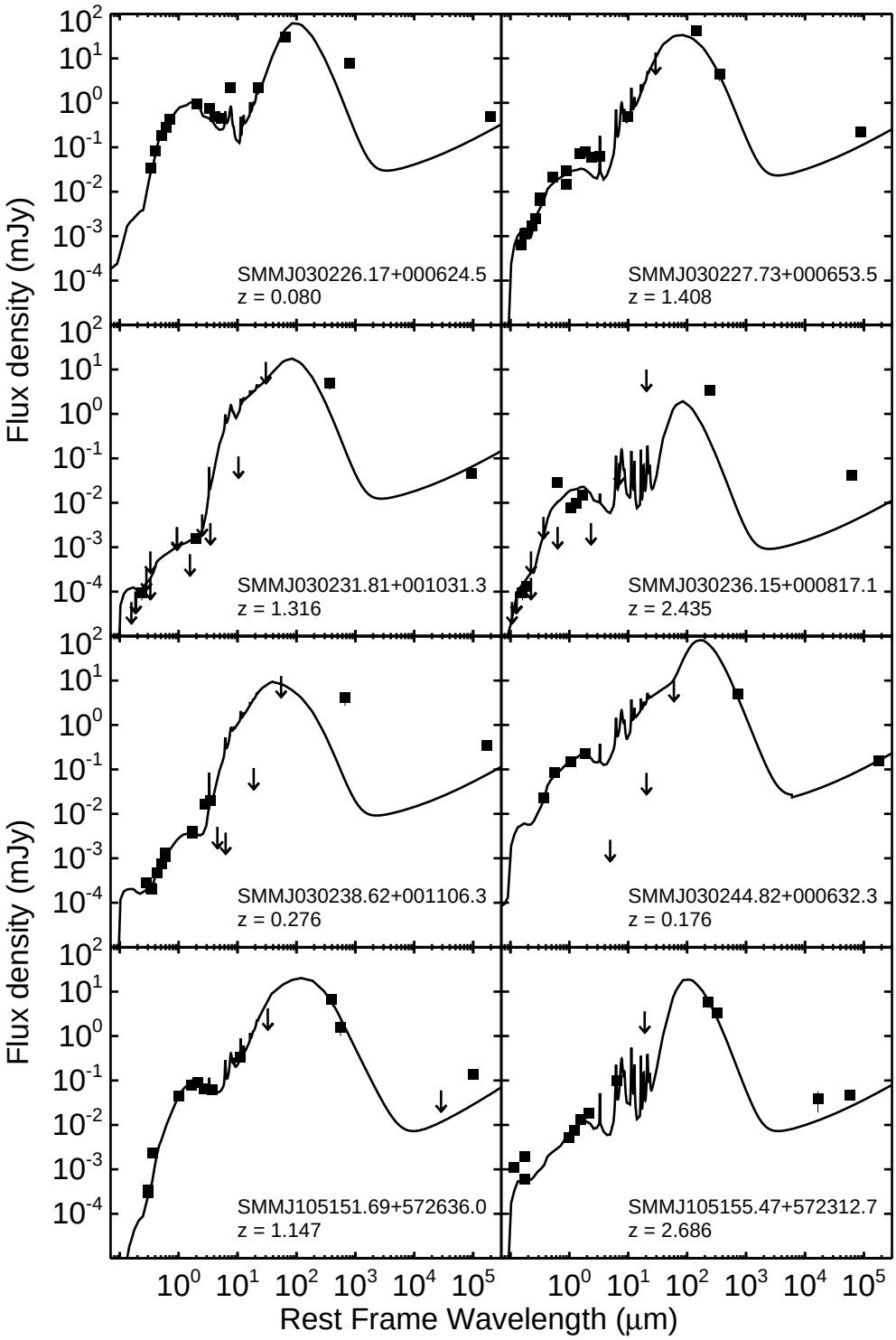

Figure 6.7: *Spectral energy distributions (SEDs) of SMGs. Solid lines: the best GRASIL fits. Dashed lines: SEDs of GRB hosts (Michałowski et al., 2008) shown for comparison. Squares: detections with errors, in most cases, smaller than the size of the symbols. Arrows: 3σ upper limit (values marked at the base). In the cases where our fits strongly underpredict the observed data at 850 μm, we adopted $L_{\rm IR}$ and T_d of Chapman et al. (2005).*

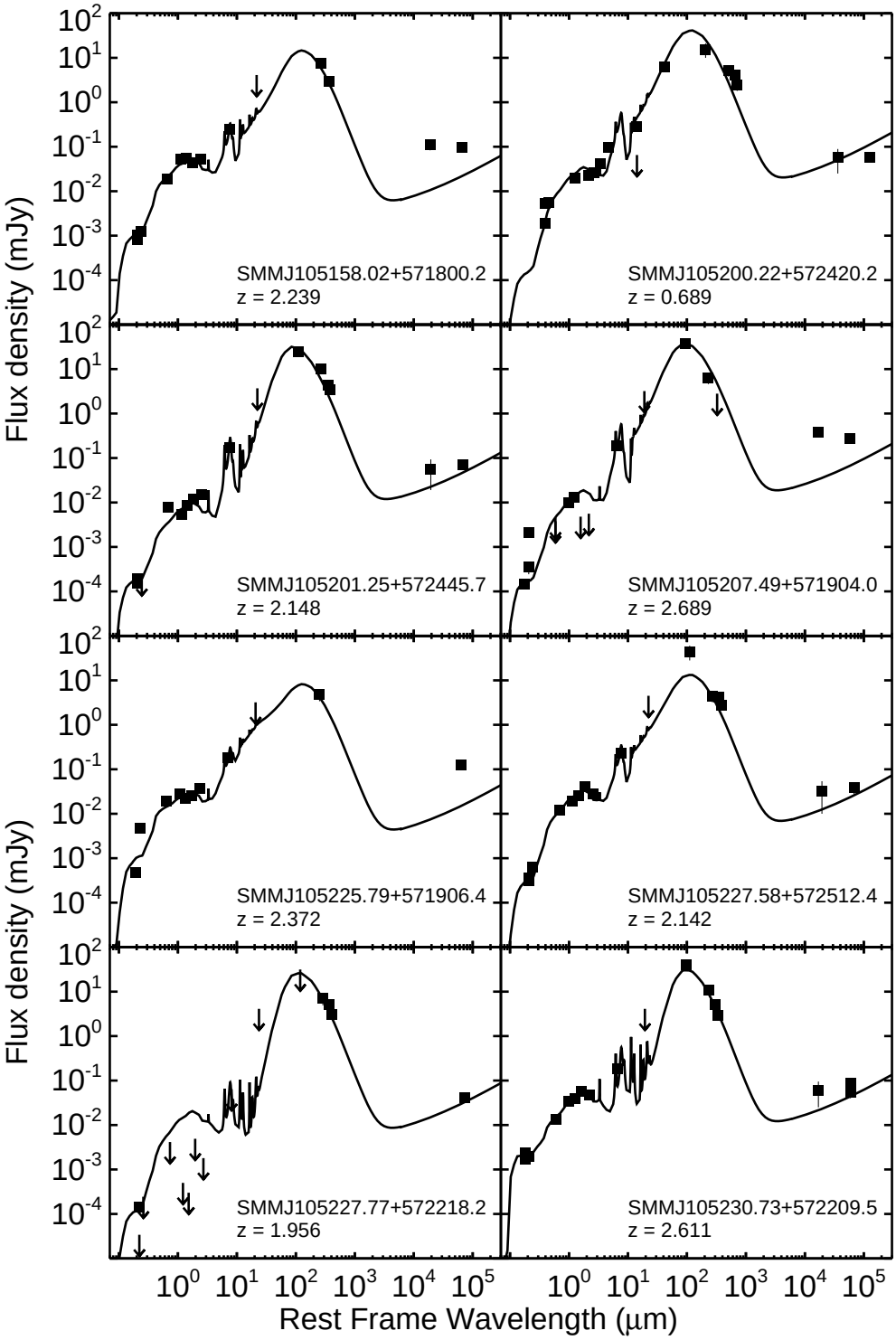

Figure 6.7: *(continued).*

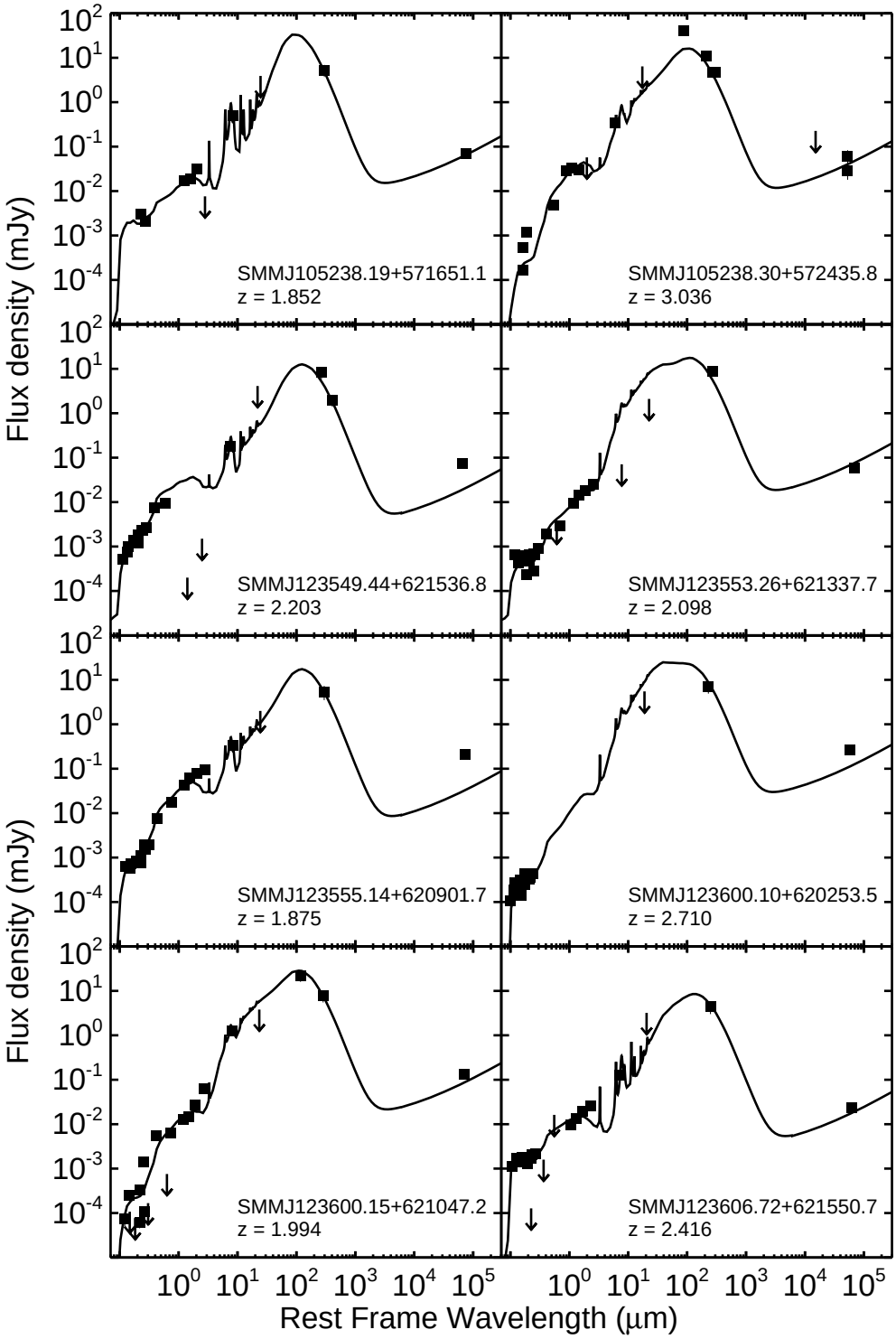

Figure 6.7: *(continued).*

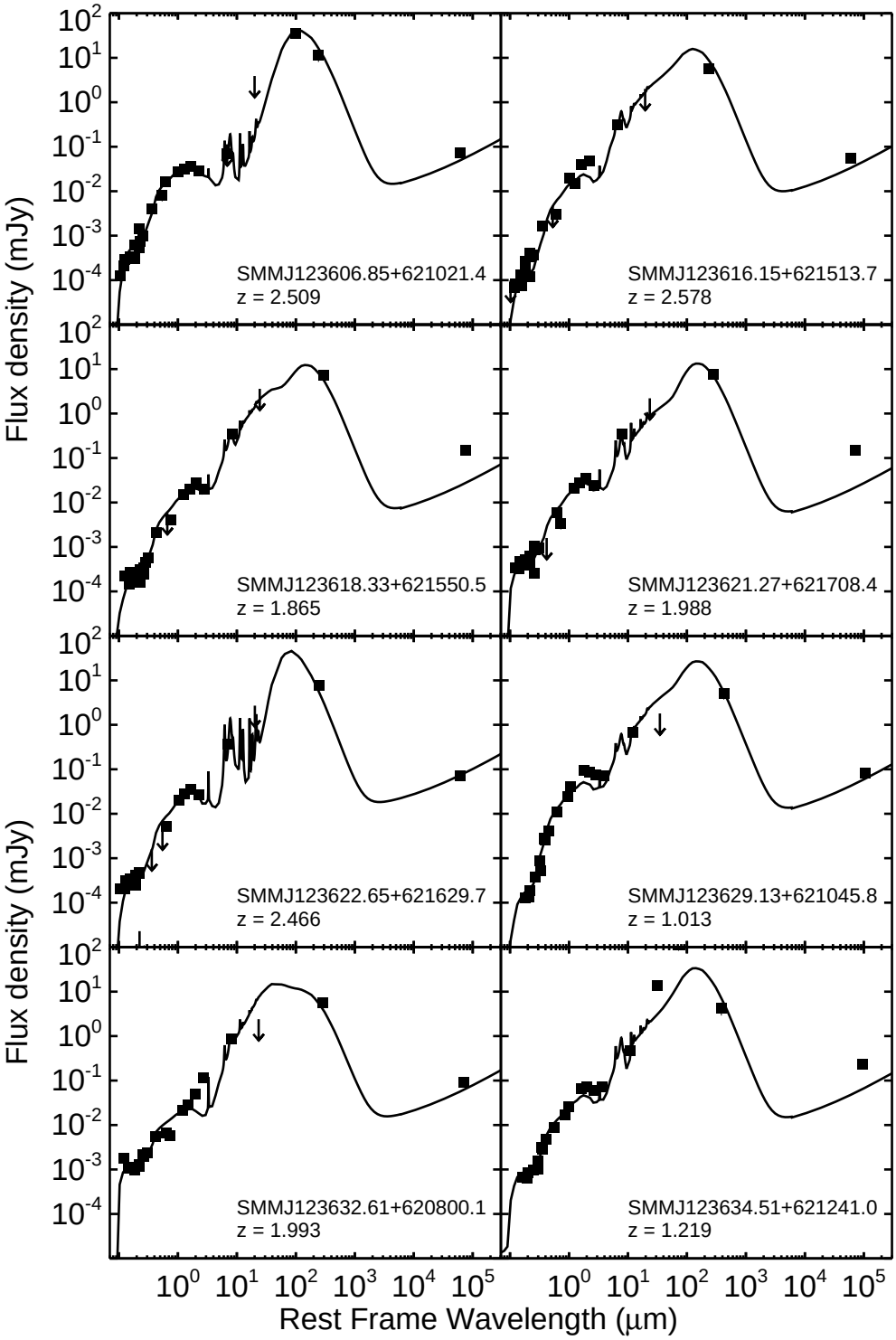

Figure 6.7: *(continued).*

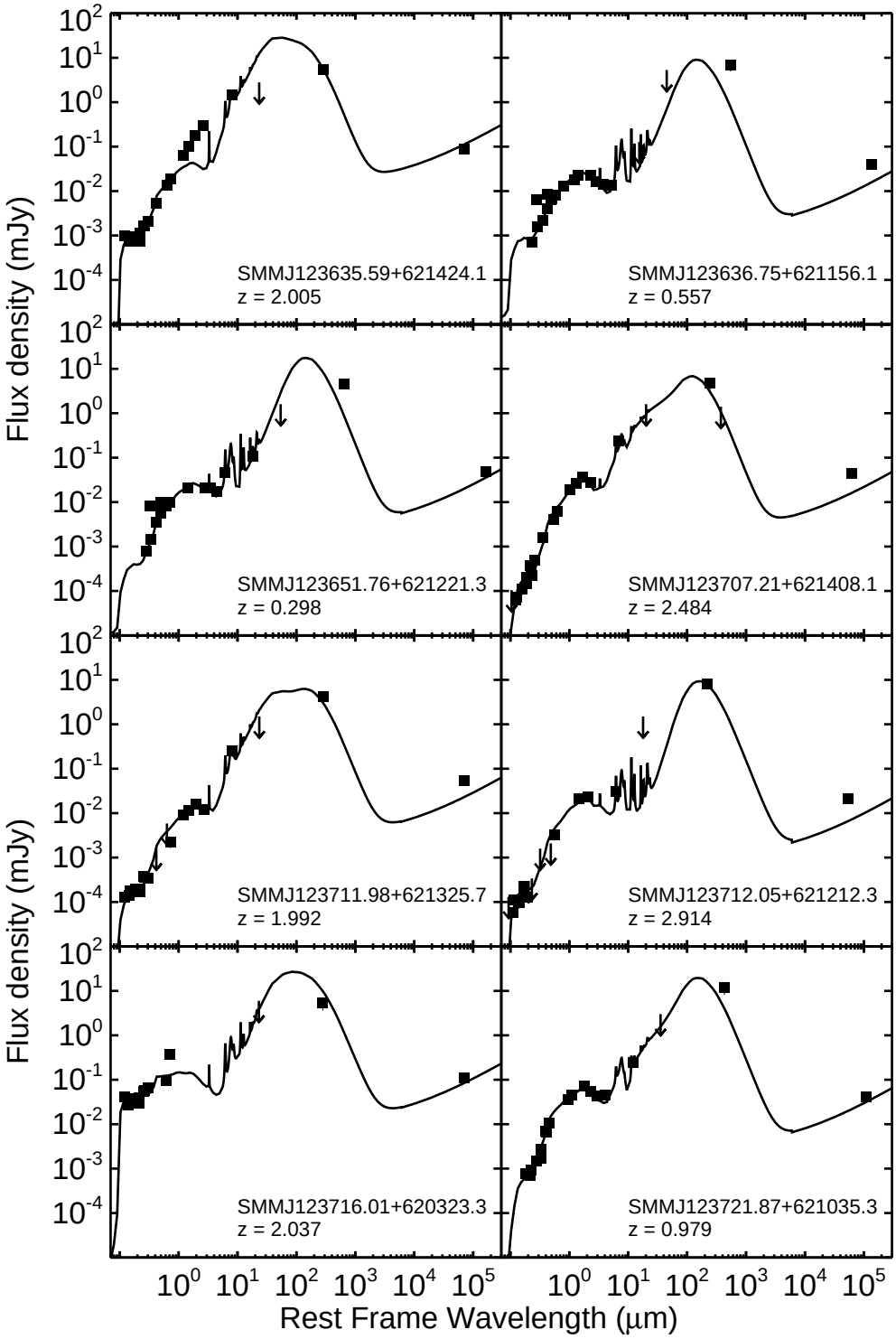

Figure 6.7: *(continued).*

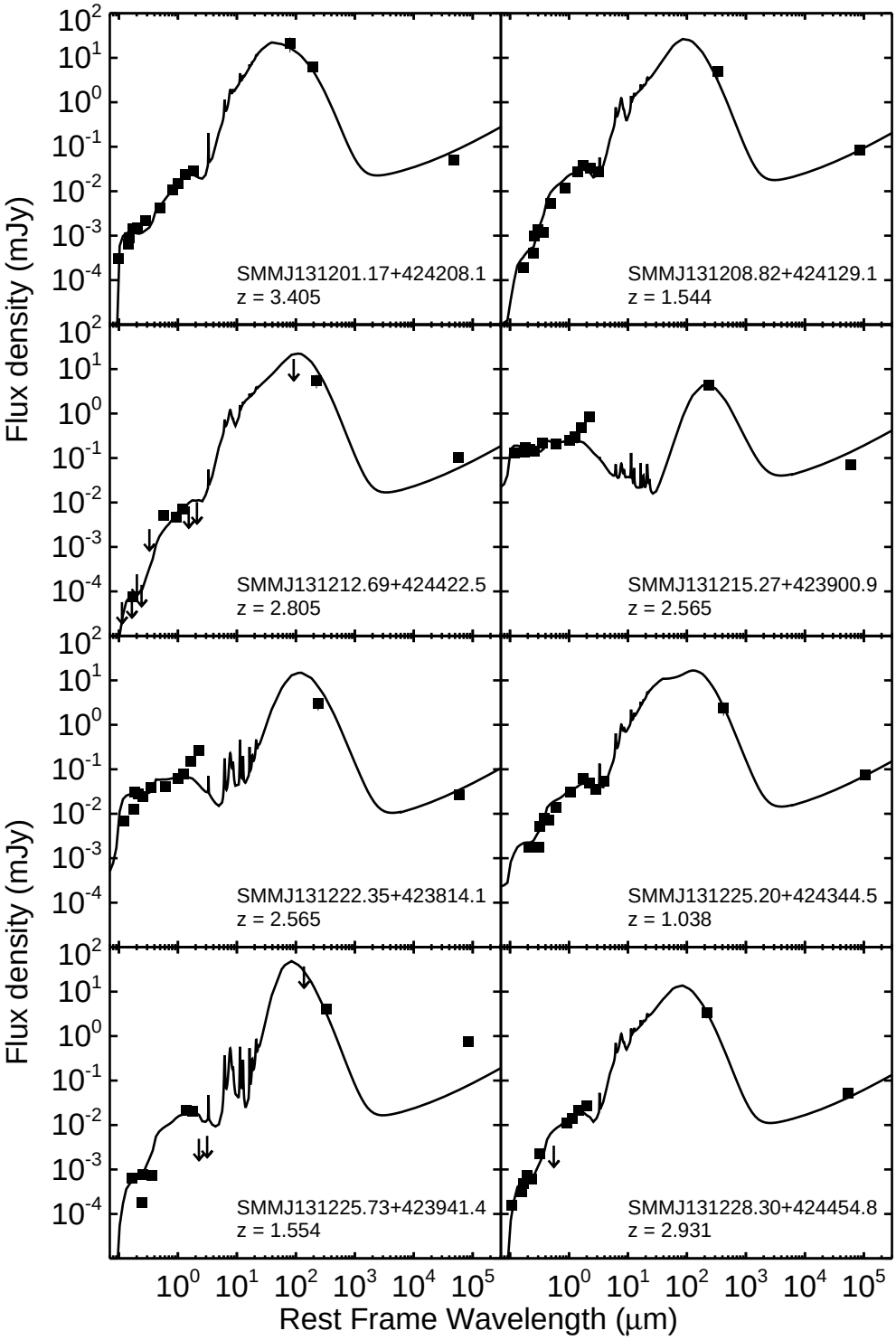

Figure 6.7: *(continued).*

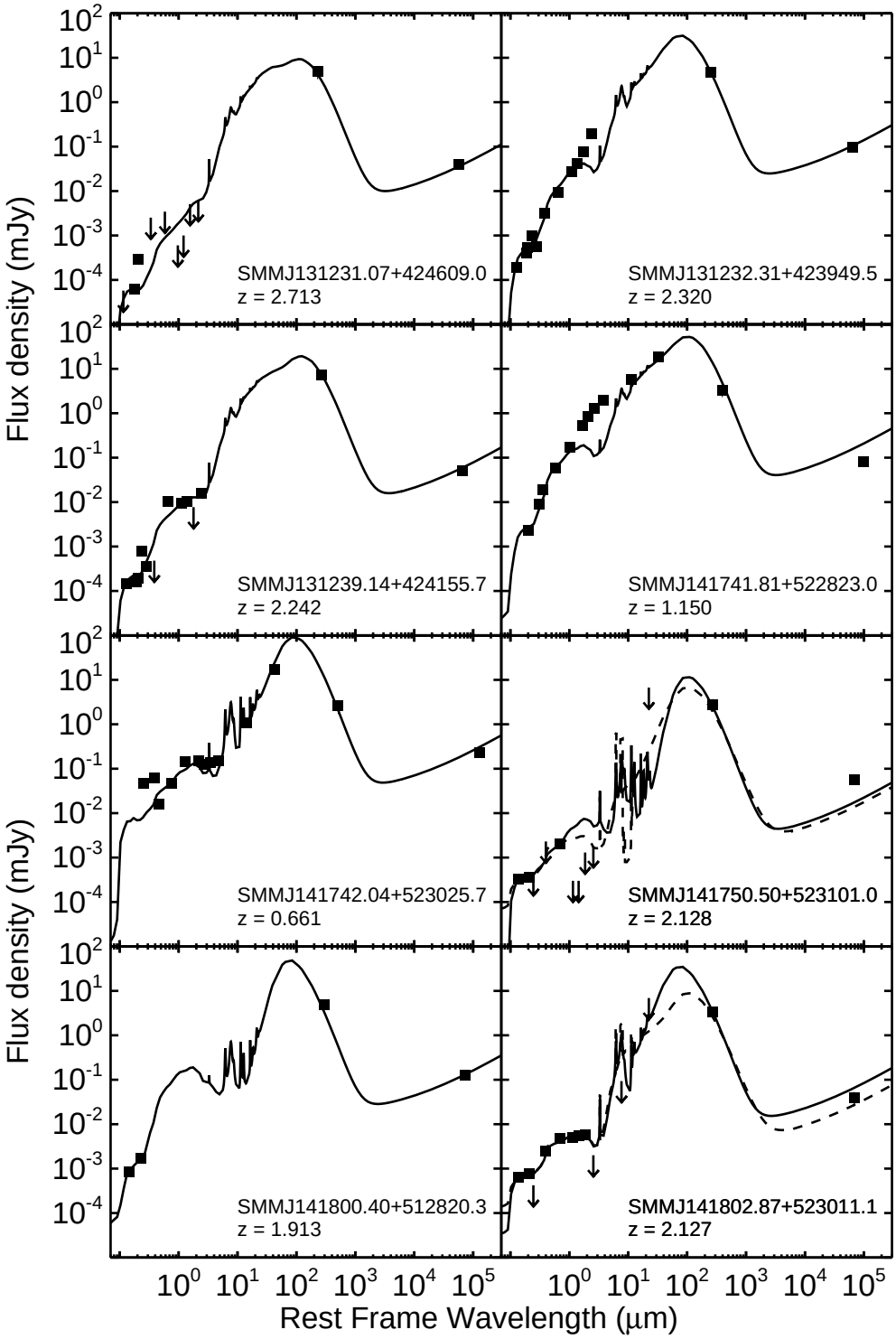

Figure 6.7: *(continued).*

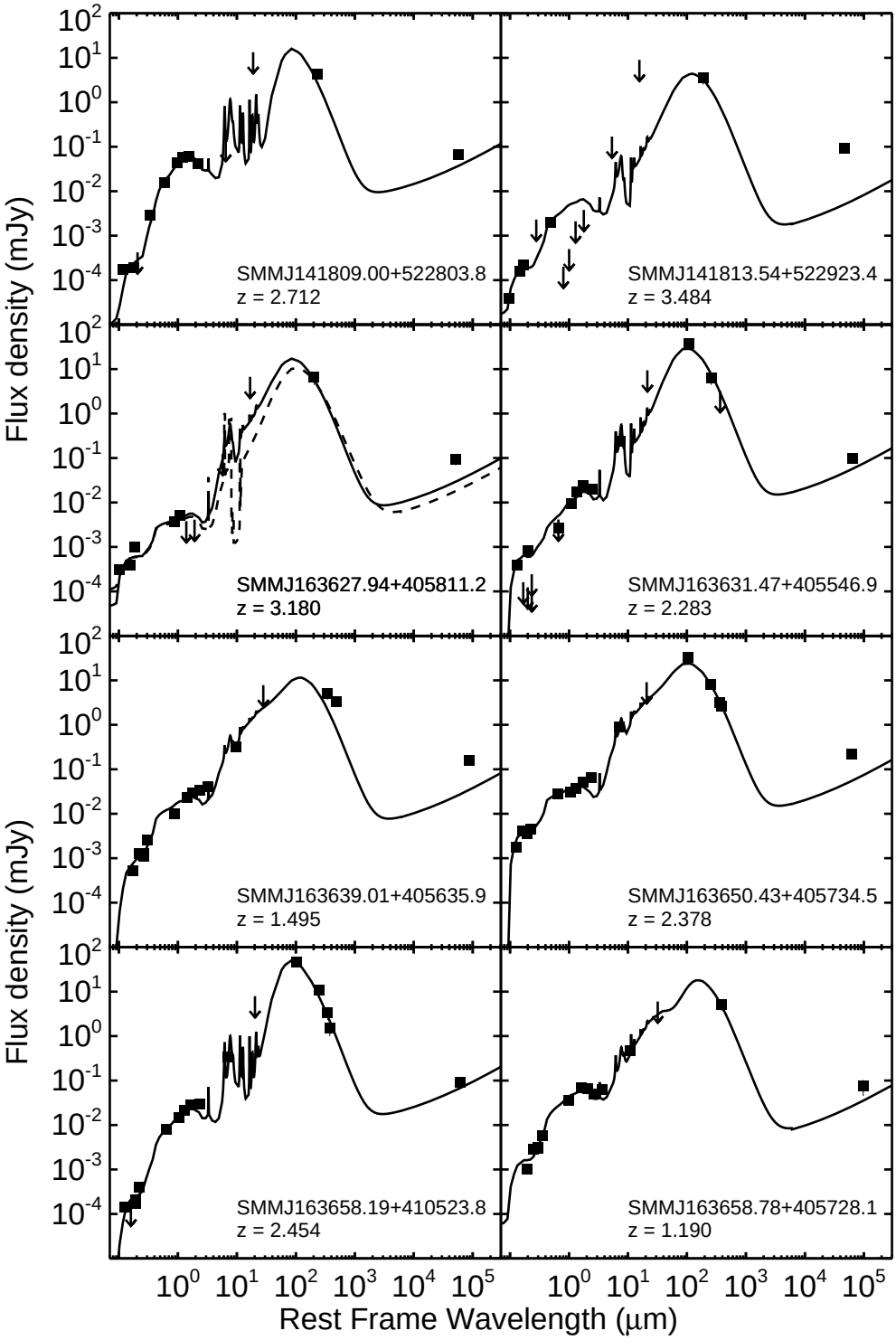

Figure 6.7: *(continued).*

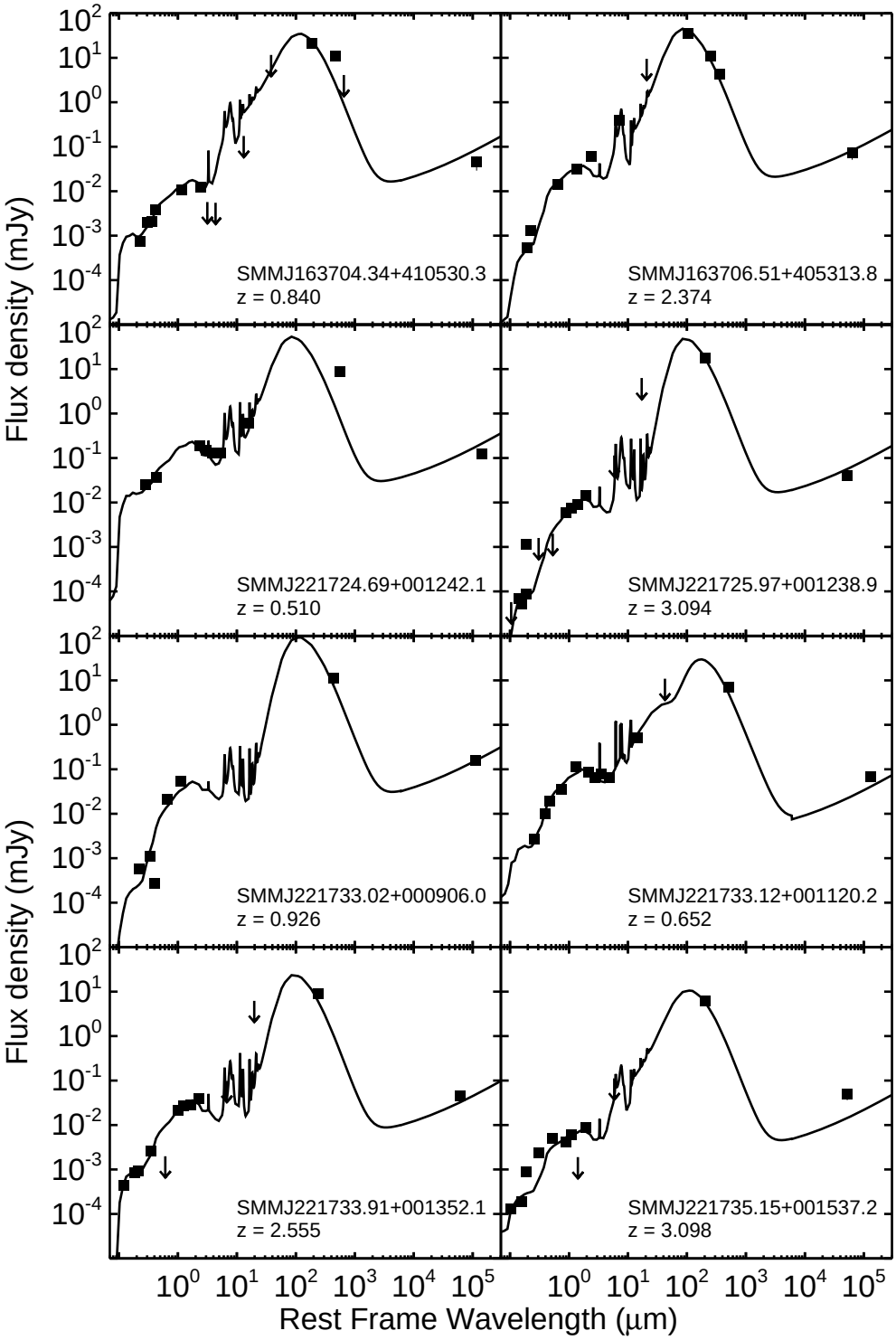

Figure 6.7: *(continued).*

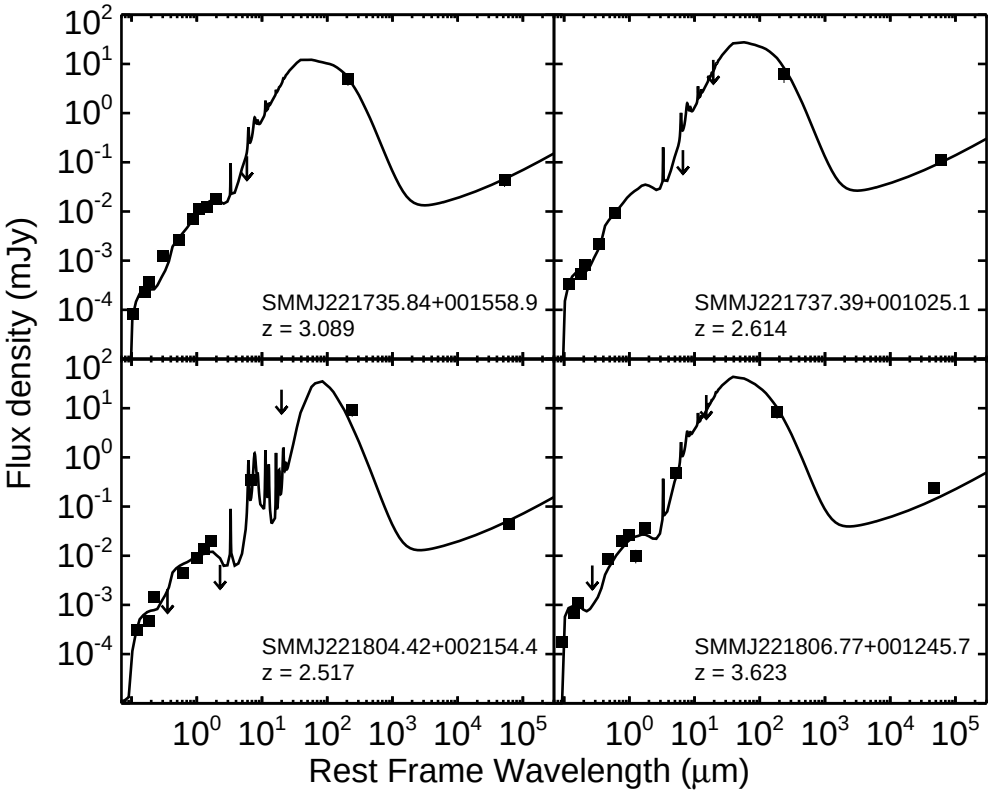

Figure 6.7: *(continued).*

Published as: Michałowski, M. J., Watson, D. & Hjorth, J. – *Rapid dust production in submillimeter galaxies at $z > 4$?*, Astrophysical Journal, submitted.

7

FORMATION OF STARS AND DUST IN SUBMILLIMETER GALAXIES AT REDSHIFTS $z > 4$

ABSTRACT –

The existence of submillimeter-selected galaxies (SMGs) at redshifts $z > 4$ has recently been confirmed. Using simultaneously all the available data from UV to radio we have modelled the spectral energy distributions of the six known spectroscopically confirmed SMGs at $z > 4$. We find that their star formation rates (average $\sim 2500\ M_{\odot}\ yr^{-1}$), stellar ($\sim 3.6 \times 10^{11}\ M_{\odot}$) and dust ($\sim 6.7 \times 10^{8}\ M_{\odot}$) masses, extinction ($A_V \sim 2.2$ mag) and gas-to-dust ratios (~ 60) are within the ranges for $1.7 < z < 3.6$ SMGs. Our analysis suggests that the infrared-to-radio luminosity ratios of SMGs do not change up to redshift ~ 5 and are lower by a factor of ~ 2.1 than the value corresponding to the local IR-radio correlation. However, we also find dissimilarities between $z > 4$ and lower-redshift SMGs. Those at $z > 4$ tend to be among the most star-forming, least massive and hottest (~ 60 K) SMGs and exhibit the highest fraction of stellar mass formed in the ongoing starburst ($\sim 45\%$). This indicates that at $z > 4$ we see earlier stages of evolution of submillimeter-bright galaxies. Using the derived properties for $z > 4$ SMGs we investigate the origin of dust at epochs less than 1.5 Gyr after the Big Bang. This is significant to our understanding of the evolution of the early Universe. For three $z > 4$ SMGs asymptotic giant branch stars could be the dominant dust producers. However, for other three only supernovae are efficient and fast enough to be responsible for dust production, though requiring a very high dust yield per supernova (0.15–$0.65\ M_{\odot}$, such as that claimed in the Cassiopeia A and Kepler supernova remnants). The required dust yields are lower if a top-heavy initial mass function or significant dust growth in the interstellar medium are assumed. We estimate lower limits of the contribution of SMGs to the cosmic star formation and stellar mass densities at $z \sim 4$–5 to be $\sim 4\%$ and $\sim 1\%$, respectively.

7.1 INTRODUCTION

Submillimeter-selected galaxies (SMGs) are among the most powerful starburst galaxies in the Universe. Most of them have been found at redshifts 1.5–3 (Chapman et al., 2005). Their complex selection criteria (Blain et al., 2004), in particular the requirement of a radio detection to obtain a precise localisation, make it difficult to discover the very high-redshift tail of SMGs. This was addressed using deep, high resolution observations of SMGs (Iono et al., 2006; Tacconi et al., 2006, 2008; Wang et al., 2007, 2009; Younger et al., 2007, 2008a,b, 2009b,a; Dannerbauer et al., 2008; Cowie et al., 2009). The existence of SMGs at $z > 4$ has recently been spectroscopi-

cally confirmed by Coppin et al. (2009), Capak et al. (2008), Schinnerer et al. (2008), Daddi et al. (2009b,a) and Knudsen et al. (2008a, 2009).

At these redshifts the age of the Universe is < 1.5 Gyr, which enforces the need for careful analysis of the timescales for formation of stars and dust. The important question is if supernovae (SNe), or asymptotic giant branch (AGB) stars, or some other sources are responsible for production of dust residing in these galaxies. Locally, dust is predominantly formed by evolved, post-main-sequence stars (Gehrz, 1989), but the situation may be different at high redshifts. Dwek et al. (2007) claimed that only SNe can produce dust on timescales less than 1 Gyr, but it has been shown by Valiante et al. (2009) that AGB stars begin to dominate dust production over SNe as early as 150–500 Myr after the onset of star formation. SN-origin dust has been claimed to be present in $z \sim 6.2$ quasar (Maiolino et al., 2004) and $z \sim 6.3$ gamma-ray burst host galaxy (Stratta et al. 2007, but see other interpretation of their data in Zafar et al. 2009, in prep.)

In order to understand the formation of SMGs and their evolution through cosmic time, it is also important to compare high- and low-redshift SMG samples. This may help to constrain when their stars were formed.

SMGs at $z > 4$ are also suitable to study infrared (IR) - radio correlation. This remarkably tight correlation, found locally (Helou et al., 1985; Condon, 1992), was studied both at intermediate ($z \lesssim 1$; Garrett, 2002; Gruppioni et al., 2003; Appleton et al., 2004; Boyle et al., 2007; Marleau et al., 2007; Vlahakis et al., 2007; Yang et al., 2007) and high redshifts ($z \lesssim 3.5$; Appleton et al., 2004; Kovács et al., 2006; Beswick et al., 2008; Hainline, 2008; Ibar et al., 2008; Sajina et al., 2008; Garn et al., 2009; Michałowski et al., 2009b; Murphy et al., 2009; Murphy, 2009; Rieke et al., 2009; Seymour et al., 2009; Younger et al., 2009b). No significant evolution of the correlation was found up to these redshifts, but SMGs seem to form a correlation by their own offset towards higher radio luminosities (Kovács et al., 2006; Michałowski et al., 2009b; Murphy et al., 2009; Murphy, 2009). The only sign of evolution was reported by Ivison et al. (2009) based on stacking analysis of the 24 μm-selected galaxies, though possibly interpreted as a selection effect. It is however possible that the correlation breaks down at even earlier epochs due to changes in star-formation processes e.g. suppression of radio emission in inverse Compton losses off the CMB photons as suggested by Lacki et al. (2009), Lacki & Thompson (2009) and Murphy (2009).

In Michałowski et al. (2009b) we analysed the full UV-to-radio spectral energy distributions (SEDs) of 76 SMGs from the Chapman et al. (2005) sample with spectroscopic redshifts up to $z < 3.6$. Here we extend that study by analysing the sample of all spectroscopically confirmed SMGs at $z > 4$. The main objective of this chapter is to characterize the required efficiency of dust producers (SNe and AGB stars) at these early epochs of the evolution of the Universe. In Section 7.2 the SMG sample is presented. We outline our methodology and derive the properties of SMGs in Section 7.3 and discuss the implications in Section 7.4. Section 7.5 closes with our conclusions. We use a cosmological model with $H_0 = 70$ km s^{-1} Mpc^{-1}, $\Omega_\Lambda = 0.7$ and $\Omega_m = 0.3$.

7.2 SAMPLE

We selected all six SMGs with robust (optical or CO) redshifts at $z > 4$ identified by Coppin et al. (2009), Capak et al. (2008), Schinnerer et al. (2008), Daddi et al. (2009b,a) and Knudsen et al. (2008a, 2009) in the ECDF-S (900 arcmin^2; Coppin et al., 2009; Greve et al., 2009; Weiss et al., 2009), COSMOS (1080 arcmin^2; Scott et al., 2008), GOODS-N (100 arcmin^2; Hughes et al., 1998; Barger et al., 2000; Chapman et al., 2001; Borys et al., 2003; Serjeant et al., 2003; Wang et al., 2004) and Abell 2218 (11.8 arcmin^2; Knudsen et al., 2006) fields. The photometric data are

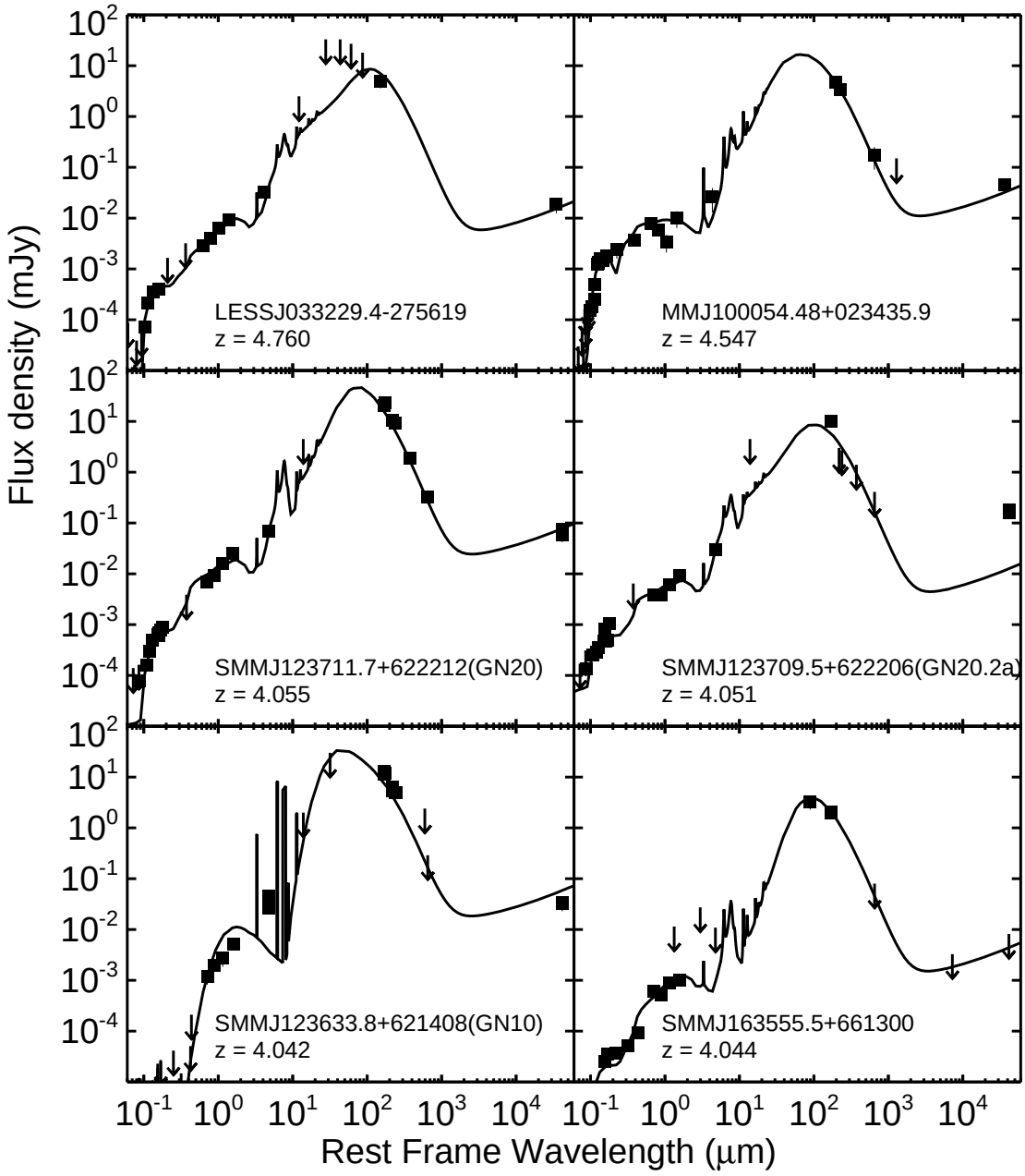

Figure 7.1: *Spectral energy distributions (SEDs) of $z > 4$ SMGs. Solid lines: the best GRASIL fits. Squares: detections with errors, in most cases, smaller than the size of the symbols. Arrows: 3σ upper limits (values marked at the base). The data for SMMJ163555.5+661300 has been corrected for lensing magnification of a factor of 5.5.*

presented in Tables 1 and 2 in Michałowski et al. (2009c) The data for SMMJ163555.5+661300 has been corrected for lensing magnification of a factor of 5.5 obtained by Knudsen et al. (2009) using the model of Elíasdóttir et al. (2007).

Our sample is not homogeneously selected. Namely, some of the sources are bright enough

in the optical to allow spectroscopy, whereas redshifts of some of them were measured based on CO emission (one even not detected at optical wavelengths). In particular, LESSJ033229.4-275619 and MMJ100054.48+023435.9 were targeted spectroscopically, because they are V-dropouts suggesting $z \approx 5$ (Coppin et al., 2009; Capak et al., 2008) and their optical counterparts (and hence, redshifts) are based on detections at radio wavelengths, which likely biases them towards high star formation rates (SFRs). The CO lines from SMMJ123711.7+622212 (called GN20 in Pope et al., 2006) and SMMJ123709.5+622206 (GN20.2a) were detected serendipitously while observing an angularly close galaxy at $z = 1.522$ (Daddi et al., 2009b); and the CO emission of SMMJ123633.8+621408 (GN10) was searched for under the assumption that it is a member of the protocluster structure containing GN20 and GN20.2a (Daddi et al., 2009a). Finally, SMMJ163555.5+661300 was detected because of its lensing magnification and is therefore intrinsically the faintest member of our sample.

It is therefore not easy to quantify how selection effects influence our results. Very likely our sample is biased towards high luminosity objects, i.e., with high SFRs. This is supported by the fact that SMMJ163555.5+661300, magnified by lensing, has a much lower SFR than blank-field members of our sample (Table 7.1). However, given the significance of the *Spitzer* IRAC detections (rest-frame ~ 1–$2\,\mu$m) of $\gtrsim 10\sigma$, our sample is *not* biased against low stellar masses.

7.3 SED Fitting and Results

We applied the SED fitting method detailed in Michałowski et al. (2008, 2009a,b, see therein a discussion of the derivation of galaxy properties and typical uncertainties) based on 35 000 templates in the library of Iglesias-Páramo et al. (2007), plus some templates of Silva et al. (1998) and Michałowski et al. (2008), all developed in GRASIL (Silva et al., 1998). The templates cover a broad range of galaxy properties and were tested to reproduce the SEDs of high-redshift galaxies (Silva et al., 1998; Iglesias-Páramo et al., 2007; Michałowski et al., 2008, 2009b).

In all but one case we obtained the best fits using the library of Iglesias-Páramo et al. (2007). For GN10 we fitted a model corresponding to a 0.1 Gyr old progenitor of an elliptical galaxy (Silva et al., 1998) with modified maximum grain temperatures from 400 to 100 K in order to suppress strong mid-IR emission in the original model, otherwise inconsistent with the data. All other models failed to reproduce its extremely red observed-frame 2.1–$3.6\,\mu$m color (Wang et al., 2009).

The best fits[1] are shown in Figure 7.1. It is apparent that GRASIL models can reproduce the SEDs of even such distant galaxies. The resulting properties of the galaxies are listed in Table 7.1.

7.4 Discussion

7.4.1 Formation of stars in $z > 4$ SMGs

All $z > 4$ SMGs in our sample are characterized by an extremely strong starburst episode (average SFR $\sim 2500\,M_\odot$ yr^{-1}, column 5 of Table 7.1) during which a substantial fraction (average $\sim 45\%$, column 9) of their stellar population was formed. They are therefore manifestations of the strongest known star-forming events in the Universe. Their high stellar masses (average $3.6 \times 10^{11}\,M_\odot$) agrees with a suggestion of Davé et al. (2009) based on numerical simulations that the most rapidly star forming galaxies coincide with the most massive galaxies.

[1] The SED fits can be downloaded from `http://archive.dark-cosmology.dk`

Table 7.1: *Properties of the $z > 4$ SMGs derived from the SED modeling*

SMG	z	SFR ($M_\odot$ yr^{-1}) SED	UV	IR	radio	SSFR (Gyr^{-1})	M_* ($10^{11} M_\odot$)	$M_{\rm burst}/M_*$ (%)	M_*/L_K ($M_\odot/L_\odot$)	M_d ($10^9 M_\odot$)	$L_{\rm IR}$ ($10^{13} L_\odot$)	T_d (K)	A_V (mag)	q	AGN?
(1)	(2)	(3)	(4)	(5)	(6)	(7)	(8)	(9)	(10)	(11)	(12)	(13)	(14)	(15)	(16)
LESSJ033229.4-275619	4.760	1718	26	1150	1636	1.82	6.3	12.5	0.68	0.7	0.7	38.7	2.01	2.36	SB,spec
MMJ100054.48+023435.9	4.547	3316	60	2725	3548	14.38	1.9	82.3	0.30	0.4	1.6	71.5	1.77	2.40	SB
SMMJ123711.7+622212(GN20,AzGN01)	4.055	6120	33	4577	4498	5.61	8.2	33.5	0.64	1.1	2.7	61.3	2.55	2.52	…
SMMJ123709.5+622206(GN20.2a,AzGN1.2)	4.051	891	27	841	10700	3.44	2.4	14.3	0.48	1.4	0.5	38.7	1.76	1.41	rad
SMMJ123633.8+621408(GN10,GN850-5,AzGN03)	4.042	2877	0	5031	1951	28.57	1.8	100.0	14.03	0.3	2.9	97.2	7.84	2.93	SB
SMMJ163555.5+661300	4.044	339	1	289	<482	3.40	0.9	18.1	0.95	0.2	0.2	45.1	2.91	>2.29	SB

Note. — Column (1): SMG name (alternative names from Wang et al., 2004, 2009; Pope et al., 2006; Daddi et al., 2009b,a; Perera et al., 2008; Chapin et al., 2009). Column (2): redshift (Coppin et al., 2009; Capak et al., 2008; Daddi et al., 2009b,a; Knudsen et al., 2009). Column (3): total star formation rate (SFR) for $0.15 - 120\,M_\odot$ stars averaged over the last 50 Myr derived from the SED model. Column (4): SFR from UV emission interpolated from the SED template (using Kennicutt, 1998). Column (5): SFR from IR emission (Column 12) used in all analysis throughout the paper (using Kennicutt, 1998). Column (6): SFR from radio emission derived directly from the radio data (using Bell, 2003). Column (7): specific SFR $\equiv$ SFR$_{\rm IR}/M_*$. Column (8): stellar mass. Column (9): Ratio of the mass of gas converted to star during the recent starburst episode to the total stellar mass. Column (10): stellar mass to light ratio (luminosity at rest-frame K was intepolated using the best SED model). Column (11): dust mass. Column (12): total $8 - 1000$ μm infrared luminosity. Column (13): dust temperature (we assumed emissivity index $\beta = 1.3$). Column (14): Average extinction $A_V = 2.5\log(V$-band starlight unextinguished / V-band starlight observed). Column (15): FIR-radio correlation parameter (Section 7.4.3). Column (16): AGN flag — SB: X-ray identified starburst (no X-ray detection; Coppin et al., 2009; Capak et al., 2008; Dannerbauer et al., 2008; Wang et al., 2009; Knudsen et al., 2009), as opposed to X-ray identified AGN (Alexander et al., 2005); spec: spectroscopically identified AGN (Coppin et al., 2009); rad: radio datapoint is more than 3σ above the starburst model.

Table 7.2: *Dust yields per star required to explain dust in $z > 4$ SMGs*

			Dust yields ($M_\odot$ per star)					
Dust producer	IMF	Total mass	LESS	MM	GN20	GN20.2a	GN10	SMM
AGB ($2.5 < M < 8M_\odot$)	Salpeter	M_*	0.03	0.06	0.04	0.17	0.05	0.07
AGB ($2.5 < M < 8M_\odot$)	Salpeter	$M_* - M_{\rm burst}$	0.04	0.31	0.06	0.20	∞	0.09
SN ($M > 8M_\odot$)	Salpeter	M_*	0.14	0.22	0.15	0.65	0.18	0.27
SN ($M > 8M_\odot$)	Top-heavy	M_*	0.05	0.08	0.05	0.23	0.06	0.10

Note. — The IMF is either Salpeter (1955) with $\alpha = 2.35$, or top-heavy with $\alpha = 1.5$. The total mass indicates if the entire stellar mass (M_*) was used to calculate number of stars (equation 7.1), or if stars created during the ongong starburst were excluded ($M_* - M_{\rm burst}$). The last six columns contain dust yields for all SMGs in the order given in Table 7.1. Only the first parts of their names are given for brevity.

The properties of the galaxies are within the ranges found by Michałowski et al. (2009b) for the $1.7 < z < 3.6$ SMG sample (Chapman et al., 2005). However, $z > 4$ SMGs tend to be among the most star-forming, least massive and hottest SMGs and exhibit the highest fraction of stellar mass formed in the ongoing starburst. Namely, 43% of $1.7 < z < 3.6$ SMGs have lower SFRs than any of the $z > 4$ SMGs[2], whereas only 2% have higher SFRs; 30% of $1.7 < z < 3.6$ SMGs have higher stellar masses, whereas only 8% have lower stellar masses; 55% have lower fraction of stellar mass formed in the ongoing starburst episode, whereas only 2% have higher fraction; and 28% have lower dust temperatures, whereas only 4% have higher temperature. This can be interpreted as SMGs at $z > 4$ representing earlier stages of the formation of submillimeter-bright galaxies at which the pre-existing stellar population is less pronounced and therefore the ongoing starburst episode contributes more to the final stellar mass.

However, we note that we cannot exclude the possibility that these galaxies are AGN-dominated. The AGN contribution would make the IR luminosities and dust temperatures higher than from pure star formation. In that case the SFRs and M_* we derive would be upper limits.

If GN10 is not AGN-dominated then the fact that we could only fit its SED using a template corresponding to a young (0.1 Gyr old) progenitor of an elliptical galaxy supports the hypothesis that SMGs evolve into ellipticals. According to our model, after 1.5 Gyr GN10 will evolve into a massive elliptical containing $\sim 10^{12}\,M_\odot$ stars. In order to explain its extremely red observed-frame 2.1–$3.6\,\mu$m color we did not need to invoke an old stellar population as suggested by Wang et al. (2009). Its spectrum is reproduced by a young stellar population residing in molecular clouds heavily obscured by dust with $A_V \sim 7.8$ mag (Table 7.1, column 14). This estimate is similar to the values obtained using only near-IR and optical data by Daddi et al. (2009a) and Wang et al. (2009). On the other hand the remaining $z > 4$ SMGs are only moderately obscured ($A_V \sim 2$ mag; column 14).

We estimate the SMG comoving volume densities of SFR, $L_{\rm IR}$, stellar and dust masses in the redshift interval 4–5[3] (comoving volume of 5.9×10^6 Mpc^3; for details of the method see Section 3.2 of Michałowski et al., 2009b): $\rho_{\rm SFR} = 2.6 \times 10^{-3}\,M_\odot$ yr^{-1} Mpc^{-3} (a similar value was found by Younger et al., 2009a, based on candidates for high-redshift SMGs), $\log \rho_{\rm LIR} =$

[2]We exclude SMMJ163555.5+661300 from this analysis, because its unlensed submillimeter flux of ~ 2 mJy makes it impossible to be detected by SCUBA in the blank-field survey similar to those used by Chapman et al. (2005).

[3]We again exclude SMMJ163555.5+661300 because it is lensed.

$7.17\,L_\odot$ Mpc^{-3}, $\log\rho_* = 5.54\,M_\odot$ Mpc^{-3} and $\log\rho_{\rm dust} = 2.81\,M_\odot$ Mpc^{-3}. However one must keep in mind that these numbers could be affected by cosmic variance, because three out of five SMGs considered here are members of a protocluster structure (Daddi et al., 2009b,a). The contributions to the cosmic SFR and stellar mass densities of SMGs at these redshifts are 4.4% and 1.0%, respectively, using the compilation of the total values in Michałowski et al. (2009b, Tables 5 and 6). These numbers indicate that currently detected SMGs did not contribute significantly to the cosmic star formation history at $z > 4$, but our estimates should be regarded as lower limits since more of such distant SMGs could still be undetected in the fields discussed here.

Our estimates of SFRs, $L_{\rm IR}$ and M_* are consistent within a factor of < 3 with those obtained by Coppin et al. (2009), Capak et al. (2008), Schinnerer et al. (2008), Younger et al. (2008b), Casey et al. (2009), Daddi et al. (2009b,a), Knudsen et al. (2009) and Wang et al. (2009) after taking into account that Daddi et al. (2009b,a) used a Chabrier (2003) initial mass function (IMF) resulting in stellar masses 1.8 times lower than for the Salpeter (1955) IMF (Erb et al., 2006).

However we obtained stellar masses for LESSJ033229.4-275619 and MMJ100054.48+023435.9 ~ 10 times larger than Coppin et al. (2009)[4] and Capak et al. (2008), respectively and for SMMJ163555.5+661300 ~ 5 times larger than Knudsen et al. (2009). The difference can be explained by the fact that Coppin et al. (2009) assumed a mass-to-light ratio of $M_*/L_K = 0.1$ and the determinations of Capak et al. (2008) and Knudsen et al. (2009) correspond to $M_*/L_K \sim 0.03$ and ~ 0.17, respectively. These are very low values (e.g. Drory et al., 2004; Portinari et al., 2004; Labbé et al., 2005; Castro Cerón et al., 2006, 2009; van der Wel et al., 2006; Courty et al., 2007; Michałowski et al., 2009b; Savaglio et al., 2009) giving lower limits on stellar masses. On the other hand, we do not assume mass-to-light ratios, but derive them from the stellar population models incorporated in GRASIL.

7.4.2 Producers of dust in $z > 4$ SMGs

The dust masses we find for $z > 4$ SMGs (Table 7.1, column 11) are similar to those derived for $z \sim 4$–6 quasars (a few$\times 10^8 M_\odot$; Dunlop et al., 1994; Benford et al., 1999; Archibald et al., 2001; Omont et al., 2001; Priddey & McMahon, 2001; Priddey et al., 2003, 2008; Isaak et al., 2002; Bertoldi et al., 2003a; Robson et al., 2004; Beelen et al., 2006; Wang et al., 2008; Martinez-Sansigre et al., 2009). These huge dust masses indicate that dust in SMGs was efficiently formed and able to survive even when the age of the Universe was only 1.2–1.5 Gyr.

As detailed below we find that *i*) AGB stars are efficient and fast enough to form dust in LESSJ033229.4-275619, GN20 and SMMJ163555.5+661300; *ii*) only SNe are efficient and fast enough to form dust in MMJ100054.48+023435.9, GN20.2a and GN10, as long as the dust yields derived for Cassiopeia A and Kepler SN remnants are correct and typical, or if a top-heavy IMF and/or significant dust growth in the interstellar medium (ISM) are assumed. If these assumptions are correct, then SNe could also produce dust in SMGs mentioned in *i*.

Asymptotic giant branch stars

In order to investigate whether AGB stars can be responsible for dust production in $z > 4$ SMGs we estimated (see Appendix) the average dust yields required per star with mass $2.5 < M < 8\,M_\odot$ and main-sequence lifetime in a range 1 Gyr – 55 Myr (calculated as 10^{10} yr $\times\,[M/M_\odot]^{-2.5}$; e.g. Kippenhahn & Weigert, 1990). The lower mass limit was chosen to ensure that the stars

[4]Note that our estimate agrees with that of Stark et al. (2007).

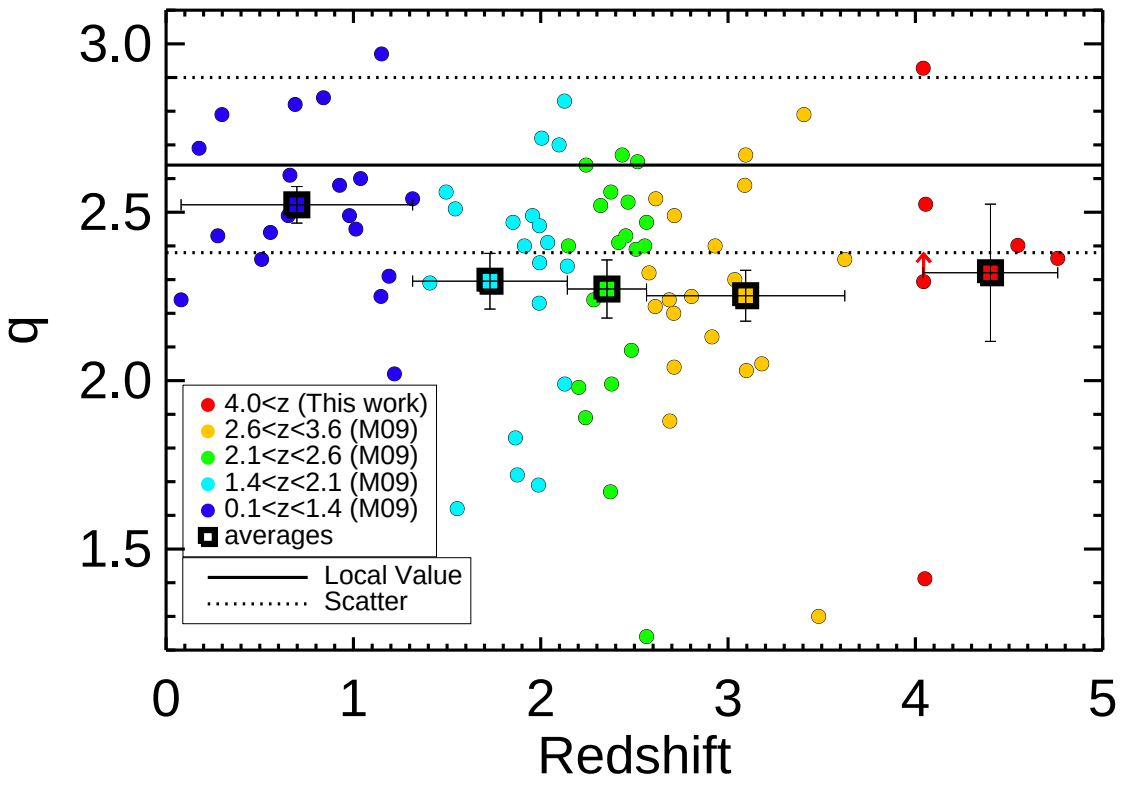

Figure 7.2: *The ratio of the infrared and radio luminosities* $q = \log(L_{\rm IR}/3.75 \times 10^{12}/I_{1.4})$ *as a function of redshift of SMGs. Both SMGs at* $z > 4$ *(red circles) and at lower redshifts (yellow, green, blue, violet circles, divided into four redshift bins) from chapter 6 (M09) are shown. In the redshift range* $1.4 < z < 5.0$ *no significant evolution of the IR-radio correlation is found for SMGs. The average* q *for SMGs (squares) is however offset towards higher radio luminosities (factor of* $\sim$ *2.1–2.3) from the local relation (*$q = 2.64$*: solid line with scatter* 0.26*: dotted lines; Bell, 2003).*

considered can start producing dust within the age of the Universe at the redshifts of our sources (1.2–1.5 Gyr).

The results are listed in the first row of Table 7.2. They are independent of the assumed star formation history of galaxies, but depend only on derived dust and stellar masses, assumed IMF and measured redshifts. We find that each AGB star would need to produce ~ 0.03–$0.07\,M_\odot$ of dust in order to explain the dust in $z > 4$ SMGs, excluding GN20.2a (see below). These numbers are close to the highest theoretical dust yields of AGB stars (Morgan & Edmunds, 2003; Ferrarotti & Gail, 2006) making them plausible dust producers. Assuming a top-heavy IMF does not change this result significantly (the required dust yields increases by $\sim 30\%$). For GN20.2a the required dust yield ($0.17\,M_\odot$) is too high to claim that AGB stars formed its dust.

However, MMJ100054.48+023435.9 and GN10 formed the majority of their stars in the ongoing starburst episode (column 9, Table 7.1), which is too short for the $2.5 < M < 8\,M_\odot$ stars considered above to finish their main-sequence phase. Therefore AGB stars could not contribute to the dust production in these two galaxies. To quantify this we calculated the required dust yields for AGB stars taking into account only stars that were born before the on-

going starburst (replacing M_* by $M_* - M_{\rm burst}$ in equation 7.1). The resulting yields (second row of Table 7.2) for LESSJ033229.4-275619, GN20, GN20.2a and SMMJ163555.5+661300 do not differ significantly from our previous estimate (first row of Table 7.2), because in this way we removed $\lesssim 30\%$ of stars (those formed during the ongoing starburst). However the yields for MMJ100054.48+023435.9 and GN10 become too high to claim that AGB stars formed dust in these galaxies.

A potential limitation of this claim is the uncertainty in determining the fraction of stellar mass formed during the ongoing starburst episode. If more stars were formed in the past, then AGB stars could be responsible for dust production in these two galaxies. However, even if it was the case, then the current SFRs would be the same as we derive, because they are fixed by strong submillimeter emission. Then the ongoing starburst becomes unfeasibly short (< 25 Myr) in order not to produce more stars than is inferred from the optical to near-infared part of the spectra. Therefore more stars in these two SMGs could have been formed before the ongoing starburst only if the current SFRs are overestimated due to a significant AGN contribution.

Supernovae

We repeated the analysis for SNe, i.e. calculated the required dust yields per one massive star ($> 8\,M_\odot$). The yields are ~ 0.15–$0.65\,M_\odot$ of dust per SN (third row of Table 7.2), consistent with the theoretical works (though without dust grain destruction implemented) of Todini & Ferrara (2001) and Nozawa et al. (2003); with a value predicted by Dwek et al. (2007) to account for dust in a $z \sim 6.4$ quasar; and with submillimeter observation of SN remnants Cassiopeia A (Dunne et al., 2003, 2009b) and Kepler (Morgan et al., 2003; Gomez et al., 2009). There is a debate about the latter results on Cassiopeia A and Kepler (e.g. Dwek, 2004; Krause et al., 2004; Gomez et al., 2005; Wilson & Batrla, 2005; Sibthorpe et al., 2009), but if these dust yields are correct and typical, then SNe are efficient enough to account for the dust in all $z > 4$ SMGs.

However our estimates are at least an order of magnitude higher than any other observed SN dust yields, which are typically in the range $\sim 10^{-3}$–$10^{-2}\,M_\odot$ (Green et al., 2004; Borkowski et al., 2006; Sugerman et al., 2006; Blair et al., 2007; Ercolano et al., 2007; Meikle et al., 2007; Rho et al., 2008, 2009; Kotak et al., 2009; Sakon et al., 2009; Sandstrom et al., 2009; Wesson et al., 2009) and theoretically predicted dust masses able to survive in SN remnants (Bianchi & Schneider, 2007). This apparent difficulty in explaining dust production in $z > 4$ SMGs can be resolved with a combination of two plausible effects.

Approximately half of the discrepancy can be accounted for with a top-heavy IMF giving more SNe per unit stellar mass (both top-heavy and Salpeter IMFs have been claimed to reproduce the number counts of SMGs; Baugh et al., 2005; Fontanot et al., 2007). Changing the IMF slope from $\alpha = 2.35$ to $\alpha = 1.5$, consistent with values for low-mass star clusters (Scalo, 1998) and a limit derived for a proto-star cluster (Sternberg, 1998), resulted in the required dust yield decreasing to 0.05–$0.23\,M_\odot$ (fourth row of Table 7.2).

The second possibility is that SNe provided only the dust seeds and that the bulk of the dust mass was accumulated during grain growth in the ISM (e.g. Draine, 2003). The timescale of this process is typically less than a few $\times\,10$ Myr (Hirashita, 2000; Zhukovska et al., 2008; Draine, 2009), i.e. short enough to contribute significantly to the growth of dust mass in $z > 4$ SMGs. This can be tested by investigation whether the grains formed by SN remnants are smaller than those present in $z > 4$ SMGs.

7.4.3 THE IR-RADIO CORRELATION AT $z > 4$

Despite the differences compared to the $1.7 < z < 3.6$ population (Section 7.4.1), the mean IR-to-radio luminosity ratio ($q \equiv \log[L_{\rm IR}/3.75 \times 10^{12}/I_{1.4}]$ with radio K-corrections assuming a slope of -0.75) for $z > 4$ SMGs of 2.32 ± 0.20 is consistent with the values derived for lower-redshift SMGs (Michałowski et al., 2009b). At $z > 4$ we find an offset of $\Delta q \sim -0.32$ (factor of ~ 2.1) from the local value of $q = 2.64$ (Bell, 2003), though due to the small sample, this offset is significant only at 1.6σ level.

Hence, with our multi-wavelength approach we confirm the results of Murphy (2009), who derived the mean $q = 2.16 \pm 0.28$ for $z > 4$ SMGs.

The offset of $\Delta q \sim -0.32$ is consistent with a hypothesis of Lacki et al. (2009) and Lacki & Thompson (2009) that SMGs are "puffy starbursts" (vertically and radially extended galaxies with vertical scale heights ~ 1 kpc) experiencing weaker bremsstrahlung and ionization losses resulting in stronger radio emission. We cannot however exclude an AGN contribution boosting their radio fluxes. Since the redshifts of four out of six $z > 4$ SMGs have been measured independently of radio detections, the radio excess cannot be a result of a bias against radio-faint sources.

In Figure 7.2 we show the q values as a function of redshift for both $z > 4$ SMGs discussed in this chapter (red circles) and lower-redshift SMGs from chapter 6 The IR-radio correlation of SMGs does not show any evolution in the redshift range $1.4 < z < 5.0$. To date there are only two q determinations at higher redshifts than presented here, namely $z = 6.2$ and 6.42 quasars (Carilli et al., 2004; Beelen et al., 2006, $q = 1.8$–2.2).

7.4.4 GAS-TO-DUST RATIO AT $z > 4$

Using the molecular gas mass estimates (based on CO[4–3] line observations) from Schinnerer et al. (2008) and Daddi et al. (2009b,a) we derive gas-to-dust ratios of $M_{H_2}/M_d = 73$, 47, 22 and 98 for MMJ100054.48+023435.9, GN20, GN20.2a and GN10, respectively. The mean value of 60 is consistent with 54^{+14}_{-11} estimated for $z \sim 1$–3.5 SMGs by Kovács et al. (2006) using the CO survey of Greve et al. (2005). SMGs at $z > 4$ have one of the lowest gas-to-dust ratios compared to other galaxies, e.g., the Milky Way ($\sim 90 - 400$; Sodroski et al., 1997), other spirals ($\sim 1000 \pm 500$; Devereux & Young, 1990; Stevens et al., 2005), the nuclear regions of local luminous IR galaxies (LIRGs), ultraluminous IR galaxies (ULIRGs) (120 ± 28; Wilson et al., 2008) and of local, far-IR-selected galaxies (~ 50; Seaquist et al., 2004) (all these results are based on IR and CO data, and are therefore directly comparable to our estimates). This is not surprising, since SMGs are selected by submillimeter emission. Similarly, a low value of $M_{H_2}/M_d = 30$ was found by Bertoldi et al. (2003b) for $z = 6.42$ quasar, but Cox et al. (2002) reported a higher value of $M_{H_2}/M_d = 150$ for $z \sim 4$ quasar. The small number of SMGs and quasars with derived gas-to-dust ratios hampers a comparison of these two samples.

7.5 CONCLUSIONS

We have analysed the spectral energy distributions of six spectroscopically confirmed $z > 4$ SMGs. Our results provide constraints on dust production at these early epochs of the evolution of the Universe. We find that AGB stars are efficient and fast enough to form the dust residing in three of these galaxies. However, for three other SMGs only SNe are efficient and fast enough. The high required SN dust yields hint at a possibility that their stars may be distributed according to a top-heavy IMF and/or that dust grains are substantially grown in the

ISM. Since the majority of the stars in these galaxies were formed on very short timescales, these properties are very likely to be similar to those of the first galaxies beyond redshift 6, which had been building up their stellar populations only for several hundred Myr, which elapsed since the Big Bang.

We present evidence that the IR-to-radio luminosity ratios of $z > 4$ SMGs are consistent with that of lower-redshiftp SMGs and are offset from the local relation by a factor of ~ 2.1.

A comparison of the $z > 4$ SMGs with the lower-redshift sample, in particular their high SFRs, dust temperatures and fraction of stars formed during the ongoing starburst as well as low stellar masses, reveals that we start to see SMGs at earlier stages of their evolution.

The improved mapping speed and sensitivity of the new SCUBA2 camera will enable studies of the evolutionary sequence of SMGs using much bigger and more homogeneously selected samples. Moreover, the study of dust production presented here will be pushed forward with a synergy of *Herschel*, SCUBA2 and ultimately ALMA. These facilities will provide a broad wavelength coverage at the IR, which will allow accurate determination of dust temperatures and, in turns, its mass.

7.6 IMF AND DUST YIELD CALCULATIONS

We calculated the dust yield per star required to explain dust mass in a galaxy in a following way. In an IMF with $M_{\rm min} = 0.15$, $M_{\rm max} = 120\,M_{\odot}$ and a slope $\alpha = 2.35$ (Salpeter, 1955, or $\alpha = 1.5$ for top-heavy IMF), the number of stars with masses between M_0 and M_1 in the stellar population with a total mass of M_* can be expressed as

$$N(M_0 < M < M_1) = M_* \frac{\int_{M_0}^{M_1} M^{-\alpha} dM}{\int_{M_{\rm min}}^{M_{\rm max}} M^{-\alpha} M dM}, \tag{7.1}$$

where the denominator provides a normalisation so that a total mass is equal to M_*. For SNe we assumed $M_0 = 8\,M_{\odot}$ and $M_1 = M_{\rm max} = 120\,M_{\odot}$, whereas for AGB stars: $M_0 = 2.5\,M_{\odot}$ and $M_1 = 8\,M_{\odot}$.

The average dust yield per star is equal to the dust mass divided by number of stars, $N(M_0 < M < M_1)$.

Acknowledgements

We thank Joanna Baradziej and Peter Laursen, for discussion and comments; Kirsten Knudsen for kindly providing the data for SMMJ163555.5+661300 prior to publication; and Jorge Iglesias-Páramo for providing his SED templates.

M. J. M. would like to acknowledge support from The Faculty of Science, University of Copenhagen. The Dark Cosmology Centre is funded by the Danish National Research Foundation.

8

CONCLUSIONS

8.1 SUMMARY

Studying the evolution of the Universe by submillimeter and radio emission has been proven to provide the view on star formation, which is complimentary to the optical wavelengths. In this thesis I investigated the properties of star-forming galaxies, in particular, gamma-ray burst (GRB) host galaxies and submillimeter galaxies (SMGs). The main results can be summarized as follows.

- **Young and old stellar populations are present in GRB hosts**

In Chapter 4 I claim that enhanced submillimeter/radio emission of $z \sim 1$ GRB hosts combined with their optical faintness and blue colors hint at very young stellar populations. On the other hand my SED fitting for the host of GRB 980425 as well as the presence of the $1.6\,\mu$m bump and the steep radio spectrum indicate that its mass is dominated by an old stellar population (Chapter 5).

- **Submillimeter/radio bright GRB hosts exhibit hot dust temperatures**

In Chapter 4 I find that those GRB hosts, which are bright enough to be detected by current submillimeter/radio facilities, have dust temperatures $T_d > 45$ K, significantly larger than those of SMGs with the same luminosity. This makes GRB hosts potential candidates for elusive hotter counterparts of SMGs. The fact that the SEDs of three SMGs are similar to those of GRB hosts (Chapter 6) supports this hypothesis.

- **The environments of GRBs are associated with high specific SFR and hot dust**

Based on spectral energy distribution of the Wolf-Rayet region close to the site of GRB 980425 (Chapter 5) I add one more evidence that the immediate environments of GRBs on 1–3 kpc scales are much more star-forming and host hotter dust than the rest of the galaxy. Such regions may dominate the emission of high-redshift GRB hosts, where they cannot be resolved.

- **SMGs are dominated by old stellar population**

In Chapter 6 I analyse the currently largest sample of SMGs with spectroscopic redshifts and I find that only a minor part (7%) of their stellar masses has been formed in the ongoing starburst episode putting constraints on their formation scenario. Namely, this implies that in the past, SMGs experienced either another starburst episode or merger of several galaxies.

However, SMGs at $z > 4$ formed much higher fraction of their stars in the ongoing starburst (45%), hinting at they are at the earlier stages of the evolution (Chapter 7).

- **SMGs are significant contributors to cosmic stellar assembly**

In Chapter 6 I find that spectroscopic SMGs host $\sim$ 5–6% of cosmic star formation and 9–15% of cosmic stellar mass at redshifts $\sim$ 2–4. After incompleteness correction these numbers increases to $\sim$ 20% and $\sim$ 30–50%, respectively. In Chapter 7 I estimated their contribution at redshifts $\sim$ 4–5 to be below 4%, but this is likely a lower limit due to small size of the sample.

- **Infrared-radio correlation holds for SMGs in an unchanged form up to redshift ~ 5 and is offset from the local relation by a factor of ~ 2.1–2.3 towards higher radio luminosities**

Combing the data presented in Chapters 6 and 7 I confirmed that the linear infrared-radio correlation does not change up to redshift ~ 5 for SMGs and is offset from the local relation by a factor of ~ 2.1–2.3.

- **Supernovae formed dust at redshifts $z > 4$**

Based on derived properties of spectroscopically confirmed SMGs at redshifts $z > 4$ (Chapter 7) I investigated the efficiency of plausible dust producers. I find that AGB stars could produce dust in three out of six $z > 4$ SMGs. However, for three other only supernovae were efficient and fast enough. This provides one more evidence that in the early Universe supernovae were significant contributors to dust formation.

8.2 OUTLOOK

Coming years are going to be exciting time for far-IR astronomy. The *Hershel* satellite has already been launched and tested. Its cameras covering a wavelength range of 60–$520\,\mu$m are going to provide crucial information on the dust emission, because they will probe very close to the peak of the dust emission in galaxies.

Hershel is ideal instrument to build-up the observational wavelength coverage of the brightest GRB hosts to confirm that their dust is indeed heated to high temperatures. *Hershel* will also detect new GRB hosts increasing the sample studied at far-IR.

In the context of SMGs, *Hershel* will detect unexplored yet portion of their SEDs. This will allow accurate determinations of their IR luminosities, temperatures and masses of dust as well as to test the hypothesis that there is significant amount of hotter dust in this galaxies, which is missed in submillimeter observations.

Next year will also bring advent of SCUBA2, the new submillimeter instrument on JCMT. Its improved mapping speed (~ 100 times faster than its precursor SCUBA), will allow much wider surveys to be performed building up larger SMG sample. Better sensitivity of SCUBA2 ensures better positional accuracy of the detected objects. Hence optical counterparts of SMGs will be able to be pinpointed without the need of radio detection. This is turn will remove the bias against high-redshift SMGs.

Ultimately, studies of the high-redshift Universe at the submillimeter wavelengths will be pushed forward by ALMA. Its unprecedented resolution and sensitivity will allow to follow up both GRB hosts and SMGs. It will be possible to study their broad-band SEDs as well as emission lines.

A

Acronyms

AGB	Asymptotic Giant Branch (star)
AGN	Active Galactic Nucleus
ALMA	Atacama Large Millimeter Array (Chajnantor/Chile)
ATCA	Australia Telescope Compact Array (Narrabri/Australia)
FWHM	Full Width at Half Maximum
GMRT	Giant Metrewave Radio Telescope (Pune/India)
GRASIL	GRAphite and SILicate (or GRAnato and SILva, radiative transfer code)
GRB	Gamma-ray Burst
HPBW	Half-Power Beamwidth (FWHM of a beam)
HST	Hubble Space Telescope
IMF	Initial Mass Function
IRAC	Infrared Array Camera (*Spitzer* instrument)
ISM	Interstellar Medium
IR	Infrared
IRAF	Image Reduction and Analysis Facility (reduction and analysis software)
JCMT	James Clerk Maxwell Telescope (Hawaii/USA)
LIRG	Luminous Infrared Galaxy
MC	Molecular Cloud
PAH	Polycyclic Aromatic Hydrocarbon
QSO	Quasi-stellar Object (or quasar)
RMS	Root Mean Square
SCUBA	Submillimetre Common-User Bolometer Array
SED	Spectral Energy Distribution
SFR	Star Formation Rate
SMG	Submillimeter Galaxy
SSFR	Specific Star Formation Rate
SSP	Simple Stellar Population
SN	Supernova
ULIRG	Ultraluminous Infrared Galaxy
UV	Ultraviolet
VLA	Very Large Array (New Mexico/USA)
VLT	Very Large Telescope (Paranal/Chile)
WSRT	Westerbork Synthesis Radio Telescope (Netherlands)
WR	Wolf-Rayet (star)

B

REDUCTION SCRIPTS

B.1 ENTIRE REDUCTION SCRIPT / LOGFILE

This script is not supposed to be run in its entirety, because it is necessary to monitor the output and change the parameters frequently, especially in the flagging part. The easiest way to use it is to copy&paste the appropriate parts to the MIRIAD terminal. This script was used to reduce data presented in Chapter 5 (Michałowski et al., 2009a).

```
miriad

#------------------------------------------------------------
# INPUT
#------------------------------------------------------------

uvfilename=2008-01-27_0550.C1741
primary=1934-638
secondary=0451-282
target=grb050915a
freq1=1344
freq2=1432

#------------------------------------------------------------
# convert RPFITS file to uv-visibilities
#------------------------------------------------------------

task atlod
in=$uvfilename
out=$uvfilename.uv
options=birdie,xycorr,noauto
go

#------------------------------------------------------------
# splitting dataset according to sources and frequencies
#------------------------------------------------------------

task uvsplit
vis= $uvfilename.uv
unset options
go


#------------------------------------------------------------
# saving the orignal uv-files in case the flagging goes bad
# NOT NECESSARY##
#------------------------------------------------------------

mkdir original_files
cp -r $primary.* original_files/
cp -r $secondary.* original_files/
cp -r $target.* original_files/

#------------------------------------------------------------
```

```
# Getting total integration time
# NOT NECESSARY##
#-----------------------------------------------------------

task uvindex
vis      =  $target.$freq1
unset  interval
unset   log
unset  options

#Total observing time is  6.98 hours

#-----------------------------------------------------------
# Flagging bad data in the primary callibrator
#-----------------------------------------------------------

task blflag
vis=$primary.$freq1
unset options
axis =time,amp
unset line
stokes=xx,yy
device =/xs
go

vis=$primary.$freq2
go

#-----------------------------------------------------------
# calibration corrections (antenna gains,delay terms and passband shapes)
#-----------------------------------------------------------

task mfcal
vis=$primary.$freq1
refant=4
unset stokes
interval =0.1
unset options
go

vis=$primary.$freq2
go

#-----------------------------------------------------------
# Gain/phase/polarization calibration
#-----------------------------------------------------------

task gpcal
options=xyvary
go

vis=$primary.$freq1
go

#-----------------------------------------------------------
# plotting uv-data of the secondary to see intererences
#-----------------------------------------------------------


task uvplt
vis=$secondary.$freq1
stokes=i,q,u,v
axis=time,amp
device=/xs
nxy=1
unset options
unset select
unset line
go

#Nothing obvious

vis=$secondary.$freq2
go
```

```
#Nothing obvious

#-------------------------------------------------------------
# Flagging bad data in the secondary callibrator
#-------------------------------------------------------------

#WHOLE PERIODS (see intereference above):
#None detected above

#INDIVIDUAL CHANNELS

task blflag
vis=$secondary.$freq1
unset options
axis =time,amp
stokes=ii
line=channel,1,1,1,1
go

line=channel,1,2,1,1
go
line=channel,1,3,1,1
go
line=channel,1,4,1,1
go
line=channel,1,5,1,1
go
line=channel,1,6,1,1
go
line=channel,1,7,1,1
go
line=channel,1,8,1,1
go
line=channel,1,9,1,1
go
line=channel,1,10,1,1
go
line=channel,1,11,1,1
go
line=channel,1,12,1,1
go
line=channel,1,13,1,1
go


vis=$secondary.$freq2

line=channel,1,1,1,1
go
line=channel,1,2,1,1
go
line=channel,1,3,1,1
go
line=channel,1,4,1,1
go
line=channel,1,5,1,1
go
line=channel,1,6,1,1
go
line=channel,1,7,1,1
go
line=channel,1,8,1,1
go
line=channel,1,9,1,1
go
line=channel,1,10,1,1
go
line=channel,1,11,1,1
go
line=channel,1,12,1,1
go
line=channel,1,13,1,1
go

AVERAGED
```

```
task blflag
unset options
unset line
axis =time,amp
stokes=xx,yy

vis=$secondary.$freq1
go

vis=$secondary.$freq2
go

#-----------------------------------------------------------
# calibration corrections (antenna gains,delay terms and passband shapes)
#-----------------------------------------------------------

task mfcal
vis=$secondary.$freq1
refant=4
unset stokes
interval =0.1
unset options
go

#I flux density:    2.118


vis=$secondary.$freq2
go

#I flux density:    2.103

#-----------------------------------------------------------
# Gain/phase/polarization calibration
#-----------------------------------------------------------

task gpcal
options=xyvary,qusolve
go

vis=$secondary.$freq1
go

#-----------------------------------------------------------
# Copy flux density corrections from primary to secondary calibrator
#-----------------------------------------------------------

task gpboot
vis=$secondary.$freq1
cal=$primary.$freq1
go

#Secondary flux density scaled by:   1.057

vis=$secondary.$freq2
cal=$primary.$freq2
go

#Secondary flux density scaled by:   1.067

#-----------------------------------------------------------
# copy calibration tables from callibrator to program source
#-----------------------------------------------------------

task gpcopy
vis=$secondary.$freq1
out=$target.$freq1
unset options
go

vis=$secondary.$freq2
out=$target.$freq2
go
```

```
#-----------------------------------------------------------
# plotting uv-plot of a source to localize interefences
#-----------------------------------------------------------

task   uvplt
vis      = $target.$freq1
unset  line
unset  select
stokes   = i
axis     = time,amp
options  = 2pass,nofqav
device   = /xs
nxy      = 1
go

#Strong interference on ~10:30 at all baselines (especially short)
#Zoom in to localize
select=time(10:15:00,10:45:00)

#To be removed:
select=time(10:30:00,10:33:30)

#Strong interference on ~7:00 at all baselines (especially short)
#Zoom in to localize
select=time(6:45:00,7:15:00)

#To be removed:
select=time(6:58:30,7:00:00)

#Strong interference on ~11:45 at all baselines (especially short)
#Zoom in to localize
select=time(11:30:00,12:00:00)

#To be removed:
select=time(11:44:00,11:48:00)

----------------

task   uvplt
vis      = $target.$freq2
unset  line
unset  select
stokes   = i
axis     = time,amp
options  = 2pass,nofqav
device   = /xs
nxy      = 1
go

#Strong interference on ~10:30 at all baselines (especially short)
#Zoom in to localize
select=time(10:15:00,10:45:00)

#To be removed:
select=time(10:30:00,10:33:30)

#Strong interference on ~7:00 at all baselines (especially short)
#Zoom in to localize
select=time(6:45:00,7:15:00)

#To be removed:
select=time(6:58:30,7:00:00)

#Strong interference on ~11:45 at all baselines (especially short)
#Zoom in to localize
select=time(11:30:00,12:00:00)

#To be removed:
select=time(11:44:00,11:48:00)

#Long interference on 6-7h at 1-2,2-3,3-4
#Long interference on 6-9h and 13-14h at 4-5
# check which channels are affected

#To be removed:
```

```
line=channel,1,1,1,1
select=time(12:45:00,15:00:00),ant(4)(5)

line=channel,1,2,1,1
select=time(13:30:00,15:00:00),ant(4)(5)

line=channel,1,5,1,1
select=time(6:00:00,7:45:00),ant(1)(2)
select=time(6:00:00,7:15:00),ant(2)(3)
select=time(6:00:00,7:15:00),ant(3)(4)
select=time(6:00:00,9:00:00),ant(4)(5)
select=time(12:30:00,15:00:00),ant(4)(5)

line=channel,1,6,1,1
select=time(8:45:00,9:05:00),ant(4)(5)

line=channel,1,7,1,1
select=time(6:00:00,9:00:00),ant(4)(5)


#-----------------------------------------------------------
# Flagging bad data in the source
#-----------------------------------------------------------

#Whole PERIODS from previous point

task uvflag
vis= $target.$freq1
flagval=flag
options=brief

select=time(10:30:00,10:33:30)
go
select=time(6:58:30,7:00:00)
go
select=time(11:44:00,11:48:00)
go

----------------

task uvflag
vis= $target.$freq2
flagval=flag
options=brief

select=time(10:30:00,10:33:30)
go
select=time(6:58:30,7:00:00)
go
select=time(11:44:00,11:48:00)
go

line=channel,1,1,1,1
select=time(12:45:00,15:00:00),ant(4)(5)
go

line=channel,1,2,1,1
select=time(13:30:00,15:00:00),ant(4)(5)
go

line=channel,1,5,1,1
select=time(6:00:00,7:45:00),ant(1)(2)
go
select=time(6:00:00,7:15:00),ant(2)(3)
go
select=time(6:00:00,7:15:00),ant(3)(4)
go
select=time(6:00:00,9:00:00),ant(4)(5)
go
select=time(12:30:00,15:00:00),ant(4)(5)
go

line=channel,1,6,1,1
select=time(8:45:00,9:05:00),ant(4)(5)
go
```

```
line=channel,1,7,1,1
select=time(6:00:00,9:00:00),ant(4)(5)
go

======================

INDIVIDUAL CHANNELS

task blflag
vis=$target.$freq1
unset options
axis =time,amp
stokes=ii
unset select
line=channel,1,1,1,1
go

line=channel,1,2,1,1
go
line=channel,1,3,1,1
go
line=channel,1,4,1,1
go
line=channel,1,5,1,1
go
line=channel,1,6,1,1
go
line=channel,1,7,1,1
go
line=channel,1,8,1,1
go
line=channel,1,9,1,1
go
line=channel,1,10,1,1
go
line=channel,1,11,1,1
go
line=channel,1,12,1,1
go
line=channel,1,13,1,1
go

------------------

vis=$target.$freq2

line=channel,1,1,1,1
go
line=channel,1,2,1,1
go
line=channel,1,3,1,1
go
line=channel,1,4,1,1
go
line=channel,1,5,1,1
go
line=channel,1,6,1,1
go
line=channel,1,7,1,1
go
line=channel,1,8,1,1
go
line=channel,1,9,1,1
go
line=channel,1,10,1,1
go
line=channel,1,11,1,1
go
line=channel,1,12,1,1
go
line=channel,1,13,1,1
go
```

```
AVERAGED

task blflag
unset options
unset line
axis =time,amp
stokes=xx,yy
go

vis=$target.$freq1
go

#-------------------------------------------------------------
# Deconvolution and cleaning
#-------------------------------------------------------------

OUTSIDE MIRIAD. Copy the script to the working directory

perl robust-weighting_imaging.pl
VIS= grb050915a.1344,grb050915a.1432,../a/grb050915a.1344,../a/grb050915a.1432
Pixel size (in arc seconds) = 1.0
Image size (xpixels,ypixels) = 1000,1000.  Accept default? [Y/n]:
Region = abspix,box(1,1,1000,1000)
10000
mv tmp_Imaging.irestor grb050915a_1as_1000pix_10000its_1390.irestor

Using gaussian beam fwhm of   13.882 by    3.633 arcsec.
Position angle:   -4.2 degrees.

perl robust-weighting_imaging.pl
VIS= grb050915a.1344,grb050915a.1432,../a/grb050915a.1344,../a/grb050915a.1432
Pixel size (in arc seconds) = 1.0
Image size (xpixels,ypixels) = 1000,1000.  Accept default? [Y/n]: N 2000 2000
Region = abspix,box(1,1,2000,2000)
10000
mv tmp_Imaging.irestor grb050915a_1as_2000pix_10000its_1390.irestor

Using gaussian beam fwhm of   14.434 by    4.105 arcsec.
Position angle:   -5.8 degrees.

perl robust-weighting_imaging.pl
VIS= grb050915a.1344,grb050915a.1432,../a/grb050915a.1344,../a/grb050915a.1432
Pixel size (in arc seconds) = 1.0
Image size (xpixels,ypixels) = 1000,1000.  Accept default? [Y/n]: N 500,500
Region = abspix,box(1,1,500,500)
10000
mv tmp_Imaging.irestor grb050915a_1as_500pix_10000its_1390.irestor

Using gaussian beam fwhm of   14.002 by    3.574 arcsec.
Position angle:   -3.8 degrees.

perl robust-weighting_imaging.pl
VIS= grb050915a.1344,grb050915a.1432,../a/grb050915a.1344,../a/grb050915a.1432
Pixel size (in arc seconds) = 2.0
Image size (xpixels,ypixels) = 1000,1000.  Accept default? [Y/n]: N 2500,2500
Region = abspix,box(1,1,2500,2500)
10000
mv tmp_Imaging.irestor grb050915a_2as_2500pix_10000its_1390.irestor

Using gaussian beam fwhm of   18.323 by    5.509 arcsec.
Position angle:   -6.2 degrees.

#Best result so far -big area make the strong sources been cleaned a bit better. There is something a few arcses
from the GRB position

perl robust-weighting_imaging.pl
VIS= grb050915a.1344,grb050915a.1432,../a/grb050915a.1344,../a/grb050915a.1432
Pixel size (in arc seconds) = 2.0
Image size (xpixels,ypixels) = 1000,1000.  Accept default? [Y/n]: N 2500,2500
Region = abspix,box(1,1,2500,2500)
50000
mv tmp_Imaging.irestor grb050915a_2as_2500pix_50000its_1390.irestor

Using gaussian beam fwhm of   18.323 by    5.509 arcsec.
Position angle:   -6.2 degrees.
```

```
#Even better

perl robust-weighting_imaging.pl
VIS= grb050915a.1344,grb050915a.1432,../a/grb050915a.1344,../a/grb050915a.1432
Pixel size (in arc seconds) = 2.0
Image size (xpixels,ypixels) = 1000,1000.  Accept default? [Y/n]: N 2500,2500
robust = +2
Region = abspix,box(1,1,2500,2500)
50000
mv tmp_Imaging.irestor grb050915a_2as_2500pix_50000its_robust+2_1390.irestor

Using gaussian beam fwhm of   23.273 by    7.438 arcsec.
Position angle:   -6.8 degrees.

#well the previous is better

#-----------------------------------------------------------
# Some image manipulation
# NOT NECESSARY##
#-----------------------------------------------------------

#Conversion of the image to the fits format

task   fits
in       = grb050915a_2as_2500pix_50000its_1390.irestor
op       = xyout
out      = grb050915a_2as_2500pix_50000its_1390.fits

unset options
unset stokes

#Following examples from GRB 980425 -more interesting case

#-----------------------------------------------------------
# Image plotting
#-----------------------------------------------------------

Task:   cgdisp
in       = grb980425_8as_1000pix_5000its_robust+2_4800.irestor
type     = contour
region   = arcsec,box(-400,-400,400,400)
xybin    =
chan     =
slev     = p,1 #percentage levels below
levs1    = -5,1,2,3,4,5,6,7,8,9,10,20,30,40,50,60,70,80
levs2    =
levs3    =
cols1    =
range    =
vecfac   =
boxfac   =
device   = /xs # OR file.ps/ps for Postscript
nxy      = 1
labtyp   = hms,dms
beamtyp  = b,l
options  =
3format  =
lines    =
break    =
csize    =
scale    =
olay     = grb980425.olay

#-----------------------------------------------------------
# Getting the position of the peaks
#-----------------------------------------------------------

The galaxies are blended so I needed to get the positions and intensities of the peaks.

Task:   cgcurs
in       = grb980425_8as_1000pix_5000its_robust+2_-Ant1_4800.irestor
type     = contour
region   = arcsec,box(-100,-150,150,40)
xybin    =
```

```
chan     =
slev     = p,1
levs     = -5,1,2,3,4,5,6,7,8,9,10,20,30,40,50,60,70,80
range    =
device   = /xs
nxy      = 1
labtyp   = hms,dms
options  = cursor
3format  =
csize    =


#------------------------------------------------------------
# Photometry
#------------------------------------------------------------

Task:   imfit
in       = grb980425_8as_1000pix_5000its_robust+2_-Ant1_4800.irestor
region   = arcsec,box(-100,-150,150,40)
clip     =
object   = gaussian,gaussian
spar     = 3.5657E-04,3.11009778E+01,-1.66885578E+01,10,5,80,4.2465E-04,1.94225856E+01,-6.46589538E+01,10,5,80
fix      =
out      = model.im
options  =

#amp,x,y,bmaj,bmin,pa
3.5657E-04,3.11009778E+01,-1.66885578E+01,10,5,80,
4.2465E-04,1.94225856E+01,-6.46589538E+01,10,5,80

imfit: Version 1.3,2007/04/16 02:52:20 UTC

-------------------------------------------------
Object grb980425
RMS residual is 1.08E-05 (theoretical image noise is 5.54E-05)

Using the following beam parameters when
deconvolving and converting to integrated flux
Beam Major,minor axes (arcsec):    75.64    37.99
Beam Position angle (degrees):     -80.7

Scaling error estimates by  7.1 to account for
noise correlation between pixels

Source  1,Object type: gaussian -GRB 980425
Peak value:                 3.3905E-04 +/- 2.0267E-05
Total integrated flux:      4.1945E-04
Offset Position (arcsec):      33.151   -15.761
Positional errors (arcsec):     2.318     1.648
Right Ascension:                19:35:06.969
Declination:                    -52:50:40.461
Major axis (arcsec):          91.071 +/- 5.426
Minor axis (arcsec):          39.031 +/- 3.589
Position angle (degrees):     -80.19 +/-      2.79
Deconvolved Major,minor axes (arcsec):   50.734    8.912
Deconvolved Position angle (degrees):     -79.3

Source  2,Object type: gaussian
Peak value:                 4.1820E-04 +/- 2.1488E-05
Total integrated flux:      4.3913E-04
Offset Position (arcsec):      19.558   -65.321
Positional errors (arcsec):     1.692     1.492
Right Ascension:                19:35:05.469
Declination:                    -52:51:30.021
Major axis (arcsec):          71.326 +/- 3.853
Minor axis (arcsec):          42.299 +/- 3.350
Position angle (degrees):     -87.49 +/-      4.40
### Warning:  Failed in attempting to deconvolve
-------------------------------------------------

out      = residual.im
options  =  residual (only the second time to get the residual image)


#------------------------------------------------------------
```

```
# Error estimation
#-----------------------------------------------------------

The region for statistics was chosen in order that it does not contain the sources and is close to the object.
Then I get the "Image pixel coordinates x,y" of the left bottom and right top corners of this image by the task
cgcurs,as done before.

Then the statistics is computed by

Task:   imstat
in       = grb980425_8as_1000pix_5000its_robust+2_-Ant1_4800.irestor
region   = box(452.43,473.83,480.52,522.53)
plot     = rms
options  =
cutoff   =
beam     =
axes     = RA,DEC
device   = /xs
log      =

IMSTAT: version 2.2 27-Oct-99
***** Statistics of image grb980425_8as_1000pix_5000its_robust+2_-Ant1_4800.ires
Bounding box: blc=(452,474,1,1),trc=(481,523,1,1)
Unit of datavalues: JY/BEAM
Unit of statistics: JY/BEAM
Axes of planes : RA---SIN,DEC--SIN

Axis 4 (STOKES):   1
Axis 3 (FREQ-LSR)
plane    Frequency    Sum      Mean      rms     Maximum   Minimum    Npoints
1        4.8     8.196E-03 5.464E-06 4.610E-05 1.181E-04-1.757E-04    1500
### Fatal Error:  X-range of plot is 0

the error is then 4.610E-05 Jy/beam = 46 uJy/beam

In order to calcuate the error of the total galaxy flux I added the contributions of all the beams inside the
galaxy:
ErrorTotal= sqrt(\sum_beams ErrorPerBeam_beams^2) = sqrt(#ofbeams * ErrorPerBeam) = ErrorPerBeam * sqrt (AreaGalaxy
/ AreaBeam)
Hence
ErrorTotal = 46 * sqrt(91.071*39.031 / (75.64*37.99)) = 51.1614 uJy

The total flux is then:
420.0 +-50 uJy
```

B.2 IMAGING SCRIPT

This script has been written by Robert Reinfrank. It should be run by a command

`perl robust-weighting_imaging.pl`

Parameters are specified interactively by a user.

```
#/usr/bin/perl

# Program "robust-weighting_imaging.pl"
# R. Reinfrank   November 2006
# Quick program to go through image processing. Same as "imaging.pl" but adds the option to change the robust
# weighting parameter (in order to change weighting on short vs. long baselines).

print "\n\nRUNNING ROBUST-WEIGHTING IMAGING SCRIPT\n\n";
print "Current directory:";
system "pwd";
print "\n\nContents:\n\n";
system "ls";
#================ INVERT OPTIONS ============================================================
print "\nEnter the filenames,or filenames (separated by a comma),as they\n";
print " would be entered in the VIS= line of INVERT: ";
$VisFiles = <STDIN>;
print "\nPixel size (in arc seconds) = ";
$CellSize = <STDIN>;
```

```
#print "\nImage size (xpixels,ypixels --eg. 500,500 = ";
print "\nImage size (xpixels,ypixels) = 1000,1000.  Accept default? [Y/n]: ";
$answer = <STDIN>;
chomp $answer; # Remove trailing 'carriage return'.
$ImageSize = "1000,1000"; # Default image size.
if ( $answer eq "N"  ||  $answer eq "n" )
{
printf "\nEnter new image size (xpixels,ypixels) --eg. 500,500:  ";
$ImageSize = <STDIN>;
chomp $ImageSize; # Remove trailing 'carriage return'(just to help print the next line!).
printf "Image size = $ImageSize pixels\n";
}

print "\nROBUST options (if any) for INVERT,ie. Default = -infinity (uniform weighting)\n";
print "(useful range is -2 [little downweighting,ie. uniform] to +2 [towards natural weighting]).\n";
print "Natural weighting,with all points treated alike,gives the best signal-to-noise ratio\n";
print "for detecting weak sources. Downside is that it emphasises data from the short spacings\n";
print "                                Accept default (minus infinity,uniform weighting)? [Y/n]: ";
$answer = <STDIN>;
chomp $answer; # Remove trailing 'carriage return'.
$Robustness = ""; # Default option.
$SideLobeSuppression = ""; # Default option.
if ( $answer eq "N"  ||  $answer eq "n" )
{
printf "\nEnter new ROBUSTness parameter (press ENTER if none):  ";
$Robustness = <STDIN>;
chomp $Robustness; # Remove trailing 'carriage return'(just to help print the next line!).
printf "robust = $Robustness\n\n";
printf "============================================================\n\n";
printf "Enter sidelobe suppression area (SUP,in arcsec). Default is to use whole image.\n";
printf "Alternatively you can enter either 1 or 2 numbers.\n";
printf "              1 = use square region\n";
printf "              2 = use numbers for RA & Dec suppression areas.\n";
printf "          ENTER = use default (corresponds to UNIFORM WEIGHTING,ie. suppress sidelobes over entire image.\n";
printf "            '0'= use NATURAL WEIGHTING.\n";
printf "Note: Natural weighting gives the best signal to noise ratio,at the expense of no sidelobe suppression.\n";
printf "      Natural weighting corresponds to SUP=0. Values between these extremes give a tradeoff between signal
to noise\n";
printf "      and sidelobe suppression.\n\n";
printf "        Enter suppression area,SUP (eg. 60 or 60,80 or ENTER for default,'0'for natural weighting):  ";
$SideLobeSuppression = <STDIN>;
chomp $SideLobeSuppression; # Remove trailing 'carriage return'.
printf "SUP = $SideLobeSuppression\n";

}

print "\nSELECT options [ eg. select = -ant(6) ] for INVERT,\n";
print "(Default,in this case is to leave it blank,ie. use ALL baselines)\n";
print "                                  Accept default (Use ALL baselines)? [Y/n]:  ";
$answer = <STDIN>;
chomp $answer; # Remove trailing 'carriage return'.
$SelectOpts = ""; # Default option.
if ( $answer eq "N"  ||  $answer eq "n" )
{
printf "\nEnter new SELECT options (press ENTER if none):  ";
$SelectOpts = <STDIN>;
chomp $SelectOpts; # Remove trailing 'carriage return'(just to help print the next line!).
printf "select = $SelectOpts\n";
}

#print "\nSTOKES = ";
#$Stokes = <STDIN>;
print "\n*** Default,at present,is to use STOKES = i,q,u,v ***\n";
print "\nOptions (if any) to use for INVERT,Default is options = mfs,double\n";
print "                                  Accept default? [Y/n]:  ";
$answer = <STDIN>;
chomp $answer; # Remove trailing 'carriage return'.
$Options= "mfs,double";
if ( $answer eq "N"  ||  $answer eq "n" )
{
printf "\nEnter new OPTIONS (press ENTER if none):  ";
$Options = <STDIN>;
chomp $Options; # Remove trailing 'carriage return'(just to help print the next line!).
printf "options = $Options\n";
}
```

```
# ================ INVERT ==========================================================
print "\n1 -Visibility files to use are $VisFiles\n";
print "Removing old temporary map,beam,clean and restor files (if they exists).....   ";
system "rm -rf tmp_Imaging.*";
print "DONE\n\n";
print "-------------------------------------------------------------------------------------------------\n\n";
system "invert \"vis=$VisFiles\" \"map=tmp_Imaging.imap,tmp_Imaging.qmap,tmp_Imaging.umap,tmp_Imaging.vmap\"
\"beam=tmp_Imaging.beam\" \"imsize=$ImageSize\" \"cell=$CellSize\" \"sup=$SideLobeSuppression\" \"robust=$Robustness\"
\"select=$SelectOpts\" \"stokes=i,q,u,v\" \"options=$Options\" ";
# ================ CLEAN OPTIONS ==========================================================
print "\n\nWill now CLEAN the image:\n";
print "\Specific REGION command(s),if any: eg. abspix,box(1,1,1000,1000) or \@cgcurs.region\n";
print "    Region = ";
$Region= <STDIN>;
print "Number of iterations to use for CLEANing (eg. 2500) = ";
$Iters= <STDIN>;
# ================ CLEAN ==========================================================
# \n\nWill just clean iMAP at present. Vary script to clean all if you wish...\n\n";
#system "clean \"map=tmp_Imaging.imap\" \"beam=tmp_Imaging.beam\" \"out=tmp_Imaging.iclean\" \"niters=$Iters\"
\"unset options\" \"unset model\" \"region=$Region\" ";
system "clean \"map=tmp_Imaging.imap\" \"beam=tmp_Imaging.beam\" \"out=tmp_Imaging.iclean\" \"niters=$Iters\"
\"region=$Region\" ";
# ================ RESTOR==========================================================
system "restor \"model=tmp_Imaging.iclean\" \"beam=tmp_Imaging.beam\" \"map=tmp_Imaging.imap\" \"out=tmp_Imaging.irestor\"
";
# ================ KVIS==========================================================
system "kvis tmp_Imaging.irestor &";
print "\n*** END OF SCRIPT ***\n\n";
```

C

CO-AUTHOR STATEMENTS

THE FACULTY OF SCIENCE
UNIVERSITY OF COPENHAGEN

The Graduate School

Declaration of co-authorship

Name: Michał Michałowski	
Civ. Reg. No. (CPR. No.): 081082-3321	E-mail: michal@dark-cosmology.dk
Department: Dark Cosmology Centre, Niels Bohr Institute	
Principal supervisor: Jens Hjorth	E-mail: jens@dark-cosmology.dk
Title of PhD thesis: Star Formation at High Redshifts and the Importance of Dust Obscuration	

This co-authorship declaration applies to the following paper:

Michałowski M. J., Hjorth J., Castro Cerón J. M., Watson D., 2008, Astrophysical Journal, 672, 817, The nature of GRB-selected submillimeter galaxies: hot and young

The student's contribution to the paper

Michał Michałowski had the idea for the paper, did the calculations and wrote the text based on discussions with co-authors.

Signatures of co-authors

Date (dd/mm/yy)	Name	Signature
29/09/2009	Jens Hjorth	
29/09/2009	Darach Watson	

THE FACULTY OF SCIENCE
UNIVERSITY OF COPENHAGEN

The Graduate School

Declaration of co-authorship

Name: Michał Michałowski	
Civ. Reg. No. (CPR. No.): 081082-3321	E-mail: michal@dark-cosmology.dk
Department: Dark Cosmology Centre, Niels Bohr Institute	
Principal supervisor: Jens Hjorth	E-mail: jens@dark-cosmology.dk
Title of PhD thesis: Star Formation at High Redshifts and the Importance of Dust Obscuration	

This co-authorship declaration applies to the following paper:

Michałowski M. J., Hjorth J., Malesani D., Michałowski T., Castro Cerón J. M., Reinfrank R. F., Garrett M. A., Fynbo J. P. U., Watson D. J., Jørgensen U. G., 2009, Astrophysical Journal, 693, 347, The properties of the host galaxy and the immediate environment of GRB 980425 / SN 1998bw from the multi-wavelength spectral energy distribution

The student's contribution to the paper

Michał Michałowski had the idea for the paper, did the calculations and wrote the text based on discussions with the co-authors. Ultraviolet-to-infrared data were reduced and analysed by the co-authors.

Signatures of co-authors

Date (dd/mm/yy)	Name	Signature
29/09/2009	Jens Hjorth	
29/09/2009	Daniele Malesani	

PhD student: _____ **Date:** 30/09/09
Signature (dd/mm/yy)

THE FACULTY OF SCIENCE
UNIVERSITY OF COPENHAGEN

The Graduate School

Declaration of co-authorship

Name: Michał Michałowski	
Civ. Reg. No. (CPR. No.): 081082-3321	E-mail: michal@dark-cosmology.dk
Department: Dark Cosmology Centre, Niels Bohr Institute	
Principal supervisor: Jens Hjorth	E-mail: jens@dark-cosmology.dk
Title of PhD thesis: Star Formation at High Redshifts and the Importance of Dust Obscuration	

This co-authorship declaration applies to the following paper:

Michałowski M. J., Hjorth J., Watson D., 2009, Monthly Notices of the Royal Astronomical Society, submitted, arXiv:0905.4499, Cosmic evolution of submillimeter galaxies and their contribution to stellar mass assembly

The student's contribution to the paper

Michał Michałowski had the idea for the paper, did the calculations and wrote the text based on discussions with the co-authors.

Signatures of co-authors

Date (dd/mm/yy)	Name	Signature
29/09/2009	Jens Hjorth	
29/09/2009	Darach Watson	

PhD student: _____ **Date:** 30/09/09
Signature (dd/mm/yy)

THE FACULTY OF SCIENCE
UNIVERSITY OF COPENHAGEN

The Graduate School

Declaration of co-authorship

Name: Michał Michałowski	
Civ. Reg. No. (CPR. No.): 081082-3321	E-mail: michal@dark-cosmology.dk
Department: Dark Cosmology Centre, Niels Bohr Institute	
Principal supervisor: Jens Hjorth	E-mail: jens@dark-cosmology.dk
Title of PhD thesis: Star Formation at High Redshifts and the Importance of Dust Obscuration	

This co-authorship declaration applies to the following paper:

Michałowski M. J., Watson D., Hjorth J., 2009, in preparation, Rapid dust production in submillimeter galaxies at z>4?

The student's contribution to the paper

Michał Michałowski and Darach Watson jointly had the ideas that went into the paper. Michał Michałowski did the calculations and wrote the text based on discussions with the co-authors.

Signatures of co-authors

Date (dd/mm/yy)	Name	Signature
~~29/09/2009~~ 30/09	Darach Watson	
29/09/2009	Jens Hjorth	

PhD student: Michałowski
Signature

Date: 30/09/09
(dd/mm/yy)

BIBLIOGRAPHY

Alexander D.M., Bauer F.E., Chapman S.C., Smail I., Blain A.W., Brandt W.N., Ivison R.J., 2005, ApJ, 632, 736

Alexander D.M., et al., 2008, AJ, 135, 1968

Almaini O., et al., 2003, MNRAS, 338, 303

Appleton P.N., et al., 2004, ApJS, 154, 147

Archibald E.N., Dunlop J.S., Hughes D.H., Rawlings S., Eales S.A., Ivison R.J., 2001, MNRAS, 323, 417

Aretxaga I., et al., 2007, MNRAS, 379, 1571

Ashby M.L.N., et al., 2006, ApJ, 644, 778

Austermann J.E., et al., 2009, MNRAS, 393, 1573

Barger A.J., Cowie L.L., Sanders D.B., Fulton E., Taniguchi Y., Sato Y., Kawara K., Okuda H., 1998, Nature, 394, 248

Barger A.J., Cowie L.L., Sanders D.B., 1999, ApJ, 518, L5

Barger A.J., Cowie L.L., Richards E.A., 2000, AJ, 119, 2092

Barnard V.E., et al., 2003, MNRAS, 338, 1

Baugh C.M., Lacey C.G., Frenk C.S., Granato G.L., Silva L., Bressan A., Benson A.J., Cole S., 2005, MNRAS, 356, 1191

Beelen A., Cox P., Benford D.J., Dowell C.D., Kovács A., Bertoldi F., Omont A., Carilli C.L., 2006, ApJ, 642, 694

Bell E.F., 2003, ApJ, 586, 794

Bell E.F., et al., 2005, ApJ, 625, 23

Bell E.F., Zheng X.Z., Papovich C., Borch A., Wolf C., Meisenheimer K., 2007, ApJ, 663, 834

Benford D.J., Cox P., Omont A., Phillips T.G., McMahon R.G., 1999, ApJ, 518, L65

Berciano Alba A., Koopmans L.V.E., Garrett M.A., Wucknitz O., Limousin M., 2009, A&A, accepted, `arXiv:0910.1213 [astro-ph.CO]`

Berger E., et al., 2001a, ApJ, 556, 556

Berger E., Kulkarni S.R., Frail D.A., 2001b, ApJ, 560, 652

Berger E., Cowie L.L., Kulkarni S.R., Frail D.A., Aussel H., Barger A.J., 2003a, ApJ, 588, 99

Berger E., Soderberg A.M., Frail D.A., Kulkarni S.R., 2003b, ApJ, 587, L5

Bertelli G., Bressan A., Chiosi C., Fagotto F., Nasi E., 1994, A&AS, 106, 275

Bertoldi F., Carilli C.L., Cox P., Fan X., Strauss M.A., Beelen A., Omont A., Zylka R., 2003a, A&A, 406, L55

Bertoldi F., et al., 2003b, A&A, 409, L47

Best P.N., Kauffmann G., Heckman T.M., Brinchmann J., Charlot S., Ivezić Ž., White S.D.M., 2005, MNRAS, 362, 25

Beswick R.J., Muxlow T.W.B., Thrall H., Richards A.M.S., Garrington S.T., 2008, MNRAS, 385, 1143

Bianchi S., Schneider R., 2007, MNRAS, 378, 973

Björnsson G., Hjorth J., Pedersen K., Fynbo J.U., 2002, ApJ, 579, L59

Blain A.W., 1997, MNRAS, 290, 553

Blain A.W., Longair M.S., 1996, MNRAS, 279, 847

Blain A.W., Kneib J., Ivison R.J., Smail I., 1999, ApJ, 512, L87

Blain A.W., Smail I., Ivison R.J., Kneib J.P., Frayer D.T., 2002, Phys. Rep., 369, 111

Blain A.W., Chapman S.C., Smail I., Ivison R., 2004, ApJ, 611, 52

Blair W.P., Ghavamian P., Long K.S., Williams B.J., Borkowski K.J., Reynolds S.P., Sankrit R., 2007, ApJ, 662, 998

Bloom J.S., Djorgovski S.G., Kulkarni S.R., Frail D.A., 1998a, ApJ, 507, L25

Bloom J.S., et al., 1998b, ApJ, 508, L21

Bloom J.S., et al., 1999, Nature, 401, 453

Bloom J.S., Djorgovski S.G., Kulkarni S.R., 2001, ApJ, 554, 678

Bloom J.S., Kulkarni S.R., Djorgovski S.G., 2002, AJ, 123, 1111

Bloom J.S., Berger E., Kulkarni S.R., Djorgovski S.G., Frail D.A., 2003, AJ, 125, 999

Borkowski K.J., et al., 2006, ApJ, 642, L141

Borys C., Chapman S., Halpern M., Scott D., 2003, MNRAS, 344, 385

Borys C., Smail I., Chapman S.C., Blain A.W., Alexander D.M., Ivison R.J., 2005, ApJ, 635, 853

Boyle B.J., Cornwell T.J., Middelberg E., Norris R.P., Appleton P.N., Smail I., 2007, MNRAS, 376, 1182

Bressan A., Silva L., Granato G.L., 2002, A&A, 392, 377

Briggs M.S., 1995, Ap&SS, 231, 3

Calzetti D., et al., 2007, ApJ, 666, 870

Campana S., et al., 2007, ApJ, 654, L17

Cannon J.M., Skillman E.D., 2004, ApJ, 610, 772

Capak P., et al., 2004, AJ, 127, 180

Capak P., et al., 2008, ApJ, 681, L53

Cardelli J.A., Clayton G.C., Mathis J.S., 1989, ApJ, 345, 245

Carilli C.L., et al., 2004, AJ, 128, 997

Casey C.M., et al., 2009, MNRAS, accepted arXiv:0908.3675 [astro-ph.CO]

Castro Cerón J.M., Michałowski M., Hjorth J., Watson D.J., Fynbo J.P.U., Gorosabel J., 2006, ApJL, 653, L85

Castro Cerón J.M., Michałowski M.J., Hjorth J., Malesani D., Gorosabel J., Watson D., Fynbo J.P.U., 2009, ApJ, submitted, arXiv:0803.2235v1 [astro-ph]

Castro-Tirado A.J., Gorosabel J., 1999, A&AS, 138, 449

Castro-Tirado A.J., et al., 1999, ApJ, 511, L85

Chabrier G., 2003, ApJ, 586, L133

Chanial P., Flores H., Guiderdoni B., Elbaz D., Hammer F., Vigroux L., 2007, A&A, 462, 81

Chapin E.L., et al., 2009, MNRAS, 398, 1793

Chapman S.C., Richards E.A., Lewis G.F., Wilson G., Barger A.J., 2001, ApJ, 548, L147

Chapman S.C., et al., 2003a, ApJ, 585, 57

Chapman S.C., Blain A.W., Ivison R.J., Smail I.R., 2003b, Nature, 422, 695

Chapman S.C., Windhorst R., Odewahn S., Yan H., Conselice C., 2003c, ApJ, 599, 92

Chapman S.C., Smail I., Blain A.W., Ivison R.J., 2004a, ApJ, 614, 671

Chapman S.C., Smail I., Windhorst R., Muxlow T., Ivison R.J., 2004b, ApJ, 611, 732

Chapman S.C., Blain A.W., Smail I., Ivison R.J., 2005, ApJ, 622, 772

Chary R., Becklin E.E., Armus L., 2002, ApJ, 566, 229

Chary R., Berger E., Cowie L., 2007, ApJ, 671, 272

Chen H.W., Prochaska J.X., Bloom J.S., Thompson I.B., 2005, ApJ, 634, L25

Chen S.L., Li A., Wei D.M., 2006, ApJ, 647, L13

Cheng K.S., Lu T., 2001, ChJAA, 1, 1

Christensen L., Hjorth J., Gorosabel J., 2004, A&A, 425, 913

Christensen L., Vreeswijk P.M., Sollerman J., Thöne C.C., Le Floc'h E., Wiersema K., 2008, A&A, 490, 45

Clemens M.S., Vega O., Bressan A., Granato G.L., Silva L., Panuzzo P., 2008, A&A, 477, 95

Clements D., et al., 2004, MNRAS, 351, 447

Clements D.L., et al., 2008, MNRAS, 387, 247

Cobb B.E., Bailyn C.D., van Dokkum P.G., Buxton M.M., Bloom J.S., 2004, ApJ, 608, L93

Condon J.J., 1992, ARA&A, 30, 575

Coppin K., et al., 2006, MNRAS, 372, 1621

Coppin K., et al., 2008, MNRAS, 384, 1597

Coppin K.E.K., et al., 2009, MNRAS, 395, 1905

Courty S., Björnsson G., Gudmundsson E.H., 2004, MNRAS, 354, 581

Courty S., Björnsson G., Gudmundsson E.H., 2007, MNRAS, 376, 1375

Cowie L.L., Barger A.J., Kneib J., 2002, AJ, 123, 2197

Cowie L.L., Barger A.J., Wang W., Williams J.P., 2009, ApJ, 697, L122

Cox P., et al., 2002, A&A, 387, 406

Daddi E., Cimatti A., Renzini A., 2000, A&A, 362, L45

Daddi E., Dannerbauer H., Krips M., Walter F., Dickinson M., Elbaz D., Morrison G.E., 2009a, ApJ, 695, L176

Daddi E., et al., 2009b, ApJ, 694, 1517

Dale D.A., Helou G., 2002, ApJ, 576, 159

Dale D.A., Helou G., Contursi A., Silbermann N.A., Kolhatkar S., 2001, ApJ, 549, 215

Dannerbauer H., Walter F., Morrison G., 2008, ApJ, 673, L127

Davé R., Finlator K., Oppenheimer B.D., Fardal M., Katz N., Kereš D., Weinberg D.H., 2009, MNRAS, submitted, `arXiv:0909.4078 [astro-ph.CO]`

de Ravel L., et al., 2009, A&A, 498, 379

de Vries W.H., Hodge J.A., Becker R.H., White R.L., Helfand D.J., 2007, AJ, 134, 457

Della Valle M., et al., 2006, Nature, 444, 1050

Devereux N.A., Young J.S., 1990, ApJ, 359, 42

Devlin M.J., et al., 2009, Nature, 458, 737

Djorgovski S.G., Kulkarni S.R., Bloom J.S., Goodrich R., Frail D.A., Piro L., Palazzi E., 1998, ApJ, 508, L17

Djorgovski S.G., Frail D.A., Kulkarni S.R., Bloom J.S., Odewahn S.C., Diercks A., 2001, ApJ, 562, 654

Draine B.T., 2003, ARA&A, 41, 241

Draine B.T., 2009, `arXiv:0903.1658v1 [astro-ph.GA]`

Draine B.T., et al., 2007, ApJ, 663, 866

Driver S.P., Popescu C.C., Tuffs R.J., Liske J., Graham A.W., Allen P.D., de Propris R., 2007, MNRAS, 379, 1022

Drory N., Bender R., Feulner G., Hopp U., Maraston C., Snigula J., Hill G.J., 2004, ApJ, 608, 742

Drory N., Salvato M., Gabasch A., Bender R., Hopp U., Feulner G., Pannella M., 2005, ApJ, 619, L131

Duncan W.D., Robson E.I., Ade P.A.R., Sandell G., Griffin M.J., 1990, MNRAS, 243, 126

Dunlop J.S., Hughes D.H., Rawlings S., Eales S.A., Ward M.J., 1994, Nature, 370, 347

Dunne L., Eales S., Edmunds M., Ivison R., Alexander P., Clements D.L., 2000, MNRAS, 315, 115

Dunne L., Eales S., Ivison R., Morgan H., Edmunds M., 2003, Nature, 424, 285

Dunne L., et al., 2009a, MNRAS, 394, 3

Dunne L., et al., 2009b, MNRAS, 394, 1307

Dwek E., 2004, ApJ, 607, 848

Dwek E., Galliano F., Jones A.P., 2007, ApJ, 662, 927

Dye S., et al., 2008, MNRAS, 386, 1107

Dye S., et al., 2009, ApJ, 703, 285

Eales S., Lilly S., Gear W., Dunne L., Bond J.R., Hammer F., Le Fèvre O., Crampton D., 1999, ApJ, 515, 518

Eales S., et al., 2009, ApJ, accepted, arXiv:0907.4156 [astro-ph.CO]

Egami E., et al., 2004, ApJS, 154, 130

Elíasdóttir Á., et al., 2007, arXiv:0710.5636 [astro-ph]

Elsner F., Feulner G., Hopp U., 2008, A&A, 477, 503

Erb D.K., Steidel C.C., Shapley A.E., Pettini M., Reddy N.A., Adelberger K.L., 2006, ApJ, 646, 107

Ercolano B., Barlow M.J., Sugerman B.E.K., 2007, MNRAS, 375, 753

Ferrarotti A.S., Gail H.P., 2006, A&A, 447, 553

Ferrero P., et al., 2006, A&A, 457, 857

Filippenko A.V., 1997, ARA&A, 35, 309

Foley S., Watson D., Gorosabel J., Fynbo J.P.U., Sollerman J., McGlynn S., McBreen B., Hjorth J., 2006, A&A, 447, 891

Fomalont E.B., Kellermann K.I., Cowie L.L., Capak P., Barger A.J., Partridge R.B., Windhorst R.A., Richards E.A., 2006, ApJS, 167, 103

Fontana A., et al., 2006, A&A, 459, 745

Fontanot F., Monaco P., Silva L., Grazian A., 2007, MNRAS, 382, 903

Frail D.A., et al., 2002, ApJ, 565, 829

Frail D.A., Kulkarni S.R., Berger E., Wieringa M.H., 2003, AJ, 125, 2299

Frayer D.T., et al., 2004, ApJS, 154, 137

Fruchter A.S., et al., 1999a, ApJ, 516, 683

Fruchter A.S., et al., 1999b, ApJ, 519, L13

Fruchter A.S., et al., 2006, Nature, 441, 463

Fynbo J.P.U., et al., 2000, ApJ, 542, L89

Fynbo J.P.U., et al., 2002, A&A, 388, 425

Fynbo J.P.U., et al., 2003, A&A, 406, L63

Fynbo J.P.U., et al., 2006a, A&A, 451, L47

Fynbo J.P.U., et al., 2006b, Nature, 444, 1047

Fynbo J.P.U., et al., 2009, ApJS, submitted, arXiv:0907.3449v1 [astro-ph.CO]

Gal-Yam A., et al., 2004, ApJ, 609, L59

Gal-Yam A., et al., 2006, Nature, 444, 1053

Galama T.J., Wijers R.A.M.J., 2001, ApJ, 549, L209

Galama T.J., et al., 1998, Nature, 395, 670

Galama T.J., et al., 1999, GRB Coordinates Network, 388, 1

Galama T.J., et al., 2003, ApJ, 587, 135

Garn T., Green D.A., Riley J.M., Alexander P., 2009, MNRAS, 397, 1101

Garrett M.A., 2002, A&A, 384, L19

Gehrz R., 1989, In: L. J. Allamandola & A. G. G. M. Tielens (ed.) Interstellar Dust, vol. 135 of IAU Symposium, 445

Genzel R., et al., 2008, ApJ, 687, 59

Goicoechea J.R., Le Bourlot J., 2007, A&A, 467, 1

Goldader J.D., Meurer G., Heckman T.M., Seibert M., Sanders D.B., Calzetti D., Steidel C.C., 2002, ApJ, 568, 651

Gomez H.L., Dunne L., Eales S.A., Gomez E.L., Edmunds M.G., 2005, MNRAS, 361, 1012

Gomez H.L., et al., 2009, MNRAS, 397, 1621

Gooch R., 1996, In: Jacoby G.H., Barnes J. (eds.) Astronomical Data Analysis Software and Systems V, vol. 101 of Astronomical Society of the Pacific Conference Series, 80

Gorosabel J., et al., 2003a, A&A, 400, 127

Gorosabel J., et al., 2003b, A&A, 409, 123

Gorosabel J., et al., 2005, A&A, 444, 711

Green D.A., Tuffs R.J., Popescu C.C., 2004, MNRAS, 355, 1315

Greiner J., 1999, Memorie della Societa Astronomica Italiana, 70, 891

Greve T.R., Ivison R.J., Bertoldi F., Stevens J.A., Dunlop J.S., Lutz D., Carilli C.L., 2004, MNRAS, 354, 779

Greve T.R., et al., 2005, MNRAS, 359, 1165

Greve T.R., et al., 2009, ApJ, submitted, arXiv:0904.0028 [astro-ph.CO]

Gruppioni C., Pozzi F., Zamorani G., Ciliegi P., Lari C., Calabrese E., La Franca F., Matute I., 2003, MNRAS, 341, L1

Hainline L.J., 2008, Multi-Wavelength Properties of Submillimeter-Selected Galaxies, Ph.D. thesis, California Institute of Technology

Hainline L.J., Blain A.W., Greve T.R., Chapman S.C., Smail I., Ivison R.J., 2006, ApJ, 650, 614

Hainline L.J., Blain A.W., Smail I., Frayer D.T., Chapman S.C., Ivison R.J., Alexander D.M., 2009, ApJ, 699, 1610

Hammer F., Flores H., Schaerer D., Dessauges-Zavadsky M., Le Floc'h E., Puech M., 2006, A&A, 454, 103

Hanlon L., et al., 2000, A&A, 359, 941

Hatsukade B., et al., 2007, PASJ, 59, 67

Hauser M.G., Dwek E., 2001, ARA&A, 39, 249

Heckman T.M., 2005, in Starbursts: From 30 Doradus to Lyman Break Galaxies, Astrophysics and Space Science Library, Vol. 329, ed. R. de Grijs, & R. M. González Delgado (Dordrecht: Springer), 3

Helou G., Soifer B.T., Rowan-Robinson M., 1985, ApJ, 298, L7

Hildebrand R.H., 1983, QJRAS, 24, 267

Hirashita H., 2000, PASJ, 52, 585

Hirashita H., Hunt L.K., 2006, A&A, 460, 67

Hjorth J., Pedersen H., Jaunsen A.O., Andersen M.I., 1999, A&AS, 138, 461

Hjorth J., Holland S., Courbin F., Dar A., Olsen L.F., Scodeggio M., 2000, ApJ, 534, L147

Hjorth J., et al., 2002, ApJ, 576, 113

Hjorth J., et al., 2003a, ApJ, 597, 699

Hjorth J., et al., 2003b, Nature, 423, 847

Hjorth J., Pian E., Fynbo J.P.U., 2004, Nuclear Physics B Proceedings Supplements, 132, 271

Högbom J.A., 1974, A&AS, 15, 417

Hogg D.W., Fruchter A.S., 1999, ApJ, 520, 54

Holland S., 2001, In: Wheeler J.C., Martel H. (eds.) AIP Conf. Proc. 586: 20th Texas Symposium on relativistic astrophysics, 593

Holland S., Hjorth J., 1999, A&A, 344, L67

Holland S., et al., 2001, A&A, 371, 52

Holland W.S., et al., 1999, MNRAS, 303, 659

Holmberg E.B., Lauberts A., Schuster H.E., West R.M., 1977, A&AS, 27, 295

Hopkins A.M., 2004, ApJ, 615, 209

Hopkins A.M., Beacom J.F., 2006, ApJ, 651, 142

Huchra J.P., Vogeley M.S., Geller M.J., 1999, ApJS, 121, 287

Hughes D.H., et al., 1998, Nature, 394, 241

Hunt L., Bianchi S., Maiolino R., 2005, A&A, 434, 849

Huynh M.T., Pope A., Frayer D.T., Scott D., 2007, ApJ, 659, 305

Ibar E., et al., 2008, MNRAS, 386, 953

Iglesias-Páramo J., et al., 2006, ApJS, 164, 38

Iglesias-Páramo J., et al., 2007, ApJ, 670, 279

Indebetouw R., Whitney B.A., Johnson K.E., Wood K., 2006, ApJ, 636, 362

Infante L., Garnavich P.M., Stanek K.Z., Wyrzykowski L., 2001, GRB Coordinates Network, 1152, 1

Iono D., et al., 2006, ApJ, 640, L1

Isaak K.G., Priddey R.S., McMahon R.G., Omont A., Peroux C., Sharp R.G., Withington S., 2002, MNRAS, 329, 149

Ivison R.J., Smail I., Le Borgne J.F., Blain A.W., Kneib J.P., Bezecourt J., Kerr T.H., Davies J.K., 1998, MNRAS, 298, 583

Ivison R.J., Dunlop J.S., Smail I., Dey A., Liu M.C., Graham J.R., 2000, ApJ, 542, 27

Ivison R.J., et al., 2002, MNRAS, 337, 1

Ivison R.J., et al., 2004, ApJS, 154, 124

Ivison R.J., et al., 2005, MNRAS, 364, 1025

Ivison R.J., et al., 2007, MNRAS, 380, 199

Ivison R.J., et al., 2009, MNRAS, submitted, `arXiv:0910.1091 [astro-ph.CO]`

Iwamoto K., et al., 1998, Nature, 395, 672

Jakobsson P., Hjorth J., Fynbo J.P.U., Watson D., Pedersen K., Björnsson G., Gorosabel J., 2004, ApJ, 617, L21

Jakobsson P., et al., 2005, MNRAS, 362, 245

Jakobsson P., et al., 2006a, A&A, 460, L13

Jakobsson P., Hjorth J., Fynbo J.P.U., Gorosabel J., Jaunsen A.O., 2006b, `arXiv:astro-ph/0611561`

Jakobsson P., et al., 2006c, A&A, 447, 897

Jakobsson P., Malesani D., Fynbo J.P.U., Hjorth J., Milvang-Jensen B., 2009, In: C. Meegan, C. Kouveliotou, & N. Gehrels (ed.) American Institute of Physics Conference Series, vol. 1133 of American Institute of Physics Conference Series, 455–463

Jarrett T.H., Chester T., Cutri R., Schneider S., Skrutskie M., Huchra J.P., 2000, AJ, 119, 2498

Jaunsen A.O., Fynbo J.P.U., Andersen M.I., Vreeswijk P., 2007, GRB Coordinates Network, 6216, 1

Jha S., et al., 2001, ApJ, 554, L155

Kann D.A., Klose S., Zeh A., 2006, ApJ, 641, 993

Kennicutt R.C., 1998, ARA&A, 36, 189

Kippenhahn R., Weigert A., 1990, Stellar Structure and Evolution, (Berlin:Springer)

Klebesadel R.W., Strong I.B., Olson R.A., 1973, ApJ, 182, L85

Klose S., et al., 2000, ApJ, 545, 271

Kneib J.P., Neri R., Smail I., Blain A., Sheth K., van der Werf P., Knudsen K.K., 2005, A&A, 434, 819

Knudsen K.K., et al., 2006, MNRAS, 368, 487

Knudsen K.K., Kneib J.P., Egami E., 2008a, In: Chary R.R., Teplitz H.I., Sheth K. (eds.) Infrared Diagnostics of Galaxy Evolution, vol. 381 of Astronomical Society of the Pacific Conference Series, 372

Knudsen K.K., van der Werf P.P., Kneib J.P., 2008b, MNRAS, 384, 1611

Knudsen K.K., Kneib J.P., Richard J., Petitpas G., Egami E., 2009, ApJ, submitted

Kocevski D., West A.A., Modjaz M., 2009, ApJ, 702, 377

Kommers J.M., Lewin W.H.G., Kouveliotou C., van Paradijs J., Pendleton G.N., Meegan C.A., Fishman G.J., 2000, ApJ, 533, 696

Kotak R., et al., 2009, ApJ, 704, 306

Kouveliotou C., Meegan C.A., Fishman G.J., Bhat N.P., Briggs M.S., Koshut T.M., Paciesas W.S., Pendleton G.N., 1993, ApJ, 413, L101

Kouveliotou C., et al., 2004, ApJ, 608, 872

Kovács A., Chapman S.C., Dowell C.D., Blain A.W., Ivison R.J., Smail I., Phillips T.G., 2006, ApJ, 650, 592

Kraus J.D., 1966, Radio astronomy, New York: McGraw-Hill

Krause O., Birkmann S.M., Rieke G.H., Lemke D., Klaas U., Hines D.C., Gordon K.D., 2004, Nature, 432, 596

Kulkarni S.R., et al., 1998, Nature, 395, 663

Labbé I., et al., 2005, ApJ, 624, L81

Lacki B.C., Thompson T.A., 2009, ApJ, submitted, `arXiv:0910.0478 [astro-ph.CO]`

Lacki B.C., Thompson T.A., Quataert E., 2009, ApJ, submitted, `arXiv:0907.4161 [astro-ph.CO]`

Lamb D.Q., Reichart D.E., 2000, ApJ, 536, 1

Lapi A., Kawakatu N., Bosnjak Z., Celotti A., Bressan A., Granato G.L., Danese L., 2008, MNRAS, 386, 608

Laurent G.T., et al., 2006, ApJ, 643, 38

Law D.R., Steidel C.C., Erb D.K., Larkin J.E., Pettini M., Shapley A.E., Wright S.A., 2009, ApJ, 697, 2057

Le Floc'h E., et al., 2003, A&A, 400, 499

Le Floc'h E., Charmandaris V., Forrest W.J., Mirabel I.F., Armus L., Devost D., 2006, ApJ, 642, 636

Li L.X., 2008, MNRAS, 388, 1487

Lilly S.J., Tresse L., Hammer F., Crampton D., Le Fevre O., 1995, ApJ, 455, 108

Lilly S.J., Eales S.A., Gear W.K.P., Hammer F., Le Fèvre O., Crampton D., Bond J.R., Dunne L., 1999, ApJ, 518, 641

MacFadyen A.I., Woosley S.E., 1999, ApJ, 524, 262

Madau P., Ferguson H.C., Dickinson M.E., Giavalisco M., Steidel C.C., Fruchter A., 1996, MNRAS, 283, 1388

Madau P., Pozzetti L., Dickinson M., 1998, ApJ, 498, 106

Maiolino R., Schneider R., Oliva E., Bianchi S., Ferrara A., Mannucci F., Pedani M., Roca Sogorb M., 2004, Nature, 431, 533

Malesani D., et al., 2004, ApJ, 609, L5

Mao S., Mo H.J., 1998, A&A, 339, L1

Marchesini D., van Dokkum P.G., Förster Schreiber N.M., Franx M., Labbé I., Wuyts S., 2009, ApJ, 701, 1765

Marleau F.R., Fadda D., Appleton P.N., Noriega-Crespo A., Im M., Clancy D., 2007, ApJ, 663, 218

Martin C., et al., 2003, In: Blades J.C., Siegmund O.H.W. (eds.) Future EUV/UV and Visible Space Astrophysics Missions and Instrumentation. Edited by J. Chris Blades, Oswald H. W. Siegmund. Proceedings of the SPIE, Volume 4854, pp. 336-350 (2003)., vol. 4854 of Presented at the Society of Photo-Optical Instrumentation Engineers (SPIE) Conference, 336–350

Martin D.C., et al., 2005, ApJ, 619, L1

Martinez-Sansigre A., et al., 2009, ApJ, accepted, `arXiv:0910.1099 [astro-ph.GA]`

Matheson T., et al., 2003, ApJ, 599, 394

Meegan C.A., Fishman G.J., Wilson R.B., Horack J.M., Brock M.N., Paciesas W.S., Pendleton G.N., Kouveliotou C., 1992, Nature, 355, 143

Meikle W.P.S., et al., 2007, ApJ, 665, 608

Menéndez-Delmestre K., et al., 2007, ApJ, 655, L65

Menéndez-Delmestre K., et al., 2009, ApJ, 699, 667

Mentuch E., et al., 2009, ApJ, accepted, `arXiv:0905.0910 [astro-ph.CO]`

Metzger M.R., Djorgovski S.G., Kulkarni S.R., Steidel C.C., Adelberger K.L., Frail D.A., Costa E., Frontera F., 1997, Nature, 387, 879

Michałowski M.J., 2006, *Spectral Energy Distributions of Gamma Ray Burst Host Galaxies*, Master's thesis, University of Copenhagen

Michałowski M.J., Hjorth J., 2007, in AIP Conf. Ser. 924, The Multicolored Landscape of Compact Objects and Their Explosive Origins, ed. L. A. Antonelli et al. (Melville, NY: AIP), 143

Michałowski M.J., Hjorth J., Castro Cerón J.M., Watson D., 2008, ApJ, 672, 817

Michałowski M.J., et al., 2009a, ApJ, 693, 347

Michałowski M.J., Hjorth J., Watson D., 2009b, `arXiv:0905.4499 [astro-ph.CO]`

Michałowski M.J., Watson D., Hjorth J., 2009c, ApJ, submitted

Miller N.A., Owen F.N., 2001, AJ, 121, 1903

Mirabal N., Halpern J.P., An D., Thorstensen J.R., Terndrup D.M., 2006, ApJ, 643, L99

Modjaz M., et al., 2006, ApJ, 645, L21

Morgan H.L., Edmunds M.G., 2003, MNRAS, 343, 427

Morgan H.L., Dunne L., Eales S.A., Ivison R.J., Edmunds M.G., 2003, ApJ, 597, L33

Mortier A.M.J., et al., 2005, MNRAS, 363, 563

Murphy E.J., 2009, ApJ, 706, 482

Murphy E.J., Chary R.R., Alexander D.M., Dickinson M., Magnelli B., Morrison G., Pope A., Teplitz H.I., 2009, ApJ, 698, 1380

Narayan R., Piran T., Kumar P., 2001, ApJ, 557, 949

Narayanan D., Cox T.J., Hayward C., Younger J.D., Hernquist L., 2009a, MNRAS, accepted, arXiv:0905.2184 [astro-ph.CO]

Narayanan D., Hayward C.C., Cox T.J., Hernquist L., Jonsson P., Younger J.D., Groves B., 2009b, MNRAS, accepted, arXiv:0904.0004 [astro-ph.CO]

Nemiroff R.J., 1994, In: Fishman G.J. (ed.) AIP Conf. Proc. 307: Gamma-Ray Bursts, 730

Nomoto K., Yamaoka H., Pols O.R., van den Heuvel E.P.J., Iwamoto K., Kumagai S., Shigeyama T., 1994, Nature, 371, 227

Nozawa T., Kozasa T., Umeda H., Maeda K., Nomoto K., 2003, ApJ, 598, 785

Omont A., Cox P., Bertoldi F., McMahon R.G., Carilli C., Isaak K.G., 2001, A&A, 374, 371

Östlin G., Zackrisson E., Sollerman J., Mattila S., Hayes M., 2008, MNRAS, 387, 1227

Ovaldsen J.E., et al., 2007, ApJ, 662, 294

Paczyński B., 1986, ApJ, 308, L43

Paczyński B., 1991, Acta Astronomica, 41, 257

Paczyński B., 1995, PASP, 107, 1167

Paczyński B., 1998, ApJ, 494, L45

Panuzzo P., Granato G.L., Buat V., Inoue A.K., Silva L., Iglesias-Páramo J., Bressan A., 2007, MNRAS, 375, 640

Pascale E., et al., 2009, ApJ, accepted, arXiv:0904.1206 [astro-ph.CO]

Patat F., et al., 2001, ApJ, 555, 900

Perera T.A., et al., 2008, MNRAS, 391, 1227

Pérez-González P.G., et al., 2005, ApJ, 630, 82

Pérez-González P.G., et al., 2008, ApJ, 675, 234

Pian E., et al., 2006, Nature, 442, 1011

Piro L., et al., 2002, ApJ, 577, 680

Plante S., Sauvage M., 2002, AJ, 124, 1995

Pope A., et al., 2006, MNRAS, 370, 1185

Pope A., et al., 2008, ApJ, 675, 1171

Portinari L., Sommer-Larsen J., Tantalo R., 2004, MNRAS, 347, 691

Price P.A., et al., 2002a, ApJ, 573, 85

Price P.A., et al., 2002b, ApJ, 571, L121

Price P.A., et al., 2003, ApJ, 589, 838

Priddey R.S., McMahon R.G., 2001, MNRAS, 324, L17

Priddey R.S., Isaak K.G., McMahon R.G., Robson E.I., Pearson C.P., 2003, MNRAS, 344, L74

Priddey R.S., Tanvir N.R., Levan A.J., Fruchter A.S., Kouveliotou C., Smith I.A., Wijers R.A.M.J., 2006, MNRAS, 369, 1189

Priddey R.S., Ivison R.J., Isaak K.G., 2008, MNRAS, 383, 289

Prochaska J.X., et al., 2004, ApJ, 611, 200

Prochaska J.X., et al., 2007a, ApJS, 168, 231

Prochaska J.X., Chen H.W., Dessauges-Zavadsky M., Bloom J.S., 2007b, ApJ, 666, 267

Prochaska J.X., Dessauges-Zavadsky M., Ramirez-Ruiz E., Chen H.W., 2008, ApJ, 685, 344

Rawat A., Hammer F., Kembhavi A.K., Flores H., 2008, ApJ, 681, 1089

Reddy N.A., Steidel C.C., Fadda D., Yan L., Pettini M., Shapley A.E., Erb D.K., Adelberger K.L., 2006, ApJ, 644, 792

Rho J., et al., 2008, ApJ, 673, 271

Rho J., Reach W.T., Tappe A., Hwang U., Slavin J.D., Kozasa T., Dunne L., 2009, ApJ, 700, 579

Rieke G.H., Alonso-Herrero A., Weiner B.J., Pérez-González P.G., Blaylock M., Donley J.L., Marcillac D., 2009, ApJ, 692, 556

Robson I., Priddey R.S., Isaak K.G., McMahon R.G., 2004, MNRAS, 351, L29

Rol E., Wijers R.A.M.J., Kouveliotou C., Kaper L., Kaneko Y., 2005, ApJ, 624, 868

Ruiz-Velasco A.E., et al., 2007, ApJ, 669, 1

Ryle M., Vonberg D.D., 1946, Nature, 158, 339

Sagar R., et al., 2001, Bulletin of the Astronomical Society of India, 29, 91

Sajina A., et al., 2008, ApJ, 683, 659

Sakon I., et al., 2009, ApJ, 692, 546

Salpeter E.E., 1955, ApJ, 121, 161

Salvaterra R., et al., 2009, Nature, submitted, `arXiv:0906.1578v2 [astro-ph.CO]`

Sandstrom K.M., Bolatto A.D., Stanimirović S., van Loon J.T., Smith J.D.T., 2009, ApJ, 696, 2138

Sault R.J., Killeen N.E.B., 2004, The Miriad User's Guide. Australia Telescope National Facility, Sydney, (`http://www.atnf.csiro.au/computing/software/miriad/`)

Sault R.J., Teuben P.J., Wright M.C.H., 1995, In: Shaw R.A., Payne H.E., Hayes J.J.E. (eds.) Astronomical Data Analysis Software and Systems IV, vol. 77 of Astronomical Society of the Pacific Conference Series, 433

Savaglio S., Fall S.M., Fiore F., 2003, ApJ, 585, 638

Savaglio S., Glazebrook K., Le Borgne D., 2006, In: Holt S.S., Gehrels N., Nousek J.A. (eds.) Gamma-Ray Bursts in the Swift Era, vol. 836 of American Institute of Physics Conference Series, 540–545

Savaglio S., Glazebrook K., LeBorgne D., 2009, ApJ, 691, 182

Sawicki M., 2002, AJ, 124, 3050

Scalo J., 1998, In: Gilmore G., Howell D. (eds.) The Stellar Initial Mass Function (38th Herstmonceux Conference), vol. 142 of Astronomical Society of the Pacific Conference Series, 201

Schinnerer E., et al., 2008, ApJ, 689, L5

Schlegel D.J., Finkbeiner D.P., Davis M., 1998, ApJ, 500, 525

Schwarz U.J., 1978, A&A, 65, 345

Scott K.S., et al., 2008, MNRAS, 385, 2225

Scott S.E., et al., 2002, MNRAS, 331, 817

Scoville N.Z., et al., 1998, ApJ, 492, L107

Seaquist E., Yao L., Dunne L., Cameron H., 2004, MNRAS, 349, 1428

Serjeant S., et al., 2003, MNRAS, 344, 887

Serjeant S., et al., 2008, MNRAS, 386, 1907

Seymour N., Huynh M., Dwelly T., Symeonidis M., Hopkins A., McHardy I.M., Page M.J., Rieke G., 2009, MNRAS, 398, 1573

Sibthorpe B., et al., 2009, ApJ, submitted `arXiv:0910.1094v1 [astro-ph.HE]`

Silva L., Granato G.L., Bressan A., Danese L., 1998, ApJ, 509, 103

Smail I., Ivison R.J., Blain A.W., 1997, ApJ, 490, L5

Smail I., Ivison R.J., Blain A.W., Kneib J.P., 2002, MNRAS, 331, 495

Smail I., Chapman S.C., Blain A.W., Ivison R.J., 2004, ApJ, 616, 71

Smith I.A., Tilanus R.P.J., Wijers R.A.M.J., Tanvir N., Vreeswijk P., Rol E., Kouveliotou C., 2001, A&A, 380, 81

Smith I.A., et al., 2005, A&A, 439, 987

Soderberg A.M., et al., 2006, Nature, 442, 1014

Sodroski T.J., Odegard N., Arendt R.G., Dwek E., Weiland J.L., Hauser M.G., Kelsall T., 1997, ApJ, 480, 173

Soifer B.T., et al., 1984, ApJ, 283, L1

Soifer B.T., Sanders D.B., Madore B.F., Neugebauer G., Danielson G.E., Elias J.H., Lonsdale C.J., Rice W.L., 1987, ApJ, 320, 238

Sokolov V.V., et al., 2001, A&A, 372, 438

Sollerman J., et al., 2002, A&A, 386, 944

Sollerman J., Östlin G., Fynbo J.P.U., Hjorth J., Fruchter A., Pedersen K., 2005, New Astronomy, 11, 103

Sollerman J., et al., 2006, A&A, 454, 503

Solomon P.M., Downes D., Radford S.J.E., Barrett J.W., 1997, ApJ, 478, 144

Stanek K.Z., et al., 2003, ApJ, 591, L17

Stanek K.Z., et al., 2006, Acta Astronomica, 56, 333

Stark D.P., Bunker A.J., Ellis R.S., Eyles L.P., Lacy M., 2007, ApJ, 659, 84

Sternberg A., 1998, ApJ, 506, 721

Stevens J.A., Amure M., Gear W.K., 2005, MNRAS, 357, 361

Stratta G., Fiore F., Antonelli L.A., Piro L., De Pasquale M., 2004, ApJ, 608, 846

Stratta G., Maiolino R., Fiore F., D'Elia V., 2007, ApJ, 661, L9

Sugerman B.E.K., et al., 2006, Science, 313, 196

Swinbank A.M., Smail I., Chapman S.C., Blain A.W., Ivison R.J., Keel W.C., 2004, ApJ, 617, 64

Swinbank A.M., Chapman S.C., Smail I., Lindner C., Borys C., Blain A.W., Ivison R.J., Lewis G.F., 2006, MNRAS, 371, 465

Swinbank A.M., et al., 2008, MNRAS, 391, 420

Tacconi L.J., et al., 2006, ApJ, 640, 228

Tacconi L.J., et al., 2008, ApJ, 680, 246

Takagi T., Hanami H., Arimoto N., 2004, MNRAS, 355, 424

Takata T., Sekiguchi K., Smail I., Chapman S.C., Geach J.E., Swinbank A.M., Blain A., Ivison R.J., 2006, ApJ, 651, 713

Tamura Y., et al., 2009, Nature, 459, 61

Tantalo R., Chiosi C., Bressan A., Fagotto F., 1996, A&A, 311, 361

Tanvir N.R., et al., 2004, MNRAS, 352, 1073

Tanvir N.R., et al., 2008, MNRAS, 388, 1743

Tanvir N.R., et al., 2009, Nature, submitted, `arXiv:0906.1577v2 [astro-ph.CO]`

Taylor E.L., et al., 2005, MNRAS, 361, 1352

Thomsen B., et al., 2004, A&A, 419, L21

Thöne C.C., et al., 2006, GRB Coordinates Network, 5373, 1

Thöne C.C., Greiner J., Savaglio S., Jehin E., 2007a, ApJ, 671, 628

Thöne C.C., Perley D.A., Bloom J.S., 2007b, GRB Coordinates Network, 6663, 1

Thöne C.C., et al., 2008, ApJ, 676, 1151

Thöne C.C., Michałowski M.J., Leloudas G., Cox N.L.J., Fynbo J.P.U., Sollerman J., Hjorth J., Vreeswijk P.M., 2009, ApJ, 698, 1307

Tinney C., et al., 1998, IAU Circ., 6896, 1

Todini P., Ferrara A., 2001, MNRAS, 325, 726

Tody D., 1986, In: Crawford D.L. (ed.) Instrumentation in astronomy VI; Proceedings of the Meeting, Tucson, AZ, Mar. 4-8, 1986. Part 2 (A87-36376 15-35). Bellingham, WA, Society of Photo-Optical Instrumentation Engineers, 1986, p. 733., vol. 627 of Presented at the Society of Photo-Optical Instrumentation Engineers (SPIE) Conference, 733

Tody D., 1993, In: Hanisch R.J., Brissenden R.J.V., Barnes J. (eds.) Astronomical Data Analysis Software and Systems II, vol. 52 of Astronomical Society of the Pacific Conference Series, 173

Totani T., 1997, ApJ, 486, L71

Trentham N., Blain A.W., Goldader J., 1999, MNRAS, 305, 61

Trentham N., Ramirez-Ruiz E., Blain A.W., 2002, MNRAS, 334, 983

Valiante E., Lutz D., Sturm E., Genzel R., Tacconi L.J., Lehnert M.D., Baker A.J., 2007, ApJ, 660, 1060

Valiante R., Schneider R., Bianchi S., Andersen A.C., 2009, MNRAS, 397, 1661

van de Ven G., van Dokkum P.G., Franx M., 2003, MNRAS, 344, 924

van der Horst A.J., Rol E., Wijers R.A.M.J., Strom R., Kaper L., Kouveliotou C., 2005, ApJ, 634, 1166

van der Wel A., Franx M., Wuyts S., van Dokkum P.G., Huang J., Rix H.W., Illingworth G.D., 2006, ApJ, 652, 97

van Dokkum P.G., Franx M., 2001, ApJ, 553, 90

Vlahakis C., Eales S., Dunne L., 2007, MNRAS, 379, 1042

Vreeswijk P.M., et al., 1999, ApJ, 523, 171

Vreeswijk P.M., Fender R.P., Garrett M.A., Tingay S.J., Fruchter A.S., Kaper L., 2001a, A&A, 380, L21

Vreeswijk P.M., et al., 2001b, ApJ, 546, 672

Vreeswijk P.M., et al., 2004, A&A, 419, 927

Wall J.V., Pope A., Scott D., 2008, MNRAS, 383, 435

Wang R., et al., 2008, AJ, 135, 1201

Wang W., Cowie L.L., Barger A.J., 2006, ApJ, 647, 74

Wang W.H., Cowie L.L., Barger A.J., 2004, ApJ, 613, 655

Wang W.H., Cowie L.L., van Saders J., Barger A.J., Williams J.P., 2007, ApJ, 670, L89

Wang W.H., Barger A.J., Cowie L.L., 2009, ApJ, 690, 319

Watabe Y., Risaliti G., Salvati M., Nardini E., Sani E., Marconi A., 2009, MNRAS, 396, L1

Watson D., Hjorth J., Jakobsson P., Pedersen K., Patel S., Kouveliotou C., 2004, A&A, 425, L33

Watson D., et al., 2006, ApJ, 652, 1011

Watson D., Hjorth J., Fynbo J.P.U., Jakobsson P., Foley S., Sollerman J., Wijers R.A.M.J., 2007, ApJ, 660, L101

Webb T.M., et al., 2003a, ApJ, 587, 41

Webb T.M.A., Lilly S.J., Clements D.L., Eales S., Yun M., Brodwin M., Dunne L., Gear W.K., 2003b, ApJ, 597, 680

Weiß A., Ivison R.J., Downes D., Walter F., Cirasuolo M., Menten K.M., 2009, ApJ, 705, L45

Weiss A., et al., 2009, ApJ, submitted

Wesson R., et al., 2009, MNRAS, submitted, arXiv:0907.0246v1 [astro-ph.GA]

Wheeler J.C., Harkness R.P., 1990, Reports of Progress in Physics, 53, 1467

Wiersema K., et al., 2007, A&A, 464, 529

Wijers R.A.M.J., Bloom J.S., Bagla J.S., Natarajan P., 1998, MNRAS, 294, L13

Wilson C.D., et al., 2008, ApJS, 178, 189

Wilson T.L., Batrla W., 2005, A&A, 430, 561

Woo J., Courteau S., Dekel A., 2008, MNRAS, 390, 1453

Woo J.H., Urry C.M., van der Marel R.P., Lira P., Maza J., 2005, ApJ, 631, 762

Woosley S.E., 1993, ApJ, 405, 273

Yang M., Greve T.R., Dowell C.D., Borys C., 2007, ApJ, 660, 1198

Younger J.D., et al., 2007, ApJ, 671, 1531

Younger J.D., et al., 2008a, MNRAS, 387, 707

Younger J.D., et al., 2008b, ApJ, 688, 59

Younger J.D., et al., 2009a, ApJ, 704, 803

Younger J.D., et al., 2009b, MNRAS, 394, 1685

Yun M.S., Carilli C.L., 2002, ApJ, 568, 88

Yun M.S., Reddy N.A., Condon J.J., 2001, ApJ, 554, 803

Zheng X.Z., Bell E.F., Papovich C., Wolf C., Meisenheimer K., Rix H.W., Rieke G.H., Somerville R., 2007, ApJ, 661, L41

Zhukovska S., Gail H.P., Trieloff M., 2008, A&A, 479, 453